UNIVERSITY OF CALIFORNIA

Los Angeles

Leaf hydraulics and evolution

A dissertation submitted in partial satisfaction of the

requirements for the degree Doctor of Philosophy

in Biology

by

Christine Scoffoni

2014

ABSTRACT OF THE DISSERTATION

Leaf hydraulics and evolution

by

Christine Scoffoni

Doctor of Philosophy in Biology

University of California, Los Angeles, 2014

Professor Lawren Sack, Chair

There has been increasing worldwide recognition of the importance of hydraulic physiology—the transport of water through the plant—in explaining plant growth and drought tolerance. By combining physiology and anatomy within an evolutionary framework, we can discover the mechanisms underlying species differences in hydraulic function, especially those of the leaf, the central organ in plant metabolism. I refined and developed new methods to investigate leaf water transport and its decline during drought, focusing on a critical measure of the capacity for water movement (leaf hydraulic conductance, K_{leaf}). I found that species most tolerant of K_{leaf} decline had small leaves with dense major veins, providing pathways for the water to bypass embolized conduits during drought giving a new, direct explanation to the fact that species of dry areas have small leaves. I also developed a new method to investigate the role of leaf shrinkage on water movement. As leaves shrink with dehydration, mesophyll cells lose connectivity, physically impacting water movement outside the xylem. I found that species most sensitive to K_{leaf} decline were those with strongest shrinkage in thickness. I then developed a new method to measure xylem hydraulic decline in leaves to test for a possible artifact of cutting leaf petioles under

tension while under water. Such artifact has been recently found to occur in stems, and has put into question measurements of K_{leaf}. Across four diverse species, I found no sign of such an artifact in leaves, likely due to the lesser mechanical stress imposed when cutting a petiole vs. stem. Finally, I took an evolutionary perspective. I quantified the anatomical and physiological plasticity in leaves of six species of endemic Hawaiian lobeliads grown under different light regimes and found a high degree of plasticity in K_{leaf} with light, relating to leaf anatomical changes. Across 30 species of *Viburnum* I have identified the evolutionary shifts of leaf anatomy, water transport and drought tolerance. This work provides new techniques, clarity and applications toward understanding leaf water transport and its role in plant performance and drought tolerance, with applications for ecology, paleobiology and the conservation of species and ecosystems.

The dissertation of Christine Scoffoni is approved.

Phil Rundel

Louis Santiago

Lawren Sack, Committee Chair

University of California, Los Angeles

2014

TABLE OF CONTENTS

LIST OF TABLES

LIST OF SUPPLEMENTARY TABLES

CHAPTER 2

CHAPTER 3

CHAPTER 4

TABLE S7.2 Akaike Information Criterion (AIC) scores for the two models of trait evolution in the different tested correlations. Model: Brownian motion (BM) and Ornstein-Uhlenbeck (OU). Best chosen model appears in bold

LIST OF FIGURES

ACKNOWLEDGMENTS

These past five years have been quite an amazing journey, and I would like to thank many people without whom I would not be where I am today.

First, I would like to thank Prof. Henri Sandoz for his incredible passion for plants and pushing me to leave Aix to pursue functional plant ecology. I am forever grateful to Stephan Hättenschwiler for giving me the opportunity to work in his lab for several months, with unforgettable field experiences in the Swiss Alps and French Guyana, and for exposing me to the amazing diversity of leaf vein architecture for the first time. To Guillermo Goldstein and all the team at Iguazu National Park, thanks for such a wonderful experience, and teaching me the exciting complexities of field plant ecophysiology in the most beautiful place in the world. I would like to thank Sylvain Delzon for convincing me to enroll in the Master Program at the Université de Bordeaux, it was definitely the best decision I ever made. To Fernando Valladares, thanks for hosting me in your lab for a year, and giving me the opportunity to work on stem hydraulics. I learned so much from everyone there! Above all, I really want to thank my advisor, Lawren Sack. There are no words to thank you enough for all your support, patience, availability and mentorship throughout the years. You introduced me to the field of leaf hydraulics and taught me everything I know and for that I will be forever grateful. Your passion for plant sciences is really contagious, and I feel truly lucky to have been your student. Finally, to my lab mates and Rodrigo: thanks for being so supportive and such an inspiration to me. You guys are AWESOME! (Chris, thanks for paving the road! Faith, that first year would have been so much harder without you…! Megan, thanks for all the hilarious and cute YouTube animal videos you shared with us and inventing the smashing game: you are brilliant! Grace, thanks for being my

"desk buddy" for the past three years and making lab such a fun place to be. And Marissa, thanks for the incredible enthusiasm you carry with you at all times and share!)

I would also like to thank my committee members Phil Rundel, Louis Santiago and Mike Alfaro, as well as Rasoul Sharifi for their encouragement and feedback. To Jocelyn Yamadera, there are no words to thank you enough for your patience and availability throughout the years. I would not have made it through grad school without you!!

I especially would like to thank my collaborators David Chatelet, Hervé Cochard, Michael Donoghue, Erika Edwards, Tom Givnish, Justin Kunkle, Athena Mckown and Rebecca Montgomery, as well as Jonathan Chang and many students who helped me with my research. Thanks so much for all your hard work/help. You have all taught me so much and I couldn't have done it without you!

Finally, I would like to thank my family for their love, understanding and support; I wouldn't be who I am and where I am without them. Un grand merci à toi Mamy, pour avoir partagé mon voyage en bus jusqu'à la fac presque tous les matins par téléphone, me permettant de toujours commencer le boulot dans la bonne humeur. Y sobre todo Marcos, gracias por tu constante apoyo y amor, por siempre creer en mi, por haberme seguido por todo el mundo y haber tenido que pasar el bar exam en tres paises.... Sos increible!

Co-authored work: **Chapter 2** is from Scoffoni C, McKown A, Rawls M, Sack L (2012) Dynamics of leaf hydraulic conductance with water status: quantification and analysis of species differences under steady-state. *Journal of Experimental Botany* 63, 643-658. A McKown and M Rawls assisted with measurements and provided feedback on the manuscript, L Sack mentored at all stages of the project. **Chapter 3** is from Scoffoni C, Rawls M, McKown A, Cochard H, Sack

L (2011) Decline of leaf hydraulic conductance with dehydration: relationship to leaf size and venation architecture. *Plant Physiology* 156, 832-843. M Rawls, A Mckown assisted with measurements and provided feedback on the manuscript, H. Cochard assisted with the model analysis and provided feedback on the manuscript. L Sack mentored at all stages of the project. **Chapter 4** is from Scoffoni C, Vuong C, Diep S, Cochard H, Sack L (2014) Leaf shrinkage with dehydration: coordination with hydraulic vulnerability and drought tolerance. *Plant Physiology* 164, 1772-1788. C Vuong and S Diep assisted with measurements, H Cochard assisted with the model analysis and provided feedback on the manuscript, L Sack mentored at all stages of the project. **Chapter 5** is from Scoffoni C & Sack L (*in review*) Are leaves "freewheelin'"? Testing for a Wheeler-type effect in leaf xylem hydraulic decline. L Sack mentored at all stages of the project. **Chapter 6** is a version of Scoffoni C, Kunkle J, Pasquet-kok J, Vuong C, Patel A, Montgomery R, Givnish T, Sack L (*in preparation*) Testing "optimality" in light induced plasticity: responses of leaf hydraulics and anatomy for Hawaiian Lobeliads diverse in light adaptation. J Kunkle grew the plants and provided the gas exchange measurements and feedback on the manuscript, J Pasquet-kok, C Vuong and A Patel assisted with measurements, R Montgomery and T Givnish helped with the design of the project and provided feedback. L Sack mentored at all stages of the project. **Chapter 7** is a version of Scoffoni C, Chatelet D, Pasquet-kok J, Rawls M, Donoghue M, Edwards E, Sack L (*in preparation*) Leaf hydraulic architecture drives the evolution of gas exchange in *Viburnum*. D Chatelet provided the gas exchange, leaf area and minor vein length per area measurements, helped with the analyses and provided feedback on the manuscript; J Pasquet-kok and M Rawls assisted with the measurements, M Donoghue and E Edwards helped with the design of the project and provided feedback; L Sack mentored at all stages of the project.

Funding: This work was supported by Vavra Fellowships and Research grants, the UCLA Bartholomew Fellowship, the Charles E. and Sue K. Young student Award, the UCLA Dissertation Year Fellowship, and National Science Foundation Grants #0546784, #0614813, IOS-0753233, IOS-0842771, IOS-1147292 (L. Sack), IOS-0843231 (E. J. Edwards), IOS-0842800 (M. J. Donoghue).

BIOGRAPHICAL SKETCH

PROFESSIONAL PREPARATION

2010 OTS PASI Embedded Sensors Network Course (La Selva Biological Station, Costa Rica)
2008 MS in Plant Functional Biology (Université Bordeaux 1)
2006 BSc. in Plant Biology (Université Aix-Marseille 3)

PUBLICATIONS

Published work

Scoffoni C, Pou A, Aasamaa K, Sack L. 2008. The rapid light response of the leaf hydraulic conductance: new evidence from two experimental methods. *Plant, Cell and Environment* 13:1803-1812

Scoffoni C, Rawls M, McKown A, Cochard H, Sack L. 2011. Decline of leaf hydraulic conductance with dehydration: relationship to leaf size and venation architecture. *Plant Physiology* 156:832-843

Scoffoni C, McKown A, Rawls M, Sack L. 2012. Dynamics of leaf hydraulic conductance with water status: quantification and analysis of species differences under steady-state. *Journal of Experimental Botany.* 63, 643-658

Scoffoni C, Vuong C, Diep S, Cochard H, Sack L. 2014. Leaf shrinkage with dehydration: coordination with hydraulic vulnerability and drought tolerance. *Plant Physiology*.164, 1772-1788

Bartlett M, **Scoffoni C**, Sack L. 2012. The determinants of leaf turgor loss point and prediction of drought tolerance of species and biomes: a global meta-analysis. *Ecology Letters*. 15, 393-405

Bartlett M, **Scoffoni C**, Ardy R, Zhang Y, Shanwen S, Cao K, Sack L. 2012. Rapid determination of comparative drought tolerance traits: using an osmometer to predict turgor loss point. *Methods in Ecology & Evolution*. 3: 880-888.

Guyot G, **Scoffoni C**, Sack L. 2012. Combined impacts of irradiance and dehydration on leaf hydraulic conductance: insights into vulnerability and stomatal control. *Plant, Cell & Environment.* 35, 857-871

John GP, **Scoffoni C**, Sack L. 2013. Allometry of cells and tissues within leaves. *American Journal of Botany*. 100:1936-1948

Li S, Zhang YJ, Ishida A, Sack L, **Scoffoni C,** Chen YJ, Cao KF. 2013. The heterogeneity and spatial patterning of structure and physiology across the leaf surface in giant leaves of *Alocasia macrorrhiza. PLoS One.* 8, e64502

Pivovaroff J, Sharifi R, **Scoffoni C**, Sack L, Rundel PW. 2013. Making the best of the worst of times: traits underlying combined shade and drought tolerance of *Ruscus aculeatus* and *R. microglossum*. *Functional Plant Biology. In press*

Sack L, **Scoffoni C**, McKown AD, Frole K, Rawls M, Havran JC, Tran H, Tran S. 2012. Developmentally-based scaling laws for leaf venation architecture explain global patterns. *Nature communications.* 3, 837

Sack L, **Scoffoni C**. 2012. Measurement of leaf hydraulic conductance and stomatal conductance and their responses to irradiance and dehydration using the evaporative flux method (EFM). *Journal of Visualized Experiments*.

Sack L, **Scoffoni C.** 2013. *Tansley Review*. Leaf venation: structure, function, development, evolution, ecology and applications in past, present and future. *New Phytologist.* 198: 983-1000

Sack L, **Scoffoni C,** John GP, Poorter H, Mason CM, Mendez-Alonzo R, Donovan LA. 2013. How do leaf veins influence the worldwide leaf economic spectrum? Review and synthesis. *Journal of Experimental Botany* 64: 4053-4080.

Flexas J, **Scoffoni C**, Gago J, Sack L. 2013. Leaf mesophyll conductance and leaf hydraulic conductance: an introduction to their measurement and coordination. *Journal of Experimental Botany* 64: 3965-3981.

Granda A, **Scoffoni C,** Rubio-Casal AE, Sack L, Valladares F. (In press). Leaf and stem physiological responses to summer and winter extremes of woody species across temperate ecosystem. *Oikos*.

Papers in review or in revision

Sack L, Pasquet-Kok J, Taylor SH, **Scoffoni C**, Diener AC, Edwards EJ, Christin PA, Osborne CP (In revision). Constrasting hydraulic constraints on photosynthesis and adaptation to climate in C_3 and C_4 grasses.

Sack L, Caringella M, **Scoffoni C**, Mason C, Rawls M, Markesteijn L, Poorter L. (In review). Leaf vein length per area is not intrinsically scale dependent: avoiding measurement artifacts for accuracy and precision.

Sack L, **Scoffoni C,** John GP, Poorter H, Mason CM, Mendez-Alonzo R, Donovan LA. (In review). Leaf mass per area (LMA) is independent of vein length per area: avoiding pitfalls when modeling phenotypic integration (reply to Blonder *et al*. 2014)

SYNERGISTIC ACTIVITIES

• Instructor of two-week course, "*Ecophysiology of Drought Tolerance*" (with co-instructor Lawren Sack) at University of La Serena, Chile, June 2012

• Conference presentation at UCLA's Ecolunch series (April 2010, November 2011), Botanical Society of America (August 2010), Southern California Academy of Sciences symposium (May 2011, May 2012), International Botanical Congress (August 2011), MEDECOS (September 2011), ESA (August 2012)

• Poster presentation at the Department of Ecology and Evolutionary Biology's annual research symposium (UCLA; 2010, 2011, 2012)

• Referee for >20 papers for *Annals of Botany, Annals of Botany Plants, American Journal of Botany, Ecology, Functional Ecology, Functional Plant Biology, International Journal of Heat and mass Transfer, International Journal of Plant Biology, Journal of Experimental Botany, Oecologia, Plant Cell & Environment, Plant Ecology, Plant and Soil, Tree Physiology, TREES structure and function*

• Member of the American Society of Plant Biologists, the Botanical Society of America and the Ecological Society of America

• Co-chair of the UCLA Ecolunch Committee at the Department of Ecology and Evolutionary Biology (fall 2010- June 2011)

• Member of the UCLA EEB Departmental Awards board (2012-2013)

• Dissemination of research findings on web pages for public access

CHAPTER 1

PREMISE OF THE DISSERTATION

"In order to show the real correlation between structure and function, anatomical investigations must always be followed by physiological experiments"— Maximov (1931).

To understand how plants function as organisms and determinants of ecosystems, we need a greater understanding of plant physiology and how it relates to the anatomy. Leaves are a major determinant of whole-plant function, providing through photosynthesis the sugars necessary for plant growth, and they represent a critical bottleneck in the plant water transport system, accounting for more than 30% of the whole-plant hydraulic resistance (Sack and Holbrook, 2006). My dissertation focuses on fundamental questions that have remained unanswered relating to leaf function, structure and its evolution. Recent work has shown an importance for hydraulic physiology in explaining many aspects of leaf diversity, and I have aimed to further our understanding of the underlying mechanisms shaping species differences in leaf hydraulic vulnerability by combining physiology and anatomy within an evolutionary framework.

Since the early Devonian (about 400 Mya), leaves have evolved independently multiple times in different lineages (Wilson, 1953; Crane and Kenrick, 1997; Harrison et al., 2005; Floyd and Bowman, 2006; Tomescu, 2009). Since then, leaves have diversified in various size, shape and form, and are especially diverse in their venation architecture. This can be surprising at first given they share the exact same function in virtually all plants: they transport the water, nutrients, sugars and signals necessary for plant growth, and provide mechanical support to display the leaf toward the light for energy capture. New approaches have suggested much of the diversity in leaf form and venation can relate to achieving adequate hydraulic supply (Zwieniecki et al., 2002; Sack and Holbrook, 2006; Brodribb et al., 2010). Indeed, leaves face a

great design challenge, as they harvest solar energy for photosynthesis and growth while requiring an adequate hydraulic supply to replace water lost to transpiration that occurs when stomata open to capture CO_2. Our understanding of the hydraulic functions of leaf veins and mesophyll and their relationship to physiological traits and habitat has remained rudimentary.

My PhD work focuses on clarifying the mechanical, ecological and evolutionary understanding of leaf hydraulics and its relationship to physiological traits and habitat. In Chapter 2, I have refined the method for measurement of leaf hydraulic conductance (K_{leaf}) and developed a new framework to analyze and interpret the dynamics of K_{leaf} with dehydration and rehydration. This work enabled a detailed investigation of the relationship between leaf hydraulic conductance, venation architecture and leaf size. In Chapter 3, I improved the understanding of the mechanistic basis for the decline observed in K_{leaf} during dehydration using both a modeling and experimental approach and proposed a new direct explanation to one of the most well-known biogeographic trends: the tendency of leaves to be smaller in drier areas. In Chapter 4, using modeling and empirical results, I investigated the physical impact of leaf dehydration on the cells outside the xylem on the outside-xylem pathways in water movement during drought. Chapter 5 presents new methods and analyses of leaf xylem hydraulic vulnerability, presented specifically to answer a recent paper that raised a concern about methods of K_{leaf} measurements including those described in my Chapter 2, based on the fact that measurements of stem hydraulic conductance were found to be subject to an artifact of cutting xylem under water while under tension. I developed a new method to directly measure leaf xylem hydraulic conductance for dehydrated leaves and thereby to construct leaf xylem hydraulic vulnerability curves. These experiments validated our method against that artifact, which was not seen in leaves. In Chapters 6 and 7 of my dissertation, I take a specifically evolutionary perspective on leaf hydraulics

within a tropical and a temperate clade. In Chapter 6, I investigated anatomical and physiological plasticity in leaves from six species of Hawaiian lobeliads grown under different light regimes. Finally, in Chapter 7, I investigate for the first time the coordinated evolution of leaf hydraulics and gas exchange in a well resolved lineage, along with the evolution of hydraulic partitioning in leaves of 30 *Viburnum* species grown in a common garden.

REFERENCES

Brodribb TJ, Feild TS, Sack L (2010) Viewing leaf structure and evolution from a hydraulic perspective. Functional Plant Biology **37:** 488-498

Crane PR, Kenrick P (1997) Diverted development of reproductive organs: A source of morphological innovation in land plants. Plant Systematics and Evolution **206:** 161-174

Floyd SK, Bowman JL (2006) Distinct developmental mechanisms reflect the independent origins of leaves in vascular plants. Current Biology **16:** 1911-1917

Harrison CJ, Corley SB, Moylan EC, Alexander DL, Scotland RW, Langdale JA (2005) Independent recruitment of a conserved developmental mechanism during leaf evolution. Nature **434:** 509-514

Maximov NA (1931) The physiological significance of the xeromorphic structure of plants. Journal of Ecology **19:** 273-282

Sack L, Holbrook NM (2006) Leaf hydraulics. Annual Review of Plant Biology **57:** 361-381

Tomescu AMF (2009) Megaphylls, microphylls and the evolution of leaf development. Trends in Plant Science **14:** 5-12

Wilson CL (1953) The telome theory. Botanical Review **19:** 417-437

Zwieniecki MA, Melcher PJ, Boyce CK, Sack L, Holbrook NM (2002) Hydraulic architecture of leaf venation in *Laurus nobilis* L. Plant Cell and Environment **25:** 1445-1450

CHAPTER 2

DYNAMICS OF LEAF HYDRAULIC CONDUCTANCE WITH WATER STATUS: QUANTIFICATION AND ANALYSIS OF SPECIES DIFFERENCES UNDER STEADY-STATE

ABSTRACT

Leaf hydraulic conductance (K_{leaf}) is a major determinant of photosynthetic rate in well-watered and drought-stressed plants. Previous work assessed the decline of K_{leaf} with decreasing leaf water potential (Ψ_{leaf}), most typically using rehydration kinetics methods, and found that species varied in the shape of their vulnerability curve, and that hydraulic vulnerability correlated with other leaf functional traits and with drought sensitivity. We tested and extended these findings, using a new steady-state evaporative flux method under high irradiance, and determined the function for the vulnerability curve of each species individually using maximum likelihood for 10 species varying strongly in drought tolerance. Additionally, we assessed the ability of excised leaves to recover in K_{leaf} with rehydration, and developed a new theoretical framework to estimate how rehydration of measured leaves may affect estimation of hydraulic parameters. As hypothesized, species differed in their vulnerability function. Drought-tolerant species showed shallow linear declines and more negative Ψ_{leaf} at 80% loss of K_{leaf} (P_{80}), whereas drought-sensitive species showed steeper, non-linear declines, and less negative P_{80}. Across species, the maximum K_{leaf} was independent of hydraulic vulnerability. Recovery of K_{leaf} after 1 h rehydration of leaves dehydrated below their turgor loss point occurred only for four out of ten species. Across species without recovery, a more negative P_{80} correlated with the ability to maintain K_{leaf} through both dehydration and rehydration. These findings indicate that resistance

to K_{leaf} decline is important not only in maintaining open stomata during the onset of drought, but also in enabling sustained function during drought recovery.

Key words: Cavitation, dehydration, EFM, K_{leaf}, rehydration, refilling, safety margins, turgor loss point, vulnerability curves

INTRODUCTION

In dicotyledons, the leaf hydraulic conductance strongly constrains gas exchange and growth (Sack *et al.*, 2003; Sack and Holbrook, 2006). The resistance of open stomata to vapor diffusion out of the leaf is typically far greater than the hydraulic resistance to bulk flow of the liquid transport through the plant, and transpiration rates are thus dictated by this diffusion process, which in turn depends on the stomatal and boundary layer conductances and the difference in vapor pressure between the intercellular air spaces of the leaf and the atmosphere (Cowan, 1972; Sack and Tyree, 2005; Sack and Holbrook, 2006). However, the maintenance of open stomata depends on the leaf being well-hydrated, i.e., having a high leaf water potential (Ψ_{leaf}), which in turn depends on the plant hydraulic conductance being sufficiently high. Because in dicotyledons, the leaf accounts for on average 30% of the plant hydraulic resistance (Sack *et al.*, 2003; Sack and Holbrook, 2006), the leaf hydraulic conductance (K_{leaf} = flow rate / water potential driving force, i.e., 1/ leaf hydraulic resistance) is thus a critical variable. Water enters the petiole, moves through several vein orders of diminishing size, then exits into the bundle sheath and moves through or around cells before evaporating into the intercellular airspace and being transpired from the stomata. The K_{leaf} declines with Ψ_{leaf} during drought, due to losses of conductance resulting from cavitation and/or collapse of xylem conduits, and/or to decline in the permeability of extra-xylem tissues, and this response drives stomatal closure to prevent leaf desiccation (e.g., Salleo *et al.*, 2000; Brodribb and Holbrook, 2004a; Sack and Holbrook, 2006;

Scoffoni *et al.*, 2008; Brodribb and Cochard, 2009; Brodribb *et al.*, 2010; Scoffoni *et al.*, 2011). Understanding species variation in hydraulic vulnerability is thus critical, and several techniques have been applied, especially the rehydration kinetics method (RKM; Table S2.1; Brodribb and Holbrook, 2003a). The aim of this study was to quantify this response using an independent, steady-state method, for species varying strongly in drought tolerance, and to determine the ability of dehydrated leaves to recover in K_{leaf} after rehydration.

Previous studies using the RKM found species to vary strongly in leaf hydraulic vulnerability, quantified as the Ψ_{leaf} at 50% loss of K_{leaf} (P_{50}; e.g. Hao *et al.*, 2008; Blackman *et al.*, 2009; Chen *et al.*, 2009; Johnson *et al.*, 2009a; Saha *et al.*, 2009). Additionally, species with a low P_{50} also had low osmotic potential at turgor loss point (Blackman *et al.*, 2010), and could thus maintain stomata open as leaves dehydrate. Further, these studies tested the classic trade-off between hydraulic efficiency and safety, previously found for stems, and showed this to be absent in leaves: the maximum K_{leaf} for hydrated leaves (K_{max}) was independent of P_{50} (Sack and Holbrook, 2006; Blackman *et al.*, 2010).

Notably, the various methods for measuring K_{leaf} all have value but can raise potential concerns (Sack and Tyree, 2005). There was thus a need to test leaf hydraulic vulnerability with a method independent of the RKM. The typically used RKM measures K_{leaf} from water uptake into the mesophyll of a dehydrated leaf for a known time, and involves some uncertainty because uptake to leaf cells continues even after leaf collection for Ψ_{leaf} determination, though a recently modified version of the RKM ("dynamic RKM") has overcome this limitation (Brodribb and Cochard, 2009; Blackman and Brodribb, 2011; Brodribb and Blackman, and PrometheusWiki contributors 2011). Additionally, in the RKM, water uptake into mesophyll cells might not always mimic the complete pathways of natural transpiration (Scoffoni et al., 2008). Additionally, the RKM may give low resolution of K_{leaf} declines in the well hydrated range of

the vulnerability curve if such leaves rehydrate completely during measurement. The evaporative flux method (EFM) has the advantage of allowing K_{leaf} measurement during steady state transpiration and, further, using the EFM, leaves can be acclimated to high irradiance, which influences K_{leaf} for many species (Sack *et al.*, 2002; Nardini *et al.*, 2005; Tyree *et al.*, 2005; Cochard *et al.*, 2007; Sellin and Kupper, 2007; Scoffoni *et al.*, 2008; Sellin *et al.*, 2008). One previous study applied a variant of the EFM to generate vulnerability curves (the heat-flux method, "Heat-FM"; Brodribb and Holbrook, 2006) which involved some complexity. A heat gun was used on the leaf to drive a transiently high transpiration rate, after which the stomata closed, establishing a lower flow rate. The leaf was removed, and K_{leaf} was determined as the steady state flow rate divided by the final Ψ_{leaf} (Ψ_{final}), and the vulnerability curve was determined as K_{leaf} plotted against Ψ_{final}. However, that method could not determine the lowest Ψ_{leaf} induced in the leaf during the high transpiration rates driven by the hot air (Ψ_{lowest}), which may have triggered the K_{leaf} decline. In this study, the EFM was modified to allow measurement of both Ψ_{lowest} and Ψ_{final}, such that K_{leaf} could be plotted against both.

A second aim of this study was to refine the statistical analysis of the K_{leaf} decline with dehydration for improved accuracy and mechanistic insight. Typically, studies have fitted the same function for all species, chosen for approximate fit to the data; polynomial (including linear), sigmoidal and logistic functions have all been used (Table S2.1). However, species may differ in the shape of their vulnerability curve, and choosing the appropriate function is important both for accuracy and also to allow interpretation of the underlying processes (Brodribb and Holbrook, 2006, 2007). Notably few studies have directly discussed the underlying basis for different shapes of vulnerability curves, probably due to the lack of an approach to objectively select the appropriate function, but the literature has pointed to several potential mechanisms for differently shaped curves (reviewed in Table 2.1). As a next step a rigorous analysis is needed to

resolve species differences in the shape of the function. Thus, for ten diverse species, the maximum likelihood function was selected for each species. Drought tolerant species were hypothesized to show shallower, linear declines, whereas drought-sensitive species were expected to show stronger initial K_{leaf} declines due to greater sensitivity in one or more components of the water transport system. Tests were made of the impact on estimated hydraulic vulnerability parameters of using different functions as in previous studies (Table S2.1), and the degree to which it matters how vulnerability curves are plotted, i.e, whether unbinned data for K_{leaf} are plotted against Ψ_{lowest} or Ψ_{final}, or whether data are binned by Ψ_{leaf} intervals.

A third aim in this study was to quantify the recovery of K_{leaf} with rehydration, a related, essential process that has received little attention. One previous study found that excised and dehydrated sunflower leaves recovered rapidly in K_{leaf} when rehydrated with petioles under water (Trifilo *et al.*, 2003a). We tested for species differences in this ability. Species with greatest hydraulic vulnerability were hypothesized to show greatest recovery, as they would derive most benefit. Further, all studies of vulnerability have involved leaf rehydration during measurement, but none have accounted for this in interpretation; we developed tests to determine how our measurements might be affected. The main benefit of a low hydraulic vulnerability has typically been framed as the ability to keep stomata open without dehydrating the mesophyll. We hypothesized that a low hydraulic vulnerability would also confer the ability to maintain K_{leaf} through both dehydration and rehydration.

MATERIAL AND METHODS

Plant material

This study was conducted alongside a study of the importance of venation architecture and leaf size in determining species-variation in hydraulic vulnerability (Scoffoni *et al.*, 2011). Ten

species were selected across nine families and spanning a wide range of drought sensitivity; five species were native to dry habitats (mainly California chaparral) and five species to moist habitats (Table 2.2). Study species included mature trees and shrubs in and around the campus of University of California, Los Angeles and Will Rogers State Park, Los Angeles, California, and sunflower *Helianthus annuus* var. Sunspot grown from seeds (Botanical Interests; Broomfield, Colorado, USA) in 3.6 L pots in a greenhouse (average minimum, mean and maximum values for temperature: 21.1, 23.2 and 26.0^{o}C; for humidity: 44, 51 and 59%). Sunflowers were irrigated every two days, with 200-250 ppm of 20:20:20 N:P:K; the irradiance measured at mid-day on a sunny day was up to 550 µmol photon $\cdot$ m^{-2} $\cdot$ s^{-1}, and on average 300 µmol photon $\cdot$ m^{-2} $\cdot$ s^{-1} (LI-250 light meter; LI-COR Biosciences, Lincoln, Nebraska, USA).

Experiments were conducted in May-September 2008. On the day prior to measurements, for three to ten plants per species, exposed branches with mature, healthy leaves were collected into plastic bags with moist paper towel; for sunflowers, whole shoots were collected. Each shoot was re-cut by at least two nodes in the laboratory under ultrapure water (MilliPore, 0.22 µm Thornton 200CR, Molshem, France) and rehydrated overnight at laboratory temperature (20-25ºC), covered with dark plastic bags.

Measuring dehydration response of K_{leaf} with the evaporative flux method

Using the evaporative flux method (EFM), K_{leaf} is determined as the ratio of steady-state transpirational flow rate (E, mmol $\cdot$ m^{-2} $\cdot$ s^{-1}) to the water potential driving force ($\Delta\Psi_{leaf}$, MPa; Sack et al., 2002). Notably, in this system, the overall driving force for flow through the whole leaf is the water potential gradient between the outside air and the water entering the petiole, but the important component of that driving force is the vapor pressure gradient between the outside air and leaf airspaces; this vapor pressure driving force, and stomatal conductance, determine the

transpiration rate (see *Introduction*). However, for the liquid-phase part of flow (i.e., the hydraulic system), the driving force at steady state is the water potential gradient between the leaf mesophyll where water evaporates (estimated as the Ψ_{leaf} measured at the end of the measurement, i.e., the Ψ_{final}) and the water entering the petiole at atmospheric pressure (i.e., 0 MPa relative pressure).

In this study, we focused on the dehydration response of the whole-leaf hydraulic system, including the petiole. The leaf was cut from the shoot with a fresh razor blade under ultrapure water that was used as flow solution (0.22 mm Thornton 200 CR; MilliPore, Molsheim, France) degassed at least 8 h with a vacuum pump (Gast, Benton Harbor, MI), and refiltered (0.2µm; Syringe filter, Cole-Parmer, Vernon Hills, IL). The petiole was then rapidly connected to silicon tubing (Cole-Parmer, Vernon Hills, IL) under ultrapure water to prevent air entering the system. The tubing connected the leaf to a cylinder on a balance (models XS205 and AB265, ±10 µg sensitivity; Mettler Toledo, Columbus, OH) that logged data every 30 s to a computer for the calculation of flow rate through the leaf (*E*). Leaves were held adaxial surface upwards in wood frames strung with fishing line above a large box fan (Lakewood Engineering & Manufacturing Company, Chicago, IL). Leaves were illuminated with > 1000 mmol · m^{-2} · s^{-1} photosynthetically active radiation at the leaf surface by floodlights (model 73828 1000 W, "UV filter"; Sears, Roebuck, Hoffman Estates, IL) suspended above a Pyrex container (Corning Incorporated, Corning, NY) filled with water to absorb the heat of the lamp. Leaf temperature was determined using a thermocouple (Cole-Parmer, Vernon Hills, IL) and maintained between 23 and 28°C.

Leaves were allowed to transpire on the apparatus for at least 30 min and until flow rate stabilized, with no upward or downward trend, and with a coefficient of variation <5% for at least five measurements made at 30 sec flow intervals. When flow rate was very low (<8 µg s^{-1}),

stability was determined with the same criterion, but using the running averages of the last five 30 sec intervals. Previous studies found these criteria to be sufficient for stabilization of E, Ψ_{leaf} and K_{leaf}; tests with longer measurement periods after stable flow was established showed no relationship of K_{leaf} to measurement time for seven species of a wide range of leaf capacitance (Scoffoni *et al.*, 2008; Pasquet-Kok *et al.*, 2010). The minimum 30 min flow period was chosen to ensure that leaves had sufficient time to acclimate to high irradiance, which has been found to enhance K_{leaf} by up to eightfold depending on species apparently due to the expression and/or activation of aquaporins (Sack *et al*., 2002; Nardini *et al*., 2005; Tyree *et al*., 2005; Cochard *et al.*, 2007; Scoffoni *et al.*, 2008; Voicu *et al*., 2008). Measurements were discarded if the flow suddenly changed, either due to apparent leakage from the seal or blockage in the system by particles or air bubbles. Following the stabilization of the flow rate, leaf temperature was recorded with a thermocouple and the final five flow rate measurements were averaged. The leaf was quickly removed from the tubing, the petiole was dabbed dry, and the leaf was placed into a sealable bag (Whirl-Pak; Nasco, Fort Atkinson, WI, USA), which had been previously exhaled in, to halt transpiration. Following at least 30 min equilibration, the final leaf water potential (Ψ_{final}) was measured with a pressure chamber (Plant Moisture Stress, Model 1000, Albany, Oregon, USA). K_{leaf} was calculated as E / $-\Delta\Psi_{leaf}$ (where $\Delta\Psi_{leaf} = \Psi_{final}$ - 0 MPa) and further normalized by leaf area measured with a LI-COR 3100 leaf area meter (Li-Cor 3100 meter, Lincoln, Nebraska, USA). To correct for changes in K_{leaf} induced by the temperature dependence of water viscosity, K_{leaf} values were standardized to 25° (Weast, 1974; Yang and Tyree, 1993; Sack *et al*., 2002).

To determine the stomatal conductance of leaves measured with the EFM, the final E was divided by the mole fraction vapor pressure deficit (VPD), derived from temperature and relative humidity (RH) measurements in the lab from a weather station that logged measurements each 5

min (HOBO Micro Station with Smart Sensors; Onset, Bourne, Massachusetts, USA), where mole fraction VPD = (1-(RH × VP_{sat}))/ 101.3 kPa, and VP_{sat} is saturation vapor pressure determined using the Arden-Buck equation (Buck, 1981).

The EFM was modified to allow determination of K_{leaf} for dehydrated leaves. Shoots were cut into segments with at least three leaves under ultrapure water and then dehydrated with a fan for different periods of time to a range of Ψ_{leaf} values. The bench drying of shoots to achieve a leaf vulnerability curve has been used in studies using the rehydration kinetics method (e.g.; Brodribb and Holbrook, 2003a; Blackman *et al.*, 2009), and previous studies found similar vulnerability curves when constructed from bench-drying shoots as from leaves on plants progressively droughted (Brodribb and Holbrook, 2004a; Blackman *et al.*, 2009; Pasquet-Kok *et al.*, 2010). In our study, shoots were allowed to equilibrate for at least 30 min before two leaves were excised and measured for initial Ψ_{leaf} (Ψ_o) using a pressure chamber. If the difference in the Ψ_{leaf} of those two leaves was greater than 0.1 MPa, the shoot was discarded; for very dehydrated shoots, this range was extended to 0.3 MPa. The third leaf (typically the middle leaf) was used to determine K_{leaf} with the EFM. When dehydrated leaves are measured with the EFM, the stomata open (see *Results*); before steady state flow is achieved, the leaf may rehydrate such that Ψ_{final} is less negative than Ψ_o, or, alternatively, the leaf may further dehydrate such that Ψ_{final} is more negative than Ψ_o. For each species, at least six K_{leaf} values were obtained for each 0.5 MPa interval from full hydration to strong dehydration. Outlier tests were conducted for each 0.5 MPa interval (Dixon test; Sokal and Rohlf, 1995); 0-4 outliers were removed over the whole curve for given species (representing 0-8% of the 26-74 data points per curve).

To test the importance of method for constructing vulnerability curves, we determined these in three ways previously applied (Table S2.1). First, K_{leaf} was plotted against whichever

was lowest, Ψ_o or Ψ_{final} (= "Ψ_{lowest}"), i.e., the Ψ_{leaf} associated with the strongest dehydration experienced during the experiment, and each leaf was considered as a data point ("unbinned Ψ_{lowest}"). Additionally, K_{leaf} was plotted against Ψ_{lowest} with data averaged in 0.5 MPa bins ("binned Ψ_{lowest}"), with the exception of *H. annuus* averaged in 0.2 MPa bins because of its distinctively narrower K_{leaf} response, with negligible values below -1.5 MPa. Finally, K_{leaf} was plotted against Ψ_{final} rather than Ψ_{lowest} ("Ψ_{final}"), with each leaf considered as a data point. Determination of these alternative versions of the vulnerability curve also allowed interpretation of the recovery of K_{leaf} during the measurement (see section below).

In the above-described methods, as in previous studies of K_{leaf}, the pressure chamber balance pressure was taken as Ψ_{leaf}. In actuality, the balance pressure for an equilibrated leaf gives the xylem pressure potential (P_x), and - P_x is less negative than the bulk Ψ_{leaf} by the amount of the vein xylem solute potential (π_x, Tyree and Zimmermann, 2002). Notably, previous studies on a range of species have measured π_x values of approximately -0.05 MPa, a difference that would not affect our findings significantly (Boyer, 1967). We made tests to verify such low π_x for *C. sasanqua*, *H. arbutifolia* and *L. camara*. Shoots of four leaves were rehydrated overnight and dehydrated to a range of Ψ_{leaf} (-0.04 to -1.5 MPa). Two leaves were excised for initial Ψ_{leaf} measurement, a third was bagged for determination of initial π_x, and the fourth was placed in the EFM apparatus until a steady-state flow rate was achieved. Leaf vein π_x was determined using vapor pressure osmometry (Vapro 5520, Wescor Inc., UT). The leaf margin was excised to open the tips of the midrib and second-order veins, and the leaf was pressurized in the pressure chamber and xylem sap exuded from the petiole was collected onto a filter paper, while moist paper towels surrounded the chamber and petiole to minimize evaporation. The filter paper was transported to the osmometer in a weighing bottle filled with moist paper towel. All π_x values were less negative than the least negative measurable value with this instrument, -0.05

MPa, and thus indistinguishable from pure water in our instrument, indicating that our findings would not be significantly impacted by π_x.

Model testing and estimation of parameters for the decline of K_{leaf} with dehydration

Maximum likelihood was used to select the function for each species' K_{leaf} vulnerability response (Burnham and Anderson, 2002), using the *optim* function in R 2.9.2 (http://www.r-project.org; Burnham and Anderson, 2004; Sack et al., 2006; our scripts are available on request). A linear function ($K_{leaf} = a\,\Psi_{leaf} + y_o$), was tested, in addition to sigmoidal ($K_{leaf} = \frac{a}{1+e^{-\left(\frac{\Psi_{leaf}-x_0}{b}\right)}}$) and logistic functions ($K_{leaf} = a/(1+(\frac{\Psi_{leaf}}{x_0})^b)$) as used previously in the literature on leaf vulnerability (Table S2.1) and an exponential function ($K_{leaf} = y_0 + ae^{-b\Psi_{leaf}}$), as previously used for whole-plant vulnerability (Iovi *et al.*, 2009). The maximum likelihood parameters were determined by the Simulated Annealing procedure for global optimization, followed by the Nelder–Mead simplex procedure for local optimization; standard errors for parameters were generated from the Hessian matrix. For each data set, functions were compared using the Akaike Information Criterion (AIC), corrected for low *n*. The function with the lowest AIC value was chosen as the best fit function for that dataset, with differences > 2 considered as meaningful (Burnham and Anderson, 2002, 2004).

To compare species in their hydraulic parameters, and to determine correlations between hydraulic parameters and other leaf traits, values for the maximum K_{leaf} at full hydration (K_{max}) and the Ψ_{leaf} at which K_{leaf} had declined by 50% and 80% (P_{50} and P_{80}) were determined from the vulnerability curves. For these parameters, each species' maximum likelihood function was used—i.e., that with lowest Akaike Information Criterion (AIC) and highest r^2 determined from

the unbinned data plots ("unbinned Ψ_{lowest}" and "Ψ_{final}"). The steepness of the vulnerability curve was also determined, as the first derivative of the maximum likelihood function at Ψ_{leaf} = -0.5 MPa, where the steepest declines were observed. As an additional method for determining K_{max}, we calculated for each species the average K_{leaf} for points above -0.5 MPa; this was the method used in most previous leaf hydraulics studies that measured only K_{leaf} for hydrated leaves, and not its vulnerability to dehydration (e.g., Sack *et al.*, 2002; Brodribb and Holbrook, 2003b; Nardini *et al.*, 2005).

To determine the degree to which the choice of function and dataset matters, tests were made of the sensitivity of vulnerability curve parameters (K_{max}, P_{50} and P_{80}) to the choice of function, and, for each function, of plotting K_{leaf} against "unbinned Ψ_{lowest}", "binned Ψ_{lowest}" or "Ψ_{final}".

Hydraulic safety margins were calculated as the difference between the Ψ_{leaf} at which the leaves of a given species lose turgor (π_{TLP}; data from Scoffoni *et al.*, 2011) and those at which hydraulic function was substantially lost (P_{50} or P_{80}). Positive numbers indicate a safety margin, whereas negative numbers indicate a loss of hydraulic function even above the turgor loss point.

Testing the recovery of leaf hydraulic conductance after dehydration

Experiments were performed to test the recovery of K_{leaf} for leaves rehydrated after dehydration (method after Trifilo *et al.*, 2003a). For the 10 species, shoots were dehydrated with a fan to a known Ψ_{leaf} below their respective turgor loss points (determined as described in following section). Leaves from each shoot were excised in air using a fresh razor blade and measured for Ψ_{leaf} ($\Psi_{dehydration}$), and other leaves were excised under ultrapure water, and rehydrated 1 h with petiole under water in a beaker, covered with a dark plastic bag. Following rehydration, leaves were equilibrated in a plastic bag for at least 10 min and either had petioles cut in air and were

measured for Ψ_{leaf} ($\Psi_{rehydration}$), or had petioles re-cut under ultrapure water and were immediately connected to the EFM to determine K_{leaf} (n = 4-12 per species). The % recovery of K_{leaf} was determined as the K_{leaf} after rehydration divided by the K_{leaf} at $\Psi_{dehydration}$, which was estimated from the species' maximum likelihood vulnerability curve × 100%. The recovery was considered significant if the K_{leaf} after 1-h rehydration was greater than the K_{leaf} at $\Psi_{dehydration}$ (*t*-test; Minitab Release 15). The recovery was determined as complete if K_{leaf} after 1-h rehydration was not significantly lower than the K_{leaf} at $\Psi_{rehydration}$ which was estimated from the species' maximum likelihood vulnerability curve.

Testing for the recovery of leaf hydraulic conductance during EFM measurement

As in other methods for determining leaf hydraulic vulnerability (i.e., RKM and Heat-FM; see *Introduction*), the EFM partially rehydrates the dehydrated leaf, as the petiole is connected to water at atmospheric pressure. We developed two analyses to test for the potential recovery of K_{leaf} during the EFM measurement. The first analysis was a test of residual variation. If K_{leaf} recovered completely during the EFM measurement, one would expect no influence of the dehydration treatment prior to measurement on the final K_{leaf} value; rather, the measured K_{leaf} would simply relate to Ψ_{final}, i.e., the leaf water potential during the final steady state flow. Thus, for each species, from the maximum likelihood vulnerability curve for the "Ψ_{final}" plot, the residuals of K_{leaf} against Ψ_{final} were calculated. These residuals represented the variation in K_{leaf} unrelated to Ψ_{final}. A test was made for correlation of these residuals with Ψ_{lowest} values (Minitab Release 15). If the residual K_{leaf} variation was negatively correlated with Ψ_{lowest}, there was a persistent impact of Ψ_{lowest} on K_{leaf}, independently of Ψ_{final}. In other words, the effect of the dehydration treatment persisted even at the end of the EFM measurement, and thus, the K_{leaf} had not recovered completely during the measurement. The second analysis was the calculation of an

index of the recoverability of K_{leaf} during the EFM. For each species, a sample of the vulnerability data was selected that was analogous to the 1-h rehydration experiment (see previous section). Data were selected for leaves that had been dehydrated to a Ψ_{leaf} below turgor loss point but that had rehydrated during the EFM measurement to Ψ_{leaf} values similar to those for leaves measured by the EFM after the 1-h rehydration experiment (n = 4-7 for each species). The % recovery of K_{leaf} during EFM was determined as the average measured K_{leaf} for this leaf sample divided by the K_{leaf} at $\Psi_{dehydration}$, which was estimated from the species' maximum likelihood vulnerability curve × 100%. The significance of the recovery of K_{leaf} was tested as for leaves in the 1-h rehydration experiment.

Given that some species showed a partial recovery of K_{leaf} with rehydration during the EFM (see *Results*), a theoretical consideration was made of how K_{leaf} recovery during measurement should influence the calculation of vulnerability parameters. Based on the diversity of tissues in the leaf hydraulic pathway, the vulnerability of K_{leaf} is expected to involve several components, some of which might be recoverable on a short time scale, while others might be reversible after a longer time scale under low tension (cf. Brodribb and Holbrook, 2006; Scoffoni *et al.*, 2008). The most appropriate vulnerability plot would depend on the degree that leaves are recoverable in the short term (Fig. 2.1). Bounding cases were considered in which (a) leaves were non-recoverable in K_{leaf} during the measurement, (b) leaves were totally recoverable, and (c) leaves were partially recoverable. In case (a) in which K_{leaf} is non- recoverable, an accurate vulnerability curve would be obtained by plotting K_{leaf} against Ψ_{lowest}, as only the minimum Ψ_{leaf} during the whole experiment is important for influencing K_{leaf}. In case (a), plotting K_{leaf} against Ψ_{final} would overestimate the leaf's vulnerability. By contrast, in case (b) in which K_{leaf} recovers completely during measurement, an accurate vulnerability curve would be determined by plotting K_{leaf} against Ψ_{final}, because only the Ψ_{leaf} during steady-state at the end of the

measurement is important for influencing K_{leaf}. In case (b), plotting K_{leaf} against Ψ_{lowest} would underestimate the leaf's vulnerability. Finally, in case (c), in which K_{leaf} is partially recoverable, the accurate vulnerability curve would be intermediate between the plots of K_{leaf} against Ψ_{final} and against Ψ_{lowest}. Additional scenarios were not considered, e.g., if leaves recover in K_{leaf} differently depending on their degree of dehydration; notably, such scenarios should fall within the bounding cases considered. We tested whether the estimation of vulnerability parameters K_{max}, P_{50} and P_{80} was improved by using for each species the plot appropriate to its K_{leaf} recovery. Thus, for the species that showed no K_{leaf} recovery during EFM measurement, parameters were re-calculated from the maximum likelihood function for the "Ψ_{lowest} unbinned" plot, and for the species with partial recovery, parameters were averaged from those determined from the "Ψ_{final}" and "Ψ_{lowest} unbinned" plots. These re-calculated parameters were compared with those determined using the "Ψ_{lowest} unbinned" for all species, as has been the most typical procedure in previous studies (Table S2.1).

Statistical analysis of differences among species and trait correlations across species

Trait differences between moist and dry habitat species were tested using ANOVAs with species nested within habitat type, and using *t*-tests on species means (Table 2.1; Minitab Release 15). All data were log-transformed to improve normality and heteroscedasticity (Sokal and Rohlf, 1995). Correlations among traits were considered significant only if $P < 0.05$ for both Spearman and Pearson coefficients (r_s and r_p respectively); when relationships were non-linear, correlations for log-transformed data were determined. Standard major axes were fitted when determining slopes of relationships between traits, to account for error in both *x* and *y*-variables (using SMATR; Sokal and Rohlf, 1995; Warton *et al.*, 2006).

RESULTS

Vulnerability curves: species-differences in the response of K_{leaf} to dehydration

The evaporative flux method (EFM) was effective for determining vulnerability curves for leaves dehydrated from near full turgor to beyond turgor loss point (Fig. 2.2). Leaves that had been previously dehydrated opened their stomata and established steady state transpiration during the EFM measurement, as indicated by even the lowest transpiration rates observed representing stomatal conductance values 2.2- to 7.3-fold higher than cuticular conductance for these species (Table S2.2).

Species differed significantly in the shape of the leaf hydraulic vulnerability curves. For four species the linear function was selected by maximum likelihood for K_{leaf} plotted against "Ψ_{lowest} unbinned", and for six species a non-linear function was selected (Fig. 2.2; Table S2.3). The logistic function was selected for five species and the sigmoidal for *C. betuloides*. Species from dry habitats had a greater tendency to show a linear decline in K_{leaf} as one of their selected functions, i.e., within AIC of 2 of the maximum likelihood function (4/5 species vs 1/5 for moist habitats; $P = 0.018$; proportion test). The slope of the vulnerability curve at $\Psi_{leaf} = -0.5$ MPa varied from -10 to -0.5 mmol m^{-2} s^{-1} MPa^{-2}, and drought sensitive species had on average 3-fold steeper slopes than drought tolerant species (-6.5 vs. -1.6 mmol m^{-2} s^{-1} MPa^{-2} respectively; *t*-test; $P = 0.009$, $n = 5$).

Vulnerability curves: sensitivity of derived parameters to the choice of function and plot

The use of maximum likelihood to select the vulnerability function for each species based on plots of K_{leaf} against "Ψ_{lowest} unbinned" was considered to be the most appropriate practice, and was the one used for interpretation and comparison among species. However, because many previous studies have applied a single function and plot to all species' data, we tested the

sensitivity of the derived vulnerability parameters to the choice of function and plot and whether such choices affected the resolution of species-ranking in vulnerability. Notably, the functions selected by maximum likelihood with AIC values within 2 of the minimum depended on the choice of plot, and multiple functions were often selected for given species (Fig. 2.2, Table S2.3). Thus, when using the "Ψ_{lowest} binned" plot, the linear function was selected for 8/10 species, the logistic for two and the exponential for one species. By contrast, when using the "Ψ_{lowest} unbinned" plot, the logistic function was selected for eight species, the sigmoidal for six, the linear for five and the exponential for four. When using the "Ψ_{final}" plot, the logistic was selected for nine species, the exponential for eight, the sigmoidal for five and the linear for two. The best fit function selected using the "Ψ_{lowest} unbinned" plot was one of those selected when using the "Ψ_{lowest} binned" dataset for 5/10 species, and when using the "Ψ_{final}" plot for only 3/10 species.

The estimation of vulnerability parameters K_{max}, P_{50} and P_{80}, was sensitive to the function and the plot used, but typically the values determined in different ways were correlated across species (Fig. 2.2, data in Table S2.4). When using the "Ψ_{lowest} unbinned" plot, the K_{max}, P_{50} and P_{80} values generated by the four different functions, averaged across species, varied by 12-27%, 0.21-0.76 MPa and 0.12-0.74 MPa respectively, and correlated across species in 15/18 comparisons (r_p= 0.81-0.99; $P < 0.05$). The use of the three plots produced K_{max} values from the four given functions that varied on average by 3-40%, and correlated across species in 11/12 comparisons (r_p= 0.64-0.99; $P < 0.05$; Fig. 2.2). Notably, for a species such as *Platanus*, with a steep initial hydraulic decline, determining K_{max} from a "Ψ_{lowest} unbinned" plot was critical to resolve its high K_{max}. For P_{50} and P_{80}, the use of the "Ψ_{lowest} unbinned" and "Ψ_{lowest} binned" plots produced values for given functions that differed on average by 0.08-0.6 MPa, and correlated across species in 7/8 comparisons (r_p= 0.56-0.99; $P < 0.05$). By contrast, the use of the "Ψ_{final}"

plot produced P_{50} and P_{80} values 0.8-2 MPa less negative than when using the other plots (Fig. 2.2; paired *t*-test; $P < 0.05$), and values were not correlated across species (r_p= -0.40 to 0.48; P = 0.11-0.81). The values of K_{max} determined using the function selected using the "Ψ_{lowest} unbinned" or "Ψ_{lowest} binned" plots did not differ on average across species from those determined by taking the mean of K_{leaf} values at Ψ_{leaf} of 0 to -0.5 MPa (data in Table S2.5; P = 0.10-0.15; paired *t*-test). However, K_{max} determined using the "Ψ_{final}" plot was on average 44% higher than K_{max} determined by taking the mean of K_{leaf} values at Ψ_{leaf} of 0 to -0.5 MPa (P = 0.02), but again the species' values with the two methods were correlated (r_p = 0.74; $P < 0.01$).

Species variation in maximum K_{leaf} and vulnerability, and lack of an efficiency-safety trade-off

Species were compared in the parameters determined from their maximum likelihood functions using the "Ψ_{lowest} unbinned" plot (Table 2.2). Species differed by more than 11-fold in K_{max}, with no average differences between species from moist and dry habitats, though species-differences were significant considering K_{max} as the mean of K_{leaf} values at Ψ_{leaf} of 0 to -0.5 MPa (ANOVA; $P < 0.001$). Species also differed strongly in their vulnerabilities, varying 32-fold in P_{50} and 15-fold in P_{80}, from the most vulnerable species (*H. annuus* and *P. racemosa*) with values less than -1 MPa to the least vulnerable species, *C. diversifolia*, with P_{50} and P_{80} values of -3.54 and -5.25 MPa respectively (Fig. 2.2). Species' P_{50} and P_{80} values were strongly correlated (r_p and r_s = 0.88-0.96, $P < 0.01$). Species with greater vulnerability (i.e., with less negative P_{50} and P_{80} values) had steeper vulnerability curve slopes (r_p and r_s = -0.72 to -0.83, $P < 0.01$; data in Table S2.5). On average, species from dry habitats had 2.4 to 2.9-fold more negative P_{50} and P_{80} than species from moist habitats.

Species with lower vulnerability had greater hydraulic safety margins. Thus, safety margins based on P_{50} were negatively correlated with P_{50}, and safety margins based on P_{80} were

negatively correlated with both P_{50} and P_{80} (r_p and r_s =- 0.70 to -0.95; $P < 0.05$; data in Table S2.5). Safety margins based on P_{50} ranged from -1.9 to 0.17 MPa and were positive for two species (*C. diversifolia* and *H. arbutifolia*); thus, most species lost leaf turgor at lower Ψ_{leaf} than P_{50} as determined using the steady-state method. However, safety margins calculated from P_{80} ranged from -1.7 to 2.7 MPa, and 7 species had positive safety margins. Safety margins did not differ between habitat types (*t*-test, $P < 0.05$).

Both P_{50} and P_{80} were independent of K_{max} across species ($|r_p|$ and $|r_s|$ = 0.37-0.62, $P > 0.05$).

Recovery of K_{leaf} with leaf rehydration and a new importance for leaf hydraulic vulnerability

Species varied strongly in the ability to recover in K_{leaf} after dehydration below their turgor loss point (such that K_{leaf} declined by 57-97% depending on species) followed by 1-h rehydration with petiole under water (Fig. 2.3). For four species (*C. diversifolia*, *H. annuus*, *L. camara*, and *M. grandiflora*), , K_{leaf} increased 2.2 to 2.8-fold (Fig. 2.3; $P < 0.05$); *C. diversifolia* and *M. grandiflora* recovered fully in K_{leaf} to their expected values. Three of these species were moist-habitat species (*L. camara*, *H. annuus* and *M. grandiflora*) and one was a dry-habitat species (*C. diversifolia*). The six other species showed no significant recovery. The % of recovery of K_{leaf} after rehydration did not correlate with K_{max}, P_{50} or P_{80} ($P > 0.05$; data in Table S2.5).

For the six species that did not recover in K_{leaf} with 1-h rehydration, a nearly perfect correlation was found of the ability to maintain K_{leaf} after dehydration and rehydration episodes and low P_{50} and P_{80} (r_s and r_p = -0.94 to -0.98; $P < 0.005$; Fig. 2.4). Thus, among the species that did not recover in K_{leaf} with rehydration, a low vulnerability predicted the ability to retain hydraulic capacity despite strong, short-term dynamics in water status.

Testing K_{leaf} recovery during EFM, and its impact on the estimation of hydraulic parameters

No species showed full recovery in K_{leaf} of dehydrated leaves during EFM measurements; for all species there was a persistent impact of dehydration. When the residuals of K_{leaf} against Ψ_{final} were plotted against Ψ_{lowest} (see *Methods*), this correlation was significant for seven species (r_p = -0.49 to -0.79; n = 25-74; $P < 0.05$; Table 2.3). For the other three species (*C. sasanqua, H. annuus* and *H. canariensis*) the lack of significant correlation of residuals with Ψ_{lowest} did not imply a complete recovery of K_{leaf} during EFM measurement. In the case of *H. annuus* and *H. canariensis*, the Ψ_{lowest} values were typically the Ψ_{final} values because the leaves dehydrated further during measurement, rather than recovering in Ψ_{leaf}, and in the case of *C. sasanqua*, because the Ψ_{lowest} correlated with Ψ_{final} (r_p = 0.53; $P < 0.001$) there may not have been sufficient residual variation for a powerful test. There were broadly consistent results in the second analysis of the recovery of K_{leaf} during the EFM measurement, i.e., the calculation of the % recovery of K_{leaf} for leaves that rehydrated over the same Ψ_{leaf} interval as the 1-h rehydration experiment. Again there was no evidence for total recovery of K_{leaf}. There was a significant partial recovery of K_{leaf} in 3/10 species ($P < 0.007$; Table 2.3), with K_{leaf} increasing by 158-178%. Across species, the recovery of K_{leaf} during the EFM was positively correlated with that observed after 1-h rehydration (r_p and r_s = 0.83-0.84; $P < 0.05$). The % recovery of K_{leaf} during the EFM was 13% lower on average than that after 1-h rehydration, consistent with the leaf rehydrating a shorter period of time, under subatmospheric pressure (paired t-test; P = 0.04).

Given that three species indicated partial K_{leaf} recovery during EFM measurement, an analysis was made of its potential influence on derived vulnerability parameters (see *Methods*). Re-calculating these species' K_{max}, P_{50} and P_{80} values while considering the partial K_{leaf} recovery produced values that were correlated with those determined using both the "Ψ_{lowest} unbinned" and "Ψ_{lowest} binned" plots (r_s and r_p = 0.57-0.99; $P < 0.001$ to 0.09), indicating that species

comparisons using those vulnerability plots are robust even despite partial K_{leaf} recovery. However, the re-calculated parameters accounting for partial recovery did not correlate with those determined using the "Ψ_{final}" plot (r_s and r_p = 0.08-0.30; P = 0.16-0.83).

DISCUSSION

The new steady-state evaporative flux method developed for determining the hydraulic vulnerability of leaves acclimated to high irradiance allowed an independent confirmation and extension of key relationships first shown using rehydration methods. Additionally, refined statistical methods for analyzing vulnerability data allowed fitting the appropriate function for each species and considering the effect of recovery during the measurement. These approaches showed novel variation among species in leaf vulnerability, and relationships with species' habitat. Further, rehydration experiments quantifying the rapid recovery of K_{leaf} after dehydration indicated novel species variation, and a new role for leaf vulnerability in determining function after episodes of dehydration and rehydration. This work provided new insights into the vulnerability response, and will additionally enable higher resolution in future work investigating the underlying mechanisms for leaf hydraulic vulnerability.

Species' differences in K_{leaf} decline and potential mechanisms

Species differed strikingly in their vulnerability parameters P_{50} and P_{80}, and in the shape of their vulnerability curves. Notably, because species varied strongly in initial K_{leaf} values (K_{max}) and in the steepness of their decline in K_{leaf}, P_{80} was useful to allow comparison of species' vulnerabilities at a similar stage of their trajectory, i.e., after the steepest decline phase (Fig. 2.2), whereas P_{50} values often occurred in the middle of the steepest decline, which for some species occurred at very high Ψ_{leaf}. For such species the P_{50} may not be an effective index of drought

resistance. Further, we note that several species (e.g., *Platanus racemosa*) had very high K_{max}, with substantial K_{leaf} decline before Ψ_{leaf} reached -0.5 MPa. Though part of the true range of leaf hydraulic behavior in such species, such very high K_{leaf} values are outside of the range found in nature, as they would not occur for leaves transpiring *in vivo*, in which the soil and plant hydraulic resistance would cause a further Ψ_{leaf} drop not experienced by leaves in the EFM. Species with such steep, non-linear decline were typical of moist habitat species whereas species with shallow, linear declines were associated with dry habitats.

The K_{leaf} decline during dehydration arises due to loss of hydraulic conductance in the petiole and/or vein xylem, and/or the extra-xylem pathways (Table 2.1). The importance of (1) cavitation due to air seeding in major veins leading to subsequent embolism was supported by studies showing ultra-acoustic emissions that may reflect cavitation events (Kikuta et al., 1997; Salleo et al., 2000; Johnson et al., 2009a), as well as dye and cryo-scanning electron microscope studies showing embolism in vein xylem (Salleo *et al.*, 2001; Nardini *et al.*, 2003; Nardini *et al.*, 2008; Johnson *et al.*, 2009a), measurement of relatively low air-seedling pressures in the leaf petiole and midrib (Choat *et al.*, 2005), and a correlation across species of hydraulic vulnerability with low major vein length per leaf area, as such leaves have less xylem redundancy to protect from the impact of embolism (Scoffoni *et al.*, 2011). Another mechanism may be (2) the collapse of xylem conduits in the leaf veins; indeed xylem cell collapse has been found for tracheids in the vein of pine needles and in the transfusion tissue of a tropical conifer, at Ψ_{leaf} values as high as -1.5 MPa, in advance of cavitation (Cochard *et al.*, 2004; Brodribb and Holbrook, 2005). Indeed, xylem cell collapse has been hypothesized to occur in the minor vein xylem in angiosperms too, but not yet visualized directly (Blackman *et al.*, 2010). Additionally, K_{leaf} decline might relate to (3) the loss of turgor in living cells in the extra-xylem flow pathways (Brodribb and Holbrook, 2006) in particular the cells of the bundle sheath, mesophyll and

epidermis, which may shrink with walls retracting, and/or may undergo plasmolysis. Tissues with low solute potential, such as bundle sheath, might lose turgor in advance of the mesophyll (Giles *et al.*, 1974; Palta and Leestadelmann, 1983; Nonami and Schulze, 1989; Canny and Huang, 2006). Such changes in cell volume and turgor may alter the flow pathways, and additionally reduce membrane permeability, e.g., via deactivation of aquaporins (Kim and Steudle, 2007). A final mechanism for the K_{leaf} decline especially in well-hydrated leaves is (4) the evaporation of liquid water in the cells walls during transpiration, leaving walls moist but with empty pores and thus lower permeability (Kim and Steudle, 2007; Lee *et al.*, 2009; Voicu *et al.*, 2009).

The shapes of functions fitted to K_{leaf} data from our study using maximum likelihood provide several key insights and hypotheses for the action of these mechanisms and point to a diversity in specific impacts across species. Given that embolism or collapse of vein xylem conduits is a principal driver of the K_{leaf} decline, the linear decline observed for four species implies that air seeding or collapse begins at high Ψ_{leaf} for these species (see references in Table 2.1). The linear decline also implies that conduits of different sizes tend to have approximately equal distributions of air seeding pressures and tendencies to collapse, and/or that a high major vein density provides redundancy that protects the leaf from a disproportionate effect of cavitation of the major vein xylem. A linear decline of K_{leaf} would also be consistent with a direct role for loss in mesophyll, epidermis or bundle sheath cell volume or turgor, or the number of water pathways through cell walls declining approximately linearly with Ψ_{leaf} above turgor loss point (Table 2.1). The logistic decline observed in five species and sigmoidal decline in *C. betuloides* indicate a qualitative difference. Given that xylem cavitation and/or collapse play a principal role, for these species the steep decline at high Ψ_{leaf} that slows with ongoing dehydration are consistent with an unequal distribution of air seeding pressures, e.g., the larger

vessels that confer the bulk of vein xylem conductivity cavitating and/or collapsing first, and smaller vessels having lower air seeding pressures or wall strength and losing function at lower Ψ_{leaf} (Table 2.1). A disproportionate decline at high Ψ_{leaf} could also relate to species having low major vein densities and thus that embolism occurring early in these veins leading to substantial declines in K_{leaf} (Table 2.1). If losses in cell permeability are important, the disproportionate decline at high Ψ_{leaf} could relate to a strong sensitivity of K_{leaf} to losses in volume in particular cells, with low solute potential, e.g, bundle sheath cells, that may shrink at high Ψ_{leaf} and/or undergo aquaporin deactivation (Table 2.1). If losses of cell wall pathways contribute to the loss of K_{leaf}, a disproportionate decline at high Ψ_{leaf} would be consistent with the cell walls behaving as observed for other porous media that show non-linear declines in conductivity with declining water potential, e.g., soil (Laio *et al.*, 2001). The species-variation in vulnerability curves points to the critical importance of research to disentangle the specific mechanisms of K_{leaf} decline for given species. Notably, previous work has shown species variation in partitioning of hydraulic resistance between petiole and lamina, and among vein orders, and between the vein xylem and extra-xylem pathways (Trifilo *et al.*, 2003b; Sack *et al.*, 2004; Sack *et al.*, 2005). These species differences would also result in variation in the important mechanisms underlying sensitivity to hydraulic decline because K_{leaf} would be most sensitive to declines in conductance in the component that accounted for the greatest part of the leaf resistance (Scoffoni *et al.*, 2011).

In this study we focused on the response of K_{leaf} to dehydration under high irradiance. We note that many species show an increase of K_{leaf} under high irradiance, and this response may interact with the response to dehydration (Kim and Steudle, 2007; Lee *et al.*, 2009; Voicu *et al.*, 2009). The decline of conductance under low irradiance occurs in the extra-xylem tissues (Nardini *et al.*, 2005); thus, under low irradiance, the extra-xylem tissues would account for a greater proportion of leaf resistance, and cavitation or collapse of vein xylem would have a lesser

impact on K_{leaf}, and any reduction in the permeability of extra-xylem tissues due to dehydration would have a stronger impact (Nardini *et al.*, 2005; Scoffoni *et al.*, 2008; Voicu *et al.*, 2008). The interaction of the light and dehydration responses of K_{leaf} is an important area for future investigation.

Quantifying the vulnerability of K_{leaf}: importance and limitations of the steady state method

Since it is not yet possible to directly determine K_{leaf} across a full range of Ψ_{leaf} in *vivo*, hydraulic methods have been applied to excised leaves. The EFM is the latest of several approaches to measuring K_{leaf} vulnerability on excised leaves. These methods have advantages over indirect methods, such as the *audio method*, which registers amplified ultrasonic acoustic emissions within drying plant tissue, hypothesized to arise from cavitation (UAE; Milburn and Johnson, 1966; Tyree and Dixon, 1983, 1986; Kikuta et al., 1997; Johnson *et al.*, 2009a), or *visual methods* using dye or cryo-scanning electron microscopy that directly demonstrate embolism in dehydrated leaves (Salleo *et al.*, 2000; Salleo *et al.*, 2001), and collapse of conduits in dehydrated conifer leaves (Cochard et al., 2004; Brodribb and Holbrook, 2005), because these methods do not provide information of possible extra-xylem decline, or directly measure hydraulic vulnerability. Hydraulic methods applied to excised leaves include, in addition to the EFM, the high pressure flowmeter (Nardini et al., 2001), the vacuum pump method (Lo Gullo et al., 2003), and the rehydration kinetics method (RKM), most frequently used for determining leaf hydraulic vulnerability, which estimates K_{leaf} from the uptake of water during rehydration by analogy to the charging of a capacitor in series with a resistor (RKM; Brodribb and Holbrook, 2003a, 2004a, b, 2006; Woodruff *et al.*, 2007; Hao *et al.*, 2008; Woodruff *et al.*, 2008; Blackman *et al.*, 2009; Brodribb and Cochard, 2009; Johnson *et al.*, 2009a; Johnson *et al.*, 2009b; Saha *et al.*, 2009; Blackman and Brodribb, 2011). As described in the *Introduction*, these methods all

have merits and disadvantages. The steady state EFM is independent of the RKM, and here confirmed and extended key findings.

Several limitations of the EFM applied to excised leaves equally apply to the other methods for leaf vulnerability. These methods cannot assess the decline of K_{leaf} and Ψ_{leaf} that occurs *in vivo*, when xylem water is under tension, and leaf cells are equilibrated at very low water potentials; the xylem cells may be collapsed, leaf cells shrunken, and aquaporins inactivated (Cochard et al., 2002; Cochard et al., 2004; Brodribb and Holbrook, 2005, 2006; Canny and Huang, 2006). Excising the leaf under water relieves the tension, and some of these effects might be reversed rapidly. Discovery of such effects would require new *in vivo* methods for measuring K_{leaf} decline. In the meantime, vulnerability measured on excised leaves must be considered as conservative, because these methods measure only the K_{leaf} decline that is *not* instantly recoverable, e.g., embolism in veins, which may require many minutes to hours of low tension and active processes to recover (Tyree and Zimmermann, 2002; Bucci *et al.*, 2003; Trifilo *et al.*, 2003a), and persistent effects on living tissues. Further, all the methods may be affected by recovery of K_{leaf} with rehydration during the measurement itself, but the analysis in this study showed that comparative estimates of hydraulic vulnerability remained robust despite such recovery.

Linkage of vulnerability with drought sensitivity

Species of dry habitats had lower vulnerability (i.e., lower P_{50} and P_{80}) than species of moist habitat. This finding was consistent with that of a study of Australian species using the RKM (Blackman *et al.*, 2010), here extended with the steady state method to a set of species very diverse in drought tolerance. This study also confirmed no trade-off across species between K_{max} and hydraulic vulnerability, as previously reported using RKM (Blackman *et al.*, 2010) and in a

meta-analysis combining data collected with different methods (Sack and Holbrook, 2006), a relationship frequently found for stems (Tyree and Zimmermann, 2002; Maherali *et al.*, 2004; Meinzer et al., 2010). Notably, species from dry and moist habitats did not differ on average in their K_{max}. This finding is consistent with multiple types of adaptation to drought. Some drought-tolerant species use water sparingly via low maximum rates of gas exchange, consistent with low K_{max}, while others conduct rapid gas exchange when water is available, consistent with high K_{max}, and then "gear-down" during shortage, (Maximov, 1931; Grubb, 1998), as illustrated by species such as *H. arbutifolia* (maximum photosynthetic rate of 14 μmol CO_2 m^{-2} s^{-1}; Valladares and Pearcy, 1997).

We also found that across species P_{50} and P_{80} were strongly correlated with bulk leaf turgor loss point (π_{TLP}) and osmotic potential (Scoffoni *et al.*, 2011 ; Fig. 2.5). This finding confirmed and extended the correlation previously reported between P_{50} and π_{TLP} for 19 species using the RKM (Blackman *et al.*, 2010). A low π_{TLP} might confer resistance to K_{leaf} decline directly, if it allows cells to preserve turgor and maintain their structural integrity at lower bulk Ψ_{leaf} (Blackman *et al.*, 2010). Previous work has demonstrated the heterogeneity of solute potential and across lamina locations and tissues (Slavik, 1959; Nonami and Schulze, 1989; Koroleva *et al.*, 1997; Koroleva *et al.*, 2002), and the correlation with vulnerability might be even stronger with the turgor loss point of individual tissues important in the water flow pathways, e.g., the bundle sheath, rather than for the bulk leaf.

One consequence of the correlation of vulnerability and π_{TLP} is a mechanism for inducing protective stomatal closure in drought sensitive species (Brodribb and Cochard, 2009; Hao et al., 2010). The narrow safety margins found in this study were consistent with past studies showing angiosperms often operating at close to cavitation thresholds (Lo Gullo *et al.*, 2003; Brodribb and Holbrook, 2004a, b) in contrast with conifers and ferns which can have wide safety margins

(Brodribb and Holbrook, 2004b). Declines in K_{leaf} accelerate further declines in Ψ_{leaf} at a given transpiration rate, and guard cells lose turgor against the background of epidermal cell pressure (Franks and Farquhar, 1999; Damour *et al.*, 2010). After that point, cuticular water loss would lead to slower declines of Ψ_{leaf} and of K_{leaf} (Pasquet-Kok *et al.*, 2010). By contrast, in species with low hydraulic vulnerability, the maintenance of K_{leaf} would allow stomata to remain open without desiccating the mesophyll during diurnal water stress or soil drought (Brodribb and Holbrook, 2003a). This contribution of K_{leaf} sensitivity to stomatal control is important in whole-plant drought tolerance (Brodribb and Cochard, 2009; Blackman *et al.*, 2010).

Species differences in K_{leaf} recovery and a new importance of resistance to K_{leaf} decline

We found a strong, novel variation across species in the ability of dehydrated leaves to recover rapidly in K_{leaf} with 1-h of rehydration. Six species showed no recovery and four increased in K_{leaf} by 2.5- to 2.8-fold. This study thus partially confirmed one previous report of a complete recovery for sunflower (Trifilo *et al.*, 2003a). Typically K_{leaf} did not fully recover after 1-h rehydration, indicating a partial irreversibility consistent with embolisms that require refilling, or losses of cell permeability that might require energy transduction for recovery (Bucci et al., 2003).

Our data on vulnerability and recovery highlighted a new importance for leaf hydraulics in determining performance with changing plant water status. A recent meta-analysis of data for 31 species found that at minimum daily Ψ_{leaf}, species varied strongly in their K_{leaf} decline, with roughly half the species being below P_{50} (Johnson *et al.*, 2009b). Our study showed that among species that did not recover rapidly in K_{leaf} with rehydration, a low hydraulic vulnerability conferred the ability to maintain K_{leaf} at a high value through both dehydration and rehydration. Species resistant to hydraulic decline could thus maintain K_{leaf} at high levels despite transient but

severe dynamics in Ψ_{leaf}, and gain a benefit in maintaining performance during diurnal water stress or soil drought. These findings are consistent with the correlation of low leaf hydraulic vulnerability and the ability of severly droughted plants to recover in transpiration after rewatering (Blackman *et al.*, 2009; Brodribb and Cochard, 2009). Tests are needed of the degree that rapid leaf hydraulic recovery as shown in this study contributes to whole plant hydraulic recovery and tolerance of dynamic water regimes.

ACKNOWLEDGMENTS

We thank M. Bartlett, W. Dang, A. Gibson, P. Rundel and Y. Taniguchi for logistical assistance, and T. Brodribb for discussion. This research was supported by UCLA Department of Ecology and Evolutionary Biology, a UCLA Vavra Research Fellowship and by National Science Foundation Grant #0546784.

Table 2.1. Mechanisms that would theoretically influence the shape of the response of leaf hydraulic conductance (K_{leaf}) to dehydration (i.e., decreasing leaf water potential, Ψ_{leaf}) and thus the function that best fitted to the data. A linear decline implies no threshold Ψ_{leaf} before which K_{leaf} declines (i.e., K_{leaf} declines immediately as Ψ_{leaf} declines), and also a proportional decline of K_{leaf} with Ψ_{leaf}. A non-linear decline of K_{leaf} with Ψ_{leaf} can include a threshold Ψ_{leaf} before the decline begins and/or a disproportionate decline of K_{leaf} as Ψ_{leaf} declines. For these possibilities we included three types of mechanisms—those relating to air seeding causing cavitation in the xylem conduits (and analogous effects would occur given collapse of xylem conduit walls), those arising from venation architecture, and those arising in the pathways outside the xylem. References are provided to studies of these potential mechanisms *per se* and/or on their influence on the shape of stem or leaf vulnerability curves.

Shape of K_{leaf} decline	**Air seeding**	**Venation architecture**	**Pathways outside the xylem**
Linear decline:			
No threshold before decline	• If air seeding begins at high Ψ_{leaf} because of large pit membrane pore size (Neufeld *et al.*, 1992 Pammenter and Vander Willigen, 1998)		• If a loss of membrane permeability (e.g., due to aquaporin activity or loss of cell turgor) begins immediately as Ψ_{leaf} declines (Brodribb and Holbrook, 2006)
Proportional decline of K_{leaf} with declining Ψ_{leaf}	• If conduits of different sizes all have a wide range in maximum pit membrane pore size such that cavitation occurs equally across conduit sizes (Pammenter and Vander Willigen, 1998; Choat *et al.*, 2005)	• If higher major vein length/area (=vein density) confers hydraulic redundancy, such that first embolisms of the vein xylem conduits do not cause a dramatic decline (Scoffoni *et al.*, 2011)	• If membrane permeability declines linearly as the average cell tugor declines with Ψ_{leaf} (Kubiske and Abrams, 1990; Brodribb and Holbrook, 2006) • If the K_{leaf} declines due to loss of water-filled pathways through cell walls as cells dehydrate (Pieruschka *et al.*, 2010)
Non-linear decline (logistic, sigmoidal, exponential):			
Threshold before decline	• If a threshold for air-seeding determined by the largest pit membrane pore size leads to a retention of K_{leaf} until a Ψ_{leaf} threshold (Neufeld *et al.*, 1992; Pammenter and Vander Willigen, 1998; Domec *et al.*, 2006)		• If there is a threshold Ψ_{leaf} below which aquaporins are deactivated and membrane permability declines (North and Nobel, 2000; Miyazawa *et al.*, 2008) • If the K_{leaf} is insensitive to turgor or turgor is maintained by osmotic adjustment until a cavitation threshold is reached (Brodribb and Holbrook, 2006).
Disproportionate decline of K_{leaf} with declining Ψ_{leaf}	• If larger conduits conferring the bulk of the vein xylem conductivity have larger pit membrane pores or greater pore numbers, and cavitate first, followed by smaller conduits that have decreasing impact on K_{leaf} (Neufeld *et al.*, 1992; Pammenter and Vander Willigen, 1998; Tyree and Zimmermann, 2002)	• If leaves with lower major vein density suffer strong decline in K_{leaf} with first embolism of xylem conduits in the low-order veins (Scoffoni *et al.*, 2011)	• If strong declines due to aquaporin deactivation occur at high Ψ_{leaf} (Johansson *et al.*, 1998; Kim and Steudle, 2007; Scoffoni *et al.*, 2008) • If a greater loss of turgor in cells with relatively weak solute potential (e.g., bundle sheath cells) during leaf dehydration lead to especially rapid decline in K_{leaf} (Nonami and Schulze, 1989; Koroleva *et al.*, 1997)

Table 2.2. Study species, family, native range, and mean values ± standard error for pressure volume curve parameters and leaf hydraulic vulnerability parameters, i.e., leaf hydraulic conductance at full hydration (K_{max}), leaf water potential at 50% and 80% decline of leaf hydraulic conductance (P_{50} and P_{80}), calculated from the maximum likelihood function for the "Ψ_{lowest} unbinned" plot, and results of *t*-tests on species' means (for hydraulics parameters) and of analyses of variance for the difference between moist and dry area species, and among species nested within those categories (for pressure volume parameters).$^{NS}P > 0.05$; $*P < 0.025$;$***P < 0.001$. †Croat, 1978; Kitamura and Murata, 1979; eFloras, 2008

Species	Family	Native range†	K_{max} (mmol m^{-2} s^{-1} MPa^{-1})	P_{50} (-MPa)	P_{80} (-MPa)	Turgor loss point (-MPa)	Osmotic Potential (-MPa)	Modulus of elasticity (MPa)	Saturated water content ($g.g^{-1}$)
Dry habitat species :									
Cercocarpus betuloides	Rosaceae	California. Mexico	4.36	2.76	5.25	2.59 ± 0.03	1.64 ± 0.04	10.1 ± 0.701	0.79 ± 0.02
Comarostaphylis diversifolia	Ericaceae	California. Mexico	2.96	2.85	4.56	3.45 ± 0.34	2.51 ± 0.34	17.3 ± 2.23	0.70 ± 0.01
Hedera canariensis	Araliacaeae	Canary Islands	5.73	0.64	1.18	1.98 ± 0.09	1.49 ± 0.07	17.9 ± 1.28	2.81 ± 0.09
Heteromeles arbutifolia	Rosaceae	California. Mexico	20.7	2.57	4.12	2.53 ± 0.10	2.08 ± 0.10	16.4 ± 0.486	1.38 ± 0.07
Quercus agrifolia	Fagaceae	California. Mexico	3.96	2.40	3.83	3.00 ± 0.12	2.31 ± 0.12	12.8 ± 0.787	0.93 ± 0.01
Moist habitat species :									
Camellia sasanqua	Theaceae	Japan	5.99	1.78	2.84	2.12 ± 0.18	1.61 ± 0.04	7.98 ± 1.11	1.74 ± 0.03
Helianthus annuus	Asteraceae	Across N. America	6.45	0.83	1.16	1.09 ± 0.12	0.875 ± 0.10	13.3 ± 1.31	11.2 ± 0.79
Lantana camara	Verbenaceae	Pantropical	11.4	0.80	1.41	1.37 ± 0.04	1.10 ± 0.04	9.14 ± 0.525	2.73 ± 0.15
Magnolia grandiflora	Magnoliaceae	Southern U.S.	5.24	0.42	2.06	2.06 ± 0.05	1.43 ± 0.34	5.49 ± 0.792	1.50 ± 0.07
Platanus racemosa	Platanaceae	California, Mexico	34.12	0.09	0.35	2.03 ± 0.06	1.54 ± 0.12	4.85 ± 0.331	1.34 ± 0.03
Average ± SE	Dry habitat species		7.55 ± 3.32	2.24 ± 0.41	3.79 ± 0.69	2.71 ± 0.14	2.01 ± 0.19	14.9 ± 1.49	1.32 ±0.04
	Moist habitat species		12.64 ± 5.48	0.78 ± 0.28	1.56 ± 0.42	1.74 ± 0.09	1.31 ± 0.14	8.16 ± 1.51	3.71 ±0.21
ANOVA	Dry /moist		^{NS}	*	*	***	***	***	***
	Species					***	***	***	***

Table 2.3. Results from the tests of the recovery of leaf hydraulic conductance (K_{leaf}) during the evaporative flux method (EFM), and during *1*-hour rehydration in the dark. (*P < 0.05; **P < 0.01; ***P < 0.001). In the Residual test for recovery during the EFM, significance indicates that K_{leaf} did not fully recover. For the indices of K_{leaf} recovery during the EFM, and during the 1-hour rehydration experiments, significance before the comma indicates some degree of significant recovery, and significance after the comma indicates that K_{leaf} did not recover fully (see *Methods*).

Species	Residual test for recovery during EFM	Index of recovery in K_{leaf} during EFM	Index of recovery in K_{leaf} after 1-hour rehydration
	R^2 (n)	(% Increase)	(% Increase)
Camellia sasanqua	0.029^{NS}(41)	114^{NS,} **	58.9^{NS}, ***
Cercocarpus betuloides	0.48***(70)	119^{NS}, **	119^{NS}, **
Comarostaphylos diversifolia	0.33***(57)	178**, *	259***, ^{NS}
Hedera canariensis	0.036^{NS}(41)	159**, **	150^{NS}, ***
Helianthus annuus	0.017^{NS}(36)	124^{NS}, *	230**, *
Heteromeles arbutifolia	0.62***(58)	66.4^{NS}, *	79.3^{NS}, *
Lantana camara	0.61***(25)	161^{NS}, **	284**, **
Magnolia grandiflora	0.24* (74)	158**, ***	218*, ^{NS}
Platanus racemosa	0.35***(38)	104^{NS}, *	130^{NS}, *
Quercus agrifolia	0.38***(46)	72.2^{NS}, **	113^{NS}, ***

FIGURE CAPTIONS

Figure 2.1. A theoretical framework for the construction of vulnerability curves according to the degree that leaves recover in leaf hydraulic conductance (K_{leaf}) with rehydration. The black line is the "true" vulnerability curve, the grey line is the vulnerability curve plotting K_{leaf} against "Ψ_{lowest}", and the grey dotted line is the vulnerability curve plotting K_{leaf} against "Ψ_{final}". Bounding cases were considered: (a) leaves were non-recoverable in their K_{leaf} during the measurement, (b) leaves were totally recoverable in their K_{leaf} and (c) leaves were partially recoverable in their K_{leaf} (see *Methods*).

Figure 2.2. Vulnerability curves for leaf hydraulic conductance (K_{leaf}) for 10 species varying widely in drought tolerance, determined using the evaporative flux method using three different plots ("Ψ_{lowest} unbinned", "Ψ_{lowest} binned" and "Ψ_{final}"). For the "Ψ_{lowest} unbinned" and "Ψ_{final}" panels, each point represents a different leaf measured. Standard errors are represented for each bin point in the "Ψ_{lowest} binned" plot. The lines plotted are the maximum likelihood functions using each plot for each species (Table S2.3).

Figure 2.3. Recovery of leaf hydraulic conductance (K_{leaf}) after 1-hour rehydration with petiole under water, for 10 species varying widely in drought tolerance. The grey curves are the best-fit functions of the species' response to dehydration from Fig. 2; open and filled symbols represent the predicted K_{leaf} at the dehydrated leaf water potential, and K_{leaf} after *1*-hour rehydration respectively; stars on the *x*-axis represent the turgor loss point. Species depicted in the upper four panels showed significant recovery in K_{leaf} (*P = 0.04; **P = 0.001; ***P < 0.001); only *C. diversifolia* and *M. grandiflora* showed total recovery. Species depicted in the lower panels showed no significant recovery in K_{leaf}.

Figure 2.4. The ability of hydraulic vulnerability to predict the degree that leaf hydraulic conductance (K_{leaf}) was maintained after strong dehydration and rehydration for *1*-hour with petiole in water, calculated as K_{leaf} after rehydration divided by maximum K_{leaf} (K_{max}). Filled dots represent species without recovery of K_{leaf} and open dots species that did show recovery of K_{leaf}. The line was fitted only for species without recovery of K_{leaf} (**P = 0.005; ***P < 0.001).

Figure 2.5. Correlation of the leaf water potential at 80% loss of leaf hydraulic conductance (P_{80}) with osmotic potentials (a) at full turgor (π_o) and (b) at turgor loss point (π_{TLP}), for ten species of a wide range of drought tolerance. Fitted standard major axes: (a) $\pi_o = 0.30 \times P_{80} + 0.85$; (b) $\pi_{TLP} = 0.42 \times P_{80} + 1.1$, Data for π_o and π_{TLP} from Scoffoni et al. (2011).

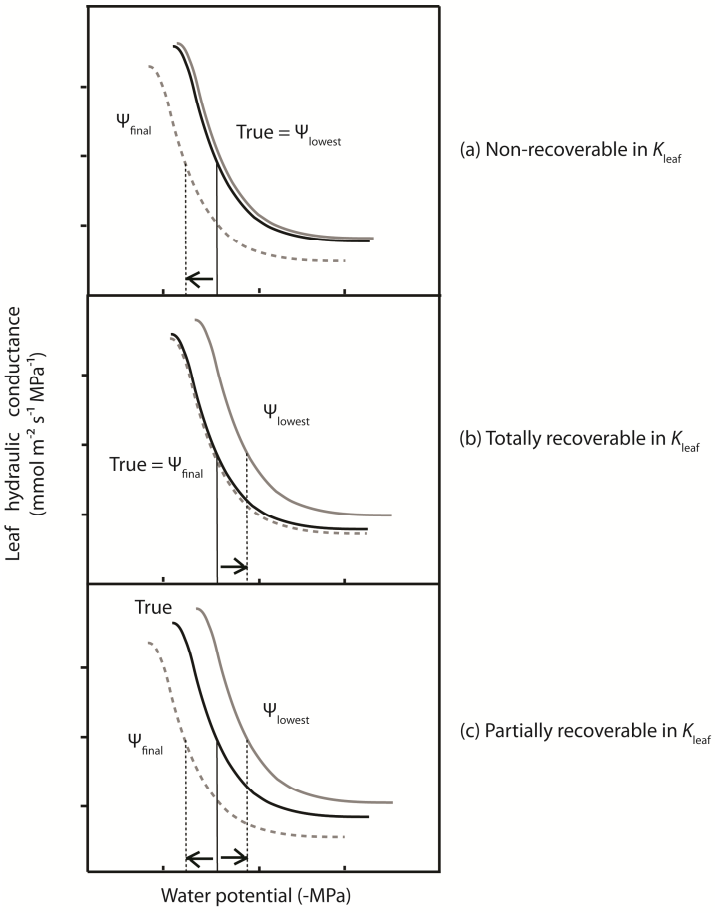
Leaf hydraulic conductance (mmol m-2 s-1 MPa-1)
Ψfinal
True = Ψlowest
(a) Non-recoverable in Kleaf
Ψlowest
True = Ψfinal
(b) Totally recoverable in Kleaf
True
Ψlowest
Ψfinal
(c) Partially recoverable in Kleaf
Water potential (-MPa)

Figure 2.1

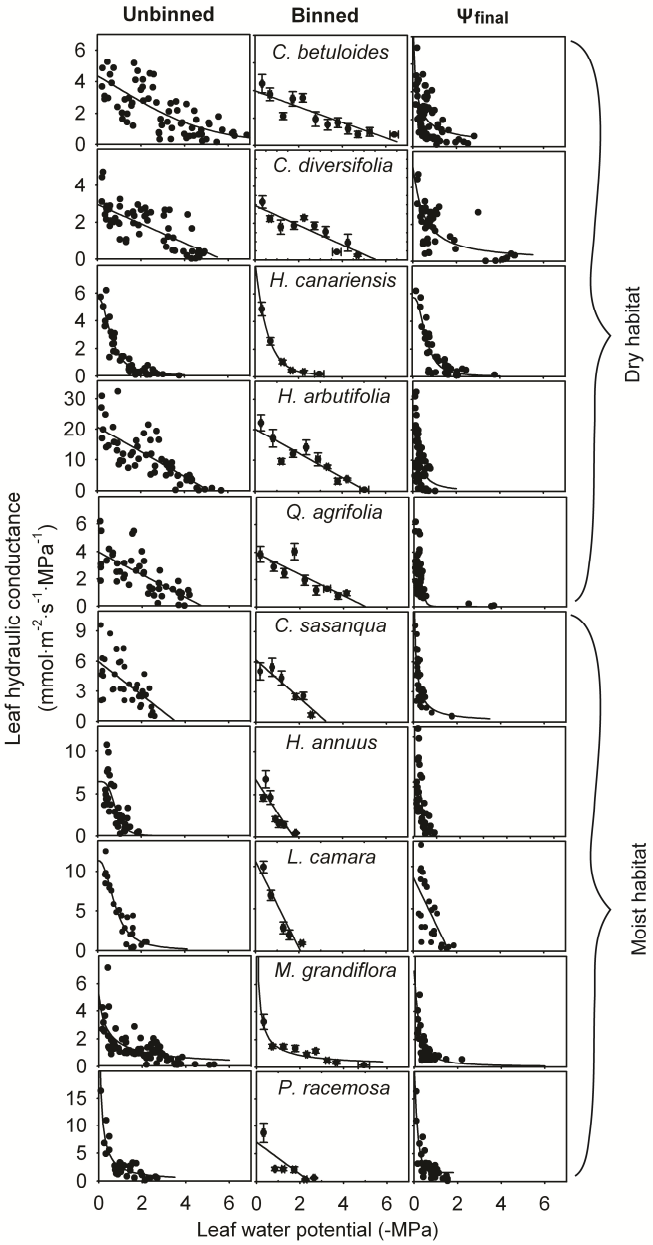
Unbinned
Binned
Ψfinal
C. betuloides
C. diversifolia
H. canariensis
H. arbutifolia
Q. agrifolia
C. sasanqua
H. annuus
L. camara
M. grandiflora
P. racemosa
Dry habitat
Moist habitat
Leaf hydraulic conductance (mmol·m-2·s-1·MPa-1)
Leaf water potential (-MPa)

Figure 2.2

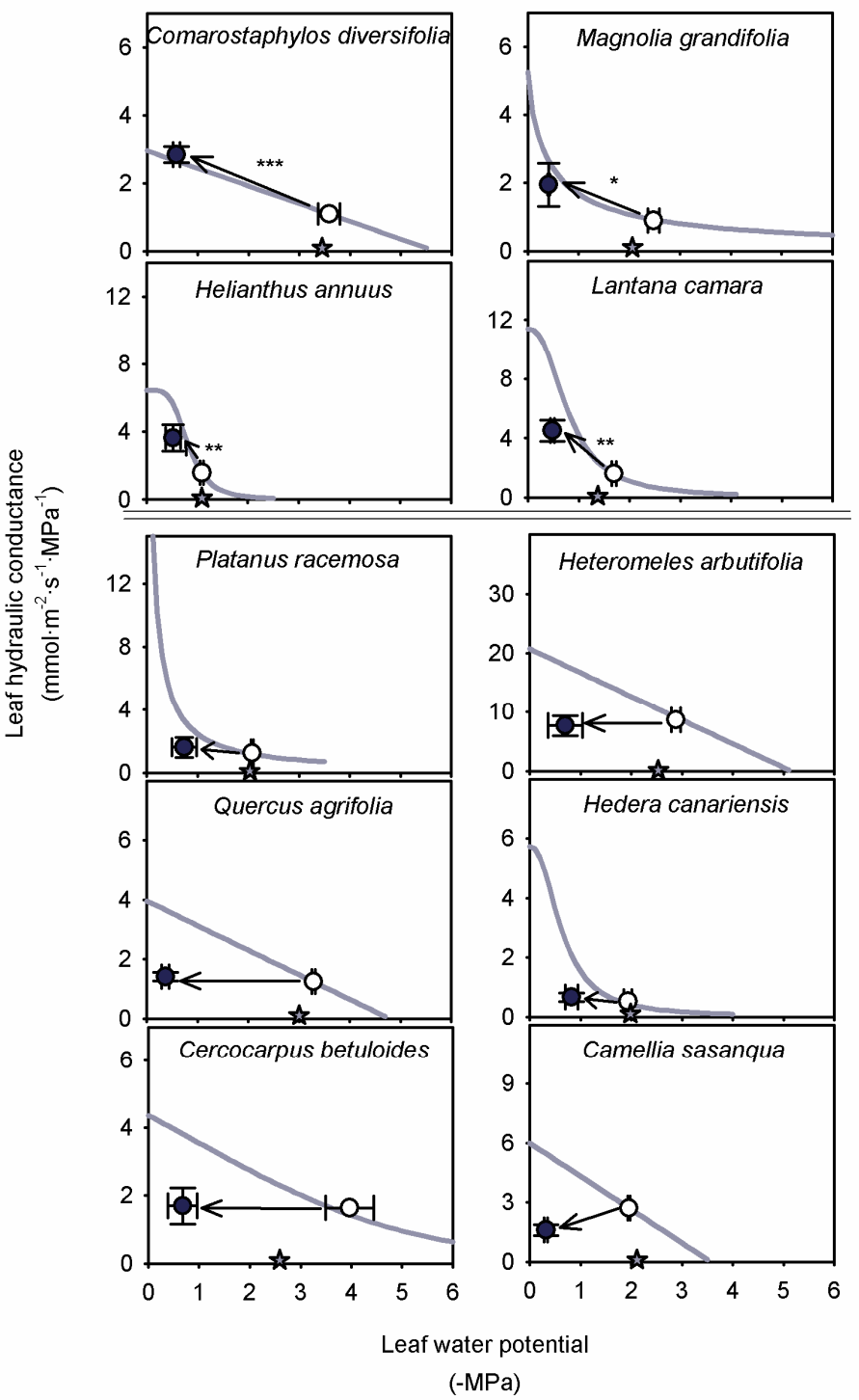
Comarostaphylos diversifolia
Magnolia grandifolia
Helianthus annuus
Lantana camara
Platanus racemosa
Heteromeles arbutifolia
Quercus agrifolia
Hedera canariensis
Cercocarpus betuloides
Camellia sasanqua
***
*
**
**
Leaf hydraulic conductance
(mmol·m-2·s-1·MPa-1)
Leaf water potential
(-MPa)

Figure 2.3

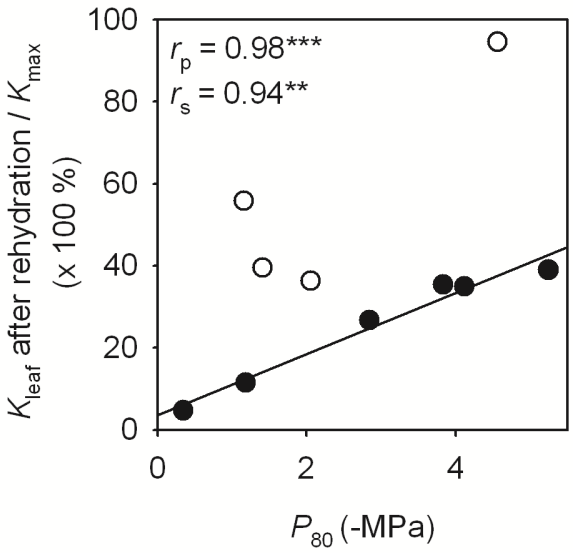
100
80
60
40
20
0
0
2
4
r_p = 0.98***
r_s = 0.94**
K_{leaf} after rehydration / K_{max} (x 100 %)
P_{80} (-MPa)

Figure 2.4

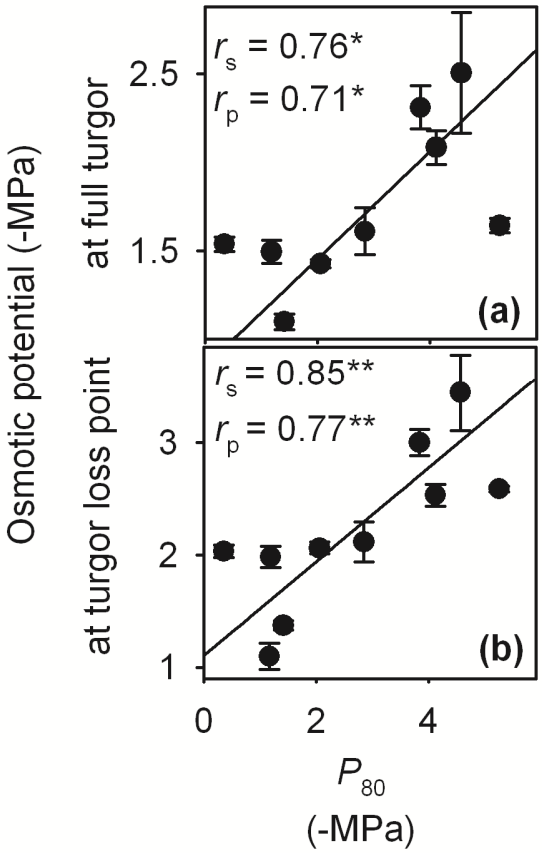
Osmotic potential (-MPa)
at full turgor
at turgor loss point
r_s = 0.76*
r_p = 0.71*
r_s = 0.85**
r_p = 0.77**
(a)
(b)
2.5
1.5
3
2
1
0
2
4
P_{80}
(-MPa)

Figure 2.5

SUPPLEMENTAL MATERIAL

Table S2.1. A summary of previous studies of leaf hydraulic vulnerability on whole leaves, indicating the various methods used, the different functions fitted to the data, and whether the data were binned or not before line-fitting.

Table S2.2. Minimum and maximum transpirational flow rates (*E*) for each species measured with the evaporative flux method and corresponding estimated stomatal conductances (*g*), and cuticular conductances for these species.

Table S2.3. Parameters for the decline of leaf hydraulic conductance (K_{leaf}) with declining leaf water potential for 10 species, fitted with four different functions, R^2 for observed values plotted against predicted values from the fitted function, and values for the Akaike Information Criterion (AIC). For each function, three plots were tested for K_{leaf} against leaf water potential: (1) "Ψ_{lowest} unbinned", (2) "Ψ_{lowest} binned", (3) and "Ψ_{final}" (see "*Methods*" for additional information). Bold and grey shading indicate the best fit model(s) for each plot for each species. Cells were left blank when the maximum likelihood parameters were extremely large or small values.

Table S2.4. **(spreadsheet file)** Parameters of leaf hydraulic vulnerability curves (K_{max}, P_{50} and P_{80}) determined by fitting four functions to the data for each species (linear, sigmoidal, logistic and exponential) and using three kinds of plots ("Ψ_{lowest} unbinned", "Ψ_{lowest} binned" and" Ψ_{final}").

Table S2.5 (spreadsheet file) Species means ± standard errors for leaf hydraulic vulnerability parameters and pressure-volume parameters for 10 species ranging widely in drought tolerance.

Table S2.1. A summary of previous studies of leaf hydraulic vulnerability on whole leaves, indicating the various methods used, the different functions fitted to the data, and whether the data were binned or not before line-fitting. *Functions were selected for apparent fit "by eye" in most studies, though two studies used maximum likelihood to select the sigmoidal over a linear function for their species and method (Johnson *et al.*, 2009a; Johnson *et al.*, 2009b).

Study	Measurement method	Function fitted*	Plot for fitting function
Kikuta et al., 1997	UAE	No function	Ψ_{lowest} unbinned
Salleo et al., 2000	UAE	No function	Ψ_{lowest} unbinned
Nardini et al., 2001	UAE/VPM	Polynomial	Ψ_{lowest} binned
Salleo et al., 2001	UAE /Visual	No function	Ψ_{lowest} unbinned
Brodribb and Holbrook, 2003a	RKM	Cumulative normal distribution	Ψ_{lowest} unbinned
Lo Gullo et al., 2003	UAE /VPM	Polynomial	Ψ_{lowest} unbinned
Nardini *et al.*, 2003	VPM/Visual	Sigmoidal	Ψ_{lowest} binned
Nardini and Salleo, 2003	UAE/HPFM	No function	Ψ_{lowest} unbinned
Salleo et al., 2003	VPM/ Visual	Polynomial	Ψ_{lowest} binned
Trifilo *et al.*, 2003a	VPM	Linear ($y = ax + b$)	Ψ_{lowest} unbinned
Trifilo *et al.*, 2003b	VPM/Visual	Linear ($y = ax + b$)	Ψ_{lowest} unbinned
Brodribb and Holbrook, 2004a	RKM	Cumulative normal distribution	Ψ_{lowest} unbinned
Brodribb and Holbrook, 2004b	RKM	Cumulative normal distribution	Ψ_{lowest} binned
Brodribb and Holbrook, 2006	RKM/ Heat-FM	Linear ($y = ax + b$) and sigmoidal ($y = a/(1 + e^{-((x-x_0)/b)})$)	Ψ_{final}
Brodribb and Holbrook, 2007	Heat-FM	Linear ($y = ax + b$) and sigmoidal ($y = a/(1 + e^{-((x-x_0)/b)})$)	Ψ_{final}
Woodruff et al., 2007	RKM	Sigmoidal ($y = a/(1 + e^{-((x-x_0)/b)})$)	Ψ_{lowest} unbinned
Hao et al., 2008	RKM	Sigmoidal	Ψ_{lowest} unbinned
Woodruff et al., 2008	RKM for K_{shoot} as proxy for K_{leaf}	Logistic ($y = a/(1 + (x/x_0)^b)$)	Ψ_{lowest} binned
Blackman et al., 2009	RKM	Sigmoidal ($y = a/(1 + e^{-((x-x_0)/b)})$)	Ψ_{lowest} unbinned
Brodribb and Cochard, 2009	Dynamic RKM	Sigmoidal ($y = a/(1 + e^{-((x-x_0)/b)})$)	Ψ_{lowest} unbinned
Chen et al., 2009	DKM	Sigmoidal ($y = a/(1 + e^{-b(x-c)})$)	Ψ_{lowest} binned
Johnson *et al.*, 2009a	UAE/RKM	Linear and sigmoidal	Ψ_{lowest} unbinned
Johnson *et al.*, 2009b	RKM	Sigmoidal ($y = a/(1 + e^{-((x-x_0)/b)})$)	Ψ_{lowest} unbinned
Saha *et al*., 2009	RKM	No function	Ψ_{lowest} unbinned
Blackman *et al.*, 2010	Dynamic RKM	Sigmoidal ($y = a/(1 + e^{-((x-x_0)/b)})$)	Ψ_{lowest} unbinned

Abbreviations: DKM, dehydration kinetics method; Heat-FM, evaporative flux method with heat gun; HPFM, high pressure flow method; RKM, rehydration kinetics method; UAE, ultrasonic acoustic emissions; Visual, visual method using dyes (i.e., Fluorescein, Phloxine B); VPM, vacuum pump method.

Table S2.2. Minimum and maximum transpirational flow rates (*E*) for each species measured with the evaporative flux method and corresponding estimated stomatal conductances (*g*), and cuticular conductances for these species. The *g* was determined by dividing by laboratory average mole fraction vapor pressure deficit (0.015 mol mol^{-1}). Means ± standard errors are reported for the five highest and five lowest *E* and *g* values for each species ($E_{highest}$, E_{lowest}, g_{higest} and g_{lowest} respectively).

Species	$E_{highest}$ ± SE ($mmol \cdot m^{-2} \cdot s^{-1}$)	E_{lowest} ± SE ($mmol \cdot m^{-2} \cdot s^{-1}$)	$g_{highest}$ ($mmol \cdot m^{-2} \cdot s^{-1}$)	g_{lowest} ($mmol \cdot m^{-2} \cdot s^{-1}$)	g_{min}* ($mmol \cdot m^{-2} \cdot s^{-1}$)
Camellia sasanqua	1.52 ± 0.091	0.453 ± 0.047	101 ± 6.70	30.2 ± 3.14	1.77 ± 0.13
Cercocarpus betuloides	2.82 ± 0.199	0.300 ± 0.037	188 ± 13.2	20.0 ± 2.48	3.99 ± 0.41
Comarostaphylos diversifolia	2.28 ± 0.056	0.314 ± 0.087	152 ± 3.73	20.9 ± 5.78	2.87 ± 0.35
Hedera canariensis	2.30 ± 0.111	0.226 ± 0.032	153 ± 7.43	15.04 ± 2.15	0.44 ± 0.03
Helianthus annuus	4.30 ± 0.191	0.618 ± 0.089	286 ± 12.7	41.2 ± 5.95	18.3 ± 1.92
Heteromeles arbutifolia	5.57 ± 0.087	0.156 ± 0.023	384 ± 5.80	10.4 ± 1.50	4.21 ± 1.22
Lantana camara	4.73 ± 0.116	0.618 ± 0.088	315 ± 7.70	41.2 ± 5.88	12.0 ± 0.85
Magnolia grandiflora	1.51 ± 0.146	0.286 ± 0.041	100 ± 9.76	19.1 ± 2.72	3.88 ± 0.41
Platanus racemosa	2.66 ± 0.170	0.545 ± 0.150	177 ± 11.4	36.3 ± 10.0	6.61 ± 0.41
Quercus agrifolia	1.14 ± 0.074	0.152 ± 0.006	76.0 ± 4.96	10.1 ± 0.43	1.72 ± 0.23

* data from Scoffoni *et al.*, 2011

Table S2.3. Parameters for the decline of leaf hydraulic conductance (K_{leaf}) with declining leaf water potential for 10 species fitted with four different functions, R^2 for observed values plotted against predicted values from the fitted function, and values for Akaike Information Criterion (AIC). For each function, three plots were tested for K_{leaf} against leaf water potential: (1) "Ψ_{lowest} unbinned", (2) "Ψ_{lowest} binned", (3) and "Ψ_{final}" (see "*Methods*" for additional information). Bold and grey shading indicate the best fit model(s) for each plot for each species. Cells were left blank when the maximum likelihood parameters were extremely large or small values.

Species	Plot	LINEAR: $K_{leaf} = a\,\Psi_{leaf} + y_o$				SIGMOIDAL: $K_{leaf} = a/(1 + e^{-(\frac{\Psi_{leaf}-x_0}{b})})$					LOGISTIC: $K_{leaf} = a/(1 + (\frac{\Psi_{leaf}}{x_0})^b)$					EXPONENTIAL: $K_{leaf} = y_0 + ae^{-b\times\Psi_{leaf}}$				
		a	y_0	r^2	AIC	a	b	x_0	r^2	AIC	a	B	x_0	r^2	AIC	a	b	y_0	r^2	AIC
C. betuloides	(1)	**-0.60±0.07**	**4.01±0.25**	**0.49**	**217.24**	**7.09±5.76**	**-2.16±1.06**	**1.01±3.53**	**0.52**	**215.81**	**4.02±0.49**	**2.06±0.76**	**2.94±0.54**	**0.51**	**216.56**	**5.24±1.38**	**0.23±0.13**	**-0.66±1.59**	**0.52**	**216.14**
	(2)	**-0.56±0.08**	**4.00±0.30**	**0.78**	**28.15**						4.43±0.82	1.14±0.59	2.59±0.92	0.82	30.84	4.58±1.11	0.27±0.18	0.02±1.36	0.83	30.36
	(3)	-1.46 ±0.27	3.31±0.25	0.29	240.75						**9.43±14.1**	**0.82±0.49**	**0.13±0.42**	**0.38**	**234.25**	**4.36±0.74**	**1.72±0.90**	**0.59±0.65**	**0.36**	**235.55**
C. diversifolia	(1)	**-0.52±0.06**	**2.96±1.78**	**0.54**	**130.60**	3.09±1.49	-1.32±0.10	2.81±1.71	0.53	134.94	7.06±12.6	0.60±0.47	0.23±0.13	0.52	136.01					
	(2)	**-0.53±0.08**	**2.95±0.24**	**0.80**	**19.08**	2.55±0.47	-0.83±0.50	3.30±0.50	0.59	27.21	2.33±0.21	5.56±2.82	3.44±0.28	0.78	25.75					
	(3)	-0.50± 0.06	2.62±0.12	0.64	116.45						**5.13±1.80**	**1.08±0.27**	**0.49±0.33**	**0.74**	**101.97**	**3.70±0.38**	**0.91±0.23**	**0.22±0.21**	**0.73**	**103.32**
H. arbutifolia	(1)	**-4.02±0.42**	**20.7±1.22**	**0.61**	**350.53**	34.7±34.1	-1.73±0.95	0.87±3.45	0.60	354.64	22.3 ±3.95	1.52±0.57	1.95±0.68	0.58	357.58	56.8±82.0	0.09±0.16	-35.3±83.4	0.61	352.534
	(2)	**-3.94±0.41**	**20.2±0.53**	**0.84**	**56.74**	54.9±163	-2.06±0.79	-0.79±10.2	0.82	63.97	23.0±5.63	1.40±0.59	1.73±0.84	0.80	65.19	63.8±156	0.07±0.22	-42.9±158	0.84	62.64
	(3)	**-19.2±4.44**	**17.0±1.71**	**0.24**	**389.29**						**20.8 ±7.11**	**1.61±0.78**	**0.29±0.14**	**0.28**	**389.02**	**22.0±4.78**	**3.29±2.39**	**1.97±5.15**	**0.27**	**389.17**
H. canariensis	(1)	-1.53±0.18	3.79±0.30	0.63	121.51	**26.7±53.3**	**-0.59±0.15**	**-0.60±0.15**	**0.87**	**79.75**	**5.74±0.57**	**2.27±0.34**	**0.64±0.08**	**0.88**	**79.13**	**7.49±0.57**	**1.55±0.21**	**0.05±0.21**	**0.88**	**79.92**
	(2)	**-1.61±0.39**	**4.06±0.69**	**0.74**	**33.21**						**5.88±0.22**	**2.24±0.12**	**0.63±0.03**	**0.999**	**31.95**	**8.10±0.19**	**1.73±0.07**	**0.15±0.05**	**0.999**	**31.30**
	(3)	-1.71±0.24	3.68±0.33	0.56	129.08	**15.7±16.8**	**-0.45±0.13**	**-0.08±0.80**	**0.83**	**91.89**	**5.75±0.63**	**2.53±0.44**	**0.60±0.07**	**0.84**	**91.06**	**7.98±0.73**	**1.73±0.27**	**-0.06±0.07**	**0.83**	**92.45**
Q. agrifolia	(1)	**-0.83±0.12**	**3.96±0.29**	**0.49**	**141.72**	**3.99±0.82**	**-0.93±0.43**	**2.39±0.53**	**0.50**	**143.46**	**3.45±0.28**	**3.77±1.53**	**2.61±0.24**	**0.50**	**143.55**					
	(2)	**-0.78±0.16**	**3.95±0.42**	**0.75**	**26.96**	3.76±0.87	-0.88±0.54	2.71±0.63	0.76	35.68	3.37±0.35	4.21±2.07	2.86±0.33	0.77	35.39					
	(3)	-0.86±0.25	2.68±0.22	0.20	162.96	**3.17±0.60**	**-0.09±0.08**	**0.37±0.05**	**0.32**	**157.64**	**2.98±0.28**	**4.94±2.93**	**0.37±0.05**	**0.32**	**157.50**	**3.77±0.83**	**2.07±0.92**	**0.04±0.70**	**0.31**	**158.56**
C. sansanqua	(1)	**-1.69±0.33**	**5.99±0.52**	**0.39**	**160.18**	**5.53±0.78**	**-0.54±0.24**	**1.93±0.23**	**0.41**	**161.08**	**5.26±0.48**	**3.49±1.44**	**1.94±0.20**	**0.42**	**160.93**					
	(2)	**-1.90 ±0.29**	**-6.22±0.48**	**0.88**	**28.43**	5.46±0.46	-0.47±0.12	1.90±0.14	0.94	54.56	5.27±0.32	3.93±0.98	1.88±0.13	0.94	54.4					
	(3)	-3.36±0.78	4.98±0.40	0.31	168.09						**13.8±13.2**	**1.05±0.54**	**0.10±0.18**	**0.54**	**153.60**	**8.95±1.54**	**4.09±1.52**	**0.86±0.90**	**0.54**	**154.24**
H. annuus	(1)	-4.63±0.76	7.50±0.73	0.51	153.57	**7.41±2.06**	**-0.24±0.12**	**0.78±1.17**	**0.58**	**150.94**	**6.45±0.75**	**4.15±1.45**	**0.83±0.08**	**0.59**	**149.49**	11.71±1.80	1.17±0.72	-1.20±2.61	0.55	152.99
	(2)	**-3.88±0.82**	**6.80±0.88**	**0.76**	**34.45**	6.17±1.10	-0.19±0.11	0.88±0.10	0.86	44.68	5.83±0.59	4.96±1.80	0.88±0.07	0.88	43.47	10.83±2.49	0.92±0.75	-1.82±3.66	0.81	46.98
	(3)	-4.28±0.92	6.64±0.77	0.38	162.26	**5.61±0.76**	**-0.13±0.07**	**0.79±0.07**	**0.44**	**160.78**	**5.48±0.58**	**5.72±2.55**	**0.79±0.07**	**0.46**	**159.77**	11.1±5.66	0.74±0.86	-3.18±6.96	0.39	164.01
L. camara	(1)	-5.40±0.52	10.8±0.67	0.81	103.21	**34.6±55.5**	**-0.61±0.21**	**-0.19±1.54**	**0.89**	**91.66**	**11.4±1.44**	**2.43±0.49**	**0.80±0.12**	**0.89**	**91.17**	**16.4±1.33**	**1.31±0.36**	**-0.20±1.19**	**0.89**	**91.89**
	(2)	**-5.12±0.74**	**10.6±1.01**	**0.90**	**44.53**	38.5±13.3	-0.63±0.04	-0.29±0.33	0.999	Inf	11.4±0.06	2.45±0.02	0.81±0.01	0.999	Inf	16.50±0.35	1.29±0.09	-0.23±0.28	0.998	Inf
	(3)	**-5.27±1.16**	**8.71±1.04**	**0.44**	**130.84**	**7.73±2.03**	**-0.23±0.16**	**0.87±0.18**	**0.47**	**132.46**	**7.11±0.96**	**4.31±2.32**	**0.89±0.13**	**0.47**	**132.22**	17.1±19.1	0..49±0.93	-7.35±21.0	0.45	133.36
M. grandiflora	(1)	-0.58±0.08	2.54±0.19	0.40	194.76						**5.24±2.62**	**0.87±0.29**	**0.42±0.50**	**0.48**	**187.02**	3.22±0.63	1.14±0.67	0.68±0.33	0.46	189.47
	(2)	**-0.55±0.10**	**2.47±0.28**	**0.76**	**21.07**						**21.4±34.6**	**0.75±0.13**	**0.03±0.09**	**0.89**	**20.94**	3.33±0.48	0.71±0.41	0.22±0.49	0.86	23.66
	(3)	-0.68±0.11	2.06±0.16	0.32	203.52											**7.43±1.50**	**4.49±0.94**	**0.64±0.15**	**0.67**	**153.15**
P. racemosa	(1)	-3.25±0.63	7.28±0.90	0.46	154.75						**34.1±23.2**	**1.06±0.23**	**0.09±0.11**	**0.82**	**121.24**	19.45±2.73	3.39±0.64	1.53±0.38	0.81	123.73
	(2)	**-2.87±0.83**	**7.08±1.42**	**0.66**	**40.80**											20.2±6.28	2.89±0.95	1.06±0.41	0.95	58.91
	(3)	-4?92±1.08	6.73±0.90	0.39	158.119											**20.4±5.97**	**6.41±2.33**	**1.63±0.58**	**0.69**	**139.85**

REFERENCES

Blackman CJ, Brodribb TJ, Jordan GJ. 2009. Leaf hydraulics and drought stress: response, recovery and survivorship in four woody temperate plant species. *Plant Cell and Environment* **32**, 1584-1595.

Blackman CJ, Brodribb TJ, Jordan GJ. 2010. Leaf hydraulic vulnerability is related to conduit dimensions and drought resistance across a diverse range of woody angiosperms. *New Phytologist* **188**, 1113-1123.

Blackman CJ, Brodribb TJ. 2011. Two measures of leaf capacitance: insights into the water transport pathway and hydraulic conductance in leaves. *Functional Plant Biology* **38**, 118-126.

Boyer JS. 1967. Leaf water potentials measured with a pressure chamber. *Plant Physiology* **42**, 133-137.

Brodribb TJ, Holbrook NM. 2003a. Stomatal closure during leaf dehydration, correlation with other leaf physiological traits. *Plant Physiology* **132**, 2166-2173.

Brodribb TJ, Holbrook NM. 2003b. Changes in leaf hydraulic conductance during leaf shedding in seasonally dry tropical forest. *New Phytologist* **158**, 295-303.

Brodribb TJ, Holbrook NM. 2004a. Diurnal depression of leaf hydraulic conductance in a tropical tree species. *Plant Cell and Environment* **27**, 820-827.

Brodribb TJ, Holbrook NM. 2004b. Stomatal protection against hydraulic failure: a comparison of coexisting ferns and angiosperms. *New Phytologist* **162**, 663-670.

Brodribb TJ, Holbrook NM. 2005. Water stress deforms tracheids peripheral to the leaf vein of a tropical conifer. *Plant Physiology* **137**, 1139-1146.

Brodribb TJ, Holbrook NM. 2006. Declining hydraulic efficiency as transpiring leaves desiccate: two types of response. *Plant Cell and Environment* **29**, 2205-2215.

Brodribb TJ, Holbrook NM. 2007. Forced depression of leaf hydraulic conductance in situ: effects on the leaf gas exchange of forest trees. *Functional Ecology* **21**, 705-712.

Brodribb TJ, Cochard H. 2009. Hydraulic Failure Defines the Recovery and Point of Death in Water-Stressed Conifers. *Plant Physiology* **149**, 575-584.

Brodribb TJ, Feild TS, Sack L. 2010. Viewing leaf structure and evolution from a hydraulic perspective. *Functional Plant Biology* **37**, 488-498.

Brodribb TJ, Blackman CJ. and PrometheusWiki contributors. PROTOCOL: non-steady state rehydration to determine leaf hydraulic conductance, vulnerability and capacitance. *PrometheusWiki.* Retrieved 02,June2011, from http://www.publish.csiro.au/prometheuswiki/tiki-pagehistory.php?page=PROTOCOL:Non-steady state rehydration to determine leaf hydraulic conductance, vulnerability and capacitance&preview=

Bucci SJ, Scholz FG, Goldstein G, Meinzer FC, Sternberg LDL. 2003. Dynamic changes in hydraulic conductivity in petioles of two savanna tree species: factors and mechanisms contributing to the refilling of embolized vessels. *Plant Cell and Environment* **26**, 1633-1645.

Buck AL. 1981. New equations for computing vapor-pressure and enhancement factor. *Journal of Applied Meteorology* **20**, 1527-1532.

Burnham KP, Anderson DR. 2002. *Model selection and multimodel inference, 2nd ed*. New York, New York, USA. : Springer.

Burnham KP, Anderson DR. 2004. Multimodel inference - understanding AIC and BIC in model selection. *Sociological Methods & Research* **33**, 261-304.

Canny MJ, Huang CX. 2006. Leaf water content and palisade cell size. *New Phytologist* **170**, 75-85.

Chen JW, Zhang Q, Li XS, Cao KF. 2009. Independence of stem and leaf hydraulic traits in six Euphorbiaceae tree species with contrasting leaf phenology. *Planta* **230**, 459-468.

Choat B, Lahr EC, Melcher P, Zwieniecki MA, Holbrook NM. 2005. The spatial pattern of air seeding thresholds in mature sugar maple trees. *Plant, Cell & Environment* **28**, 1082-1089.

Cochard H, Coll L, Le Roux X, Ameglio T. 2002. Unraveling the effects of plant hydraulics on stomatal closure during water stress in walnut. *Plant Physiology* **128**, 282-290.

Cochard H, Froux F, Mayr FFS, Coutand C. 2004. Xylem wall collapse in water-stressed pine needles. *Plant Physiology* **134**, 401-408.

Cochard H, Venisse JS, Barigah TS, Brunel N, Herbette S, Guilliot A, Tyree MT, Sakr S. 2007. Putative role of aquaporins in variable hydraulic conductance of leaves in response to light. *Plant Physiology* **143**, 122-133.

Cowan IR. 1972. Electrical analog of evaporation from, and flow of water in plants. *Planta* **106**, 221-226.

Croat TB. 1978. Flora of Barro Colorado Island. *Flora of Barro Colorado Island*. California: Stanford University Press, 735.

Damour G, Simonneau T, Cochard H, Urban L. 2010. An overview of models of stomatal conductance at the leaf level. *Plant Cell and Environment* **33**, 1419-1438.

Domec JC, Lachenbruch B, Meinzer FC. 2006. Bordered pit structure and function determine spatial patterns of air-seeding thresholds in xylem of Douglas-fir (*Pseudotsuga menziesii*; Pinaceae) trees. *American Journal of Botany* **93**, 1588-1600.

eFloras. 2008. Flora of North America *Missouri Botanical Garden & Harvard University Herbaria*, Vol. 2010. St. Louis, MO &Cambridge, MA: http://www.efloras.org/.

Franks PJ, Farquhar GD. 1999. A relationship between humidity response, growth form and photosynthetic operating point in C-3 plants. *Plant Cell and Environment* **22**, 1337-1349.

Giles KL, Beardsel.Mf, Cohen D. 1974. Cellular and ultrastructural changes in mesophyll and bundle sheath-cells of maize in response to water stress. *Plant Physiology* **54**, 208-212.

Grubb PJ. 1998. A reassessment of the strategies of plants which cope with shortages of resources. *Perspectives in Plant Ecology Evolution and Systematics* **1**, 3-31.

Hao GY, Hoffmann WA, Scholz FG, Bucci SJ, Meinzer FC, Franco AC, Cao KF, Goldstein G. 2008. Stem and leaf hydraulics of congeneric tree species from adjacent tropical savanna and forest ecosystems. *Oecologia* **155**, 405-415.

Hao GY, Sack L, Wang AY, Cao KF, Goldstein G. 2010. Differentiation of leaf water flux and drought tolerance traits in hemiepiphytic and non-hemiepiphytic *Ficus* tree species. *Functional Ecology* **24**, 731-740.

Iovi K, Kolovou C, Kyparissis A. 2009. An ecophysiological approach of hydraulic performance for nine Mediterranean species. *Tree Physiology* **29**, 889-900.

Johansson I, Karlsson M, Shukla VK, Chrispeels MJ, Larsson C, Kjellbom P. 1998. Water transport activity of the plasma membrane aquaporin PM28A is regulated by phosphorylation. *Plant Cell* **10**, 451-459.

Johnson DM, Meinzer FC, Woodruff DR, McCulloh KA. 2009a. Leaf xylem embolism, detected acoustically and by cryo-SEM, corresponds to decreases in leaf hydraulic conductance in four evergreen species. *Plant Cell and Environment* **32**, 828-836.

Johnson DM, Woodruff DR, McCulloh KA, Meinzer FC. 2009b. Leaf hydraulic conductance, measured in situ, declines and recovers daily: leaf hydraulics, water potential and stomatal conductance in four temperate and three tropical tree species. *Tree Physiology* **29**, 879-887.

Kikuta SB, LoGullo MA, Nardini A, Richter H, Salleo S. 1997. Ultrasound acoustic emissions from dehydrating leaves of deciduous and evergreen trees. *Plant Cell and Environment* **20**, 1381-1390.

Kim YX, Steudle E. 2007. Light and turgor affect the water permeability (aquaporins) of parenchyma cells in the midrib of leaves of *Zea mays*. *Journal of Experimental Botany* **58**, 4119-4129.

Kitamura S, Murata G. 1979. Colored illustrations of woody plants of Japan, Revised editions *Colored illustrations of woody plants of Japan, Revised editions* Vol. II. Osaka, Japan: Hoikusha, 158-159.

Koroleva OA, Farrar JF, Tomos AD, Pollock CJ. 1997. Patterns of solute in individual mesophyll, bundle sheath and epidermal cells of barley leaves induced to accumulate carbohydrate. *New Phytologist* **136**, 97-104.

Koroleva OA, Tomos AD, Farrar J, Pollock CJ. 2002. Changes in osmotic and turgor pressure in response to sugar accumulation in barley source leaves. *Planta* **215**, 210-219.

Kubiske ME, Abrams MD. 1990. Pressure-volume relationships in non-rehydrated tissue at various water deficits. *Plant Cell and Environment* **13**, 995-1000.

Laio F, Porporato A, Ridolfi L, Rodriguez-Iturbe I. 2001. Plants in water-controlled ecosystems: active role in hydrologic processes and response to water stress - II. Probabilistic soil moisture dynamics. *Advances in Water Resources* **24**, 707-723.

Lee SH, Chung GC, Zwiazek JJ. 2009. Effects of irradiance on cell water relations in leaf bundle sheath cells of wild-type and transgenic tobacco (*Nicotiana tabacum*) plants overexpressing aquaporins. *Plant Science* **176**, 248-255.

Lo Gullo MA, Nardini A, Trifilo P, Salleo S. 2003. Changes in leaf hydraulics and stomatal conductance following drought stress and irrigation in *Ceratonia siliqua* (Carob tree). *Physiologia Plantarum* **117**, 186-194.

Maherali H, Pockman WT, Jackson RB. 2004. Adaptive variation in the vulnerability of woody plants to xylem cavitation. *Ecology* **85**, 2184-2199.

Maximov NA. 1931. The physiological significance of the xeromorphic structure of plants. *Journal of Ecology* **19**, 273-282.

Meinzer FC, McCulloh KA, Lachenbruch B, Woodruff DR, Johnson DM. 2010. The blind men and the elephant: the impact of context and scale in evaluating conflicts between plant hydraulic safety and efficiency. *Oecologia* **164**, 287-296.

Milburn JA, Johnson RPC. 1966. Conductance of sap. 2. Detection of vibrations produced by sap cavitation in *Ricinus* xylem. *Planta* **69**, 43-52.

Miyazawa S, Yoshimura S, Shinzaki Y, Maeshima M, Miyake C. 2008. Deactivation of aquaporins decreases internal conductance to CO2 diffusion in tobacco leaves grown under long-term drought. *Functional Plant Biology* **35**, 553-564.

Nardini A, Tyree MT, Salleo S. 2001. Xylem cavitation in the leaf of *Prunus laurocerasus* and its impact on leaf hydraulics. *Plant Physiology* **125**, 1700-1709.

Nardini A, Salleo S. 2003. Effects of the experimental blockage of the major veins on hydraulics and gas exchange of *Prunus laurocerasus* L. leaves. *Journal of Experimental Botany* **54**, 1213-1219.

Nardini A, Salleo S, Raimondo F. 2003. Changes in leaf hydraulic conductance correlate with leaf vein embolism in *Cercis siliquastrum* L. *Trees-Structure and Function* **17**, 529-534.

Nardini A, Salleo S, Andri S. 2005. Circadian regulation of leaf hydraulic conductance in sunflower (*Helianthus annuus* L. cv Margot). *Plant Cell and Environment* **28**, 750-759.

Nardini A, Ramani M, Gortan E, Salleo S. 2008. Vein recovery from embolism occurs under negative pressure in leaves of sunflower (*Helianthus annuus*). *Physiologia Plantarum* **133**, 755-764.

Neufeld HS, Grantz DA, Meinzer FC, Goldstein G, Crisosto GM, Crisosto C. 1992. Genotypic variability in vulnerability of leaf xylem to cavitation in water-stressed and well-irrigated sugarcane. *Plant Physiology* **100**, 1020-1028.

Nonami H, Schulze ED. 1989. Cell water potential, osmotic potential, and turgor in the epidermis and mesophyll of transpiring leaves - Combined measurements with the cell pressure probe and nanoliter osmometer. *Planta* **177**, 35-46.

North GB, Nobel PS. 2000. Heterogeneity in water availability alters cellular development and hydraulic conductivity along roots of a desert succulent. *Annals of Botany* **85**, 247-255.

Palta JP, Leestadelmann OY. 1983. Vacuolated plant-cells as ideal osmometer- Reversibility and limits of plasmolysis, and estimation of protoplasm volume in control and water-stress tolerant cells. *Plant Cell and Environment* **6**, 601-610.

Pammenter NW, Vander Willigen C. 1998. A mathematical and statistical analysis of the curves illustrating vulnerability of xylem to cavitation. *Tree Physiology* **18**, 589-593.

Pasquet-Kok J, Creese C, Sack L. 2010. Turning over a new 'leaf': multiple functional significances of leaves versus phyllodes in Hawaiian *Acacia koa*. *Plant Cell and Environment* **33**, 2084-2100.

Pieruschka R, Huber G, Berry JA. 2010. Control of transpiration by radiation. *Proceedings of the National Academy of Sciences of the United States of America* **107**, 13372-13377.

Sack L, Melcher PJ, Zwieniecki MA, Holbrook NM. 2002. The hydraulic conductance of the angiosperm leaf lamina: a comparison of three measurement methods. *Journal of Experimental Botany* **53**, 2177-2184.

Sack L, Cowan PD, Jaikumar N, Holbrook NM. 2003. The 'hydrology' of leaves: co-ordination of structure and function in temperate woody species. *Plant Cell and Environment* **26**, 1343-1356.

Sack L, Streeter CM, Holbrook NM. 2004. Hydraulic analysis of water flow through leaves of sugar maple and red oak. *Plant Physiology* **134**, 1824-1833.

Sack L, Tyree MT. 2005. Leaf hydraulics and its implications in plant structure and function. *Vascular Transport in Plants*. Oxford, UK.: eds N.M. Holbrook & M.A. Zweiniecki, Elsevier/Academic Press, 93–114.

Sack L, Tyree MT, Holbrook NM. 2005. Leaf hydraulic architecture correlates with regeneration irradiance in tropical rainforest trees. *New Phytologist* **167**, 403-413.

Sack L, Holbrook NM. 2006. Leaf hydraulics. *Annual Review of Plant Biology* **57**, 361-381.

Sack L, Melcher PJ, Liu WH, Middleton E, Pardee T. 2006. How strong is intracanopy leaf plasticity in temperate deciduous trees? *American Journal of Botany* **93**, 829-839.

Saha S, Holbrook NM, Montti L, Goldstein G, Cardinot GK. 2009. Water Relations of *Chusquea ramosissima* and *Merostachys claussenii* in Iguazu National Park, Argentina. *Plant Physiology* **149**, 1992-1999.

Salleo S, Nardini A, Pitt F, Lo Gullo MA. 2000. Xylem cavitation and hydraulic control of stomatal conductance in laurel (*Laurus nobilis* L.). *Plant Cell and Environment* **23**, 71-79.

Salleo S, Lo Gullo MA, Raimondo F, Nardini A. 2001. Vulnerability to cavitation of leaf minor veins: any impact on leaf gas exchange? *Plant Cell and Environment* **24**, 851-859.

Salleo S, Raimondo F, Trifilo P, Nardini A. 2003. Axial-to-radial water permeability of leaf major veins: a possible determinant of the impact of vein embolism on leaf hydraulics? *Plant Cell and Environment* **26**, 1749-1758.

Scoffoni C, Pou A, Aasamaa K, Sack L. 2008. The rapid light response of leaf hydraulic conductance: new evidence from two experimental methods. *Plant Cell and Environment* **31**, 1803-1812.

Scoffoni C, Rawls M, McKown A, Cochard H, Sack L. 2011. Decline of leaf hydraulic conductance with dehydration: relationship to leaf size and venation architecture. *Plant Physiology* **156**, 832-843.

Sellin A, Kupper P. 2007. Temperature, light and leaf hydraulic conductance of little-leaf linden (*Tilia cordata*) in a mixed forest canopy. *Tree Physiology* **27**, 679-688.

Sellin A, Ounapuu E, Kupper P. 2008. Effects of light intensity and duration on leaf hydraulic conductance and distribution of resistance in shoots of silver birch (*Betula pendula*). *Physiologia Plantarum* **134**, 412-420.

Slavik B. 1959. Gradients of osmotic pressure of cell sap in the area of one leaf blade. *Biol Plant [Praha]* **1**, 39-47.

Sokal RR, Rohlf FJ. 1995. *Biometry: the principles and practice of statistics in biological research. Third edition*: W.H. Freeman and Company, New York, New Yord, USA.

Trifilo P, Gasco A, Raimondo F, Nardini A, Salleo S. 2003a. Kinetics of recovery of leaf hydraulic conductance and vein functionality from cavitation-induced embolism in sunflower. *Journal of Experimental Botany* **54**, 2323-2330.

Trifilo P, Nardini A, Lo Gullo MA, Salleo S. 2003b. Vein cavitation and stomatal behaviour of sunflower (*Helianthus annuus*) leaves under water limitation. *Physiologia Plantarum* **119**, 409-417.

Tyree MT, Dixon MA. 1983. Cavitation events in *Thuja occidentalis* L.- Ultrasonic acoustic emissions from the sapwood can be measured. *Plant Physiology* **72**, 1094-1099.

Tyree MT, Dixon MA. 1986. Water-stress induced cavitation and embolism in some woody plants. *Physiologia Plantarum* **66**, 397-405.

Tyree MT, Zimmermann MH. 2002. *Xylem Structure and the Ascent of Sap*. Berlin, Germany.: Springer.

Tyree MT, Nardini A, Salleo S, Sack L, El Omari B. 2005. The dependence of leaf hydraulic conductance on irradiance during HPFM measurements: any role for stomatal response? *Journal of Experimental Botany* **56**, 737-744.

Valladares F, Pearcy RW. 1997. Interactions between water stress, sun-shade acclimation, heat tolerance and photoinhibition in the sclerophyll *Heteromeles arbutifolia*. *Plant Cell and Environment* **20**, 25-36.

Voicu MC, Zwiazek JJ, Tyree MT. 2008. Light response of hydraulic conductance in bur oak (Quercus macrocarpa) leaves. *Tree Physiology* **28**, 1007-1015.

Voicu MC, Cooke JEK, Zwiazek JJ. 2009. Aquaporin gene expression and apoplastic water flow in bur oak (Quercus macrocarpa) leaves in relation to the light response of leaf hydraulic conductance. *Journal of Experimental Botany* **60**, 4063-4075.

Warton DI, Wright IJ, Falster DS, Westoby M. 2006. Bivariate line-fitting methods for allometry. *Biological Reviews* **81**, 259-291.

Weast RC, ed. 1974. *Handbook of Chemistry and Physics, 54th ed*. Cleveland, Ohio: CRC Press.

Woodruff DR, McCulloh KA, Warren JM, Meinzer FC, Lachenbruch B. 2007. Impacts of tree height on leaf hydraulic architecture and stomatal control in Douglas-fir. *Plant Cell and Environment* **30**, 559-569.

Woodruff DR, Meinzer FC, Lachenbruch B. 2008. Height-related trends in leaf xylem anatomy and shoot hydraulic characteristics in a tall conifer: safety versus efficiency in water transport. *New Phytologist* **180**, 90-99.

Yang SD, Tyree MT. 1993. Hydraulic resistance in *Acer saccharum* shoots and its influence on leaf water potential and transpiration. *Tree Physiology* **12**, 231-242.

CHAPTER 3

DECLINE OF LEAF HYDRAULIC CONDUCTANCE WITH DEHYDRATION: RELATIONSHIP TO LEAF SIZE AND VENATION ARCHITECTURE

ABSTRACT

Across plant species, leaves vary enormously in their size and their venation architecture, of which one major function is to replace water lost to transpiration. The leaf hydraulic conductance (K_{leaf}) represents the capacity of the transport system to deliver water, allowing stomata to remain open for photosynthesis. Previous studies showed that K_{leaf} relates to the vein density (= vein length per area). Additionally, venation architecture determines the sensitivity of K_{leaf} to damage; severing the midrib caused K_{leaf} and gas exchange to decline, with lesser impacts in leaves with higher major vein density that provided more numerous water flow pathways around the damaged vein. Because xylem embolism during dehydration also reduces K_{leaf}, we hypothesized that higher major vein density would also reduce hydraulic vulnerability. Smaller leaves, which generally have higher major vein density, would thus have lower hydraulic vulnerability. Tests using simulations with a spatially explicit model confirmed that smaller leaves with higher major vein density were more tolerant of major vein embolism. Additionally, for ten species ranging strongly in drought tolerance, hydraulic vulnerability determined as the leaf water potential at 50% and 80% loss of K_{leaf} was lower with greater major vein density and smaller leaf size ($|r| = 0.80\text{-}0.86$; $P < 0.01$). These relationships were independent of other aspects of physiological and morphological drought tolerance. These findings point to a new functional role of venation architecture and small leaf size in drought tolerance, potentially contributing to well-known biogeographic trends in leaf size.

INTRODUCTION

The leaf venation architecture has common functions across plant species, serving for mechanical support (Niklas, 1999), sugar and hormone transport (Kehr and Buhtz, 2008), and the replacement of water lost to transpiration during photosynthesis (Sack and Holbrook, 2006). However, venation architecture is highly diverse across species (Uhl and Mosbrugger, 1999; Roth-Nebelsick et al., 2001; Sack and Frole, 2006; Ellis et al., 2009; Brodribb et al., 2010). In dicotyledons, the leaf venation system typically consists of three orders of major veins and up to five higher orders of minor veins embedded in the mesophyll, with the vein orders arranged in a hierarchy; lower order veins are larger in diameter, with greater xylem conduit numbers and sizes, whereas higher order veins have greater length per area (= vein density; Sack and Holbrook, 2006; McKown et al., 2010). Species vary strongly in the density of given vein orders and their conductivities (Cochard et al., 2004b; Sack and Frole, 2006). The aim of this study was to test for novel functional consequences of variation in leaf venation architecture and leaf size, and particularly a role in drought tolerance.

The leaf is a critical component in the plant water transport system, accounting for 30% or more of whole-plant hydraulic resistance (Sack and Holbrook, 2006). The leaf hydraulic conductance (K_{leaf}; flow rate / water potential driving force, i.e., the inverse of hydraulic resistance) quantifies a complex microhydrological system, including the conductances in series of the vein xylem (K_x) and the mesophyll pathways outside the xylem (K_{ox}). The venation architecture is thus an important determinant of K_{leaf} and its dynamics. Total vein density is a determinant of both K_x and K_{ox}, because, all else being equal, higher densities represent more numerous xylem flow pathways in parallel per leaf area, and shorter pathways for water movement outside the xylem (Sack and Frole, 2006; Brodribb et al., 2007; McKown et al., 2010). Additionally, venation structure may contribute to the ability of K_{leaf} to withstand vein

damage (Sack et al., 2008). Minor veins had been classically hypothesized to provide "conductive overload", consisting of many parallel pathways for water flow such that a leaf could tolerate hydraulic disruption of major veins (Wylie, 1938). However, detailed studies found that K_{leaf}, stomatal conductance and photosynthesis were very sensitive to damage of the large major veins, which supply water to the downstream vein hierarchy (Nardini et al., 2001; Huve et al., 2002; Nardini and Salleo, 2003; Sack et al., 2003a; Salleo et al., 2003; Delaney and Higley, 2006). Additionally, the impact of severing the midrib near its base differed among species. The decline of K_{leaf} was lower in palmately-veined species with greater major vein density providing flow pathways around the disrupted vein (Sack et al., 2008). The impact of midrib damage on K_{leaf} also varied among pinnately veined species. Smaller leaves, with their major veins spaced more closely and thus greater major vein densities, had greater tolerance of midrib damage (Sack et al., 2008).

Just as for leaves with damaged veins, K_{leaf} declines in dehydrating leaves, resulting in reductions of leaf gas exchange and whole plant growth (Salleo et al., 2000; Brodribb and Holbrook, 2003; Sack and Holbrook, 2006; Johnson et al., 2009b). The K_{leaf} decline with dehydration arises at least in part from embolism in the vein xylem (Kikuta et al., 1997; Salleo et al., 2000; Salleo et al., 2001; Nardini et al., 2003; Trifilo et al., 2003a; Trifilo et al., 2003b; Cochard et al., 2004a; Brodribb and Holbrook, 2005; Choat et al., 2005; Brodribb et al., 2009; Johnson et al., 2009a). Cavitation in turn will depend on the intrinsic vulnerability of each vein, with major veins likely to be more vulnerable because of their long and wide conduits (Choat et al., 2005). We hypothesized that higher major vein density, by providing transport pathways around embolised major veins, would confer tolerance of K_{leaf} to dehydration, i.e., more negative Ψ_{leaf} values at 50% and 80% loss of K_{leaf} (P_{50} and P_{80} respectively). Such a role for leaf venation could be important in the optimization of leaf size. Leaf size is highly variable across

environments, with smaller leaves more frequent in dry habitats, both within and among species (Givnish, 1987; Sultan and Bazzaz, 1993; Gibson, 1998; Cunningham et al., 1999; Ackerly, 2003, 2004), as well as among community assemblages (Dolph and Dilcher, 1980; Fonseca et al., 2000). One advantage for small leaves is their thinner boundary layer enabling more rapid convective cooling (Vogel, 1968, 1970; Parkhurst and Loucks, 1972; Gibson, 1998; Vogel, 2009; Nobel, 2010). There may additionally be a direct hydraulic benefit of small leaves, if their greater major vein redundancy protects K_{leaf} from decline and thus contributes to drought tolerance. To test these hypotheses, we conducted computer simulations of the impact of vein cavitation on K_{leaf}. We compared theoretical results with experimentally-measured relationships among leaf hydraulic vulnerability, leaf size, venation architecture and other aspects of leaf drought tolerance for species diverse in leaf form and drought sensitivity.

MATERIAL AND METHODS

Computer simulations of the importance of vein architecture in leaf hydraulic vulnerability

Simulations of the impact of cavitation in leaves with varying venation architecture were generated using the program *K_leaf*, version 6 (written by H. Cochard, Institut National de la Recherche Agronomique, Clermont-Ferrand, France; Cochard et al., 2004b; McKown et al., 2010; available on request, *Herve.Cochard*@clermont.inra.fr). Based on specified parameters, *K_leaf* creates a spatially explicit model of a leaf with up to six vein orders represented as a square grid of xylem resistors and outside-xylem resistors ("mesophyll" resistors) branching orthogonally from each junction of the vein grid. In modeled leaves, water exits through the mesophyll resistor located at each vein junction, and the bulk of the water thus exits from the numerous minor veins. The model determines three parameters, K_x (leaf xylem conductance per leaf area), K_{ox} (outside-xylem conductance per leaf area), and K_{leaf}, where:

$$K_{leaf} = (K_x^{-1} + K_{ox}^{-1})^{-1}) \quad \text{eqn 1}$$

for leaves given specified size, densities and cross-sectional conductivities for each vein order, and mesophyll conductance. Simulations were modeled using an elliptical leaf with 12 pairs of second-order veins (2^o veins) and with vein densities and conductivities based on those for a *Juglans regia* terminal leaflet (Cochard et al. 2004). Our findings should be applicable to other leaves with hierarchical, reticulate venation (McKown et al., 2010). Individual vein conductivities (k_v) were based on estimations from xylem conduit lumen dimensions in *Juglans* vein cross-sections using the formula:

$$k_v = \sum \left(\frac{\pi a^3 b^3}{64\eta(a^2+b^2)}\right) \quad \text{eqn 2}$$

where *a* and *b* are the major and minor axes of ellipses, and η is the viscosity of water at 25°C (units are mmol m s^{-1} MPa^{-1}; Lewis and Boose, 1995; Cochard et al., 2004b; Sack and Frole, 2006). The K_x calculated by the model depends on the individual vein order conductivities and densities, and K_{ox} depends on the specified mesophyll conductance and the total vein density, which determines the number of junctions and thus of mesophyll resistors in parallel.

Values of K_x, K_{ox}, and K_{leaf} were determined in typical units, normalized by leaf area (mmol m^{-2} s^{-1} MPa^{-1}). The relative responses of K_x, K_{ox} and K_{leaf} to alteration of venation features in our simulations are expected to accurately indicate relative trends and principles of leaf venation design; however, the empirical values are not to be taken as meaningful, and units are not presented in our simulation results. For instance, the simulations based on the *Juglans* leaflet anatomical data set produced a K_x of 462 mmol m^{-2} s^{-1} MPa^{-1}, which is very high relative to experimentally measured K_x and many times greater than measured K_{ox} (Cochard et al., 2004b). Cochard et al. (2004b) introduced the "xylem hydraulic efficiency" parameter in *K_leaf* (XHE; modeled K_x divided by measured K_x) to calibrate the modeled K_x with measured values and thus

to account for other factors than xylem conduit numbers and diameters that cannot currently be modeled, such as pit membrane resistance (Sperry et al., 2005) or conduit blockage by embolism or tyloses (Salleo et al., 2002; Choat et al., 2005). In our simulations, XHE was set to 1. While not significant for this study, future work should better reconcile modeled K_x with experimentally measured values (McKown et al., 2010).

For this study, we focused on the impacts of simulated cavitation on K_x values, which would result in a reduction of K_{leaf}, by a degree that depends on the value of K_x relative to K_{ox}. The ratio of K_{ox} and K_x depends on species and on environmental variables that affect these compartments differently, but the available data suggest that K_{ox} and K_x are of similar magnitudes on average (Sack and Holbrook, 2006), and in that case, a given decline of K_x would reduce K_{leaf} by approximately half that amount. We also note that dehydration could also impact on the extra-xylem pathways, e.g., due to cell shrinkage and/or aquaporin deactivation (Kim and Steudle, 2007), which would lead to stronger overall impacts on K_{leaf}.

The program generates leaves of a specified size and number and arrangement of 2^o veins, from which it determines the 2^o vein density. Thus, designating leaves of given sizes leads to the 2^o veins being spaced further apart, just as observed in real leaves (Sack et al., 2008; see *Results*). The density of the minor veins (in this model, 3^o and higher) depends on the areole size, which is specified independently, and thus is manipulated independently of major vein density. We altered leaf size (and thus the density of 1^o and 2^o veins) and also minor vein densities, simulating a total of 42 leaves of six different sizes (4.8 to 65.4 cm²), associated with a 3.5-fold range of major vein densities (0.15-0.53 mm mm^{-2}) × seven different minor vein densities (spanning a 3.5-fold range; 2.8-8.7 mm mm^{-2}). For each leaf, we additionally applied cavitation "treatments" to determine the impact on K_x: (1) To test the impact of cavitating the major veins, we reduced the cross-sectional conductivities of the 1^o and 2^o veins by 90%, to simulate the great

majority of vessels being cavitated; and (2) To test the impact of cavitating the minor veins, we reduced the cross-sectional conductivities of the 3^{o}, 4°, 5° and 6° veins by 90%. For the simulated leaves of contrasting venation architecture, we present the percent loss of conductance of K_x that resulted from these treatments, i.e., the decline relative to a control, uncavitated leaf.

Plant material and leaf hydraulic vulnerability

Leaf hydraulic vulnerability was determined for ten species sampled in and around the campus of University of California, Los Angeles and Will Rogers State Park, Los Angeles, California in May-September 2008 (Table 3.1). Leaves were collected from mature trees and shrubs of nine species. Leaves from sunflowers (*Helianthus annuus*, var. Sunspot; Botanical Interests, Colorado, USA) were collected from greenhouse plants grown from seeds in 3.6 L pots (average minimum, mean and maximum values for temperature: 21.1, 23.2 and 26.0^{o}C; for humidity: 44, 51 and 59%). Sunflowers were irrigated every two days, with 200-250 ppm of 20:20:20 N:P:K; the light availability measured at mid-day on a sunny day was up to 550 µmol photon · m^{-2} · s^{-1}, and on average 300 µmol photon · m^{-2} · s^{-1} (LI-250 light meter; LI-COR Biosciences, Lincoln, Nebraska, USA). Species spanning a wide range of drought sensitivity were selected across nine families to include phylogenetic diversity. Five species were native to dry habitats and five species to moist habitats (Table 3.2).

Mature, healthy leaves were excised from sun-exposed branches rehydrated overnight. We used the evaporative flux method (EFM) to determine leaf vulnerability curves. We measured K_{leaf} as the light-acclimated steady-state transpirational flow rate for excised leaves (E, mmol · m^{-2} · s^{-1}) divided by the water potential driving force ($\Delta\Psi_{leaf}$, MPa; Sack et al., 2002; Scoffoni et al., 2008). The EFM was modified to allow determination of K_{leaf} at low Ψ_{leaf}. Shoots were cut into segments of three or more leaves under ultrapure water, and dehydrated with a fan

for different periods of time to achieve a range of Ψ_{leaf} values. Shoots were allowed to equilibrate for at least 30 min and then two leaves were excised and measured for initial Ψ_{leaf} (Ψ_o) using a pressure chamber (Plant Moisture Stress Model 1000; PMS Instrument Co, Albany, OR, USA). The third leaf (typically the middle leaf) was used to determine K_{leaf} with the EFM. The vulnerability curve was obtained by plotting K_{leaf} against whichever was lowest, Ψ_o or Ψ_{final} ("Ψ_{lowest}"), assuming this to be the Ψ_{leaf} associated with the strongest dehydration experienced during the experiment (bench-drying and K_{leaf} measurement). Species show different shapes in their vulnerability curve trajectories, as expected given variation in the importance of multiple mechanisms for the decline of K_{leaf} with dehydration (Brodribb and Holbrook, 2006). Thus, we determined each species' vulnerability curve, selecting among four functions used in the previous literature using maximum likelihood (Burnham and Anderson, 2002), using the *optim* function in R 2.9.2 (http://www.r-project.org; Burnham and Anderson, 2004; Sack et al., 2006; our scripts are available on request): linear ($K_{\mathrm{leaf}} = a\,\Psi_{\mathrm{leaf}} + y_o$), sigmoidal ($K_{\mathrm{leaf}} = \frac{\mathrm{a}}{1+\mathrm{e}^{-\left(\frac{\Psi_{\mathrm{leaf}}-x_0}{\mathrm{b}}\right)}}$), logistic ($K_{\mathrm{leaf}} = a/(1+(\frac{\Psi_{\mathrm{leaf}}}{x_0})^{\mathrm{b}})$) and exponential ($K_{\mathrm{leaf}} = y_0 + ae^{-b\Psi_{\mathrm{leaf}}}$). We used the best fit function for each species to estimate the maximum K_{leaf} for the hydrated leaf (K_{max}), and the Ψ_{leaf} at 50% and 80% loss of K_{leaf} (P_{50} and P_{80} respectively).

Quantification of leaf form and venation architecture

We determined venation traits for leaves from one leaf from an exposed branch for three individuals per species, from the same individuals measured for hydraulic vulnerability. Leaves were collected in May-September 2007 and fixed in formalin-acetic-acid solution (37% aqueous formaldehyde solution, 50% ethanol and 13% glacial acetic acid solution). Leaves were chemically cleared with 5% NaOH in ethanol, stained with safranin and counterstained with fast-

green (Berlyn and Miksche, 1976). Leaves were mounted with water in transparency film (CG5000, 3M Visual Systems Division, Austin, TX, USA) and scanned (flatbed scanner; Canon Scan Lide 90; 1200 pixels/inch). The leaf area, length, width, perimeter, and numbers and lengths of 1^o and 2^o veins were measured using Image J software, v. 1.42q (U. S. National Institutes of Health, Bethesda, Maryland, USA). Two indices of leaf shape were calculated: the length: width ratio and the perimeter^2: area ratio (a size-independent index of edge relative to size; Sack et al., 2003b). The 3^o vein lengths were measured for three rectangles per leaf (10 to 300 mm^2, depending on leaf size), located centrally in the top, middle and bottom thirds of the leaf. For each vein order, the vein density was calculated as length divided by leaf area; for 3^o veins, the vein densities were averaged across the three subsampled rectangles. Vein diameters, excluding the bundle sheath, were measured for each vein order by averaging six measurements (two made centrally in veins in the top, middle and bottom thirds of the leaf).

Measurements of the minor vein system were made under a light microscope (DMRB Leica Microsystems, Germany) with a 5× or 10× objective and digital camera (14.2 Color Mosaic, DIAGNOSTIC Instruments Inc., ENG0950, USA). Three rectangles were imaged (areas of 1.5 mm^2 or 6 mm^2) centrally in the top, middle and bottom thirds of the leaf, and the number of vein orders, density of minor veins (length per area) and the number of free vein endings per area, and vein diameters measured centrally in six segments were averaged across the rectangles. The major vein density was determined as the sum of 1^o, 2^o and 3^o vein densities and the minor vein density as the sum for 4° and higher order veins. The ratio of major to minor vein density was calculated for each leaf for every species.

Quantifying other key traits related to leaf drought tolerance

Morphological and physiological traits related to leaf drought tolerance were measured for six leaves from each of three to six individuals per species. Measurements were made of leaf area and of dry mass after oven-drying at least 48h at > 70°C to allow calculation of leaf mass per area (LMA, $g \cdot m^{-2}$). Leaf thickness was determined using digital calipers (Fowler, Chicago, IL), and leaf density was calculated as LMA divided by leaf thickness (Witkowski and Lamont, 1991). Cuticular conductance (g_{min}), the minimum conductance to vapor diffusion across the epidermis when the stomata are closed, was measured by weighing leaves as they dehydrated (Sack et al., 2003b; Sack et al., 2010). Parameters were determined from pressure-volume curves constructed by measuring leaf water potential and relative water content as leaves dehydrated (Tyree and Hammel, 1972; Sack et al., 2003b), including osmotic potential at full turgor (π_o, MPa) and at turgor loss point (π_{TLP}, MPa), saturated water content (*SWC*, $g \cdot g^{-1}$), modulus of elasticity (ε, MPa), and capacitances at full turgor and at turgor loss point (C_{FT} and C_{TLP}, MPa^{-1}; Sack and PrometheusWiki, 2010).

Statistical analysis of trait differences and correlations across species

To test trait differences between moist and dry habitat species (Table 3.2 and Table S3.1), we performed ANOVAs with species nested within habitat type (Minitab Release 15). Prior to tests, data were log-transformed to improve normality and heteroscedasticity (Sokal and Rohlf, 1995). We performed *t*-tests for leaf density, maximum K_{leaf}, P_{50} and P_{80} where only species mean values were available (Table S3.1).

A correlation matrix was determined to reveal the inter-correlative structure of hydraulic parameters, leaf size, venation architecture, and other traits putatively related to drought tolerance. For a conservative estimation, correlations were considered significant only if $P < 0.05$

for both Spearman and Pearson coefficients (r_s and r_p respectively). Because many relationships were non-linear, we determined Pearson correlations for both raw and log-transformed data.

When three variables of interest were inter-correlated across species, we performed partial correlation analysis (Sokal and Rohlf, 1995), testing the relationship between two variables holding the third variable constant (*corpcor* package; R; Schaefer et al., 2007).

RESULTS

Impacts of vein cavitation depend on venation architecture: computer simulations

Simulations implemented in the program *K_leaf* showed that the impacts of vein cavitation depended on vein density and leaf size (Fig. 3.1A, B and C; Table 3.1). Leaves were simulated of different sizes but with the same number of second-order (2^o) veins, and thus larger leaves had their 2^o veins spaced further apart, and major vein density declined geometrically with increasing leaf size (major vein density = $1.194 \times \text{leaf size}^{-0.5}$; $r_p = 0.999$; $P < 0.001$). By contrast, across the simulated leaves, minor vein density was varied independently of leaf size ($r_p = 0.02$; $P = 0.89$). K_x for uncavitated leaves correlated positively with both major vein density and minor vein density ($r_p = 0.75$; $P < 0.001$ and $r_p = 0.15$; $P = 0.01$ respectively).

When major veins were reduced by 90% in cross-sectional conductivity to simulate dysfunction of conduits due to embolism, the smaller leaves with greater major vein density showed a lesser impact on total xylem and whole leaf hydraulic conductance per leaf area (K_x and K_{leaf}), i.e., a lower percentage loss of conductance (PLC; Fig. 3.1A). Thus, across simulated leaves, the PLC of K_x resulting from major vein cavitation correlated negatively with major vein density ($r_p = -0.85$, $P < 0.001$). For the simulated leaves with cavitated major veins, the K_x itself correlated strongly with major vein density, due both to the increase of maximum K_x by higher major vein density, and the protective role of higher major vein density ($r_p = 0.97$; $P < 0.001$).

The importance of minor vein density was opposite from that of major vein density. A *higher* minor vein density increased the impact of cavitation of the major veins on the K_x (Fig. 3.1A). Thus, across the simulated leaves, the PLC of K_x resulting from major vein cavitation correlated positively with minor vein density (r_p = 0.42, P = 0.001). For these simulated leaves with cavitated major veins, the K_x was not related to minor vein density (r_p = 0.08; P = 0.57), because the greater K_x conferred by higher minor vein density was counteracted by a greater sensitivity to major vein cavitation. Overall, because of the contrasting effect of major and minor vein density, the PLC of K_x due to the cavitation of major veins was least for leaves with highest major vein density and lowest minor vein density, and correlated negatively with the ratio of major to minor vein density (Fig. 3.1C; r_p = -0.97 P < 0.001).

When the minor veins rather than the major veins were cavitated, K_x and K_{leaf} had a different dependency on venation architecture. When minor veins were reduced by 90% in cross-sectional conductivity to simulate cavitation, the smaller leaves with greater major vein density showed *higher* PLC of K_x (Fig. 3.1B). Thus, across simulated leaves, the PLC of K_x resulting from minor vein cavitation was positively related to major vein density (r_p = 0.77, P < 0.001). By contrast, a higher minor vein density reduced the impact of cavitation of the minor veins on the K_x (Fig. 3.1B). Thus, across the simulated leaves, the PLC of K_x resulting from minor vein cavitation was negatively correlated with minor vein density (r_p = -0.48, P = 0.001). For the simulated leaves with cavitated minor veins, the K_x itself correlated positively with minor vein density, due both to the increase of maximum K_x by higher minor vein density, and the protective role of high minor vein density (r_p = 0.66; P < 0.001). For these simulated leaves with cavitated minor veins, the K_x also positively correlated with major vein density, but more weakly than for uncavitated leaves, because the increase of maximum K_x due to higher major vein density was counteracted by the greater PLC driven by minor vein cavitation in leaves with

higher major vein density (r_p = 0.35 rather than 0.75; P < 0.001). Overall, the PLC of K_x resulting from cavitation of the minor veins was strongly positively correlated with the ratio of major to minor vein density (Fig. 3.1C; r_p = 0.92; P < 0.001).

Notably, in the model simulations, the PLC of K_x resulting from major vein cavitation varied widely across the entire range of tested leaves with different major and minor vein densities (22-87%; Fig. 3.1A and C). By contrast, the PLC of K_x resulting from minor vein cavitation was very strong across the entire range of tested leaves (62-90%, and > 80% for most simulated leaves; Fig. 3.1B and C).

Diversity in leaf venation and drought tolerance traits across species of moist and dry habitat

Across the ten species diverse in drought tolerance there were strong differences in leaf hydraulic conductance at full hydration, and in their vulnerability to dehydration. The species varied in K_{max}, P_{50} and P_{80} by 12- to 32-fold. The K_{max} varied from 2.96 to 34.1 mmol m^{-2} s^{-1} MPa^{-1} for *Comarostaphylos diversifolia* and *Platanus racemosa*, in P_{50} from -0.09 to -2.85 MPa for *P. racemosa* and *C. diversifolia*; and in P_{80} from -0.35 to -5.25 MPa for *P. racemosa* and *Cercocarpus betuloides* (Table S3.1).

The species differed strongly in leaf venation architecture and gross morphology, with substantial variation between moist and dry habitat species (Table 3.2; Table S3.1). Species varied fourfold in major vein density, threefold in minor vein density, and sevenfold in the ratio of major to minor vein density. Species of moist and dry habitats did not differ significantly in minor and total vein densities (P = 0.11-0.74), but dry habitat species had 18% higher major vein density (with 14-18% higher midrib, 2° and 3° vein densities) and 50% higher ratio of major to minor vein density. Moist habitat species had 24% more free ending veinlets per area, 13% higher minor vein diameters and 14% higher number of 2° veins than dry habitat species (P <

0.001). Moist and dry habitat species did not differ in the diameters of their major veins (Table S3.1). Species varied 18-fold in leaf area, with dry habitat species having on average 30% smaller leaves than moist habitat species. Leaf shape indices (length: width and perimeter^2: area) did not differ between habitats (P = 0.35-0.46).

Several venation traits correlated with leaf size. The densities of 1^o, 2^o and 3^o veins declined with increasing leaf size (r_p and r_s = -0.70 to -0.92, $P < 0.05$), as did the total major vein density (r_p=-0.95; r_s = -0.89, $P < 0.001$; Figs 3.2A and 3.3), and the ratio of major to minor vein density (r_p = -0.67; r_s = -0.70; P = 0.03). Major vein density declined geometrically with increasing leaf size (i.e., with an exponent of -0.5; Fig. 3.2A). By contrast, minor vein density was independent of leaf size (r_p and r_s = -0.10 to -0.20, $P > 0.05$; Figs 3.2B and 3.3), as were total vein density (as minor vein density accounted for 73-95% of total vein density), vein diameters and the number of free ending veinlets per area ($|r_p|$ and $|r_s|$ = 0.02-0.43, $P > 0.05$; Fig. 3.3; Table S3.2).

Species of dry habitats also had greater expression of leaf drought tolerance traits than species from moist habitats, with 14% higher leaf mass per area (LMA), 11% thicker leaves, 18% higher modulus of elasticity, 15%-16% more negative values for osmotic potential at full turgor and at turgor loss point, and 30% lower cuticular conductance. By contrast, species of moist habitats had on average two- to threefold higher saturated water content and capacitances before and after turgor loss point (Table S3.1; $P < 0.001$).

Relationships among hydraulic vulnerability, venation, and other drought tolerance and morphological traits

Across species, P_{50} and P_{80} were strongly correlated and more negative values occurred in leaves with higher major vein density and smaller leaf size ($|r_p|$ and $|r_s|$ = 0.78-0.90, $P < 0.01$; Figs 3.3,

4A and 4B; Table S3.2). These relationships for the major vein system also held for component vein orders; the densities of 1^o, 2^o and 3^o veins, all inter-correlated, were greater in leaves with more negative P_{50} and P_{80} ($|r_p|$ and $|r_s|$ = 0.64-0.90 $P < 0.01$). Because leaf size and major vein densities were themselves negatively correlated (Fig. 3.2A), no correlation could be observed of leaf hydraulic vulnerability with leaf size or with major vein density independently of the other. Thus, in a partial correlation analysis, the relationships of P_{50} and P_{80} with leaf area were not significant after partialing out major vein density, and their relationships with major vein density were not significant after partialing out leaf area ($|r_{partial}|$ = 0.08-0.29; $P > 0.05$). By contrast with major vein densities, other vein traits, including the minor vein density, total vein density, number of secondary veins, vein diameters, and number of free-ending veinlets per area did not correlate with P_{50} or P_{80} ($|r_p|$ and $|r_s|$ = 0.01-0.57, $P > 0.05$). The ratio of major: minor vein density was positively correlated with P_{50} and P_{80} (r_p and r_s = 0.77-0.67, $P < 0.05$; Table S3.2)

Leaf hydraulic vulnerability also correlated with several other drought tolerance traits. The osmotic potentials at full and zero turgor, which were inter-correlated (r_s and r_p = 0.95-0.98, $P < 0.001$), both correlated with P_{50} and P_{80} (r_p and r_s = 0.85-0.71, $P < 0.05$; Table S3.2). Leaves with higher LMA values tended to have more negative P_{80} (r_p = 0.71, r_s = 0.73, $P < 0.05$; Table S3.2) but LMA was not correlated with P_{50} ($P > 0.05$). However, both P_{50} and P_{80} were independent of other aspects of venation architecture and leaf morphology and physiology, including leaf shape indices (length: width and perimeter^2: area), the modulus of elasticity, capacitances at full and zero turgor, saturated water content, leaf thickness and density, and cuticular conductance ($P > 0.05$; Table S3.2).

The linkage of hydraulic vulnerability (P_{50} and P_{80}) with major vein density was independent from the relationships of hydraulic vulnerability to other leaf drought tolerance traits. The linkage of P_{50} or P_{80} with major vein density was apparently more fundamental. Thus,

partialing out LMA, or osmotic potentials at full and zero turgor did not remove the correlation of P_{50} or P_{80} with major vein density ($r_{partial}$ = 0.68 – 0.78; $P < 0.05$). However, when partialing out the effect of major vein density on P_{50} or $P_{80,}$ their correlations with LMA and with osmotic potentials at full and zero turgor were lost ($|r_{partial}|$= 0.04– 0.29; $P > 0.05$). Notably, the maximum leaf hydraulic conductance at full hydration did not correlate with any venation architecture or morphological trait including leaf size, or leaf drought tolerance, for this set of diverse leaves ($P > 0.05$).

DISCUSSION

The importance of major vein density and leaf size in resistance to drought

We found novel, strong correlations of P_{50} and P_{80} with major vein density and leaf size, across ten species with diverse leaves, consistent with findings from the computer model simulations. All else being equal, leaf and whole-plant drought resistance would be conferred by a higher major vein density, which is generally associated with small leaf size (Dunbar-Co et al., 2009; McKown et al., 2010).

Such a role for venation and leaf size in determining hydraulic vulnerability has important potential ecological and biogeographic implications. A link between leaf size and P_{50} and P_{80} provides a new additional mechanism for the ecological distribution of leaf sizes. Leaf size evolves relatively quickly via several independent genetic pathways (Ackerly, 2009; Gonzalez et al., 2010). Small leaves are more common in dry and exposed habitats, and larger leaves in moister and/or shaded habitats (Dolph and Dilcher, 1980; Givnish, 1987; Fonseca et al., 2000), and fossil leaf size is thus used as an indicator of past climate (Wilf, 1997). A direct hydraulic benefit of small leaves in drought tolerance, and the greater risk associated with large leaves under dry conditions, should thus be considered in addition to other demonstrated roles

for leaf size in determining drought tolerance. A very well-established benefit of smaller leaves in warmer environments is their thinner boundary layer and more rapid convective cooling (Nobel, 1976; Nicotra et al., 2008; Vogel, 2009; Yates et al., 2010). Another advantage of small leaves in exposed conditions is that more leaves can be packed into a smaller space to capture irradiance, though this benefit carries a greater cost in support mass; more branch allocation is needed to support many small leaves than for fewer larger leaves, and this outweighs the lower requirement for petiole and midrib support of smaller leaves (Bragg and Westoby, 2002; Niinemets et al., 2006, 2007). Future work needs to tease apart the importance of the direct hydraulic mechanism in providing an advantage in drought tolerance for smaller leaves from these other benefits across different species sets.

Is the relationship of hydraulic tolerance of dehydration to leaf size and higher major vein density necessarily causal? We considered the possibility that these relationships could be coincidental, i.e., that small leaf size and high major vein density on one hand, and more negative P_{50} and P_{80} on the other might be independently selected in drought-tolerant species. In our study, two lines of evidence supported a causal relationship. First, the relationship was established by the computer simulations of leaves with altered sizes and venation architecture, all else being held fixed. In these simulations, cavitation of the major veins as often observed during dehydration (see below), was better tolerated by smaller leaves with higher major vein density. Second, the partial correlation analyses of our experimental data showed that the relationship of venation architecture to leaf hydraulic vulnerability was independent of other drought tolerance traits, including turgor loss point (π_{TLP}). Indeed, π_{TLP} is the most reliable single predictor of species' drought tolerance to our knowledge (Auge et al., 1998; Sack et al., 2003b; Baltzer et al., 2008), and thus, if selection for drought tolerance were to result in a coincidental correlation of vulnerability and venation architecture, both should show underlying correlations with π_{TLP}. For

our ten species, P_{50} and P_{80} were strongly correlated with π_{TLP} (see also Crombie et al., 1985; Blackman et al., 2010), but venation architecture was unrelated to π_{TLP}. Further, P_{50} and P_{80} lost their relationship with π_{TLP} after partialing out major vein density, whereas they remained correlated with major vein density even after partialing out π_{TLP} , indicating that the relationships of P_{50} and P_{80} to major vein density are more directly causal than any relationships with π_{TLP} (Shipley, 2000).

We propose that the relationship between leaf size and hydraulic vulnerability in both simulated and real leaves supports a general mechanism, to be tested in other species sets, including closely-related species within lineages in a phylogenetic context, because smaller leaves have evolved reliably in drier habitats (Ackerly et al., 2002; McDonald et al., 2003; Dunbar-Co et al., 2009; Santiago and Kim, 2009). In our modeled leaves and experimental species set, as across species in general, leaf size and major vein density were linked (Dunbar-Co et al., 2009; McKown et al., 2010). Future studies of species similar in leaf size but different in major vein densities are necessary to establish the role of venation independently of size in determining P_{50} and P_{80}. A similar test could be conducted using *Arabidopsis* vein mutants of similar leaf size, with variation in major vein densities.

The potential roles of venation in determining K_{leaf} decline

The linkage of hydraulic vulnerability with venation architecture shown here would be expected because of the reduction of xylem conductivity, due to cavitation or collapse of conduits in the vein xylem, as previously shown by dye experiments, cryo scanning electron microscopy (cryoSEM), and acoustic methods (e.g., Kikuta et al., 1997; Salleo et al., 2000; Nardini and Salleo, 2003; Cochard et al., 2004a; Brodribb and Holbrook, 2005; Johnson et al., 2009a). Notably, other factors besides vein density can determine leaf hydraulic vulnerability, which is a

higher-level trait influenced by multiple lower-level traits (cf. Marks and Lechowicz, 2006; McKown et al., 2010). Thus, species may additionally differ in the air-seeding thresholds of xylem conduits, and in the responses of extra-vascular tissues to dehydration. Some small-leaved species in moist habitats might not have the low vulnerability suggested by their leaf size, if other factors were to over-ride the benefit of high major vein density. However, our findings from simulated leaves and from our ten species diverse in drought tolerance indicated a strong potential role of major vein density and leaf size in determining P_{50} and P_{80} across diverse species.

Model simulations showed that the vulnerability of K_x due to cavitation of major and minor veins were associated differently with venation architecture. Thus, loss of K_x resulting from cavitation in the major veins correlated with higher major vein density, the same relationship found in our experiments. However, loss of K_x resulting from cavitation in the major veins correlated with *lower* minor vein density. Further, the opposite patterns were found for loss of K_x when cavitation was simulated in the minor veins. These various model results can be understood according to the simple principle of the relative leverage of the major or minor veins in the overall vein system (cf. McKown et al., 2010). The hydraulic leverage of one vein system depends inversely on its density, i.e., its redundancy, relative to the other vein system, and cavitation has a stronger impact on the overall system when the leverage of that vein system is strongest. Thus, when the major vein density is higher, it has less leverage relative to the minor vein system, and cavitation of the major veins will cause a lower decrease in K_x and K_{leaf} (Table 3.1). By contrast, when the minor vein density is higher, the major vein system gains leverage relative to the minor vein system, and thus cavitation of the major veins would cause a greater decrease in K_x and K_{leaf} (Table 3.1). The model indicated that a higher major vein density is more effective for reducing hydraulic vulnerability due to major vein cavitation than a lower minor

vein density. The model showed that reducing minor vein density only led to a strong reduction in PLC (i.e., to a strong gain in tolerance) at high major vein density. Further, a higher major vein density also increases maximum leaf hydraulic conductance for well-hydrated leaves (K_{max}), both in absolute terms, and relative to vein construction cost, all else being equal, whereas a lower minor vein density leads to losses of K_{max} (McKown et al., 2010). Thus, for leaves with high major vein density, a low minor vein density might be a mechanism to achieve additional drought tolerance all else being equal, but at the cost of maximum hydraulic capacity and providing no gain in absolute conductance when the major veins are cavitated. The mechanism of achieving higher major vein density with small leaf sizes was found in the model simulations and experimental study to provide a strong benefit in reducing vulnerability and thus for drought tolerance.

Notably, the model findings indicated that leaves with higher major vein density, though less sensitive to cavitation of the major veins, were *more sensitive* to cavitation of the minor vein system. Thus, our empirical findings, of reduced vulnerability in leaves with higher major vein density suggested that major vein cavitation was more important than minor vein cavitation in driving loss of K_x and K_{leaf}. There are four lines of evidence that support the greater probability of cavitation in the major than minor veins. First, the major veins have wide and long xylem conduits especially vulnerable to air seeding (Choat et al., 2005). Second, in naturally dehydrated leaves, embolism is readily observed by cryo-scanning electron microscopy (cryoSEM) of major veins (Ball et al., 2004, 2006; Marenco et al., 2006; Johnson et al., 2009a), and acoustic studies have indicated cavitation in the major veins at Ψ_{leaf} values as high as -0.3 MPa (Crombie et al., 1985; Kikuta et al., 1997; Salleo et al., 2000; Johnson et al., 2009a). By contrast, the cryoSEM studies published thus far have not shown cavitation of minor vein conduits (Canny, 2001). Studies of dye uptake into transpiring leaves did show less staining of minor veins in dehydrated

leaves (Salleo et al., 2001; Nardini et al., 2003; Trifilo et al., 2003b); these findings are consistent with cavitation occurring principally in major veins, blocking uptake to the minor veins. Third, leaves that did not render their minor vein system resistant to cavitation would tend to be extremely sensitive to decline during drought, regardless of their venation architecture. The model simulations showed that cavitation of minor veins led to drastic decline in K_x across leaves of all venation architectures. As previously argued by Brodribb & Holbrook (2006), it seems improbable that leaves would invest in a fine vein network that becomes embolized at high water potentials and thus decline strongly in function. Fourth, a study of diverse angiosperms found that the leaf P_{50} was more negative in species with thicker-walled conduits in their minor veins (Blackman et al., 2010). That finding suggested that conduits are built to resist collapse at the tensions experienced during strong dehydration. In wood, such investment to avoid collapse signifies that the xylem can withstand cavitation to close to that degree of tension, as cavitation precedes collapse (Hacke and Sperry, 2001; Hacke et al., 2001; Blackman et al., 2010). Thus, minor vein conduits too should resist both cavitation and collapse at high levels of dehydration.

The collapse of xylem conduits during leaf dehydration cannot be entirely excluded. Collapse of conduits in the major or minor veins has never yet been shown for angiosperms but has been found in conifer needles dehydrated to water potentials ranging -1.5 to -3.5 MPa (Cochard et al., 2004a; Brodribb and Holbrook, 2005). Future studies are needed to analyze in detail the progression of cavitation and collapse in veins of different orders during leaf dehydration. Such work will also need to consider other aspects of the structure of the vein system, e.g, vessel widths, lengths and the degree that conduits span across vein orders, as these factors have been found to have great importance in stem vulnerability (Sperry, 2003; Sperry et al., 2005), and vary greatly across species (Sack and Frole, 2006). These aspects may contribute

to the correlation of vulnerability with low major vein density, because the major veins have especially long and wide vessels that span multiple orders. Other aspects of leaf vein arrangement, in addition to vein density, such as looping in the major veins might also influence resistance to hydraulic decline (Corson, 2010; Katifori et al., 2010).

While this discussion has focused on the decline of K_{leaf} with dehydration that is driven by declines in the xylem pathway conductivity, i.e., in K_x, there is also a potential role for declines in K_{ox} in the correlation of P_{80} with major vein density and leaf size. The K_{ox} may decline in dehydrating leaves due to changes in the permeability of membranes (Sack and Holbrook, 2006). Notably, given that a high major vein density would entail a large bundle sheath area by which water exits the major veins, if the lamina near the major veins accounts for a large part of transpiration (Fricke, 2002; Sack et al., 2002; Nardini et al., 2010) then leaves with high major vein density would likely maintain a greater bundle sheath area, and a greater K_{ox} when cells lose turgor in dehydrating leaves (Kim and Steudle, 2007). Additionally, we note that as leaves dehydrate, it is possible that K_{leaf}, the bulk leaf parameter, may not well describe the water transport pathways, if sectors or "patches" of lamina become isolated, each with their own hydraulic supply (cf. Barbour and Farquhar, 2004). Leaves with high major vein density may better provide for access of isolated leaf sectors to the lower-order vein distribution system. Future studies are needed of the impact of dehydration on the bundle sheath and mesophyll tissues, and on the potential heterogeneity of water supply in dehydrating leaves. Detailed characterization of the causes of K_{leaf} decline and its dependence on xylem and mesophyll characters will contribute to an ability to predict variation in species' drought responses from cell and tissue-level properties.

Relationship of leaf vulnerability to leaf and whole-plant drought tolerance

Our results also highlighted the importance of cell properties and leaf morphology in drought tolerance. Species from dry habitats had higher leaf mass per area (LMA) and modulus of elasticity, more negative osmotic potentials at full and zero turgor (π_{TLP}) and lower cuticular conductance than species from moist habitats, which by contrast had higher saturated water content (SWC) and capacitance. Further, the π_{TLP} correlated with P_{50} and P_{80} as shown in two previous studies (Crombie et al., 1985; Blackman et al., 2010). Given that stomata tend to close near the π_{TLP} (Hao et al., 2010), this linkage points to a control of stomatal aperture during drought by hydraulic vulnerability. The linkage might arise mechanistically, if a low osmotic potential in leaf tissues, reflected by $\pi_{TLP,}$ acted to reduce turgor loss and decline in membrane permeability (Canny and Huang, 2006). Alternatively, the π_{TLP} might be co-selected with P_{50} and P_{80} in drought tolerant leaves such that stomatal closure precedes hydraulic dysfunction. Our results were most consistent with this second possibility. In the partial correlation analysis, π_{TLP} had no impact on P_{50} and P_{80} when major vein density was partialed out. Thus, as found in the model simulations, leaf size and major vein density are putative causes of high P_{50} and P_{80}, whereas π_{TLP} is apparently a structurally independent but coordinated trait that modulates the leaf and plant response to drought.

The finding that major vein density and small leaf size reduce leaf hydraulic vulnerability points to potential roles in determining whole-plant drought tolerance. These traits may be especially important because the leaf is a key locus in whole-plant vulnerability, with typically greater hydraulic sensitivity than stems and roots (Hao et al., 2008; Brodribb and Cochard, 2009; Domec et al., 2009). Thus, for three of the four chaparral species in this study, the leaf P_{50} was 2.7 to 4.7 MPa lower than that previously reported for stems (Jacobsen et al., 2007), with only *Q. arbutifolia* having stems apparently similar to leaves in their vulnerability (-2 versus -2.4 MPa respectively). The importance of leaf hydraulic vulnerability in whole-plant drought tolerance

was further supported in this study both by the more negative P_{50} and P_{80} values for species of dry than moist habitats, and by the general correlation of these traits with others related to leaf drought tolerance. It is important to recognize, however, that there can be other possible routes to leaf drought tolerance than a low hydraulic vulnerability and thus being able to maintain hydraulic and photosynthetic function during drought. Thus, some species can achieve substantial drought tolerance via a low g_{min} and water storage, with an extreme development of this mechanism in succulent plants (Ogburn and Edwards, 2009). In this study, *Hedera canariensis* showed these mechanisms (Sack et al., 2003c; Metcalfe, 2005) possibly explaining its relatively high K_{leaf} vulnerability. Other species can achieve drought tolerance via an ability to tolerate low tissue water potentials via dehydrin expression that prevents mechanical failure of the cell walls (e.g., the resurrection fern *Polypodium polypodioide*; Layton et al., 2010). Species with these alternative mechanisms to maintaining hydraulic function can achieve large leaf sizes even given dry conditions (Nobel and Jordan, 1983). Further, we note that drought tolerance achieved at the level of the whole plant may not always correspond to leaf-level drought tolerance. Some species with drought-sensitive leaves can tolerate dry soil by shedding leaves or achieving deep roots, as is the case for *Lantana camara* (Castillo et al., 2007), which had relatively high K_{leaf} vulnerability. By contrast, some species with drought-tolerant leaves may be sensitive to drought in the field, due to relatively shallow roots (e.g., *Magnolia grandiflora*; Klos et al., 2009). Future work will establish the degree that even despite such complexity, key leaf traits such as major vein density, leaf size, and P_{50} and P_{80} contribute to drought tolerance. This work has strong potential to explain leaf function during drought from cell, tissue and organ-level physiological properties, and to predict the drought tolerance of diverse species and landscapes in current and extinct vegetation from their leaf traits.

ACKNOWLEDGMENTS

We thank Weimin Dang and the UCLA Plant Growth Facility, Art Gibson, and Phil Rundel for logistical assistance.

Table 3.1. Results of computer model simulations of the percentage loss of whole-leaf xylem hydraulic conductance (PLC of K_x) after reducing (a) major and (b) minor vein conductivities to simulate cavitation, in realistic leaves varying in major or minor vein density.

Leaf simulation	(a) Cavitation in major veins	(b) Cavitation in minor veins
Higher major vein density	Lower K_x decline	Greater K_x decline
Higher minor vein density	Greater K_x decline	Lower K_x decline
Higher major : minor vein density	Lower K_x decline	Greater K_x decline

Note: Contrasting impacts were found for the impacts of higher major and minor vein densities on the PLC of K_x due to vein cavitation, and contrasting impacts were found when cavitating major or minor veins. These effects can be understood in terms of the relative leverage of major or minor veins on the overall vein system. When the major vein density is increased, its greater redundancy gives the minor vein system a greater leverage; thus, the leaf is less sensitive to cavitation in the major veins and more sensitive to cavitation in the minor veins. By contrast, when the minor vein density is increased, its greater redundancy gives the major vein system a greater leverage; thus, the leaf is more sensitive to cavitation in the major veins and less sensitive to cavitation in the minor veins.

Table 3.2. Species, family, native range, and mean values ± standard error for morphological and physiological traits, and results of analyses of variance for the difference between moist and dry habitat species and among species nested within those categories. ***$P < 0.001$; NS, $P > 0.05$

Species	Family	Native range	Leaf area (cm^2)	Leaf mass per area ($g.m^{-2}$)	Major vein density (mm^{-1})	Minor vein density (mm^{-1})	Ratio major : minor vein density	Cuticular conductance ($mmol \cdot m^{-2} \cdot s^{-1}$)
Dry habitat species :								
Cercocarpus betuloides	Rosaceae	California. Mexico	7.04 ± 1.73	156 ± 19.9	1.40 ± 0.14	7.74 ± 0.76	0.19 ± 0.03	3.99 ± 0.41
Comarostaphylis diversifolia	Ericaceae	California. Mexico	7.93 ± 1.89	254 ± 7.73	1.57 ± 0.18	4.17 ± 0.18	0.38 ± 0.04	2.87 ± 0.35
Hedera canariensis	Araliacaeae	Canary Islands	53.2 ± 14.4	78.1 ± 6.32	0.53 ± 0.06	3.00 ± 0.10	0.18 ± 0.01	0.44 ± 0.03
Heteromeles arbutifolia	Rosaceae	California. Mexico	14.6 ± 2.89	146 ± 13.2	0.88 ± 0.04	4.63 ± 0.11	0.19 ± 0.005	4.21 ± 1.22
Quercus agrifolia	Fagaceae	California. Mexico	13.5 ± 1.32	166 ± 7.64	1.07 ± 0.07	7.30 ± 0.23	0.15 ± 0.02	1.72 ± 0.23
Moist habitat species :								
Camellia sasanqua	Theaceae	Japan	11.1 ± 0.45	144 ± 13.4	0.78 ± 0.04	3.31 ± 0.26	0.24 ± 0.03	1.77 ± 0.13
Helianthus annuus	Asteraceae	Across N. America	44.3 ± 1.64	56.2 ± 6.98	0.48 ± 0.03	9.32 ± 0.44	0.05 ± 0.002	18.3 ± 1.92
Lantana camara	Verbenaceae	Pantropical	12.8 ± 3.09	79.0 ± 4.48	0.97 ± 0.12	9.75 ± 0.40	0.11 ± 0.02	12.0 ± 0.85
Magnolia grandiflora	Magnoliaceae	Southern U.S.	69.5 ± 5.51	180 ± 17.3	0.48 ± 0.02	5.16 ± 0.29	0.09 ± 0.003	3.88 ± 0.41
Platanus racemosa	Platanaceae	California, Mexico	80.9 ± 2.79	109 ± 6.54	0.40 ± 0.06	4.97 ± 0.14	0.08 ± 0.01	6.61 ± 0.41
Average trait values	Dry area species		19.2 ± 4.44	162 ± 11	1.09 ± 0.09	5.18 ± 0.35	0.22 ± 0.04	2.65 ± 0.45
	Moist area species		43.7 ± 14.3	113 ± 9.75	0.62 ± 0.05	6.23 ± 0.33	0.12 ± 0.03	8.44 ± 0.82
ANOVA	Dry /moist		***	***	***	NS	***	***
	Species		***	***	***	***	***	***

FIGURE CAPTIONS

Figure 3.1. Results of computer model simulations of the percentage loss of whole-leaf xylem hydraulic conductance (PLC of K_x) after reducing by 90% (A) major and (B) minor vein conductivities to simulate cavitation for realistic leaves varying in major or minor vein density (n = 42 simulated leaves; see *Materials and Methods*). (C) The dependence of PLC of K_x due to cavitation of major (grey) and minor (black) veins on the ratio of major: minor vein density.

Figure 3.2. The scaling of vein density with leaf size for ten species varying strongly drought tolerance. (A) Major vein density versus leaf area. (B) The independence of minor vein density with leaf size. Symbols: grey, dry habitat species; white, moist habitat species. Fitted regression in (A): Major vein density = 0.32 × Leaf area$^{-0.53}$. ***P< 0.001; ^{NS}P > 0.05.

Figure 3.3. Relation of the vulnerability of leaf hydraulic conductance to major and minor vein densities for ten species varying strongly drought tolerance. Vulnerability curves are plotted in the left column; each point represents a different measured leaf (n = 26-74 per curve). For each vulnerability curve the fitted line is the maximum likelihood function for given species (linear for *C. sasanqua*, *C. diversifolia*, *Q. agrifolia*, and *H. arbutifolia*, logistic for *M. grandiflora*, *P. racemosa*, *H. annuus*, *H. canariensis* and *L. camara* and sigmoidal for C. betuloides; R^2 = 0.39-0.89; P < 0.001; see *Materials and Methods*) and the vertical line represents the water potential at 80% loss of conductivity (P_{80}). Leaf schematics are drawn to scale, with major veins (first- and second-order veins). Micrographs of the minor vein architecture are represented on the right, indicating the independence of minor vein density from leaf size; in each image, the largest vein

at the top is a second-order vein, with third-order veins branching off, and the minor veins make up the rest of the network.

Figure 3.4. Dependence of leaf hydraulic vulnerability, quantified as the water potential at 80% loss of conductivity (P_{80}) on (A) major vein density and (B) leaf area. Symbols: grey, dry habitat species; white, moist habitat species. Fitted regressions: (A) P_{80} = 4.2 × Major vein density – 0.92; (B) P_{80}= 28.2 × Leaf area$^{-0.84}$.

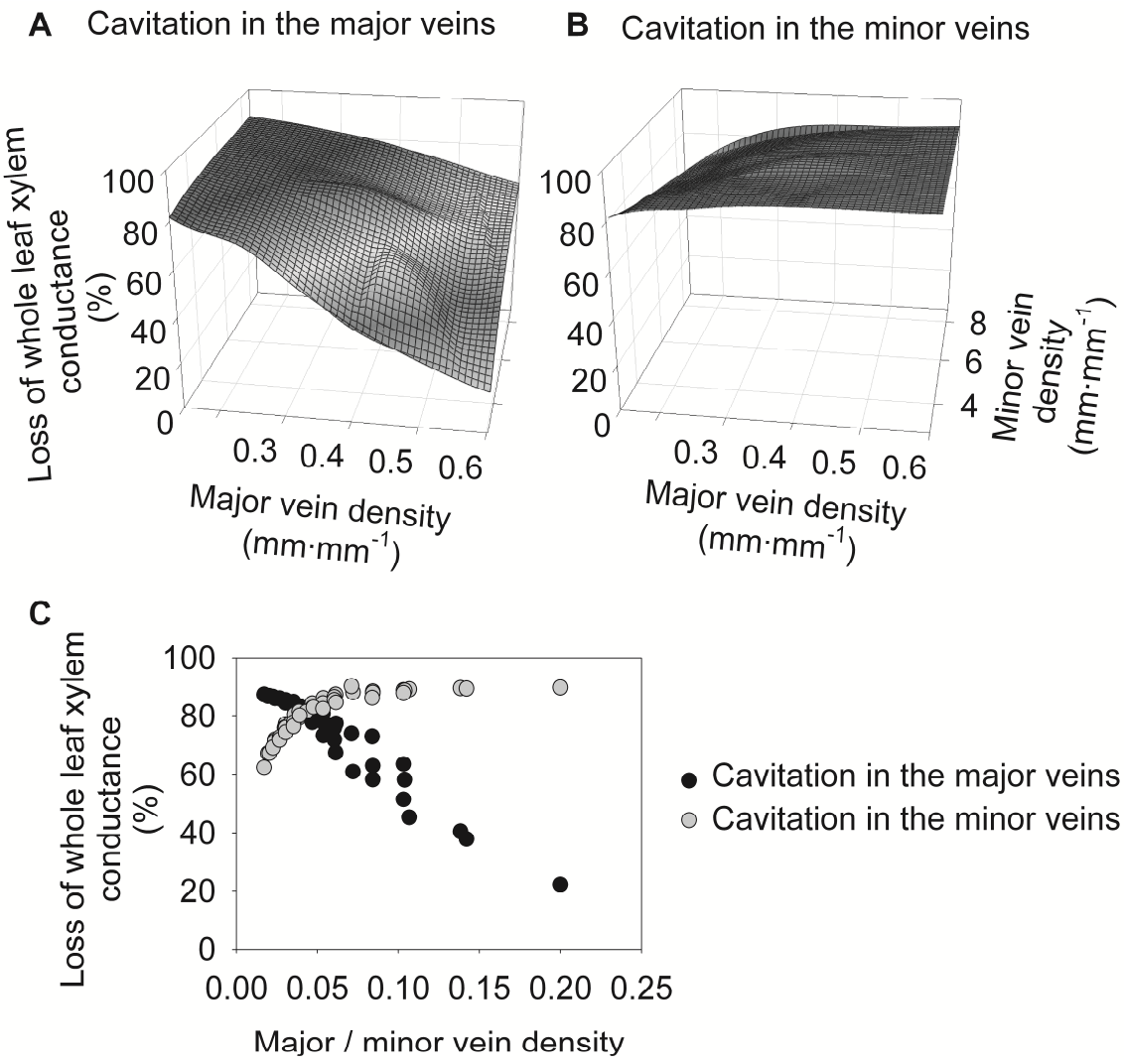
A Cavitation in the major veins
B Cavitation in the minor veins
Loss of whole leaf xylem conductance (%)
100
80
60
40
20
0
0.3 0.4 0.5 0.6
Major vein density (mm·mm-1)
8
6
4
Minor vein density (mm·mm-1)
C
0.00 0.05 0.10 0.15 0.20 0.25
Major / minor vein density
Cavitation in the major veins
Cavitation in the minor veins

Figure 3.1

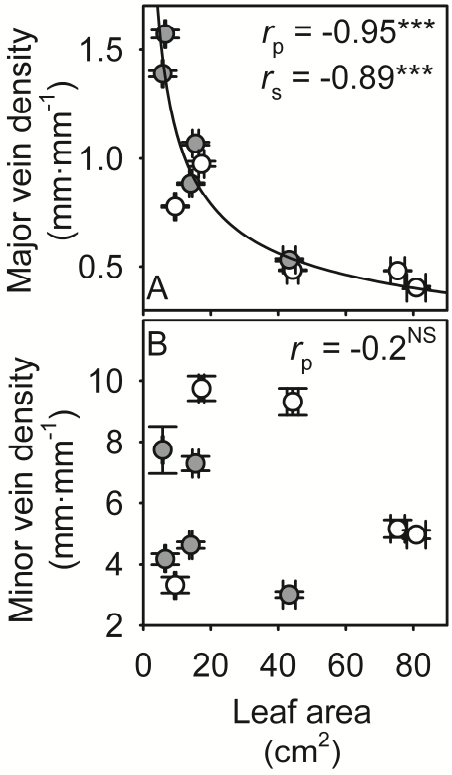
Major vein density
(mm·mm-1)
1.5
1.0
0.5
rp = -0.95***
rs = -0.89***
A
B
rp = -0.2NS
Minor vein density
(mm·mm-1)
10
8
6
4
2
0
20
40
60
80
Leaf area
(cm2)

Figure 3.2

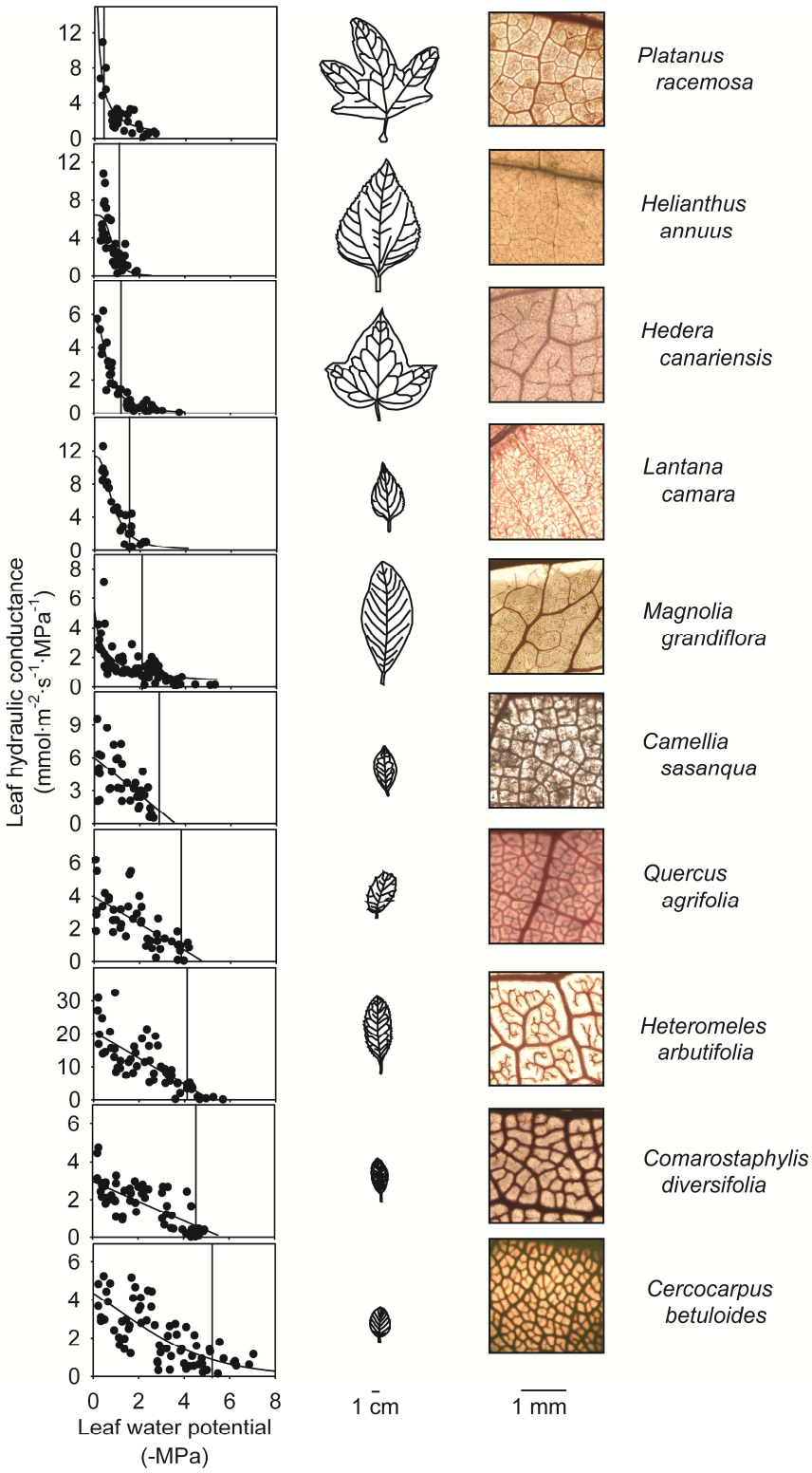
Leaf hydraulic conductance (mmol·m-2·s-1·MPa-1)
Leaf water potential (-MPa)
1 cm
1 mm
Platanus racemosa
Helianthus annuus
Hedera canariensis
Lantana camara
Magnolia grandiflora
Camellia sasanqua
Quercus agrifolia
Heteromeles arbutifolia
Comarostaphylis diversifolia
Cercocarpus betuloides

Figure 3.3

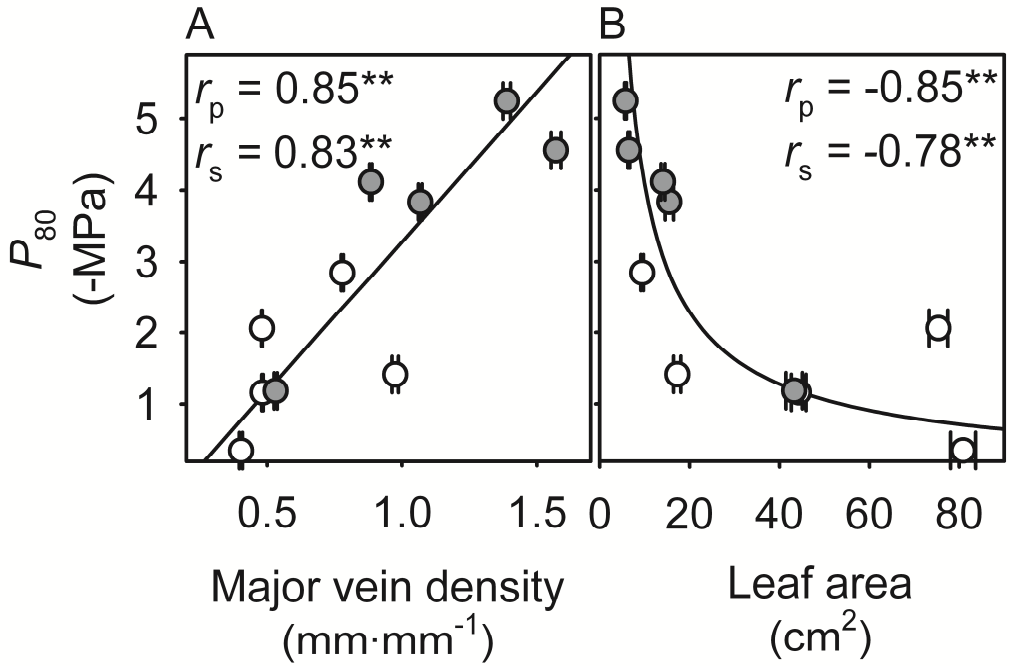
A
B
r_p = 0.85**
r_s = 0.83**
r_p = -0.85**
r_s = -0.78**
P_{80} (-MPa)
1
2
3
4
5
0.5
1.0
1.5
0
20
40
60
80
Major vein density (mm·mm^{-1})
Leaf area (cm^2)

Figure 3.4

SUPPLEMENTAL MATERIAL

Table S3.1. Species means ± standard errors for 24 morphological, anatomical and physiological traits and results of analyses of variance testing for species differences, and for differences between moist and dry habitat species. *** $P < 0.001$; ** $P < 0.01$; * $P < 0.05$; NS, $P > 0.05$.

Table S3.2. Correlation matrix for the relationship of leaf hydraulic vulnerability traits with venation architecture and other traits related to leaf morphology and drought tolerance. For each correlation the Spearman coefficient is presented, and the Pearson coefficient calculated with untransformed data and log-transformed data. Correlations are highlighted as significant only when Spearman and Pearson coefficients are both significant. *** $P < 0.001$; ** $P < 0.01$; * $P < 0.05$.

REFERENCES

Ackerly D (2009) Conservatism and diversification of plant functional traits: Evolutionary rates versus phylogenetic signal. Proceedings of the National Academy of Sciences of the United States of America **106:** 19699-19706

Ackerly DD, Knight CA, Weiss SB, Barton K, Starmer KP (2002) Leaf size, specific leaf area and microhabitat distribution of chaparral woody plants: contrasting patterns in species level and community level analyses. Oecologia **130:** 449-457

Ackerly DD (2003) Community assembly, niche conservatism, and adaptive evolution in changing environments. International Journal of Plant Sciences **164:** S165-S184

Ackerly DD (2004) Adaptation, niche conservatism, and convergence: Comparative studies of leaf evolution in the California chaparral. American Naturalist **163:** 654-671

Auge RM, Duan XG, Croker JL, Witte WT, Green CD (1998) Foliar dehydration tolerance of twelve deciduous tree species. Journal of Experimental Botany **49:** 753-759

Ball MC, Canny MJ, Huang CX, Heady RD (2004) Structural changes in acclimated and unacclimated leaves during freezing and thawing. Functional Plant Biology **31:** 29-40

Ball MC, Canny MJ, Huang CX, Egerton JJG, Wolfe J (2006) Freeze/thaw-induced embolism depends on nadir temperature: the heterogeneous hydration hypothesis. Plant Cell and Environment **29:** 729-745

Baltzer JL, Davies SJ, Bunyavejchewin S, Noor NSM (2008) The role of desiccation tolerance in determining tree species distributions along the Malay-Thai Peninsula. Functional Ecology **22:** 221-231

Barbour MM, Farquhar GD (2004) Do pathways of water movement and leaf anatomical dimensions allow development of gradients in $H_2{}^{18}0$ between veins and the sites of evaporation within leaves? Plant Cell and Environment **27:** 107-121

Berlyn GP, Miksche JP (1976) Botanical microtechnique and cytochemistry. Iowa State University Press, Ames, Iowa, USA.

Blackman CJ, Brodribb TJ, Jordan GJ (2010) Leaf hydraulic vulnerability is related to conduit dimensions and drought resistance across a diverse range of woody angiosperms. New Phytologist

Bragg JG, Westoby M (2002) Leaf size and foraging for light in a sclerophyll woodland. Functional Ecology **16:** 633-639

Brodribb TJ, Holbrook NM (2003) Stomatal closure during leaf dehydration, correlation with other leaf physiological traits. Plant Physiology **132:** 2166-2173

Brodribb TJ, Holbrook NM (2005) Water stress deforms tracheids peripheral to the leaf vein of a tropical conifer. Plant Physiology **137:** 1139-1146

Brodribb TJ, Holbrook NM (2006) Declining hydraulic efficiency as transpiring leaves desiccate: two types of response. Plant Cell and Environment **29:** 2205-2215

Brodribb TJ, Feild TS, Jordan GJ (2007) Leaf maximum photosynthetic rate and venation are linked by hydraulics. Plant Physiology **144:** 1890-1898

Brodribb TJ, Cochard H (2009) Hydraulic failure defines the recovery and point of death in water-stressed conifers. Plant Physiology **149:** 575-584

Brodribb TJ, McAdam SAM, Jordan GJ, Feild TS (2009) Evolution of stomatal responsiveness to CO_2 and optimization of water-use efficiency among land plants. New Phytologist **183:** 839-847

Brodribb TJ, Feild TS, Sack L (2010) Viewing leaf structure and evolution from a hydraulic perspective. Functional Plant Biology **37:** 488-498

Burnham KP, Anderson DR (2002) Model selection and multimodel inference, 2nd ed. New York, New York, USA. : Springer

Burnham KP, Anderson DR. (2004) Multimodel inference: understanding AIC and BIC in model selection. Sociological Methods & Research **33**, 261-304.

Canny MJ (2001) Embolisms and refilling in the maize leaf lamina, and the role of the protoxylem lacuna. American Journal of Botany **88:** 47-51

Canny MJ, Huang CX (2006) Leaf water content and palisade cell size. New Phytologist **170:** 75-85

Castillo JM, Leira-Doce P, Carrion-Tacuri J, Munoz-Guacho E, Arroyo-Solis A, Curado G, Doblas D, Rubio-Casal AE, Alvarez-Lopez AA, Redondo-Gomez S, Berjano R, Guerrero G, De Cires A, Figueroa E, Tye A (2007) Contrasting strategies to cope with drought by invasive and endemic species of *Lantana* in Galapagos. Biodiversity and Conservation **16:** 2123-2136

Choat B, Lahr EC, Melcher P, Zwieniecki MA, Holbrook NM (2005) The spatial pattern of air seeding thresholds in mature sugar maple trees. Plant, Cell & Environment **28:** 1082-1089

Cochard H, Froux F, Mayr FFS, Coutand C (2004a) Xylem wall collapse in water-stressed pine needles. Plant Physiology **134:** 401-408

Cochard H, Nardini A, Coll L (2004b) Hydraulic architecture of leaf blades: where is the main resistance? Plant Cell and Environment **27:** 1257-1267

Corson F (2010) Fluctuations and Redundancy in Optimal Transport Networks. Physical Review Letters **104:** 4

Crombie DS, Milburn JA, Hipkins MF (1985) Maximum sustainable xylem sap tensions in *Rhododendron* and other species. Planta **163:** 27-33

Cunningham SA, Summerhayes B, Westoby M (1999) Evolutionary divergences in leaf structure and chemistry, comparing rainfall and soil nutrient gradients. Ecological Monographs **69:** 569-588

Delaney KJ, Higley LG (2006) An insect countermeasure impacts plant physiology: midrib vein cutting, defoliation and leaf photosynthesis. Plant Cell and Environment **29:** 1245-1258

Dolph GE, Dilcher DL (1980) Variation in leaf size with respect to climate in the tropics of the Western-hemisphere. Bulletin of the Torrey Botanical Club **107:** 154-162

Domec JC, Noormets A, King JS, Sun G, McNulty SG, Gavazzi MJ, Boggs JL, Treasure EA (2009) Decoupling the influence of leaf and root hydraulic conductances on stomatal conductance and its sensitivity to vapor pressure deficit as soil dries in a drained loblolly pine plantation. Plant Cell and Environment **32:** 980-991

Dunbar-Co S, Sporck MJ, Sack L (2009) Leaf trait diversification and design in seven rare taxa of the Hawaiian *Plantago* radiation. International Journal of Plant Sciences **170:** 61-75

Ellis B, Daly DC, Hickley LJ, Johnson KR, Mitchell JD, Wilf P, Wing SL (2009) Manual of leaf architecture. Cornell university press and the New York botanical garden

Fonseca CR, Overton JM, Collins B, Westoby M (2000) Shifts in trait-combinations along rainfall and phosphorus gradients. Journal of Ecology **88:** 964-977

Fricke W (2002) Biophysical limitation of cell elongation in cereal leaves. Annals of Botany **90:** 157-167

Gibson AC (1998) Photosynthetic organs of desert plants. Bioscience **48:** 911-920

Givnish TJ (1987) Comparative studies of leaf form: assessing the relative roles of selective pressures and phylogenetic constraints. New Phytologist **106:** 131-160

Gonzalez N, De Bodt S, Sulpice R, Jikumaru Y, Chae E, Dhondt S, Van Daele T, De Milde L, Weigel D, Kamiya Y, Stitt M, Beemster GTS, Inze D (2010) Increased leaf size: different means to an end. Plant Physiology **153:** 1261-1279

Hacke UG, Sperry JS (2001) Functional and ecological xylem anatomy. Perspectives in Plant Ecology Evolution and Systematics **4:** 97-115

Hacke UG, Sperry JS, Pockman WT, Davis SD, McCulloch KA (2001) Trends in wood density and structure are linked to prevention of xylem implosion by negative pressure. Oecologia **126:** 457-461

Hao GY, Hoffmann WA, Scholz FG, Bucci SJ, Meinzer FC, Franco AC, Cao KF, Goldstein G (2008) Stem and leaf hydraulics of congeneric tree species from adjacent tropical savanna and forest ecosystems. Oecologia **155:** 405-415

Hao GY, Sack L, Wang AY, Cao KF, Goldstein G (2010) Differentiation of leaf water flux and drought tolerance traits in hemiepiphytic and non-hemiepiphytic *Ficus* tree species. Functional Ecology **24:** 731-740

Huve K, Remus R, Luttschwager D, Merbach W (2002) Water transport in impaired leaf vein systems. Plant Biology **4:** 603-611

Jacobsen AL, Pratt RB, Ewers FW, Davis SD (2007) Cavitation resistance among 26 chaparral species of southern California. Ecological Monographs **77:** 99-115

Johnson DM, Meinzer FC, Woodruff DR, McCulloh KA (2009a) Leaf xylem embolism, detected acoustically and by cryo-SEM, corresponds to decreases in leaf hydraulic conductance in four evergreen species. Plant Cell and Environment **32:** 828-836

Johnson DM, Woodruff DR, McCulloh KA, Meinzer FC (2009b) Leaf hydraulic conductance, measured in situ, declines and recovers daily: leaf hydraulics, water potential and stomatal conductance in four temperate and three tropical tree species. Tree Physiology **29:** 879-887

Katifori E, Szollosi GJ, Magnasco MO (2010) Damage and fluctuations induce loops in optimal transport networks. Physical Review Letters **104:** 4

Kehr J, Buhtz A (2008) Long distance transport and movement of RNA through the phloem. Journal of Experimental Botany **59:** 85-92

Kikuta SB, LoGullo MA, Nardini A, Richter H, Salleo S (1997) Ultrasound acoustic emissions from dehydrating leaves of deciduous and evergreen trees. Plant Cell and Environment **20:** 1381-1390

Kim YX, Steudle E (2007) Light and turgor affect the water permeability (aquaporins) of parenchyma cells in the midrib of leaves of *Zea mays*. Journal of Experimental Botany **58:** 4119-4129

Klos RJ, Wang GG, Bauerle WL, Rieck JR (2009) Drought impact on forest growth and mortality in the southeast USA: an analysis using forest health and monitoring data. Ecological Applications **19:** 699-708

Layton BE, Boyd MB, Tripepi MS, Bitonti BM, Dollahon MNR, Balsamo RA (2010) Dehydration induced expression of a 31-kDa dehydrin in *Polypodium Polypodioides*

(Polypodiaceae) may enable large, reversible deformation of cell walls. American Journal of Botany **97:** 535-544

Lewis AM, Boose ER (1995) Estimating volume flow-rates through xylem conduits. American Journal of Botany **82:** 1112-1116

Marenco RA, Siebke K, Farquhar GD, Ball MC (2006) Hydraulically based stomatal oscillations and stomatal patchiness in *Gossypium hirsutum*. Functional Plant Biology **33:** 1103-1113

Marks CO, Lechowicz MJ (2006) Alternative designs and the evolution of functional diversity. American Naturalist **167:** 55-66

McDonald PG, Fonseca CR, Overton JM, Westoby M (2003) Leaf-size divergence along rainfall and soil-nutrient gradients: is the method of size reduction common among clades? Functional Ecology **17:** 50-57

McKown Athena D, Cochard H, Sack L (2010) Decoding leaf hydraulics with a spatially explicit model: principles of venation architecture and implications for its evolution. The American Naturalist **175:** 447-460

Metcalfe DJ (2005) *Hedera helix* L. Journal of Ecology **93:** 632-648

Nardini A, Tyree MT, Salleo S (2001) Xylem cavitation in the leaf of *Prunus laurocerasus* and its impact on leaf hydraulics. Plant Physiology **125:** 1700-1709

Nardini A, Salleo S (2003) Effects of the experimental blockage of the major veins on hydraulics and gas exchange of *Prunus laurocerasus* L. leaves. Journal of Experimental Botany **54:** 1213-1219

Nardini A, Salleo S, Raimondo F (2003) Changes in leaf hydraulic conductance correlate with leaf vein embolism in *Cercis siliquastrum* L. Trees-Structure and Function **17:** 529-534

Nardini A, Raimondo F, Lo Gullo MA, Salleo S (2010) Leafminers help us understand leaf hydraulic design. Plant Cell and Environment **33:** 1091-1100

Nicotra AB, Cosgrove MJ, Cowling A, Schlichting CD, Jones CS (2008) Leaf shape linked to photosynthetic rates and temperature optima in South African *Pelargonium* species. Oecologia **154:** 625-635

Niinemets U, Portsmuth A, Tobias M (2006) Leaf size modifies support biomass distribution among stems, petioles and midribs in temperate plants. New Phytologist **171:** 91-104

Niinemets U, Portsmuth A, Tobias M (2007) Leaf shape and venation pattern alter the support investments within leaf lamina in temperate species: a neglected source of leaf physiological differentiation? Functional Ecology **21:** 28-40

Niklas KJ (1999) A mechanical perspective on foliage leaf form and function. New Phytologist **143:** 19-31

Nobel PS (1976) Photosynthetic rates of sun versus shade leaves of *Hyptisemoryi Torr*. Plant Physiology **58:** 218-223

Nobel PS, Jordan PW (1983) Transpiration stream of desert species: resistances and capacitances for a C3, a C4 and a CAM plant. Journal of Experimental Botany **34:** 1379-1391

Nobel PS (2010) Physicochemical and Environmental Plant Physiology Ed 4. Kindle Edition

Ogburn RM, Edwards EJ (2009) Anatomical variation in Cactaceae and relatives: trait lability and evolutionary innovation. American Journal of Botany **96:** 391-408

Parkhurst DF, Loucks OL (1972) Optimal leaf size in relation to environment. Journal of Ecology **60:** 505-537

Roth-Nebelsick A, Uhl D, Mosbrugger V, Kerp H (2001) Evolution and function of leaf venation architecture: a review. Annals of Botany **87:** 553-566

Sack L, Melcher PJ, Zwieniecki MA, Holbrook NM (2002) The hydraulic conductance of the angiosperm leaf lamina: a comparison of three measurement methods. Journal of Experimental Botany **53:** 2177-2184

Sack L, Cowan PD, Holbrook NM (2003a) The major veins of mesomorphic leaves revisited: Tests for conductive overload in *Acer saccharum* (Aceraceae) and *Quercus rubra* (Fagaceae). American Journal of Botany **90:** 32-39

Sack L, Cowan PD, Jaikumar N, Holbrook NM (2003b) The 'hydrology' of leaves: co-ordination of structure and function in temperate woody species. Plant Cell and Environment **26:** 1343-1356

Sack L, Grubb PJ, Maranon T (2003c) The functional morphology of juvenile plants tolerant of strong summer drought in shaded forest understories in southern Spain. Plant Ecology **168:** 139-163

Sack L, Frole K (2006) Leaf structural diversity is related to hydraulic capacity in tropical rain forest trees. Ecology **87:** 483-491

Sack L, Holbrook NM (2006) Leaf hydraulics. Annual Review of Plant Biology **57:** 361-381

Sack L, Melcher PJ, Liu WH, Middleton E, Pardee T (2006) How strong is intracanopy leaf plasticity in temperate deciduous trees? American Journal of Botany **93**, 829-839

Sack L, Dietrich EM, Streeter CM, Sanchez-Gomez D, Holbrook NM (2008) Leaf palmate venation and vascular redundancy confer tolerance of hydraulic disruption. Proceedings of the National Academy of Sciences of the United States of America **105:** 1567-1572

Sack L, PrometheusWiki (2010) Leaf pressure-volume curve parameters *In*. PrometheusWiki http://www.publish.csiro.au/prometheuswiki/tiki-pagehistory.php?page=Leaf pressure-volume curve parameters&preview=10

Sack L, Scoffoni C, PrometheusWiki (2010) Minimum epidermal conductance (g_{min} a.k.a. cuticular conductance) *In*. PrometheusWiki http://www.publish.csiro.au/prometheuswiki/tiki-pagehistory.php?page=Minimum epidermal conductance (gmin%2C a.k.a. cuticular conductance)&preview=

Salleo S, Nardini A, Pitt F, Lo Gullo MA (2000) Xylem cavitation and hydraulic control of stomatal conductance in Laurel (*Laurus nobilis* L.). Plant Cell and Environment **23:** 71-79

Salleo S, Lo Gullo MA, Raimondo F, Nardini A (2001) Vulnerability to cavitation of leaf minor veins: any impact on leaf gas exchange? Plant Cell and Environment **24:** 851-859

Salleo S, Nardini A, Lo Gullo MA, Ghirardelli LA (2002) Changes in stem and leaf hydraulics preceding leaf shedding in *Castanea sativa* L. Biologia Plantarum **45:** 227-234

Salleo S, Raimondo F, Trifilo P, Nardini A (2003) Axial-to-radial water permeability of leaf major veins: a possible determinant of the impact of vein embolism on leaf hydraulics? Plant Cell and Environment **26:** 1749-1758

Santiago LS, Kim SC (2009) Correlated evolution of leaf shape and physiology in the woody *Sonchus* alliance (Asteraceae: Sonchinae) in Macaronesia. International Journal of Plant Sciences **170:** 83-92

Schaefer J, Opgen-Rhein R, Strimmer K (2007) corpcor: Efficient estimation of covariance and (partial) correlation. R package version 1.4.7.

Scoffoni C, Pou A, Aasamaa K, Sack L (2008) The rapid light response of leaf hydraulic conductance: new evidence from two experimental methods. Plant Cell and Environment **31:** 1803-1812

Shipley B (2000) Cause and correlation in biology. Cambridge University Press

Sokal RR, Rohlf FJ (1995) Biometry: the principles and practice of statistics in biological research. Third edition. W.H. Freeman and Company

Sperry JS (2003) Evolution of water transport and xylem structure. International Journal of Plant Sciences **164:** S115-S127

Sperry JS, Hacke UG, Wheeler JK (2005) Comparative analysis of end wall resistivity in xylem conduits. Plant Cell and Environment **28:** 456-465

Sultan SE, Bazzaz FA (1993) Phenotypic plasticity in *Polygonum persicaria*. II. Norms of reaction to soil-moisture and the maintenance of genetic diversity. Evolution **47:** 1032-1049

Trifilo P, Gasco A, Raimondo F, Nardini A, Salleo S (2003a) Kinetics of recovery of leaf hydraulic conductance and vein functionality from cavitation-induced embolism in sunflower. Journal of Experimental Botany **54:** 2323-2330

Trifilo P, Nardini A, Lo Gullo MA, Salleo S (2003b) Vein cavitation and stomatal behaviour of sunflower (*Helianthus annuus*) leaves under water limitation. Physiologia Plantarum **119:** 409-417

Tyree MT, Hammel HT (1972) Measurement of turgor pressure and water relations of plants by pressure bomb technique. Journal of Experimental Botany **23:** 267-282

Uhl D, Mosbrugger V (1999) Leaf venation density as a climate and environmental proxy: a critical review and new data. Palaeogeography Palaeoclimatology Palaeoecology **149:** 15-26

Vogel S (1968) Sun leaves and shade leaves differences in convective heat dissipation. Ecology **49:** 1203-1204

Vogel S (1970) Convective cooling at low airspeeds and shapes of broad leaves. Journal of Experimental Botany **21:** 91-101

Vogel S (2009) Leaves in the lowest and highest winds: temperature, force and shape. New Phytologist **183:** 13-26

Wilf P (1997) When are leaves good thermometers? A new case for leaf margin analysis. Paleobiology **23:** 373-390

Witkowski ETF, Lamont BB (1991) Leaf specific mass confounds leaf density and thickness. Oecologia **88:** 486-493

Wylie RB (1938) Concerning the conductive capacity of the minor veins of foliage leaves. American Journal of Botany **25:** 567-572

Yates MJ, Verboom GA, Rebelo AG, Cramer MD (2010) Ecophysiological significance of leaf size variation in Proteaceae from the Cape Floristic Region. Functional Ecology **24:** 485-492

CHAPTER 4

LEAF SHRINKAGE WITH DEHYDRATION: COORDINATION WITH HYDRAULIC VULNERABILITY AND DROUGHT TOLERANCE

ABSTRACT

Leaf shrinkage with dehydration has attracted attention for over 100 years, especially as it becomes visibly extreme during drought. However, little has been known of its correlation with physiology. Computer simulations of the leaf hydraulic system showed that a reduction of hydraulic conductance of the mesophyll pathways outside the xylem would cause a strong decline of leaf hydraulic conductance (K_{leaf}). For 14 diverse species, we tested the hypothesis that shrinkage during dehydration (i.e., in whole leaf, cell and airspace thickness, and in leaf area) is associated with reduction in K_{leaf} at declining leaf water potentials (Ψ_{leaf}). We tested hypotheses for the linkage of leaf shrinkage with structural and physiological water relations parameters including modulus of elasticity (ε) and osmotic pressures at full turgor (π_o) and turgor loss point (TLP) and cuticular conductance. Species originating from moist habitats showed substantial shrinkage during dehydration before reaching TLP in contrast with species originating from dry habitats. Across species, the decline of K_{leaf} with mild dehydration (i.e., the initial slope of the K_{leaf} versus Ψ_{leaf} curve) correlated with the decline of leaf thickness (the slope of the leaf thickness versus Ψ_{leaf} curve), as expected based on predictions from computer simulations. Leaf thickness shrinkage before TLP correlated negatively with ε and positively with π_o, as did leaf area shrinkage between full turgor and oven-desiccation. These findings point to a role for leaf shrinkage in hydraulic decline during mild dehydration, with potential impacts on drought adaptation for cells and leaves, influencing plant ecological distributions.

INTRODUCTION

As leaves open their stomata to capture CO_2 for photosynthesis, water is lost to transpiration, which needs to be replaced by flow through the hydraulic system. The leaf hydraulic system has two components which act essentially in series: the pathways for water movement through the xylem from the petiole to leaf minor veins, and those through the living bundle sheath and mesophyll cells to the sites of evaporation (Tyree and Zimmermann, 2002; Sack et al., 2004; Sack and Holbrook, 2006). The decline in leaf hydraulic conductance (K_{leaf}) with dehydration may thus depend on both components. The importance of the xylem component is well established. Vein xylem embolism and cell collapse have been observed in dehydrating leaves (e.g., Salleo et al., 2001; Cochard et al., 2004; Johnson et al., 2009; Blackman et al., 2010), and computer modeling and experimental work showed species with high major vein length per leaf area (major VLA; i.e., for the first three vein branching orders) were more resistant to hydraulic decline, providing more pathways around embolisms (Scoffoni et al., 2011). However, the physical impacts of dehydration on the extra-xylem pathways have not been studied, even though in turgid leaves these pathways account for 26% to 88% of leaf hydraulic resistance (i.e., of $1/K_{leaf}$), depending on species (Sack et al., 2003; Cochard et al., 2004). The aim of this study was to determine whether leaf shrinkage during dehydration relates to the decline of K_{leaf}, and the structural determinants of leaf shrinkage.

The shrinkage of leaves with dehydration has drawn attention for over 100 years. Leaves shrink in their area (Bogue, 1892; Gardner and Ehlig, 1965; Jones, 1973; Tang and Boyer, 2007; Blonder et al., 2013) and, considered in relative terms, even more strongly in their thickness (Fig. 4.1; Meidner, 1952; Gardner and Ehlig, 1965; Downey and Miller, 1971; Syvertsen and Levy, 1982; Saini and Rathore, 1983; Burquez, 1987; McBurney, 1992; Sancho-Knapik et al., 2010; Sancho-Knapik et al., 2011). Leaves fluctuate in thickness daily and seasonally according to

transpiration (Kadoya et al., 1975; Tyree and Cameron, 1977; Fensom and Donald, 1982; Rozema et al., 1987; Ogaya and Peñuelas, 2006; Seelig et al., 2012). Indeed, the relation of leaf thickness to water status is so tight that using leaf thickness to guide irrigation has led to water savings of up to 45% (Seelig et al., 2012).

Previous studies of leaf shrinkage with progressive dehydration have tended to focus on single or few species. These studies showed that thickness declines with water status in two phases. Before the bulk leaf turgor loss point (leaf water potential at turgor loss point, TLP) is reached, the slope of leaf thickness versus leaf water potential (Ψ_{leaf}) or relative water content (*RWC*) is typically shallower than past TLP (Meidner, 1955, Kennedy and Booth, 1958, Burquez, 1987, McBurney, 1992, Sancho-Knapik et al., 2010; Sancho-Knapik et al., 2011). This is because before TLP, declining Ψ_{leaf} is strongly driven by declines in turgor pressure which have a relatively low impact on cell and airspace volume, whereas past the TLP, declining Ψ_{leaf} depends only on solute concentration, which increases in inverse proportion as cell water volume declines and cells and airspaces shrink (Tyree and Hammel, 1972, Sancho-Knapik et al., 2011). However, the steepness of the slope of leaf thickness versus Ψ_{leaf} before TLP seems to vary strongly across species (Meidner, 1955; Kennedy and Booth, 1958; Fellows and Boyer, 1978; Burquez, 1987; Colpitts and Coleman, 1997; Sancho-Knapik et al., 2010; Sancho-Knapik et al., 2011).

A high leaf cell volume and turgor is crucial to physiological processes (Boyer, 1968; Lawlor and Cornic, 2002). Shrinkage may affect cell connectivity and water transport (Sancho-Knapik et al., 2011). However, no studies have tested for a possible relationship of leaf shrinkage with the decline of K_{leaf} during dehydration. Such an association would arise if across species, shrinkage occurred simultaneously with vein xylem embolism, or if tissue shrinkage led to declines in the extra-xylem hydraulic conductance.

To refine our hypotheses, we modified a computer model of the leaf hydraulic system (Cochard et al., 2004; McKown et al., 2010; Scoffoni et al., 2011) to predict the impact of losses of xylem and extra-xylem conductance on the response of K_{leaf} to dehydration. We characterized the degree of leaf shrinkage in thickness, in the thickness of cells and airspaces within the leaf, and in leaf area for 14 species diverse in phylogeny, leaf traits and drought tolerance. We hypothesized that loss of extra-xylem hydraulic conductance should have a greater impact on K_{leaf} at less negative water potentials, when xylem tensions are too weak to trigger embolism and induce dramatic declines in K_{leaf}. We hypothesized that species with greater degree of shrinkage before TLP would experience greater loss of K_{leaf}. Further, we hypothesized that species from moist habitats would have greater degree of shrinkage.

For insight into the mechanisms and consequences of leaf shrinkage, we also investigated the relationships of 18 indices of leaf shrinkage with a wide range of aspects of leaf structure and composition, including gross morphology, leaf venation architecture, parameters of pressure-volume curves, and leaf water storage. We hypothesized that across species, shrinkage in whole leaf, cell, and intercellular airspace thickness would be lower for species with greater allocation to structural rigidity and osmotic concentration, and thus shrinkage would be positively correlated with a lower modulus of elasticity, higher osmotic pressure at full turgor, lower leaf mass per area and lower leaf density. Additionally, we tested the long standing hypothesis that species with higher major VLA and/or minor vein length per leaf area (minor VLA; i.e., the fourth and higher vein branching orders) would shrink less in area and/or thickness with dehydration (Gardner and Ehlig, 1965). Finally, we tested the ability of dehydrated leaves to recover in size with rehydration. We hypothesized that recovery would be greater for mildly than for strongly dehydrated leaves, and that species with greater leaf shrinkage would be better able to recover from shrinkage.

MATERIAL AND METHODS

Computer modeling of the theoretical importance of the xylem and extra-xylem water transport pathways for leaf hydraulic vulnerability

To refine our hypothesis that leaf shrinkage should influence leaf hydraulic vulnerability, we improved the *K_leaf* program (written by H. Cochard, INRA Clermont-Ferrand, France; Cochard et al., 2004; McKown et al., 2010; Scoffoni et al., 2011; available on request to Herve.Cochard@clermont.inra.fr) to generate leaf hydraulic vulnerability curves. *K_leaf* creates a spatially explicit model of a leaf with up to six vein orders represented as a square grid of xylem resistors and outside-xylem resistors ("mesophyll" resistors) branching orthogonally from each junction of the vein grid. In modeled leaves, water exits through the mesophyll resistor located at each vein junction, with the bulk of the water exiting from the junctions of the minor veins. The model determines the hydraulic conductances of the xylem and outside xylem pathways, and of the whole leaf (i.e., K_x, K_{ox}, and K_{leaf} respectively) for leaves simulated with a given leaf size, length and cross-sectional conductivity of each vein order, and mesophyll hydraulic conductance. *K_leaf* 6.1 (developed for this study from the previous v. 6.0) can simulate loss of hydraulic conductance in each vein order and the mesophyll, corresponding to the effects of embolism and shrinkage, according to a typical vulnerability curve (Pammenter and Vander Willigen, 1998):

$$PLC_i = 100/(1+e^{((s/25)\times(P_x - P_{50})}) \quad \text{(eqn 4)}$$

where PLC_i is the percent loss of hydraulic conductance in a given vein order or in the mesophyll, P_x is the pressure at that specific location, and s and P_{50} are specified parameters, i.e., the slope of the vulnerability curve and the P_x at PLC = 50%. Having specified these component PLC responses, one can use *K_leaf* 6.1 to generate leaf hydraulic vulnerability curves (i.e., K_{leaf} versus Ψ_{leaf}) by imposing different transpiration rates, obtaining leaves with a range of different

Ψ_{leaf} corresponding to different tensions across vein orders and mesophyll. Simulations were run using a realistic elliptical leaf with an area of 9.1 cm², with 12 pairs of second-order veins, and a total vein length per area of 6.9 mm mm^{-2}, and maximum vein cross-sectional conductivities (k_v) based on estimations from measured xylem conduit dimensions in *Juglans regia* (as described by Scoffoni et al., 2011). The findings would be applicable to other leaves with hierarchical reticulate venation (McKown et al., 2010).

We ran four types of simulations to test the relative impacts of differences in vulnerability between the vein xylem and extra-xylem mesophyll: (1) All the vein orders and the mesophyll were assigned the same vulnerability, with P_{50} of -1 MPa. (2) All the vein orders were assigned the same vulnerability, with P_{50} of -1 MPa, while the mesophyll was assigned greater vulnerability, with a P_{50} of -0.25 MPa. (3) All the vein orders were assigned the same vulnerability, with P_{50} of -0.25 MPa, while the mesophyll was assigned lower vulnerability, with a P_{50} of -1 MPa. (4) All the vein orders and the mesophyll were assigned the same vulnerability, with P_{50} of -0.25 MPa. We used a slope parameter of 200 MPa^{-1} in eqn 1 for all simulations, which is in the range of previously reported values (Pammenter and Vander Willigen, 1998). Because species also vary in the proportion of resistance distributed between xylem and outside-xylem pathways even when leaves are well hydrated (Sack et al., 2004; Sack et al., 2005), we ran each of the four simulations with two different parameterizations: (a) for well hydrated leaves, most hydraulic resistance was outside the xylem (the hydraulic resistance outside the xylem, R_{ox} = 71-76% of leaf resistance), or (b) for well hydrated leaves, most resistance was inside the xylem (R_{ox}= 36-42% of leaf resistance). To achieve these two types of leaves we modified the conductivities of the first and second vein orders and the mesophyll (because of their high impacts on K_x and K_{ox} respectively), such that the K_{leaf} at full hydration had a similar value (7.54-8.95 mmol m^{-2} s^{-1} MPa^{-1}).

For each simulation, we constructed vulnerability curves by plotting K_{leaf} against leaf water potential (Ψ_{leaf}), which was determined as equal to the mesophyll pressure. We fitted five types of functions to the curves, as previously used in the literature (Pammenter and Vander Willigen, 1998; Scoffoni et al., 2012) selecting the maximum likelihood model using the *optim* function in R 2.9.2 (http://www.r-project.org; Burnham and Anderson, 2002, 2004; Sack et al., 2006): linear ($K_{\mathrm{leaf}} = a\Psi_{\mathrm{leaf}} + y_0$, two-parameter sigmoidal ($K_{\mathrm{leaf}} = \frac{100}{1+e^{(a(\Psi_{\mathrm{leaf}}-\mathrm{b}))}}$) (Pammenter and Vander Willigen, 1998), three-parameter sigmoidal ($K_{\mathrm{leaf}} = \frac{a}{1+e^{-(\frac{\Psi_{\mathrm{leaf}}-x_0}{b})}}$), logistic ($K_{\mathrm{leaf}} = \frac{a}{1+(\frac{\Psi_{\mathrm{leaf}}}{x_0})^b}$) and exponential ($K_{\mathrm{leaf}} = y_0 + ae^{-b\Psi_{\mathrm{leaf}}}$). From the maximum likelihood function for each simulated whole-leaf vulnerability curve we estimated the K_{leaf} at Ψ_{leaf} = 0 MPa (K_{max}), the Ψ_{leaf} at which K_{leaf} = 0.5 K_{max} and 0.20 K_{max} (P_{50} and P_{80} respectively) and the initial slope of the vulnerability curve at Ψ_{leaf} = -0.1 MPa.

Experimental plant material

Leaf shrinkage and its relationship to other physiological traits were determined for 14 species from 12 plant families selected for diversity in leaf size, shape and drought tolerance. Species were sampled within and around the campus of University of California, Los Angeles and Will Rogers State Park, Los Angeles, California in November 2009-May 2011 (Table 4.2). Leaves from sunflowers (*Helianthus annuus*, var. Sunspot; Botanical Interests, Colorado, USA) were collected from greenhouse plants grown from seeds in 3.6 L pots (average minimum, mean and maximum values for temperature: 21.1, 23.2 and 26.0^{o}C; for humidity: 44, 51 and 59%). Sunflowers were irrigated every two days, with 200-250 ppm solution of 20:20:20 N:P:K, and the photosynthetically active radiation measured at mid-day on a sunny day was up to 550 µmol photon · m^{-2} · s^{-1}, and on average 300 µmol photon · m^{-2} · s^{-1} (LI-250 light meter; LI-COR Biosciences, Lincoln, Nebraska, USA).

Shoots with mature leaves were collected from the sun-exposed part of three individuals of each species (the entire stem for sunflowers), and re-cut and rehydrated overnight in ultrapure water (0.22 mm Thornton 200 CR; MilliPore, Molsheim, France).

Leaf shrinkage experiments: testing leaf responses to dehydration

Leaf shrinkage experiments were conducted on leaves detached from the rehydrated shoots of each species (n = 5 leaves per species), placed in sealed bags (Whirl-Pak; Nasco, Fort Atkinson,WI, USA) that had previously been exhaled in to prevent water loss. The parameters of shrinkage and hydraulics measured for excised leaves were assumed to be representative of those for leaves dehydrating on the plant (see Supplemental Materials and Methods).

To quantify leaf shrinkage, each leaf was measured for area, thickness, mass and volume at full hydration and during progressive dehydration (see Supplemental Materials and Methods for additional details). Leaves were taped by their petioles to a metal bar in front of a fan to dehydrate, and repeatedly removed for measurement. Leaf area was measured using a flatbed scanner (Canon Scan Lide 90; Canon USA Inc., NY) followed by image analysis (ImageJ software version 1.42q; National Institutes of Health). Leaf thickness was determined by averaging values taken in the centers of the bottom, middle and top thirds of the leaf, using digital calipers (± 0.01 mm; Fowler, Chicago, IL). Leaf mass was determined using an analytical balance (± 0.01 mg; XS205; Mettler Toledo, OH). Volume was determined as the product of leaf thickness and area. Once leaves had dehydrated beyond turgor loss point, or became too brittle to handle, they were placed in an oven for at least three days at 70°C before the dry leaf area, thickness and mass were determined.

We partitioned the leaf thickness (i.e., the volume per area) into that of the cells and airspace (cf. Roderick et al., 1999). The "thickness" of the cells ($T_{C,i}$), and of intercellular airspace ($T_{A,i}$) at each level i of dehydration were calculated:

$$T_{\mathrm{C,i}} = \frac{v_{water,\mathrm{i}}}{LA_{\mathrm{i}}} \quad \text{(eqn 5)},$$

$$T_{\mathrm{A,i}} = T_{\mathrm{i}} - T_{\mathrm{C,i}} \quad \text{(eqn 6)},$$

where v_{i} is the volume of water at level *i* of dehydration (i.e., fresh leaf mass minus dry mass, divided by 1.0 g cm^{-3}), and LA_{i} and T_{i} are the leaf area and thickness at dehydration level *i*. In this calculation, we assumed based on observations of anatomical cross-sections (John et al., in press) that the volume of the protoplasts and of airspace would each be much greater than that of the solid component of the cell wall. In our calculation, the volume of cell walls would be counted with that of the airspace. However, our calculation of shrinkage parameters involved changes in the dimensions of each component with changes in leaf water status, and these parameters would not be affected by the volume of cell wall, which would be effectively unchanged during leaf dehydration.

To plot leaf shrinkage responses, for leaf area (*A*); and the thickness of the leaf (*T*), cells (T_{C}) and airspace (T_{A}); and leaf volume (*V*); we calculated the absolute percentage loss at a given level of dehydration:

$$PLX_{\mathrm{i}}\ (\%) = \ (1 - \frac{X_{\mathrm{i}}}{X_{\mathrm{FT}}}) \times 100 \quad \text{(eqn 7)},$$

where X_{i}, and X_{FT} represent the leaf area, leaf thickness, leaf cell thickness, leaf airspace thickness, and leaf volume at dehydration level *i*, and for a fully turgid leaf respectively.

The relative water content (*RWC*, unitless) in the leaf at each dehydration level *i* was calculated as:

$$RWC_{\mathrm{i}} = \frac{m_{\mathrm{leaf,i}} - m_{\mathrm{leaf,dry}}}{m_{\mathrm{leaf,FT}} - m_{\mathrm{leaf,dry}}} \quad \text{(eqn 8)},$$

where $m_{\mathrm{leaf,i}}$ is the mass of the leaf at dehydration level *i*, $m_{\mathrm{leaf,FT}}$ is the mass of the leaf at full hydration and $m_{\mathrm{leaf,dry}}$ is the mass of the dry leaf (in g).

Leaf shrinkage experiments: *estimation of leaf water potential for dehydrating leaves*

For high resolution of the shrinkage responses of leaf dimensions, we plotted leaf shrinkage against leaf water potential (Ψ_{leaf}). We determined Ψ_{leaf} by summing the turgor pressure (Ψ_p), and solute potential (Ψ_s) estimated from the *RWC* using the fundamental leaf pressure-volume relationships (Bartlett et al., 2012):

$$\Psi_p = -\pi_o - (\varepsilon (1 - RWC_i)) \quad \text{(eqn 9)}$$

$$\Psi_s = \pi_o + \left(\frac{\pi_{TLP} - \pi_o}{RWC_{TLP} - 1} \right) (RWC_i - 1) \quad \text{(eqn 10)}$$

$$\Psi_{leaf} = \Psi_p + \Psi_s = \frac{(\varepsilon \times RWC_{TLP} + \pi_{TLP} - \varepsilon - \pi_o) RWC_i - \varepsilon \times RWC_{TLP} - \pi_{TLP} + \varepsilon + \pi_o}{RWC_{TLP} - 1} \quad \text{(eqn 11)}$$

where π_o and π_{TLP} are the osmotic potentials at full turgor and at turgor loss point (TLP) respectively (the negative of osmotic pressure, in MPa), ε is the modulus of elasticity (MPa) and RWC_{TLP} is the relative water content at TLP (%). Values for these parameters were species means obtained from pressure-volume curves (Table 4.2), previously published for the same plants for nine species (Scoffoni et al., 2008; Scoffoni et al., 2011) and using additional data collected in this study for *Bauhinia galpinii*, *Platanus racemosa*, *Romneya coulteri* and *Salvia canariensis* by measuring Ψ_{leaf} and *RWC* during progressive dehydration of initially rehydrated leaves (n = 5 leaves per species; Sack and PrometheusWiki, 2010). We assumed a constant ε in eqn 9, i.e, a linear decline of Ψ_p with *RWC*, though a nonlinear decline has been reported in a number of species (Robichaux, 1984), indicating a variable ε according to leaf water status. However, a linear approximation of Ψ_p with *RWC* between full turgor and TLP often fits experimental data (including for our species), and is common in the literature (Koide et al., 2000; Bartlett et al., 2012). Moreover, simulations showed that even declines of ε by several-fold between full turgor and TLP would in any case negligibly affect our calculations of Ψ_{leaf} using eqn 11 and the shrinkage traits calculated from it (data not shown).

Leaf shrinkage experiments: determination of the parameters of leaf shrinkage

To fully characterize leaf shrinkage with dehydration we calculated 18 traits for each species (see Table 4.3 for derivations and Table S4.5 for data), most of them relating to shrinkage in thickness rather than area since we found area shrinkage to be much smaller before TLP than thickness shrinkage. The 9 indices that we found to be most representative and useful included the percent loss of whole leaf thickness, leaf cell thickness, leaf airspace thickness and leaf area at turgor loss point ($PLT_{leaf,TLP}$, $PLT_{C,TLP}$, $PLT_{A,TLP}$ and $PLA_{leaf,TLP}$), the percent loss of thickness and area for the dry leaf compared with the turgid leaf, and the slopes of percent cell ($dT_C/d\Psi$), intercellular airspace ($dT_A/d\Psi$) and total leaf thickness ($dT_{leaf}/d\Psi$) against Ψ_{leaf} between full turgor and TLP. These 9 key indices were strongly correlated with 9 additional parameters of leaf shrinkage which we determined for a comprehensive approach (Table S4.4; see Supplemental Methods).

Leaf rehydration experiments

We determined the recovery of leaf thickness for dehydrated leaves after rehydration using experiments on leaf discs (after Milburn, 1966). Shoots with healthy, mature sun-exposed leaves were collected from three individuals of ten species, re-cut under pure water in the lab, and rehydrated overnight. The next day, leaves were placed underwater, and discs of 2 - 5 cm^2 depending on leaf size, were cut centrally between midrib and lamina (n= 5 per species), toweled dry and measured for thickness and mass at full hydration. Next, shoot segments containing four leaves were re-cut under water and left to dehydrate on the bench or over a fan, such that leaves could be sampled either (1) between full turgor and turgor loss point, or (2) dehydrated past turgor loss point. Then, each individual leaf on the shoot was sealed, still on the shoot, in a plastic sealable bag (Whirl-Pak; Nasco, Fort Atkinson,WI, USA) which was previously exhaled in. The shoot was then placed in a sealed plastic zipper bag with wet paper towels, and left to equilibrate for at least 15 minutes and up to 2 hours (as necessary for more dehydrated shoots),

after which the Ψ_{leaf} was measured for the top and bottom leaf of the shoot using a pressure chamber (Plant Moisture Stress, Model 1000, Albany, OR, USA), and if these differed by more than 0.2 MPa, the shoot was discarded. Leaf discs were cut from the two remaining leaves. As one treatment, leaf discs were cut under water to minimize the effect of embolism of the leaf xylem in dehydrated leaves in delaying or preventing rehydration and recovery of tissue dimensions. As a second treatment, using different shoots, leaf discs were cut in air to test whether embolism of xylem and mesophyll cell walls would affect disc rehydration; these discs were then dipped in water to achieve a similar initial condition as those that were cut under water. Leaf discs were immediately placed in sealable plastic bags which had been previously exhaled in. Initial thickness and mass was measured for each disc using digital calipers and balances described above. Discs were then submerged under ultrapure water with a height of 2- 4 mm in a petri dish to rehydrate for 1 h after which thickness and mass were measured. The percent recovery in thickness was measured by dividing thickness after 1 h rehydration by the average thickness at full hydration. If discs cut in air and under water did not differ significantly in their recovery, values were pooled.

Leaf hydraulic traits

We tested correlation of leaf shrinkage parameters with leaf hydraulics traits and cuticular conductance. Values for leaf hydraulics traits were obtained from vulnerability curves determined using the evaporative flux method for ten species (Scoffoni et al., 2011; Sack and Scoffoni, 2012; Scoffoni et al., 2012): K_{leaf} at full turgor (K_{max}) and at turgor loss point (K_{tlp}); the percent decline of K_{leaf} at turgor loss point (%K_{tlp}), the Ψ_{leaf} at 50 and 80% loss of K_{max} (P_{50} and P_{80}), and the slope of the hydraulic vulnerability curve at Ψ_{leaf} = -0.5 MPa ($dK_{leaf}/d\Psi$). For cuticular conductance (g_{min}) we used values previously published for the same plants (Scoffoni et al., 2011).

Leaf structural and compositional traits

We tested the correlation of shrinkage parameters with traits related to gross leaf morphology and composition determined from five leaves per species (sampled from at least three individuals). For the leaves used in the shrinkage experiments, we measured fully hydrated leaf area (cm^2) and thickness (mm), leaf mass per area (LMA, in g m^{-2}; dry mass / turgid leaf area), and leaf density (in g cm^{-3}; LMA / turgid leaf thickness). The fraction of leaf air, water and solid were measured for 4 to 10 leaves per species by water infiltration into the airspaces (after Roderick et al., 1999; Sack et al., 2003). The airspace "thickness" in a dry leaf was obtained by multiplying the thickness of the dry leaf by (1 – solid fraction), and the percent airspace in a dry leaf by dividing its airspace thickness by the thickness of the dry leaf.

Leaf water storage traits

Saturated water content (*SWC*), and leaf water storage capacitances at full turgor and turgor loss point (C_{FT} and C_{TLP}) were obtained for each species from the pressure-volume curves described above (Sack et al. 2003; Sack and PrometheusWiki, 2010). Leaf area specific capacitances at full turgor and turgor loss point (C^*_{FT} and C^*_{TLP} in mol m^{-2} MPa^{-1}) were then calculated:

$$C^*_{FT} = C_{FT} \times SWC \times LMA \quad \text{(eqn 20)},$$

$$C^*_{\mathrm{TLP}} = C_{\mathrm{TLP}} \times SWC \times LMA \times RWC_{\mathrm{TLP}} \quad \text{(eqn 21)}$$

Leaf venation traits

We tested the relationship of leaf shrinkage with published vein traits for the study plants (Scoffoni et al., 2011): major vein length per area, i.e., that of the first three branching orders of veins; the minor vein length per area, i.e., that higher vein branching orders; the total vein length per area (*VLA*, also known as "vein density"); the ratio of major to minor vein length per area and free vein endings per area.

Statistics

We tested *a priori* hypotheses for the coordination of shrinkage parameters with pressure-volume parameters, hydraulic traits and leaf structure and composition across species. As in previous studies using this approach (Brodribb et al., 2007; Waite and Sack, 2010; Scoffoni et al., 2011; Nardini et al., 2012), we thus did not correct individual correlations for multiple tests, and present a correlation matrix of all traits only to illustrate the inter-correlative structure of all measured traits (Table S4.3). We advise correction for multiple statistical tests before considering trait correlations that were not hypothesized *a priori*. Pearson coefficients were determined for both untransformed and log-transformed data, given that many relationships were nonlinear (Sokal and Rohlf, 1995). Spearman rank correlations were also determined, given that these are more robust to cases in which one or two outliers might drive a significant Pearson correlation (Sokal and Rohlf, 1995). For a conservative approach, we typically recognized relationships as significant only when $P < 0.05$ for both Spearman rank and Pearson correlations (r_s and r_p respectively).

Partial correlation analyses (Sokal and Rohlf, 1995) were conducted when three variables of interest were intercorrelated across species. These analyses tested the relationship between two variables when the third is statistically held constant (implemented using the *corpcor* package in *R*; Schaefer et al., 2007).

RESULTS

Computer simulations demonstrate potential importance of extra-xylem hydraulic decline

We used computer simulation modeling with *K_leaf* v. 6.1 (Cochard et al., 2004; McKown et al., 2010; Scoffoni et al., 2011) to determine the impact of vulnerability of the outside-xylem mesophyll pathways in driving decline of K_{leaf} with dehydration (Fig 4.2; Table 4.1; Table S4.1). We generated eight leaf hydraulic vulnerability curves based on different assumptions about the

distribution of hydraulic resistance and vulnerability characteristics of various components of the flow pathway. We considered two general cases: (a) most hydraulic resistance was within the outside-xylem component, i.e., the outside xylem hydraulic resistance (R_{ox}) > the xylem hydraulic resistance (R_x), or conversely, (b) $R_x > R_{ox}$. For each of these two general cases, we considered four vulnerability scenarios: (1) low vulnerability for xylem and outside-xylem components, (2) high vulnerability for only the outside-xylem component, (3) high vulnerability for only the xylem component, and (4) high vulnerability for the xylem and outside-xylem components (see *Methods* for additional details and parameterization of each scenario). Although the vulnerability of the xylem in given vein orders and in the mesophyll was specified in the *K_leaf* model by a two-parameter sigmoidal function (Pammenter and Vander Willigen, 1998; see *Methods*), in all modeled scenarios a three-parameter logistic function was selected by maximum likelihood for the leaf vulnerability curve; the emergent whole leaf response differed in structure from that specified for its components (Table S4.1).

Consistent with expectations, the simulations showed that whole leaves were more vulnerable when both xylem and outside-xylem mesophyll components were vulnerable. The outside-xylem vulnerability had a substantial impact on K_{leaf} vulnerability. Simulating a greater vulnerability to dehydration in only the outside-xylem component or only the xylem led to substantially less negative water potential at 50% and 80% loss of K_{leaf} (P_{50} and P_{80}) and steeper initial slopes than when simulating a low xylem and outside-xylem vulnerability (compare grey dashed or light grey dashed with black solid lines; Fig. 4.2; Table 4.1). Further, because the outside-xylem mesophyll component is a terminal hydraulic bottleneck, it is critical for protection of the xylem component. Across simulations, P_{50} was always considerably more negative than the pressure inside the xylem at P_{50} (2 to 8-fold more negative; Table 4.1). At given input values for the within-xylem and outside-xylem vulnerability, the leaf was less

vulnerable when more hydraulic resistance was found outside the xylem (i.e., when $R_{ox} > R_x$ rather than $R_x > R_{ox}$), with more negative P_{50} and P_{80} values and vulnerability curves with shallower slopes (Table 4.1; compare panel A and panel B in Fig. 4.2).

Further, the outside-xylem vulnerability played the greatest role in driving the initial vulnerability at mild water deficits. The initial slope of the vulnerability curve (before cavitation occurs) was steeper when the outside-xylem component was vulnerable than when only the xylem component was vulnerable (compare grey dashed and light grey dashed lines; Fig. 4.2; Table 4.1), and similar to that found when both xylem and outside-xylem components were vulnerable (compare grey dashed with grey solid lines Fig. 4.2; Table 4.1). By contrast, the behavior of the leaf vulnerability curve at stronger water deficits was strongly influenced by the xylem component; thus, the P_{80} values when both xylem and outside-xylem components were vulnerable were similar to that found in the simulation when only the xylem was vulnerable, substantially less negative than when only the outside-xylem was vulnerable (Fig. 4.2; Table 4.1). There was less difference across simulations in the P_{50} values (Table 4.1).

These findings indicated a strong impact of reduction in mesophyll hydraulic conductance on K_{leaf} vulnerability especially at high water potentials, with more pronounced effects of xylem embolism on K_{leaf} vulnerability under stronger dehydration (Fig. 4.2; Table 4.1).

Leaf shrinkage with dehydration: variation across diverse species

Species varied significantly in their leaf shrinkage with dehydration (Fig. 4.3) and in all 9 key leaf shrinkage parameters (one-way ANOVAs, $P < 0.001$; Tables 4.2, 4.3, 4.4 and 4.5 and Table S4.2; see Tables S4.2, S4.3 and S4.4 and Supplemental Results for additional parameters that were correlated with the 9 key parameters). Species varied 18-fold in the slope of thickness against Ψ_{leaf} before turgor loss point ($dT_{leaf}/d\Psi$), from -31 $\%\cdot MPa^{-1}$ for *Platanus racemosa*, which had slopes of cell and airspace thicknesses against Ψ_{leaf} before turgor loss point ($dT_C/d\Psi$

and $dT_A/d\Psi$ respectively) of -10 and -60 %·MPa^{-1} respectively, to -1.7 %·MPa^{-1} for *Quercus agrifolia* ($dT_C/d\Psi$ and $dT_A/d\Psi$ of -4.9 and -3.9 respectively). The $dT_C/d\Psi$ varied 3-fold across species from -4.1 for *Cercocarpus betuloides* to -13 %·MPa^{-1} for *Bauhinia galpinii*, and $dT_A/d\Psi$ was even more variable, ranging from an increase in airspace of 3.9 %·MPa^{-1} for *Q. agrifolia* to a reduction of airspace of 60 %·MPa^{-1} for *P. racemosa*. The maximum shrinkage in thickness (PLT_{dry}), i.e., that observed in a dry leaf relative to a fully turgid leaf, varied 4-fold across species from 23% for *Q. agrifolia* to 83% for *B. galpinii* (Table 4.5). Notably, the proportion of the leaf thickness constituted of cell versus air did not shift significantly between full turgor and turgor loss point. Across species, the mean ± SE for the percent cell and air thickness at full turgor ($PT_{C,FT}$ and $PT_{A,FT}$) were respectively 67 ± 4% and 33 ± 4%, very similar to those at turgor loss point ($PT_{C,TLP}$ and $PT_{A,TLP}$), 69 ± 5% and 31 ± 5% respectively (paired t-tests; P = 0.44-0.49; data in Table S4.2).

The coordination of leaf thickness shrinkage with turgor loss point also varied strongly across species. The percent loss of leaf thickness at turgor loss point ($PLT_{leaf,TLP}$) varied 8-fold among species from 4.6% for *Raphiolepis indica* to 38% for *Lantana camara* (Table 4.5). The cell shrinkage at turgor loss point ($PLT_{C,TLP}$) varied 2-fold among species from 11% for *C. betuloides* to 21 % for *Camellia sasanqua*, and the intercellular airspace shrinkage at turgor loss point ($PLT_{A,TLP}$) ranged from a gain in airspace in the leaf of 12% for *Q. agrifolia* to a loss of airspace of up to 77% for *L. camara* (Table 4.5). Species differences in $PLT_{leaf,TLP}$ were driven by changes in $PLT_{A,TLP}$ rather than $PLT_{C,TLP}$; there was a tight correlation of $PLT_{leaf,TLP}$ with $PLT_{A,TLP}$ (r_s = 0.94, r_p = 0.96; $P < 0.001$) but not with $PLT_{C,TLP}$ ($P > 0.05$).

Percentage shrinkage in leaf area was much lower than that for thickness. Loss of area at turgor loss point ($PLA_{leaf,TLP}$) ranged from 0.5% for *B. galpinii* to 14% for *H. annuus* (Table 4.5).

The maximum shrinkage in area (PLA_{dry}), i.e., that for a dry leaf, ranged 14-fold across species from 4.9% for *Heteromeles arbutifolia* to 69% for *H. annuus* (Table 4.5).

Species native to moist habitats experienced more shrinkage in thickness and area than species from dry habitats (see Supplemental Results for more details).

Coordination of leaf shrinkage responses and leaf hydraulic vulnerability

Across species, the slopes of the shrinkage curves for the whole leaf ($dT_{leaf}/d\Psi$) and the cells above turgor loss point ($dT_C/d\Psi$) correlated with the slope of the leaf hydraulic vulnerability curve at Ψ_{leaf} =-0.5 MPa ($dK_{leaf}/\underline{d}\Psi$), and with P_{50} and P_{80} (Fig. 4.4; Table S4.3). No significant correlations were found between the slope of the shrinkage curve for the intercellular airspaces ($dT_A/\underline{d}\Psi$) and $dK_{leaf}/\underline{d}\Psi$, P_{50} or P_{80} (Fig. 4.4; Table S4.3). Species with greater maximum shrinkage in leaf thickness (PLT_{dry}) tended to have higher maximum leaf hydraulic conductance (K_{max}) (r_p and r_s = 0.65, 0.68; $P < 0.05$; Table S4.3), and also experienced steeper $dK_{leaf}/\underline{d}\Psi$ (r_p and r_s = 0.76-0.88; $P < 0.05$; Table S4.3). No correlations were found between K_{leaf} at turgor loss point and leaf shrinkage traits ($|r_p|$ and $|r_s|$ = 0.02-0.42, $P > 0.05$; Table S4.3).

Recovery from shrinkage in thickness for leaves dehydrated before turgor loss point was high but not complete, ranging from 60% in *Magnolia grandiflora* to 99% in *Romneya coulterii* (Table S4.5). For 8/10 species tested, a similar recovery was found for leaves that had been dehydrated to before or past turgor loss point (Table S4.5 and supplemental results).

Correlation of leaf shrinkage with leaf pressure-volume parameters, water storage, structure, venation architecture and cuticular conductance

Across species, thickness shrinkage correlated with pressure-volume curve parameters (Fig. 4.5A-C), which themselves were strongly inter-correlated (Fig. 4.5F-O, Table S4.3). Species with more negative osmotic pressures at full turgor and turgor loss point (π_o and π_{tlp} respectively) and higher modulus of elasticity (ε) shrank less in thickness before turgor loss point and tended

to have shallower shrinkage slopes $dT_{leaf}/d\Psi$, $dT_C/d\Psi$, and $dT_A/d\Psi$ (r_p and r_s = 0.62-0.86, P < 0.05; Table S4.3). Leaf area shrinkage also related to pressure-volume parameters. A high $PLA_{leaf,TLP}$ correlated with low ε (r_p and r_s = -0.62 to -0.68, P < 0.05; Table S4.3). Maximum leaf shrinkage (PLA_{dry}) correlated with high π_o and π_{tlp} and low ε ($|r_p|$ and $|r_s|$ = 0.80-0.83, P < 0.001; Fig. 4.6A-D, Table S4.3).

Notably, due to the strong relationship between ε (MPa) and PLA_{dry} (%), a fitted power law equation could be used to estimate ε from PLA_{dry} (R^2= 0.66; P < 0.001):

$$\varepsilon = 41.4 \times PLA_{\mathrm{dry}}{}^{-0.522}. \qquad \text{(eqn 1)}$$

Leaf shrinkage traits also correlated with water storage traits. With few exceptions, the $dT_{leaf}/d\Psi$, $dT_C/d\Psi$, and $dT_A/d\Psi$ correlated with leaf capacitances (amount of water storage) at full turgor and turgor loss point, and with saturated water content (C_{FT}, C_{TLP}, and SWC respectively, defined in Table 4.4) (r_p and r_s values up to 0.93, P < 0.05; Table S4.3). The PLA_{dry} was positively correlated with C_{FT}, C_{TLP}, SWC and C^*_{TLP} (r_p and r_s = 0.55-0.86, P < 0.05; Table S4.3).

Across species, leaf shrinkage also related to leaf structure. The $PLT_{leaf,TLP}$ correlated negatively with leaf mass per area and leaf density (Fig. 4.5 D-E), as did $dT_{leaf}/d\Psi$, $dT_C/d\Psi$, and PLA_{dry} ($|r_p|$ and $|r_s|$ = 0.70 to 0.87, P < 0.05; Table S4.3). Species with thinner hydrated leaves tended to have higher PLA_{dry} (r_p and r_s = -0.57 to -0.62, P < 0.05; Table S4.3). Leaf shrinkage tended to be independent of leaf area across species; only Ψ_{T50} showed a positive correlation with mean leaf area (r_p and r_s = 0.55-0.58, P < 0.05; Table S4.3).

Leaf shrinkage was independent of most leaf vein traits. No correlation was found between $dT_{leaf}/d\Psi$ and major, minor or total vein length per area (r_p and r_s = 0.25-0.57, P > 0.05; Table S4.3). The few correlations observed between vein and shrinkage traits did not suggest causal dependency (Table S4.3).

Cuticular conductance (g_{min}) was positively correlated with a number of leaf shrinkage parameters, i.e., the $PLT_{leaf,TLP}$, $PLT_{A,TLP}$, $dT_{leaf}/d\Psi$, $dT_A/d\Psi$ and PLA_{dry} ($|r_p|$ and $|r_s|$ = 0.65-0.91; $P < 0.05$; Fig. 4.7, Table S4.3).

Separating the drivers of leaf shrinkage

Most leaf pressure-volume parameters and structural features that correlated with leaf shrinkage were themselves inter-correlated (Fig. 4.5 F-O, Table S4.3). To test for effects of single traits, holding others constant, partial correlation analysis was applied to (1) $PLT_{leaf,TLP}$, ε and π_o, (2) $dT_{leaf}/d\Psi$, $dK_{leaf}/d\Psi$, ε and π_o, (3) $PLT_{leaf,TLP}$, ε and g_{min}, (4) $PLT_{leaf,TLP}$, LMA, leaf density, ε and π_o, (5) PLA_{dry}, g_{min} ε and π_o (Table S4.6). These analyses enabled us to develop a model of the influences of given traits on leaf shrinkage and the hydraulic vulnerability of the xylem and outside-xylem pathways (Fig. 4.8). Briefly, a high major VLA provides lower xylem hydraulic vulnerability independently of leaf shrinkage, which influences the outside-xylem vulnerability. A low degree of shrinkage in thickness is achieved at the cellular level through both low ε and more negative π_o and linked to structural traits such as LMA and leaf density through ε. The ε also controls the maximum shrinkage in leaf area, which acts directly on cuticular conductance.

Consistent with this model for trait influences, we found that the effects of π_o and ε on leaf shrinkage were too inter-correlated to be distinguished. Thus, when accounting for the effect of either π_o or ε, the correlation between the other trait and the $PLT_{leaf,TLP}$ disappeared ($|r_{partial}|$ = 0.42-0.01, $P > 0.05$; Fig. 4.8; Table S4.6). Similarly, LMA and leaf density were strongly related to p-v parameters, and separate relationships with shrinkage could not be resolved (Figs 4.5 and 4.8); when removing the effect of LMA or leaf density, the correlation between $PLT_{leaf,TLP}$ and p-v parameters disappeared, and when removing the effect of p-v parameters, the correlation of leaf shrinkage with LMA or leaf density disappeared ($|r_{partial}|$ = 0.06-0.47, $P > 0.05$). However,

when removing the effect of $PLT_{leaf,TLP}$, the correlation between p-v parameters and LMA or leaf density remained ($r_{partial}$ = 0.70-0.82, $P < 0.01$).

Also consistent with our model for structural influences, we found that the linkages of leaf hydraulic vulnerability with the degree of leaf shrinkage were mediated by the p-v parameters π_o and π_{TLP} (Fig. 4.8). Accounting for the effect of $dT_{leaf}/d\Psi$ the correlation between $dK_{leaf}/d\Psi$ and π_o or π_{TLP} disappeared ($|r_{partial}|$ = 0.04-0.16, $P > 0.05$). However, the correlation between $dT_{leaf}/d\Psi$ and $dK_{leaf}/d\Psi$ remained even when accounting for the effects of π_o, π_{TLP} or ε, and the correlations between $dT_{leaf}/d\Psi$ and π_o, π_{TLP} and ε remained even when accounting for $dK_{leaf}/d\Psi$ ($|r_{partial}|$ = 0.61-0.74, $P < 0.05$; Table S4.6), indicating that the linkage of shrinkage to p-v parameters was more proximal than that of hydraulic vulnerability to p-v parameters.

Leaf shrinkage in thickness was apparently indirectly correlated with g_{min}. The correlation of $PLT_{leaf,TLP}$ and g_{min} seemed to be driven by their separate correlations with ε; when accounting for the effect of ε, the correlation between g_{min} and $PLT_{leaf,TLP}$ disappeared ($r_{partial}$ = 0.09 $P > 0.05$; Table S4.6), but ε and $PLT_{leaf,\ TLP}$ remained correlated after accounting for the effect of g_{min} ($r_{partial}$ = -0.66 $P < 0.05$). By contrast, maximum shrinkage in area still remained tightly correlated with g_{min} after accounting for the effect of ε or π_o ($r_{partial}$ = 0.90-0.91 $P < 0.001$; Fig. 4.8). The correlation between maximum shrinkage in area and ε or π_o lost its significance after accounting for the effect of g_{min} ($|r_{partial}|$ = 0.42-0.43 $P > 0.05$; Table S4.6).

Predicting leaf hydraulic vulnerability from thickness shrinkage and major vein density

Given the correlations of P_{50} and P_{80} with both major *VLA* and thickness shrinkage, and because according to our structural model these latter traits were related to the xylem and outside-xylem pathways, respectively, we tested whether they provided a strong prediction of P_{50} and P_{80}. Indeed, multiple regression analysis showed a greatly improved r^2 when using both thickness shrinkage and major *VLA* when predicting P_{50} or P_{80} (r^2 = 0.87 for both P_{50} or P_{80} when using

both shrinkage and major VLA versus r^2 = 0.74-0.72 for P_{50} or P_{80} respectively using only major *VLA*, and 0.52-0.55 for P_{50} or P_{80} respectively using only $dT_{leaf}/d\Psi$). The fitted models for predicting P_{50} and P_{80} were:

$$P_{50}\ predicted = 0.465 + 0.041 \times dT_{\mathrm{leaf}}/d\Psi + 1.79 \times \text{major } VLA \qquad \text{(eqn 2)}$$

$$P_{80}\ predicted = 1.20 + 0.070 \times dT_{\mathrm{leaf}}/d\Psi + 2.70 \times \text{major } VLA \qquad \text{(eqn 3)}$$

The observed P_{50} and P_{80} were strongly correlated with values predicted from these models, with the slope close to 1 (0.96-0.97) and r^2 = 0.87 (Fig. 4.9).

DISCUSSION

The results from computer modeling and experiments demonstrated that leaf shrinkage is a strong correlate and potential driver of leaf hydraulic vulnerability alongside other drivers such as xylem embolism and collapse, and aquaporin deactivation. Our detailed examination of leaf shrinkage provides new insight into its mechanisms and variation across species. Moreover, our results have strong ecological implications, given the great variation in shrinkage across species, with species native to dry habitat more resistant to shrinkage due to their more negative osmotic pressures at full turgor (π_o or turgor loss point(π_{tlp} = leaf water potential at turgor loss point, TLP) and higher modulus of elasticity (ε).

Impact of the mesophyll on leaf hydraulic vulnerability: insights from the computer model

Results from model simulations confirmed the hypothesis that decline in extra-xylem conductance should have strong impacts on leaf hydraulic conductance (K_{leaf}) vulnerability, especially at high leaf water potential (Ψ_{leaf}). The initial slope of K_{leaf} against Ψ_{leaf} was as steep when only the extra-xylem component was vulnerable to hydraulic decline as when both xylem and extra-xylem components were vulnerable. Similarly, the impact of extra-xylem vulnerability on the leaf water potential at 50% and 80% loss of hydraulic conductance (P_{50} and P_{80}) pointed

to a particular influence of the extra-xylem component on the early decline of K_{leaf}. The model simulations were consistent with a more vulnerable extra-xylem component protecting the xylem from tensions that would cause embolisms and/or stomatal closure. Along the hydraulic pathway, the tension generated by transpiration is dissipated by frictional losses proportional to hydraulic resistance. As expected, simulations showed that in leaves where the extra-xylem resistance (R_{ox}) > the xylem resistance (R_x), and thus the extra-xylem bottleneck was more pronounced, negative pressures would build up less strongly in the xylem for a given bulk leaf water potential (Ψ_{leaf}) than if $R_x > R_{ox}$. Substantial extra-xylem resistance protects the xylem water pressure from declining to values that would trigger air seeding, thus leading to the S-shaped curve seen in the simulation where only the xylem is vulnerable (Fig. 4.2, panel A, light-grey dashed line). Additionally, an $R_{ox} > R_x$ scenario allows cavitation to occur at more negative leaf water potentials than if $R_x > R_{ox}$ (Table 4.1). Further, regardless of the relative values of R_{ox} and R_x in the turgid leaf, extra-xylem vulnerability always had a strong impact on the decline of K_{leaf} at high Ψ_{leaf}. (Fig. 4.2, panel A and B, grey dashed lines). We note that this model assumed a steady state transpiration rate. The dynamics of mesophyll water potential could act directly on stomatal aperture and thus feedback on stomatal conductance and transpiration, but the principles shown here would act when steady state was established.

These model results are analogous to the hydraulic segmentation theory proposed for whole-tree architecture (Zimmermann, 1978). According to that theory, high resistances are found in the most distal parts of the trees (leaves, then lateral branches) so that tensions will be disproportionately large there, and reduced in proximal parts, thus delaying the onset of embolisms in the main trunk xylem, crucial for the tree's survival. We found that resistance in the extra-xylem component and its increase during leaf dehydration would prevent stronger tensions in the leaf vein xylem and delay the onset of xylem embolism or collapse. In essence,

vulnerability in the xylem- and extra-xylem pathways partitions the low water potential caused by a given transpiration rate; greater vulnerability in extra-xylem pathways preferentially partitions low potentials to the mesophyll, possibly delaying xylem embolism or stomatal closure.

Thus, in sum, decline in the extra-xylem conductivity, which would likely occur during leaf shrinkage, leads to strong K_{leaf} reductions, and protects the xylem from embolism during ongoing transpiration, which would lead to yet stronger K_{leaf} reductions, and potentially necessitate energy for refilling xylem conduits (Nardini et al., 2011).

Impact of leaf shrinkage on leaf hydraulic vulnerability

Previous studies showed that K_{leaf} decline in dehydrating leaves was correlated not only with xylem embolism but also with biochemical processes outside the xylem, such as aquaporin deactivation (Johansson et al., 1998, Kim and Steudle, 2007; Scoffoni et al., 2012). Our study is the first to implicate a physical influence of leaf shrinkage in the decline of K_{leaf} with dehydration, using the same correlational approach. These results support our model findings that extra-xylem hydraulic decline would in principle impact on K_{leaf}. Further, consistent with our hypotheses, and the results of the model simulations, our experiments using diverse species confirmed the hypothesis that K_{leaf} declines were correlated across species with leaf thickness shrinkage, especially at high Ψ_{leaf}. Species that experienced most severe shrinkage above turgor loss point had steeper initial K_{leaf} declines and less negative P_{80} values. The linkage of shrinkage with initial K_{leaf} decline was consistent with our hypothesis and model simulations.

Is there an adaptive hydraulic function for greater thickness shrinkage? Such a potentially adaptive mechanism was suggested by Zimmerman's segmentation theory and results from our model simulations. Thickness shrinkage reduces K_{leaf} when the mesophyll, but not yet the xylem itself, experiences more negative water potential; this would amplify any water status signal that

causes stomatal closure, thus preventing further decline in Ψ_{leaf} and sparing the xylem from embolism. Thus, species with xylem especially sensitive to air seeding would benefit from shrinkage that would reduce the conductance outside the xylem. Such "sacrifice" of mesophyll hydraulic conductance during dehydration would also be expected to delay intense cavitation during daily transpiration. This mechanism would be particularly useful given the partial reversibility of even strong leaf shrinkage shown by our rehydration experiments. After one-hour of rehydration, leaf discs had regained more than half their initial thickness, regardless of their level of dehydration (see Supplemental Results and Discussion).

Indeed, although shrinkage has not been previously investigated in this way, previous studies have pointed to a role of extra-xylem pathways in K_{leaf} decline (reviewed in Scoffoni et al., 2012). A recent study of *Arabidopsis* suggested that bundle sheath cells acted as valves during drought by converting chemical signals from the vein xylem such as ABA into a decrease in K_{leaf} by deactivating aquaporins (Shatil-Cohen et al., 2011). Our modeling and experimental work were consistent in implicating reductions in the extra-xylem pathways, whether caused by aquaporin deactivation, cell shrinkage or both, in the decline of K_{leaf} with dehydration. Future work is needed to fully resolve the roles of xylem and extra-xylem pathways, and their interaction in determining the response of K_{leaf} to dehydration.

Drivers of leaf shrinkage and its relation to leaf vulnerability

Our experiments provided insight into processes occurring within specific leaf tissues during shrinkage, especially at the epidermal cell layers (see Supplemental Discussion, "Mechanisms of leaf shrinkage"). What are the structural factors that influence leaf shrinkage and thus hydraulic vulnerability? Previous studies have reported correlation of hydraulic vulnerability with pressure-volume parameters π_o and π_{TLP} (Crombie et al., 1985; Blackman et al., 2010; Scoffoni et al., 2012). This linkage could arise because a more negative π_{TLP} enables cells to maintain

structural integrity, i.e., a higher *RWC* at lower Ψ_{leaf} (Blackman et al., 2010; Scoffoni et al., 2012). That hypothesis was supported in our study; the percent loss of thickness at turgor loss point ($PLT_{leaf,TLP}$) was lower in species with more negative π_o and higher ε. Our findings for the linkage of shrinkage with p-v parameters confirmed and expanded those of studies of fewer species. In one study of six species, leaves of woody plants shrank less than those of herbs, potentially due to their more negative π_o (Kennedy and Booth, 1958). In another study, species with low ε shrank more strongly in thickness (Syvertsen and Levy, 1982). In our study, partial correlation analysis could not tease apart the effects of π_o and ε on $PLT_{leaf,TLP}$, due to their strong association, and their combined impacts on determining cell shrinkage at turgor loss point and thus RWC_{TLP} (Bartlett et al., 2012). These results support the hypothesis that cell shrinkage depends on cell structural integrity, i.e., the p-v parameters, and shrinkage influences leaf hydraulic vulnerability.

Tissue shrinkage may affect K_{leaf} decline by altering the pathways for water movement. The precise pathways of mesophyll water movement and, indeed, the identity of the cells that are the sites of water evaporation, have remained puzzling questions for decades (Meidner, 1983). Three main pathways for water movement outside the xylem have been proposed: 1) water flows from the xylem to the bundle sheath cells and principally evaporates there (Boyer, 1985), 2) water flows mainly through or around epidermal cells, which have their walls better interconnected than mesophyll and palisade, and evaporates near stomata (Wylie, 1943; Sheriff and Meidner, 1974; Meidner, 1975) and 3) water evaporates from the mesophyll cells but an appreciable part evaporates as well from the epidermal cells (Farquhar and Raschke, 1978). Cell shrinkage can reduce connections for water to flow (Sancho-Knapik et al., 2011) and additionally would reduce evaporative surface; both effects would reduce K_{leaf}. Tissue shrinkage during transpiration might in fact highlight where water principally evaporates within the leaf,

and how it varies among species (Canny et al., 2012). While eucalyptus showed equal shrinkage throughout the mesophyll, suggesting that transpirational water evaporates throughout the leaf, cotton showed strongest shrinkage and potentially greater evaporation in the spongy mesophyll and in palisade cells surrounding the substomatal cavities (Canny et al., 2012). Whether the shrinkage of given leaf tissues or populations of cells have more effect than others on K_{leaf} (e.g., bundle sheath cells; see Scoffoni et al., 2012) remains to be elucidated. Further, it is unknown whether K_{leaf} decline is due to the direct effect of the physical impact of leaf shrinkage on hydraulic pathways, to an indirect effect of cell shrinkage on aquaporin activity (Johansson et al., 1998; Kim and Steudle, 2007), or both. The shrinkage of airspaces may reflect structural changes, i.e., cell wall buckling, that would reduce extra-xylem water flow, by reducing cell contact and/or the conductance of cell walls.

The strength of the correlation of K_{leaf} vulnerability with leaf shrinkage, together with the model simulation results, and the clear physical linkage of the pathways of water movement with cellular structure and tissue integrity, support a mechanistic linkage between vulnerability and shrinkage. An alternative argument, that the linkage of K_{leaf} vulnerability with leaf shrinkage is only circumstantial—i.e., that these responses are independently linked across species due to their association with moist habitat – remains possible. However, it is common to use physical principles to postulate a mechanistic basis for correlations. For example, this was used to establish connections between maximum K_{leaf} and leaf hydraulic vulnerability with xylem structure (i.e., with midrib conduit dimensions and vein length per area; Sack and Frole, 2006; Brodribb et al., 2007; Blackman et al., 2010; Scoffoni et al., 2011; Nardini et al., 2012), and here we have extended this approach to the extra-xylem pathways. Further validation of this hypothesis will require tests using mutant phenotypes in model species and/or mechanistic manipulations to establish absolute causality.

Coupling the effects of leaf shrinkage and leaf veins to better predict hydraulic vulnerability

Previous researchers hypothesized that leaf veins act as a "skeleton" that reduces leaf shrinkage during dehydration (Gardner and Ehlig, 1965). We found no relationship across species of the degree of shrinkage with major or total vein length per area. Instead, we found shrinkage to be closely related to leaf properties principally determined by mesophyll cells, π_o and ε. Notably, in some species, bundle sheath extensions (especially when fibrous) could play an important role in reducing shrinkage (Cutler, 2005; Pivovaroff et al., in press).

Previous work showed that the major vein length per area (major VLA) reduces the leaf hydraulic vulnerability, providing more pathways for the water to flow around embolisms (Scoffoni et al., 2011). Thus, leaf shrinkage and the venation architecture are independent factors that both influence the vulnerability of K_{leaf}, factors representing the xylem and outside-xylem components respectively. We found that including both major VLA and shrinkage led to a stronger ability to predict P_{50} and P_{80} than either factor alone, and eqns 2 and 3 provided a very strong prediction (Fig. 4.9), the strongest to our knowledge of leaf hydraulic vulnerability based on structural measurements. Previous work has also shown that P_{50} and/or P_{80} can be predicted across species by the dimensions of minor vein xylem conduits (Blackman et al., 2010) and that hydraulic decline of K_{leaf} and/or cell permeability can be related to properties of aquaporins and the effects of abscisic acid (Kim and Steudle, 2007; Shatil-Cohen et al., 2011). Our eqns 2 and 3 should be validated and extended with measurements for additional species, as they point to a great potential value for estimating hydraulic vulnerability from easily measurable traits.

Applications of leaf shrinkage for drought monitoring and drought tolerance assessment

Our findings support previous studies showing the uses of shrinkage for monitoring drought responses, i.e., for estimating *RWC* or Ψ_{leaf} from leaf thickness and area for given leaves (e.g., Meidner, 1952; Jones, 1973; Tyree and Cameron, 1977). Our study further points to the

importance of resistance to shrinkage as a trait contributing to drought tolerance (see Supplemental Discussion). Leaf shrinkage may have novel applications for rapid estimation of drought tolerance parameters. In addition to the ability of shrinkage to predict K_{leaf} vulnerability described above, the very strong relationship between the percent loss of area in a dry leaf (PLA_{dry}) and ε highlights the potential for estimation of ε using eqn 1, and easy, rapid measurements of PLA_{dry}. This equation should be validated and extended for additional species, for rapid estimation of ε, which typically is obtained from pressure-volume curves, which can take 1-2 days of measurements per species. Such rapid measurement of a key p-v parameter complements the recently described osmometer measurement of π_o and π_{TLP} (Bartlett et al., 2012).

Because species from drier habitat experienced less shrinkage in thickness, the percent loss of thickness in a dry leaf (PLT_{dry}) may be a good proxy trait for evaluating drought tolerance rapidly. By contrast PLA_{dry} may be of limited value as a drought tolerance predictor, though a good proxy for ε. Notably, ε is not a general predictor of drought tolerance—though it may contribute to tolerance of *incipient drought* by preventing early K_{leaf} decline, and/or contribute indirectly to drought tolerance by preventing cell shrinkage to lethal levels. Indeed, a recent study quantified PLA_{dry} in 380 diverse species (Blonder et al., 2013), and found PLA_{dry} to be slightly *higher* for dry habitat species, though that trend may have arisen due to error in their measurements. In that study, PLA_{dry} was determined without first rehydrating the leaves to full turgidity, and erroneous negative PLA_{dry} data were included in that study. Such errors need to be avoided for accurate species comparisons, especially if values are to be used as proxies for more intensive physiological or ecological parameters.

Summary

Leaf shrinkage was tightly correlated with hydraulic responses, leaf and cell structure and composition, and drought adaptation. Leaf shrinkage parameters can be used as proxies for estimating hydraulic vulnerability, modulus of elasticity and potentially drought adaptation. Future research on the anatomical basis of shrinkage, the precise mechanisms of leaf hydraulic decline, and the role of shrinkage-related traits in drought tolerance for a wide range of species can capitalize on these discoveries and improve the full range of their applications.

ACKNOWLEDGMENTS

We thank Megan Bartlett, Tom Buckley and Grace John for discussion and comments on the manuscript, Graham Farquhar and two anonymous reviewers for constructive suggestions and the Bartholomew Fellowship, Department of Ecology and Evolutionary Biology (UCLA) and the National Science Foundation (grants IOS-0753233 and IOS-1147292) for support.

Table 4.1. Results from model simulations testing the impacts on leaf hydraulic vulnerability of declines in conductivity in the xylem and outside-xylem pathways. For each set of simulations, we present the percent of the leaf hydraulic resistance outside the xylem for simulated leaves (R_{ox}), the input values for water potential at 50% loss for the within-xylem (xylem P_{50}) and outside-xylem components (outside-xylem P_{50}), and the results for maximum leaf hydraulic conductance (K_{max}), leaf water potential (Ψ_{leaf}) at 50% and 80% loss of leaf hydraulic conductance (P_{50} and P_{80}) and the initial slope of the leaf hydraulic vulnerability curve (at -0.1MPa), obtained from the logistic function ($K_{leaf} = \frac{a}{1+(\frac{\Psi_{leaf}}{x_0})^b}$) which was selected as the maximum likelihood model in all simulations (cf. Table S4.1).

Scenario	Simulations	Input conditions				Output of leaf-level responses			
		R_{ox} (%)	Xylem P_{50} (MPa)	Extra-xylem P_{50} (MPa)	K_{max} (mmol m^{-2} s^{-1} MPa^{-1})	P_{50} (MPa)	P_{80} (MPa)	P_{xylem} at P_{50} (MPa)	Initial slope (mmol m^{-2} s^{-1} MPa^{-2})
(a) R_{ox} > R_x	(1) Low vulnerability for xylem and outside-xylem components	74	-1.00	-1.00	8.62	-5.50	-11.6	-0.74	-0.09
	(2) high vulnerability for only the outside-xylem component	76	-1.00	-0.25	7.56	-2.37	-7.78	-0.28	-2.08
	(3) high vulnerability for only the xylem component	71	-0.25	-1.00	8.18	-1.53	-2.72	-0.32	-0.28
	(4) high vulnerability for xylem and outside-xylem components	74	-0.25	-0.25	7.26	-1.48	-3.83	-0.25	-1.97
(b) R_x > R_{ox}	(1) Low vulnerability for xylem and outside-xylem components	39	-1.00	-1.00	9.03	-2.49	-5.03	-0.78	-0.32
	(2) high vulnerability for only the outside-xylem component	42	-1.00	-0.25	8.32	-1.23	-3.92	-0.35	-4.50
	(3) high vulnerability for only the xylem component	36	-0.25	-1.00	8.02	-0.83	-1.78	-0.39	-3.06
	(4) high vulnerability for xylem and outside-xylem components	39	-0.25	-0.25	7.65	-0.68	-1.75	-0.30	-6.02

Table 4.2. Study species, family, mean ± standard error for leaf thickness, area, mass per area and pressure-volume parameters.

Species	Family	Plant habit	Leaf thickness at full turgor (mm)	Leaf area (cm^2)	Leaf mass per area ($g\ m^{-2}$)	Osmotic pressure at full turgor (MPa)	Osmotic pressure at turgor loss point (MPa)	Modulus of elasticity (MPa)	Relative water content at turgor loss point (%)
Moist habitat									
Bauhinia galpinii	*Fabaceae*	Shrub	0.17 ± 0.007	22.2 ± 1.44	45.0 ± 1.60	-1.15 ± 0.08	-1.41 ± 0.07	7.81 ± 1.61	81.4 ± 3.39
Camellia sasanqua†	Theaceae	Shrub	0.40 ± 0.01	12.8 ± 0.98	178 ± 9.08	-1.61 ± 0.13	-2.12 ± 0.18	7.98 ± 1.11	76.7 ± 3.35
Helianthus annuus†	Asteraceae	Herb	0.20 ± 0.01	101 ± 6.61	31.2 ± 1.06	-0.87 ± 0.12	-1.09 ± 0.12	5.49 ± 0.79	84.4 ± 1.50
Lantana camara†	Verbenaceae	Shrub	0.29 ± 0.01	16.8 ± 1.22	61.4 ± 4.18	-1.10 ± 0.04	-1.37 ± 0.04	4.85 ± 0.33	78.0 ± 2.30
Magnolia grandiflora†	Magnoliaceae	Tree	0.63 ± 0.04	77.2 ± 7.12	220 ± 11.0	-1.42 ± 0.02	-2.06 ± 0.05	13.3 ± 1.31	89.3 ± 1.20
Platanus racemosa	Platanaceae	Tree	0.17 ± 0.01	130 ± 14.4	56.3 ± 2.34	-0.93 ± 0.08	-1.19 ± 0.09	7.09 ± 0.25	87.0 ± 1.44
Raphiolepis indica†	Rosaceae	Shrub	0.52 ± 0.01	28.5 ± 2.55	211 ± 8.26	-1.37 ± 0.07	-2.07 ± 0.11	11.5 ± 0.81	88.3 ± 0.55
Dry habitat									
Cercocarpus betuloides†	Rosaceae	Tree	0.22 ± 0.02	8.57 ± 1.58	121 ± 23.3	-1.64 ± 0.04	-2.59 ± 0.03	10.1 ± 0.70	85.1 ± 0.80
Comarostaphylis diversifolia†	Ericaceae	Tree	0.49 ± 0.04	12.8 ± 0.61	253 ± 16.9	-2.51 ± 0.34	-3.45 ± 0.34	17.3 ± 2.23	85.5 ± 1.85
Hedera canariensis†	Araliaceae	Shrub	0.27 ± 0.02	67.2 ± 7.68	84.1 ± 11.0	-1.49 ± 0.07	-1.98 ± 0.09	12.8 ± 0.49	88.4 ± 1.40
Heteromeles arbutifolia†	Rosaceae	Shrub	0.38 ± 0.01	21.5 ± 2.06	185 ± 12.4	-2.08 ± 0.09	-2.53 ± 0.10	16.4 ± 0.49	87.4 ± 0.53
Quercus agrifolia†	Fagaceae	Tree	0.30 ± 0.01	14.2 ± 0.70	188 ± 7.53	-2.31 ± 0.12	-3.00 ± 0.12	17.9 ± 1.28	87.5 ± 1.59
Romneya coulteri	Papaveraceae	Herb	0.36 ± 0.01	23.9 ± 0.67	78.1 ± 3.67	-1.01 ± 0.08	-1.40 ± 0.07	6.78 ± 0.33	87.2 ± 0.61
Salvia canariensis	Lamiaceae	Herb	0.26 ± 0.01	54.5 ± 8.28	41.4 ± 6.01	-0.92 ± 0.05	-1.18 ± 0.07	5.49 ± 0.21	83.1 ± 0.95

†Pressure-volume parameters from Scoffoni et al. 2008 and Scoffoni et al. 2011

Table 4.3. Symbols, terms, unit, derivation and biological significance of the 9 key leaf thickness and area shrinkage traits in this study. An additional 9 traits were quantified, and their calculation and correlations with these key traits are described in the Supplementary Information (Supplementary Methods; Supplementary Results; Table S4.2, S4.3 and S4.4). *Because thickness of the leaf or tissues precisely at turgor loss point could not be determined, we interpolated the value for turgor loss point by assuming a linear decline of leaf dimensions with Ψ_{leaf} between the two surrounding measurements.

Symbol	Parameters	Units	Derivation	Significance
Thickness shrinkage				
$PLT_{leaf,TLP}$	Percent loss of thickness at turgor loss point	%	From plot of *PLT* versus Ψ_{leaf} *	Estimate of leaf thickness shrinkage at turgor loss point
$PLT_{C,TLP}$	Percent loss of cell thickness at turgor loss point	%	From plot of $PLT_{C,TLP}$ versus Ψ_{leaf} *	Estimate of the amount of cell thickness lost when cells become flaccid
$PLT_{A,TLP}$	Proportion of intercellular airspace thickness lost at turgor loss point	%	From plot of $PLT_{A,TLP}$ versus Ψ_{leaf} *	Estimate of the amount of airspace thickness lost (or gained) when cells become flaccid
$dT_{leaf}/d\Psi$	Degree of shrinkage of leaf thickness	%·MPa^{-1}	$\frac{PLT_{leaf,TLP}}{\pi_{TLP}}$	Steepness of the decline of whole leaf thickness with Ψ_{leaf} before cells become flaccid
$dT_C/d\Psi$	Degree of shrinkage of leaf cells	%·MPa^{-1}	$\frac{PLT_{C,TLP}}{\eth_{TLP}}$	Steepness of the decline of cell thickness with Ψ_{leaf} before cells become flaccid
$dT_A/d\Psi$	Degree of shrinkage of leaf intercellular airspace	%·MPa^{-1}	$\frac{PLT_{A,TLP}}{\eth_{TLP}}$	Steepness of the decline of air thickness with Ψ_{leaf} before cells become flaccid
PLT_{dry}	Percent loss of thickness in a dry leaf	%	$1-\frac{T_{leaf,dry}}{T_{leaf,FT}}$	Maximum amount of thickness shrinkage
Area shrinkage				
$PLA_{leaf,TLP}$	Percent loss of area at turgor loss point	%	From plot of *PLA* versus Ψ_{leaf} *	Estimate of leaf area shrinkage at turgor loss point
PLA_{dry}	Percent loss of area in a dry leaf	%	$1-\frac{A_{leaf,dry}}{A_{leaf,FT}}$	Maximum amount of area shrinkage

Symbols: *PLT*, percent loss of thickness; Ψ_{leaf}, leaf water potential, and the slopes of percent cell ($dT_C/d\Psi$), intercellular airspace ($dT_A/d\Psi$) and total leaf thickness ($dT_{leaf}/d\Psi$) against Ψ_{leaf} between full turgor and turgor loss point.

Table 4.4. Symbols, terms, unit, derivation and biological significance of the 28 leaf traits relating to composition, hydraulics, p-v curves, water storage and venation.

Symbol	Parameters	Units	Derivation	Significance
Leaf composition				
$PT_{cell,FT}$	Percent cell thickness at full turgor	%	$\frac{T_{C,FT} \text{ or } T_{A,FT}}{T_{leaf,FT}}$	Amount of cell thickness at full hydration
$PT_{A,FT}$	Percent air thickness at full turgor	%		Amount of air thickness at full hydration
$PT_{cell,TLP}$	Percent cell thickness at turgor loss point	%	$\frac{T_{C,TLP} \text{ or } T_{A,TLP}}{T_{leaf,TLP}}$	Amount of cell thickness at turgor loss point
$PT_{A,TLP}$	Percent air thickness at turgor loss point	%		Amount of air thickness at turgor loss point
LMA	Leaf mass per area	g m^{-2}	Leaf dry mass/ leaf area	-
Leaf density	-	g cm^{-3}	Leaf dry mass/ leaf volume	-
FA	Fraction air	-	leaf mass before – leaf mass after water infiltration of the airspaces	Estimate of the amount of airspace in the leaf
FW	Fraction water	-	leaf mass before water infiltration of the airspaces – leaf dry mass	Estimate of the amount of water in the leaf
FS	Fraction solid	-	Leaf volume – FA – FW	Estimate of the amount of solid in the leaf
%Air in a dry leaf	-	%	Leaf dry thickness × (1- FS)	Estimate of the amount of airspace in a dry leaf
Leaf hydraulics				
K_{max}	Maximum leaf hydraulic conductance	mmol m^{-2} s^{-1} MPa^{-1}	*y*-intercept of the maximum likelihood function of the vulnerability curve	Efficiency of water movement through a fully hydrated leaf
K_{TLP}	Leaf hydraulic conductance at π_{TLP}	mmol m^{-2} s^{-1} MPa^{-1}	-	Efficiency of water movement at π_{TLP}
P_{50}	Ψ_{leaf} at 50% loss of K_{leaf}	MPa	-	-
P_{80}	Ψ_{leaf} at 80% loss of K_{leaf}	MPa	-	-
$dK_{leaf}/d\Psi$	Slope of the leaf hydraulic vulnerability curve at Ψ_{leaf} = -0.5 MPa	mmol m^{-2} s^{-1} MPa^{-1}	-	Vulnerability of K_{leaf} to dehydration
g_{min}	Cuticular conductance	mmol m^{-2} s^{-1}	-	Minimal epidermal conductance after stomatal closure
Pressure-volume curve parameters				
π_{TLP}	Osmotic pressure at turgor loss point	MPa	Point at which turgor pressure = 0	Water potential at which cells become flaccid
π_o	Osmotic pressure at full turgor	MPa	-	Concentration of solutes in cells
ε	Modulus of elasticity	MPa	Δ Turgor pressure /Δ RWC	Wall stiffness
RWC_{TLP}	Relative water content at π_{TLP}	%	-	Leaf hydration when cells become flaccid
Water storage				
C_{FT}	Capacitance at full turgor	MPa^{-1}	Δ(100- RWC)/ Δ Ψ_{leaf} before π_{TLP}	Amount of water storage before π_{TLP}
C_{TLP}	Capacitance at π_{TLP}	MPa^{-1}	Δ(100- RWC)/ Δ Ψ_{leaf} past π_{TLP}	Amount of water storage after π_{TLP}
SWC	Saturated water content	g g^{-1}	Fresh mass – dry mass / Leaf dry mass	Water storage index
C^*_{FT}	Leaf area specific C_{FT}	mol m^{-2} MPa^{-1}	$C_{FT} \times SWC \times LMA$	-
C^*_{TLP}	Leaf area specific C_{TLP}	mol m^{-2} MPa^{-1}	$C_{TLP} \times SWC \times LMA \times RWC_{TLP}$	-
Leaf venation				
Major VLA	Major vein length per area	mm mm^{-2}	Major vein length/ leaf area	Sum of 1°, 2° and 3order vein lengths per leaf area
Minor VLA	Minor vein length per area	mm mm^{-2}	Minor vein length/ leaf area	Sum of 4° and higher order vein lengths per leaf area
VLA	Vein length per area	mm mm^{-2}	Vein length/ leaf area	Sum of major and minor vein lengths per leaf area
Ratio major: minor	Ratio of major to minor VLA	-	Major VLA/ Minor VLA	Leaf venation composition index
FEV	Free ending veins per area	Number per mm^2	Number of FEV/ area	-

Table 4.5. Percent loss of thicknesses and area at turgor loss point and for oven-dried leaves.

Species	$PLT_{leaf,TLP}$	PLT_{dry}	$PLT_{C,\ TLP}$	$PLT_{A,\ TLP}$	$PLA_{leaf,TLP}$	PLA_{dry}
Bauhinia galpinii	16 ± 2.3	83 ± 1.5	19 ± 0.31	14 ± 5.1	0.48 ± 0.16	21 ± 0.94
Camellia sasanqua	15 ± 1.2	43 ± 1.1	21 ± 0.30	3.3 ± 5.2	2.9 ± 0.38	5.0 ± 2.2
Cercocarpus betuloides	18 ± 3.6	33 ± 5.0	11 ± 1.2	39 ± 16	4.8 ± 0.51	21 ± 2.3
Comarostaphylis diversifolia	12 ± 1.4	44 ± 1.9	16 ± 0.32	6.8 ± 3.4	1.2 ± 0.79	10 ± 0.88
Hedera canariensis	11 ± 1.3	62 ± 3.8	11 ± 0.18	-5.9 ± 8.7	0.96 ± 0.25	16 ± 0.93
Helianthus annuus	22 ± 1.2	36 ± 1.6	-	-	14 ± 0.62	69 ± 1.4
Heteromeles arbutifolia	12 ± 2.1	53 ± 1.1	14 ± 0.51	7.8 ± 6.5	0.74 ± 0.27	4.9 ± 2.0
Lantana camara	38 ± 2.0	80 ± 1.9	16 ± 0.54	77 ± 5.3	9.4 ± 0.43	45 ± 2.1
Magnolia grandiflora	22 ± 1.8	42 ± 3.3	11 ± 0.52	30 ± 1.9	-	8.2 ± 1.1
Platanus racemosa	36 ± 4.0	70 ± 2.7	12 ± 0.48	72 ± 0.0	1.3 ± 0.47	26 ± 2.1
Quercus agrifolia	5.1 ± 0.92	23 ± 1.7	15 ± 0.15	-12 ± 3.4	1.6 ± 0.13	7.0 ± 0.14
Raphiolepis indica	4.6 ± 0.38	47 ± 2.2	12 ± 0.14	-1.8 ± 4.9	0.61 ± 0.31	14 ± 0.45
Romneya coulteri	16 ± 1.6	50 ± 1.5	12 ± 0.29	25 ± 5.3	3.9 ± 0.28	28 ± 1.4
Salvia canariensis	28 ± 7.2	66 ± 1.5	-	-	8.4 ± 1.1	57 ± 2.7
One-way ANOVA	***	***	***	***	***	***

FIGURE CAPTIONS

Figure 4.1: Sketch of (A) a fully turgid leaf versus (B) a strongly dehydrated leaf (drawing based on leaf cross-sections of *Helianthus annuus* in Fellows and Boyer, 1978). Note the strong reduction in leaf thickness, cell thickness and intercellular airspaces in the dehydrated leaf. Epidermal cells are shrunk in the dehydrated leaf inducing whole leaf area shrinkage. Note that this sketch represents shrinkage for a typical drought sensitive species. Many species such as oaks will experience less thickness shrinkage causing instead an increase in intercellular airspace (see *Discussion*).

Figure 4.2. Computer simulated leaf hydraulic vulnerability curves indicating the theoretical impact of reducing hydraulic conductance in the within-xylem and outside-xylem components, for leaves with high and low resistance outside the xylem (panels A and B respectively). Simulations were run for leaves with (1) low vulnerability for xylem and outside-xylem components (P_{50} for the vulnerability of each component = -1 MPa; black line), (2) high vulnerability for only the outside-xylem component (P_{50} = -1 MPa and -0.25 MPa for the within-xylem and outside-xylem components respectively; grey dashed line), (3) high vulnerability for only the xylem component (P_{50} = -0.25 MPa and -1 MPa for the within-xylem and outside-xylem components respectively; light-grey dashed line), and (4) high vulnerability for both the xylem and outside-xylem components (P_{50} for the vulnerability of each component = -0.25 MPa; grey solid line).

Figure 4.3. Plots of leaf thickness shrinkage versus leaf water potential for 14 species of diverse leaf form and texture and drought tolerance; a typical plot is presented for each species. The blue shaded areas represent the thickness of the cells and the white shaded areas the thickness of the intercellular airspace. The grey horizontal line represents the maximum shrinkage in leaf thickness, i.e., for an oven-dried leaf. The red vertical line represents turgor loss point and the

red horizontal line represents the thickness of the leaf at turgor loss point. Species are ordered top left to bottom right from lowest to highest modulus of elasticity. Due to area wrinkling with dehydration of *Helianthus annuus* and *Salvia canariensis*, the cell and airspace thickness could not be estimated and only the whole leaf shrinkage is shown in light blue (see *Methods*).

Figure 4.4. Coordination of leaf shrinkage and leaf hydraulic vulnerability in ten species of diverse leaf form and texture and drought tolerance. Slope of leaf hydraulic vulnerability at Ψ_{leaf} = -0.5 MPa (A) and Ψ_{leaf} at 80% loss of hydraulic conductance (B) plotted against slope of total leaf thickness shrinkage before turgor loss point. Species from moist habitat are represented in white and woody species from dry habitat are represented in black. Fitted standardized major axes in A: $dT_{\mathrm{leaf}}/d\Psi = 3.0 \times dK_{\mathrm{leaf}}/d\Psi - 0.22$; B: $dT_{\mathrm{leaf}}/d\Psi = 18 \times {P_{80}}^{-1.1}$. * $P < 0.05$; ** $P < 0.01$

Figure 4.5. Relationship with loss of leaf thickness at turgor loss point with pressure-volume curve parameters and leaf structural traits for 14 species of diverse leaf form and texture and drought tolerance. Panels (A) to (E) show traits plotted against the % loss of leaf thickness at turgor loss point: (A) Leaf osmotic potential at full turgor, (B) leaf osmotic potential at turgor loss point, (C) modulus of elasticity, (D) leaf mass per area, and (E) leaf density. Plots F-O show the inter-correlation of those five traits. Species native from moist habitat are represented in white, woody species from dry habitat in black and herbs from dry habitat in grey. Fitted standardized major axes in A: $PLT_{\mathrm{leaf,TLP}} = -28 \times {\pi_{\mathrm{o}}}^{-1.8}$; B: $PLT_{\mathrm{leaf,TLP}} = -44 \times {\pi_{\mathrm{tlp}}}^{-1.7}$; C: $PLT_{\mathrm{leaf,TLP}} = 357 \times \varepsilon^{-1.4}$; D: $PLT_{\mathrm{leaf,TLP}} = 906 \times LMA^{-0.88}$; E: $PLT_{\mathrm{leaf,TLP}} = 3.3 \times Leaf\ density^{-1.4}$; F: $\pi_{\mathrm{o}} = -0.78 \times {\pi_{\mathrm{tlp}}}^{-0.93}$; G: $\pi_{\mathrm{o}} = -0.11 \times \varepsilon - 0.27$; H: $\pi_{\mathrm{o}} = -0.09 \times LMA^{-0.59}$; I: $\pi_{\mathrm{o}} = -3.5 \times Leaf\ density - 0.20$; J: $\pi_{\mathrm{tlp}} = -0.16 \times \varepsilon - 0.31$; K: $ð_{\mathrm{tlp}} = -0.09 \times LMA^{-0.64}$; L: $\pi_{\mathrm{tlp}} = -4.9 \times Leaf\ density - 0.20$ M: $\varepsilon = 0.25 \times LMA^{0.77}$; N:

$\varepsilon = 28 \times Leaf\ density^{0.99}$; 0: $LMA = 581 \times Leaf\ density^{1.6}$. * $P < 0.05$; ** $P < 0.01$; ***$P < 0.001$

Figure 4.6. Coordination of maximum leaf area and thickness shrinkage with modulus of elasticity and leaf density for 14 species of diverse leaf form and texture and drought tolerance. A: $PLA_{\text{dry}} = 757 \times \text{å}^{-1.7}$; B: $PLA_{\text{dry}} = 2.96 \times Leaf\ density^{-1.6}$; C: $PLT_{\text{dry}} = -118 \times Leaf\ density + 94.7$. $^{\text{NS}}P > 0.05$; * $P < 0.05$; ***$P < 0.001$

Figure 4.7. Relationship between cuticular conductance and maximum leaf area shrinkage for 14 species of diverse leaf form and texture and drought tolerance. $g_{\min} = 0.27 \times PLA_{\text{FT}} - 0.08$ * $P < 0.05$; *** $P < 0.001$

Figure 4.8: Synthetic conceptual hypothesis for trait associations and impacts of leaf shrinkage and structural traits on leaf hydraulic vulnerability. Leaf hydraulic vulnerability is determined independently by major vein length per area acting on the xylem pathways and leaf shrinkage in thickness acting on the outside-xylem pathways of water movement through the leaf. Thickness shrinkage is determined by cell properties, i.e., the pressure-volume curves parameters modulus of elasticity (ε) and the osmotic pressure at full turgor (π_o) and at turgor loss point (π_{TLP}). The dotted lines signify the ε and osmotic pressures are not directly linked, but strongly associated; saltier cells need a higher ε to maintain *RWC* at turgor loss point above lethal levels (*see* Bartlett et al., 2012). The ε, being related to cell wall thickness, is correlated with leaf density and leaf mass per area, which are also related to cell wall thickness, and thus all these variables influence thickness shrinkage. The ε also influences maximum leaf area shrinkage (PLA_{dry}). PLA_{dry} and not ε acts directly on cuticular conductance, possibly through enhanced leaky stomata (*see* text). Red arrows indicate significant *negative* correlations between traits while black arrows indicate

significant *positive* correlations between traits. Double-headed arrows indicate the traits are too intrinsically linked to tease apart.

Figure 4.9: Ability of a model to predict P_{80} from an equation based on leaf shrinkage and major vein length per area (eqn 3). The plot of observed versus predicted values, with line fitted through the origin showed low bias (slope close to 1.0) and very high r^2. Similar predictive power was found for P_{50}, see text. ***$P < 0.001$.

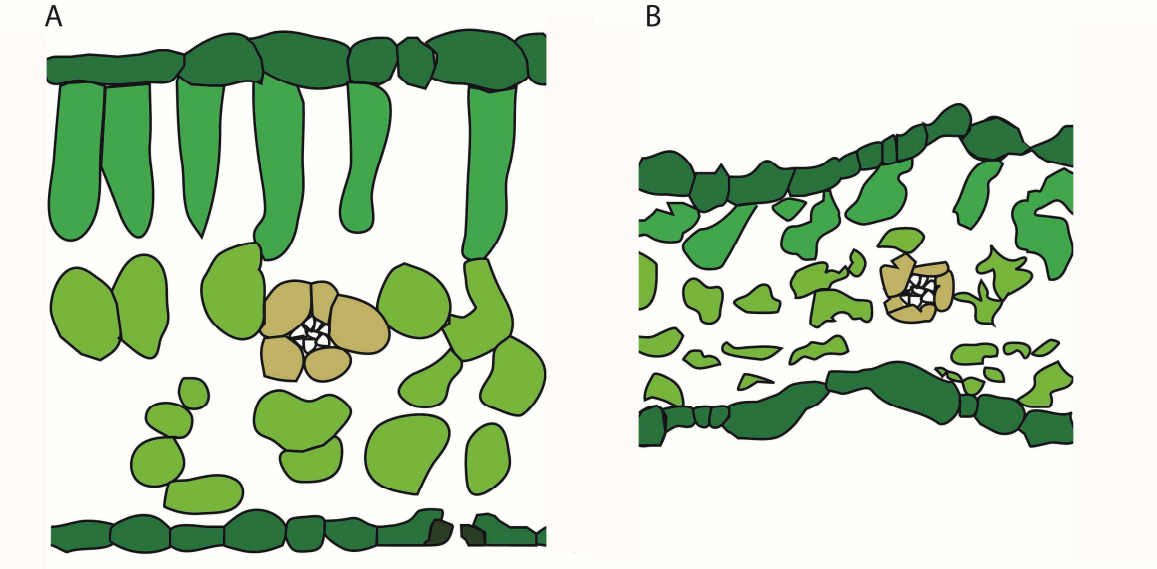

Figure 4.1

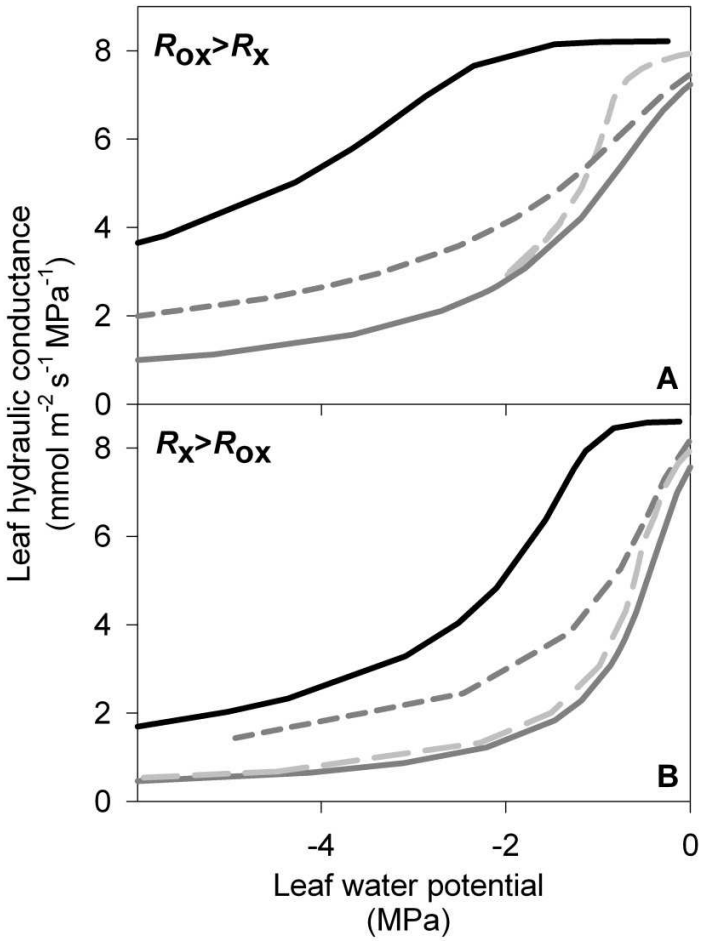
R_{ox}>R_x
R_x>R_{ox}
A
B
Leaf hydraulic conductance
(mmol m^{-2} s^{-1} MPa^{-1})
Leaf water potential
(MPa)
0
2
4
6
8
-4
-2
0

Figure 4.2

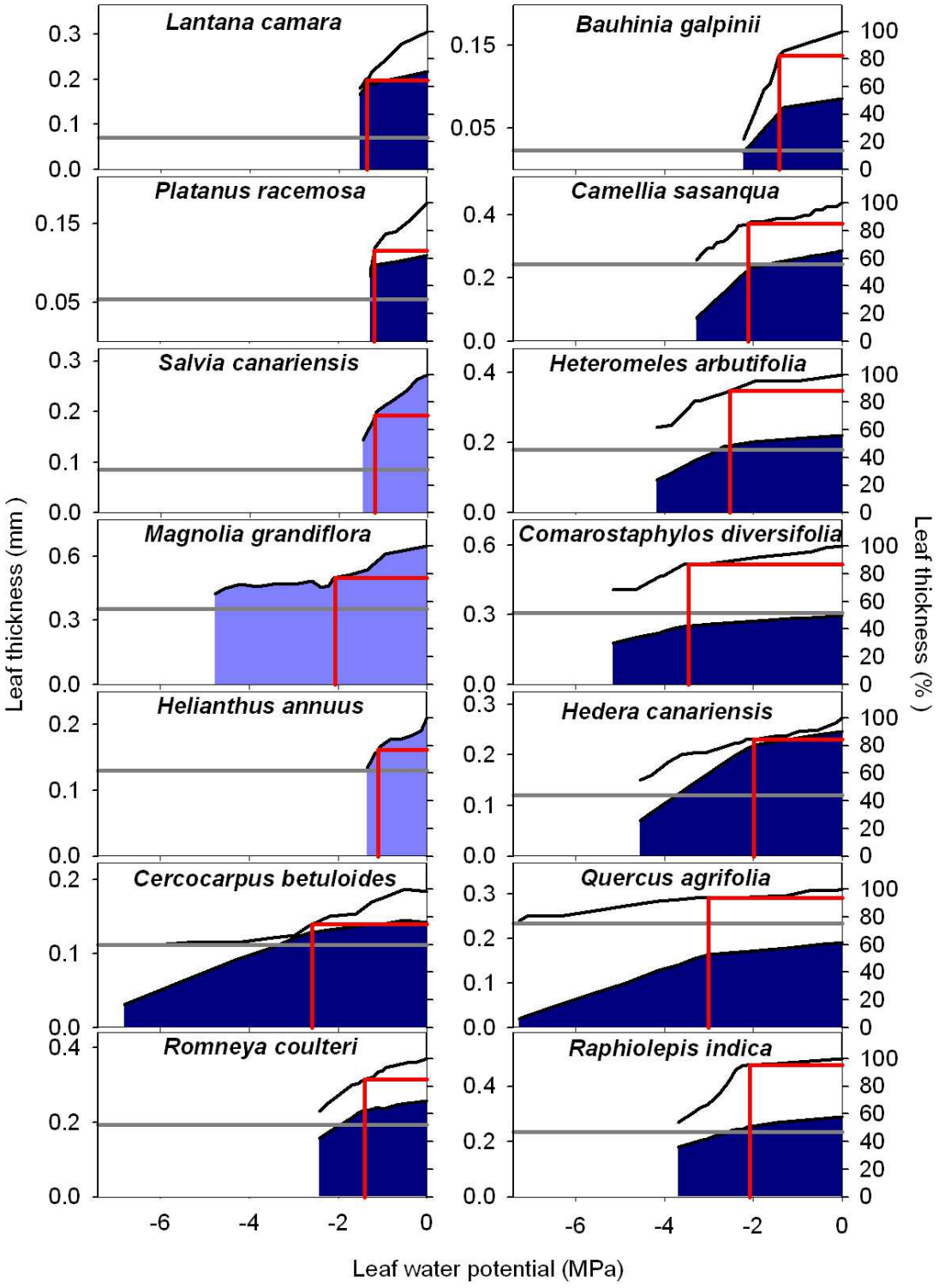
Lantana camara
Bauhinia galpinii
Platanus racemosa
Camellia sasanqua
Salvia canariensis
Heteromeles arbutifolia
Magnolia grandiflora
Comarostaphylos diversifolia
Helianthus annuus
Hedera canariensis
Cercocarpus betuloides
Quercus agrifolia
Romneya coulteri
Raphiolepis indica
Leaf thickness (mm)
Leaf thickness (%)
Leaf water potential (MPa)

Figure 4.3

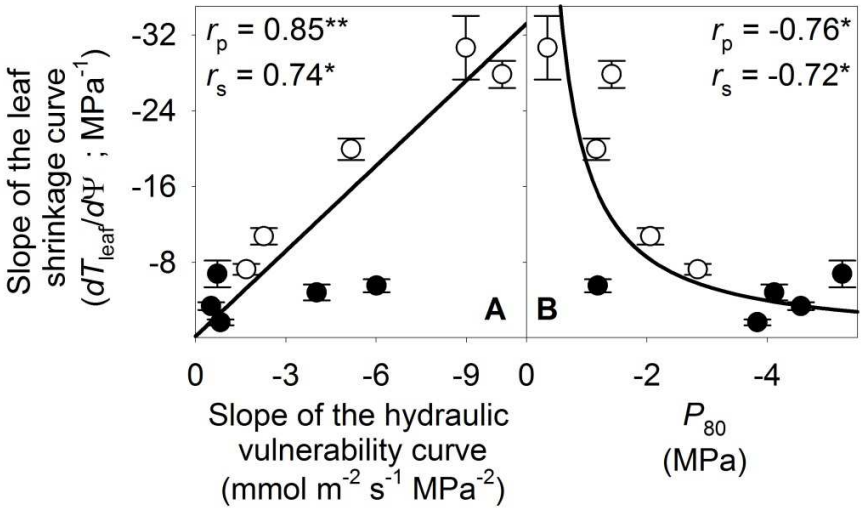
Slope of the leaf shrinkage curve ($dT_{leaf}/d\Psi$; MPa^{-1})
-32
-24
-16
-8
r_p = 0.85**
r_s = 0.74*
A
0
-3
-6
-9
Slope of the hydraulic vulnerability curve (mmol m^{-2} s^{-1} MPa^{-2})
r_p = -0.76*
r_s = -0.72*
B
0
-2
-4
P_{80} (MPa)

Figure 4.4

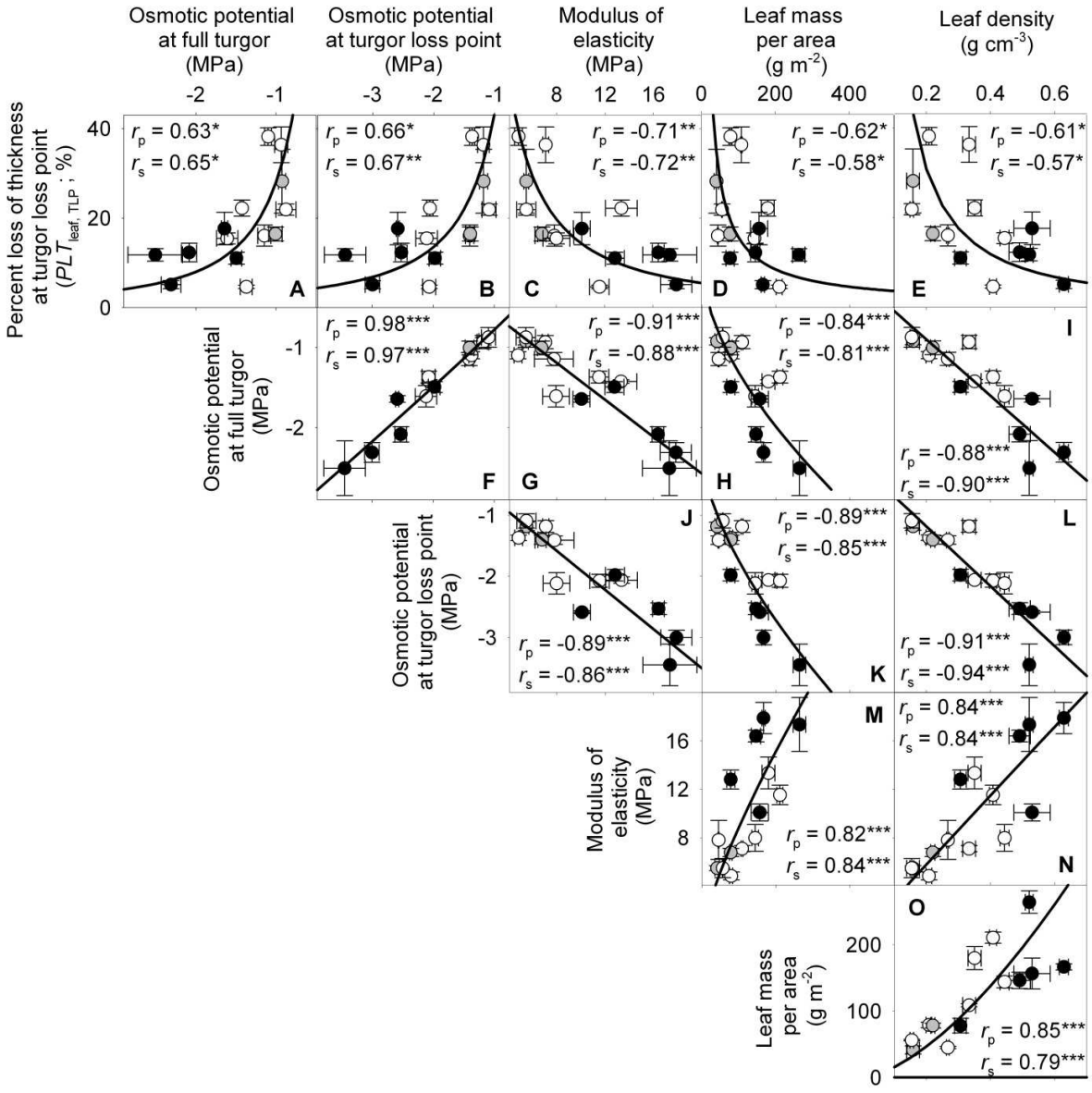
Osmotic potential at full turgor (MPa)
Osmotic potential at turgor loss point (MPa)
Modulus of elasticity (MPa)
Leaf mass per area (g m-2)
Leaf density (g cm-3)
Percent loss of thickness at turgor loss point (PLTleaf, TLP ; %)
Osmotic potential at full turgor (MPa)
Osmotic potential at turgor loss point (MPa)
Modulus of elasticity (MPa)
Leaf mass per area (g m-2)
A rp = 0.63* rs = 0.65*
B rp = 0.66* rs = 0.67**
C rp = -0.71** rs = -0.72**
D rp = -0.62* rs = -0.58*
E rp = -0.61* rs = -0.57*
F rp = 0.98*** rs = 0.97***
G rp = -0.91*** rs = -0.88***
H rp = -0.84*** rs = -0.81***
I rp = -0.88*** rs = -0.90***
J rp = -0.89*** rs = -0.86***
K rp = -0.89*** rs = -0.85***
L rp = -0.91*** rs = -0.94***
M rp = 0.82*** rs = 0.84***
N rp = 0.84*** rs = 0.84***
O rp = 0.85*** rs = 0.79***

Figure 4.5

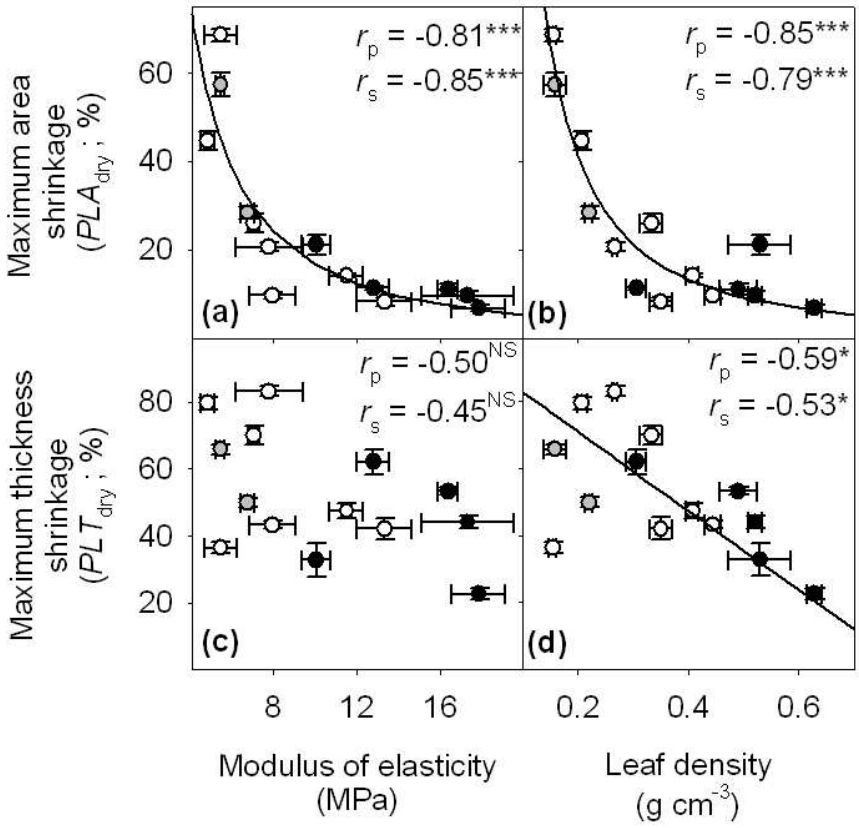
Maximum area shrinkage (PLA_{dry} ; %)
Maximum thickness shrinkage (PLT_{dry} ; %)
r_p = -0.81***
r_s = -0.85***
r_p = -0.85***
r_s = -0.79***
r_p = -0.50^{NS}
r_s = -0.45^{NS}
r_p = -0.59*
r_s = -0.53*
(a)
(b)
(c)
(d)
20
40
60
80
8
12
16
0.2
0.4
0.6
Modulus of elasticity (MPa)
Leaf density (g cm^{-3})

Figure 4.6

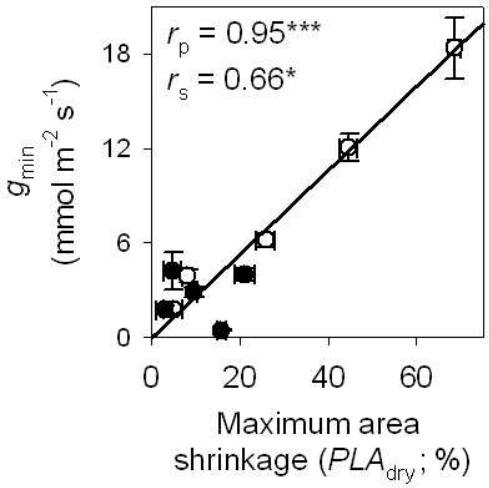
r_p = 0.95***
r_s = 0.66*
g_{min} (mmol m^{-2} s^{-1})
0
6
12
18
0
20
40
60
Maximum area shrinkage (PLA_{dry}; %)

Figure 4.7

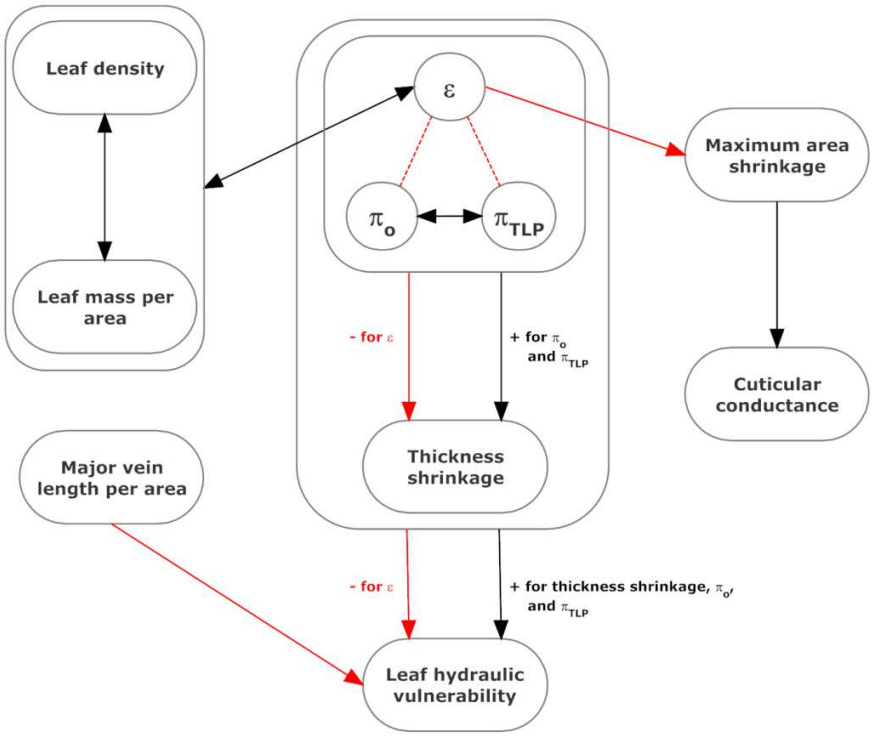
Leaf density
Leaf mass per area
ε
π_o
π_{TLP}
Maximum area shrinkage
Cuticular conductance
- for ε
+ for π_o and π_{TLP}
Thickness shrinkage
Major vein length per area
- for ε
+ for thickness shrinkage, π_o, and π_{TLP}
Leaf hydraulic vulnerability

Figure 4.8

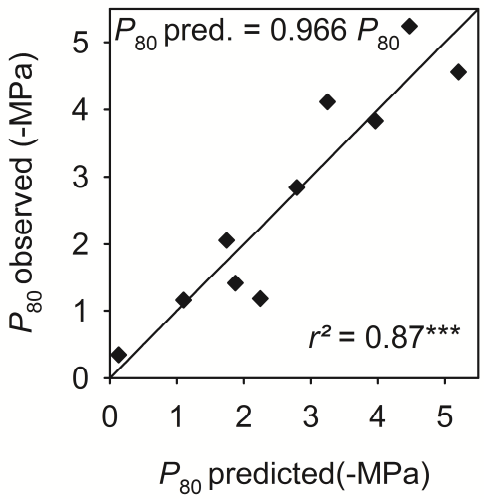
P_{80} pred. = 0.966 P_{80}
r^2 = 0.87***
P_{80} observed (-MPa)
P_{80} predicted(-MPa)
0
1
2
3
4
5

Figure 4.9

SUPPLEMENTAL MATERIAL

Table S4.1. Parameters for simulated vulnerability

Table S4.2. Mean ± standard error of shrinkage, rehydration, PV, hydraulic, water storage, leaf structure and leaf venation traits

Table S4.3. Correlation matrix of 51 traits related to shrinkage, rehydration, pressure-volume curves, hydraulics, water storage, leaf structure and venation across 14 species

Table S4.4. Symbols, terms, unit, derivation and biological significance of 9 additional leaf thickness, area and volume shrinkage traits this study.

Table S4.5. Percent recovery in thickness after 1 hour rehydration for leaves of 10 species dehydrated before and past their turgor loss point.

Table S4.6. Partial correlation analysis results.

Supplemental Results 4.1. Leaf shrinkage with dehydration: variation across diverse species of other shrinkage parameters and correlation with pressure volume parameters and cuticular conductance

Supplemental Results 4.2. Leaf shrinkage with dehydration: variation between species of wet and dry habitats

Supplemental Results 4.3. Recovery of leaf shrinkage in thickness

Supplemental Discussion 4.1. The impact of leaf shrinkage on leaf hydraulic vulnerability: studies based on rehydration kinetics

Supplemental Discussion 4.2. Mechanisms of leaf shrinkage: the role of the epidermis

Supplemental Discussion 4.3. Resistance to leaf shrinkage: an important trait contributing to drought tolerance?

Supplemental Material and Methods S4.1. Leaf shrinkage experiments: testing leaf responses to dehydration/ determination of the other parameters of leaf shrinkage/ Leaf structural and compositional traits.

REFERENCES

Bartlett MK, Scoffoni C, Ardy R, Zhang Y, Sun S, Cao K, Sack L (2012) Rapid determination of comparative drought tolerance traits: using an osmometer to predict turgor loss point. Methods in Ecology and Evolution 3: 880-888

Bartlett MK, Scoffoni C, Sack L (2012) The determinants of leaf turgor loss point and prediction of drought tolerance of species and biomes: a global meta-analysis. Ecology Letters 15: 393-405

Blackman CJ, Brodribb TJ, Jordan GJ (2010) Leaf hydraulic vulnerability is related to conduit dimensions and drought resistance across a diverse range of woody angiosperms. New Phytologist 188: 1113-1123

Blonder B, Buzzard V, Simova I, Sloat L, Boyle B, Lipson R, Aguilar-Beaucage B, Andrade A, Barber B, Barnes C, Bushey D, Cartagena P, Chaney M, Contreras K, Cox M, Cueto M, Curtis C, Fisher M, Furst L, Gallegos J, Hall R, Hauschild A, Jerez A, Jones N, Klucas A, Kono A, Lamb M, Matthai JDR, McIntyre C, McKenna J, Mosier N, Navabi M, Ochoa A, Pace L, Plassmann R, Richter R, Russakoff B, St Aubyn H, Stagg R, Sterner M, Stewart E, Thompson TT, Thornton J, Trujillo PJ, Volpe TJ, Enquist BJ (2013) The leaf area shrinkage effect can bias paleoclimate and ecology research. American Journal of Botany 99: 1756-1763

Bogue EE (1892) The shrinkage of leaves. Science 20: 163

Boyer JS (1968) Relationship of water potential to growth of leaves. Plant Physiology 43: 1056-&

Boyer JS (1985) Water transport. *In* Briggs, W. R., pp 473-516

Brodribb TJ, Feild TS, Jordan GJ (2007) Leaf maximum photosynthetic rate and venation are linked by hydraulics. Plant Physiology 144: 1890-1898

Burnham KP, Anderson DR (2002) Model selection and multimodel inference, 2nd ed. Springer, New York, New York, USA.

Burnham KP, Anderson DR (2004) Multimodel inference - understanding AIC and BIC in model selection. Sociological Methods & Research 33: 261-304

Burquez A (1987) Leaf thickness and water deficit in plants - a tool for field studies. Journal of Experimental Botany 38: 109-114

Canny M, Wong SC, Huang C, Miller C (2012) Differential shrinkage of mesophyll cells in transpiring cotton leaves: implications for static and dynamic pools of water, and for water transport pathways. Functional Plant Biology 39: 91-102

Cochard H, Froux F, Mayr FFS, Coutand C (2004) Xylem wall collapse in water-stressed pine needles. Plant Physiology 134: 401-408

Cochard H, Nardini A, Coll L (2004) Hydraulic architecture of leaf blades: where is the main resistance? Plant Cell and Environment 27: 1257-1267

Colpitts BG, Coleman WK (1997) Complex permittivity of the potato leaf during imposed drought stress. Ieee Transactions on Geoscience and Remote Sensing 35: 1059-1064

Crombie DS, Milburn JA, Hipkins MF (1985) Maximum sustainable xylem sap tensions in *Rhododendron* and other species. Planta 163: 27-33

Cutler D (2005) Design in plants. In: Collins MW, Atherton MA, Bryant JA eds. Nature and Design. Southampton, Boston: WIT Press, 95-124.

Downey LA, Miller JW (1971) Rapid measurements of relative turgidity in maize (*Zea mays* L). New Phytologist 70: 555-&

Farquhar GD, Raschke K (1978) Resistance to transpiration of sites of evaporation within leaf. Plant Physiology 61: 1000-1005

Fellows RJ, Boyer JS (1978) Altered ultrastructure of cells of sunflower leaves having low water potentials. Protoplasma 93: 381-395

Fensom DS, Donald RG (1982) Thickness fluctuations in veins of corn and sunflower detected by a linear transducer. Journal of Experimental Botany 33: 1176-1184

Gardner WR, Ehlig CF (1965) Physical aspects of internal water relations of plant leaves. Plant Physiology 40: 705-&

Johansson I, Karlsson M, Shukla VK, Chrispeels MJ, Larsson C, Kjellbom P (1998) Water transport activity of the plasma membrane aquaporin PM28A is regulated by phosphorylation. Plant Cell 10: 451-459

Johnson DM, Meinzer FC, Woodruff DR, McCulloh KA (2009) Leaf xylem embolism, detected acoustically and by cryo-SEM, corresponds to decreases in leaf hydraulic conductance in four evergreen species. Plant Cell and Environment 32: 828-836

Jones HG (1973) Estimation of plant water status with beta-gauge. Agricultural Meteorology 11: 345-355

Kadoya K, Kameda K, Chikaigumi S, Matsumoto K (1975) Studies on the hydrophysiological rhythms of Citrus trees. I.Cyclic fluctuations of leaf thickness and stem diameter of *Natsudaidai* seedlings. Journal of the Japanese Society for Horticultural Science 44: 260-264

Kennedy JS, Booth CO (1958) Water relations of leaves from woody and herbaceous plants. Nature 181: 1271-1272

Kim YX, Steudle E (2007) Light and turgor affect the water permeability (aquaporins) of parenchyma cells in the midrib of leaves of *Zea mays*. Journal of Experimental Botany 58: 4119-4129

Koide RT, Robichaux RH, Morse SR, Smith CM (2000) Plant water status, hydraulic resistance and capacitance. *In* Plant Physiological Ecology: Field and Methods and Instrumentation (eds. Pearcy RW, Ehleringer JR, Mooney HA & Rundel PW). Kluwer Dordrecht, the Netherlands, pp 161-183.

Lawlor DW, Cornic G (2002) Photosynthetic carbon assimilation and associated metabolism in relation to water deficits in higher plants. Plant Cell and Environment 25: 275-294

McBurney T (1992) The relationship between leaf thickness and plant water potential. Journal of Experimental Botany 43: 327-335

McKown Athena D, Cochard H, Sack L (2010) Decoding leaf hydraulics with a spatially explicit model: principles of venation architecture and implications for its evolution. The American Naturalist 175: 447-460

Meidner H (1952) An instrument for the continuous determination of leaf thickness changes in the field. Journal of Experimental Botany 3: 319-325

Meidner H (1955) Changes in the resistance of the mesophyll tissue with changes in the leaf water content. Journal of Experimental Botany 6: 94-99

Meidner H (1975) Water supply, evaporation, and vapor diffusion in leaves. Journal of Experimental Botany 26: 666-673

Meidner H (1983) Our understanding of plant water relations. Journal of Experimental Botany 34: 1606-1618

Milburn JA (1966) Conduction of sap. I. Water conduction and cavitation in water stressed leaves. Planta 69: 34-&

Nardini A, Lo Gullo MA, Salleo S (2011) Refilling embolized xylem conduits: Is it a matter of phloem unloading? Plant Science 180: 604-611

Nardini A, Pedà G, La Rocca N (2012) Trade-offs between leaf hydraulic capacity and drought vulnerability: morpho-anatomical bases, carbon costs and ecological consequences. New Phytologist

Ogaya R, Peñuelas J (2006) Contrasting foliar responses to drought in *Quercus ilex* and *Phillyrea latifolia*. Biologia Plantarum 50: 373-382

Pammenter NW, Vander Willigen C (1998) A mathematical and statistical analysis of the curves illustrating vulnerability of xylem to cavitation. Tree Physiology 18: 589-593

Robichaux RH (1984) Variation in the tissue water relations of two sympatric hawaiian *Dubautia* species and their natural hybrid. Oecologia 65: 75-81

Roderick ML, Berry SL, Saunders AR, Noble IR (1999) On the relationship between the composition, morphology and function of leaves. Functional Ecology 13: 696-710

Rozema J, Arp W, Vandiggelen J, Kok E, Letschert J (1987) An ecophysiological comparison of measurements of the diurnal rythm of the leaf elongation and changes of the leaf thickness of salt-resistant dicotyledonae and monocotyledonae. Journal of Experimental Botany 38: 442-453

Sack L, Cowan PD, Holbrook NM (2003) The major veins of mesomorphic leaves revisited: Tests for conductive overload in *Acer saccharum* (Aceraceae) and *Quercus rubra* (Fagaceae). American Journal of Botany 90: 32-39

Sack L, Cowan PD, Jaikumar N, Holbrook NM (2003) The 'hydrology' of leaves: co-ordination of structure and function in temperate woody species. Plant Cell and Environment 26: 1343-1356

Sack L, Frole K (2006) Leaf structural diversity is related to hydraulic capacity in tropical rain forest trees. Ecology 87: 483-491

Sack L, Holbrook NM (2006) Leaf hydraulics. Annual Review of Plant Biology 57: 361-381

Sack L, Melcher PJ, Liu WH, Middleton E, Pardee T (2006) How strong is intracanopy leaf plasticity in temperate deciduous trees? American Journal of Botany 93: 829-839

Sack L, PrometheusWiki (2010) Leaf pressure-volume curve parameters *In*. PrometheusWiki http://www.publish.csiro.au/prometheuswiki/tiki-pagehistory.php?page=Leaf pressure-volume curve parameters&preview=10

Sack L, Scoffoni C (2012) Measurement of leaf hydraulic conductance and stomatal conductance and their responses to irradiance and dehydration using the evaporative flux methods (EFM). Journal of Visualized Experiments

Sack L, Streeter CM, Holbrook NM (2004) Hydraulic analysis of water flow through leaves of sugar maple and red oak. Plant Physiology 134: 1824-1833

Sack L, Tyree MT, Holbrook NM (2005) Leaf hydraulic architecture correlates with regeneration irradiance in tropical rainforest trees. New Phytologist 167: 403-413

Saini BC, Rathore TR (1983) Adaptation of beta-ray gauge technique for measurement of water deficit of intact rice leaves. Biologia Plantarum 25: 326-330

Salleo S, Lo Gullo MA, Raimondo F, Nardini A (2001) Vulnerability to cavitation of leaf minor veins: any impact on leaf gas exchange? Plant Cell and Environment 24: 851-859

Sancho-Knapik D, Alvarez-Arenas TG, Peguero-Pina JJ, Fernandez V, Gil-Pelegrin E (2011) Relationship between ultrasonic properties and structural changes in the mesophyll during leaf dehydration. Journal of Experimental Botany 62: 3637-3645

Sancho-Knapik D, Alvarez-Arenas TG, Peguero-Pina JJ, Gil-Pelegrin E (2010) Air-coupled broadband ultrasonic spectroscopy as a new non-invasive and non-contact method for the determination of leaf water status. Journal of Experimental Botany 61: 1385-1391

Schaefer J, Opgen-Rhein R, Strimmer K (2007) corpcor: Efficient estimation of covariance and (partial) correlation. R package version 1.4.7.

Scoffoni C, McKown AD, Rawls M, Sack L (2012) Dynamics of leaf hydraulic conductance with water status: quantification and analysis of species differences under steady-state. Journal of Experimental Botany 63: 643-658

Scoffoni C, Pou A, Aasamaa K, Sack L (2008) The rapid light response of leaf hydraulic conductance: new evidence from two experimental methods. Plant Cell and Environment 31: 1803-1812

Scoffoni C, Rawls M, McKown A, Cochard H, Sack L (2011) Decline of leaf hydraulic conductance with dehydration: relationship to leaf size and venation architecture. Plant Physiology 156: 832-843

Seelig HD, Stoner RJ, Linden JC (2012) Irrigation control of cowpea plants using the measurement of leaf thickness under greenhouse conditions. Irrigation Science 30: 247-257

Shatil-Cohen A, Attia Z, Moshelion M (2011) Bundle-sheath cell regulation of xylem-mesophyll water transport via aquaporins under drought stress: a target of xylem-borne ABA? Plant Journal 67: 72-80

Sheriff DW, Meidner H (1974) Water pathways in leaves of *Hederal helix* L and *Tradescantia virginiana* L. Journal of Experimental Botany 25: 1147-1156

Sokal RR, Rohlf FJ (1995) Biometry: the principles and practice of statistics in biological research. Third edition. W.H. Freeman and Company, New York, New Yord, USA

Syvertsen JP, Levy Y (1982) Diurnal changes in citrus leaf thickness, leaf water potential and leaf to air-temperature difference. Journal of Experimental Botany 33: 783-789

Tang AC, Boyer JS (2007) Leaf shrinkage decreases porosity at low water potentials in sunflower. Functional Plant Biology 34: 24-30

Tyree MT, Cameron SI (1977) New technique for measuring oscillatory and diurnal changes in leaf thickness. Canadian Journal of Forest Research-Revue Canadienne De Recherche Forestiere 7: 540-544

Tyree MT, Hammel HT (1972) Measurement of turgor pressure and water relations of plants by pressure bomb technique. Journal of Experimental Botany 23: 267-282

Tyree MT, Zimmermann MH (2002) Xylem Structure and the Ascent of Sap. Springer, Berlin, Germany.

Waite M, Sack L (2010) How does moss photosynthesis relate to leaf and canopy structure? Trait relationships for 10 Hawaiian species of contrasting light habitats. New Phytologist 185: 156-172

Wylie RB (1943) The role of the epidermis in foliar organization and its relations to the minor venation. American Journal of Botany 30: 273-280

Zimmermann MH (1978) Hydraulic architecture of some diffuse-porous trees. Canadian Journal of Botany-Revue Canadienne De Botanique 56: 2286-2295

CHAPTER 5

ARE LEAVES "FREEWHEELIN'"? TESTING FOR A WHEELER-TYPE EFFECT IN LEAF XYLEM HYDRAULIC DECLINE

ABSTRACT

A recent study found that cutting shoots under water while xylem was under tension (which has been the standard protocol for the past few decades) could produce artifactual embolisms inside the xylem, overestimating hydraulic vulnerability relative to shoots cut under water after relaxing xylem tension (Wheeler *et al*. 2013). That study also raised the possibility that such a "Wheeler effect" might occur in studies of leaf hydraulic vulnerability. We tested for such an effect for four species by applying a modified vacuum pump method to leaves with minor veins severed, to construct leaf xylem hydraulic vulnerability curves. We tested for an impact on leaf xylem hydraulic conductance (K_x) of cutting the petiole and minor veins under water for dehydrated leaves with xylem under tension compared to dehydrated leaves on previously relaxed xylem tension in shoots. Our results showed no significant "cutting artifact" for leaf xylem. The lack of an effect for leaves could not be explained by narrower or shorter xylem conduits, and may be due to lesser mechanical stress imposed when cutting leaf petioles, and/or to rapid refilling of emboli in petioles. These findings provide the first validation of previous measurements of leaf hydraulic vulnerability against this potential artifact.

Key words: Cavitation, evaporative flux method, hydraulic resistance, xylem anatomy

INTRODUCTION

The bulk of water movement through the plant occurs to replace the water lost through stomata during transpiration: stomata open to capture CO_2 for photosynthesis, and water is lost by diffusion to the dry atmosphere. When soil water supply becomes scarce, large tensions build up in the xylem, and cavitation may occur by air seeding: small air bubbles are pulled into xylem conduits, embolizing them, thus making them nonfunctional (Tyree & Zimmermann, 2002). For the past several decades, scientists have quantified water movement through the plant under different water statuses by measuring hydraulic conductance in the lab. To do so, branches are typically dehydrated on the lab bench, samples are then cut under water (with xylem still under tension) before being measured for hydraulic conductance which avoids opening conduits to further embolism and thus maintaining the original xylem hydraulic integrity. However, a recent study challenged this methodological approach, arguing that even cutting the sample under water while xylem is under tension can lead to additional embolism in the xylem conduits (Wheeler *et al.*, 2013). Indeed, microbubbles had been hypothesized to arise a century ago from the cut end of the knife (either because it is not completely wetted when the cut is made, or because of small particles that could be found on a not perfectly clean knife) (Dixon, 1914), and/or could be released from the apoplast when the cut is made (Wheeler *et al.*, 2013), especially if the stem is subjected to strong mechanical pressure or bending that could compress xylem conduits or deform pits even transiently (Lopez *et al.*, 2014; Mayr *et al.*, 2014). Wheeler et al. (2013) tested for this artifact using stem samples on up to four temperate tree species depending on their treatments, by measuring stem hydraulic conductance of samples recut under water in the standard way (under tension) vs. samples recut under water after the tension inside the xylem was relaxed, and found a significant impact of cutting under tension underwater, which they

hypothesized to arise from bubbles entering the cut end, with their entry depending on the degree of tension and the xylem anatomy, though these mechanisms were not directly tested (Wheeler *et al.*, 2013).

While Wheeler *et al.* focused their study on the presence and impact of this artifact on stem hydraulic conductance measurements, they noted this could equally apply to hydraulic measurements for leaves and urged further testing (Wheeler *et al.*, 2013). The aim of our paper was to test for this "cutting artifact" in leaves.

Unlike in stems, water movement in leaves follows two pathways in series: xylem water transport in the leaf petioles and veins, and extra-xylary transport through the living bundle sheath and mesophyll cells to the sites of evaporation in the leaf. Thus, the leaf hydraulic conductance (K_{leaf}) is dependent on the hydraulic conductance of the xylem (K_x) and extraxylem pathways (K_{ox}):

$$K_{leaf} = (K_x^{-1} + K_{ox}^{-1})^{-1} \quad \text{eqn 1}$$

The resistance to water movement in each pathway has been shown to vary across species, from 12% to 89% in the xylem (Cochard *et al.*, 2004; Sack *et al.*, 2004; Sack *et al.*, 2005). Thus, because the "cutting artifact" theory would only affect the leaf xylem, the impact on K_{leaf} would depend on the amount of hydraulic resistance allocated to the xylem, and further whether the embolism generated by the "cutting artifact" would noticeably impact measurements of K_x. Testing for such an artifact on whole leaves would be impossible, since rehydrating shoots prior to cutting to relax the xylem tension would most likely also rehydrate mesophyll cells, which would increase K_{ox} (Scoffoni *et al.* 2012, 2014), and create the impression that there might be a "cutting artifact". Thus, to test for a cutting artifact on the hydraulic conductance of dehydrated leaves, it is necessary to test the impact on K_x directly. Methods used to measure K_x have all

involved measuring the flow of water through veins under high or low positive pressures (Cochard *et al.*, 2004; Sack *et al.*, 2004; Nardini *et al.*, 2008). Here, we directly tested this hypothesis on the leaf xylem by developing a new method to calculate K_x under vacuum conditions, with attention to simulating natural flow of water though the veins, and avoiding positive pressure that could lead to artifactual refilling of embolized conduits during the measurement. We constructed leaf xylem vulnerability curves for four diverse species varying in leaf texture, allocation to xylem vs. outside-xylem conductance and drought tolerance, and tested whether measurements differed in treatments that relaxed the xylem tension in dehydated leaves.

MATERIAL AND METHODS

Plant Material

Four species with a wide diversity in phylogeny, growth form and drought tolerance traits were selected in and around the campus of University of California, Los Angeles and Will Rogers State Park, Los Angeles, California (Table 5.1). Experiments were conducted from November 2013 to April 2014. Light exposed shoots from three mature individuals per species were collected the night prior to the start of measurements and placed in a double layer of plastic bags filled with wet paper towels. They were directly transported to the lab where they were recut at least two nodes distal to the original cut under ultra-pure water (Millipore, 0.22 μm Thornton 200CR, Molshem, France) and rehydrated overnight at laboratory temperature (20-23°C), covered in double layer of plastic bags filled with wet paper towels to halt transpiration.

Measuring leaf xylem hydraulic decline using the vacuum pump method

The vacuum pump method was first developed to measure whole shoots and roots hydraulic conductance (Kolb *et al.*, 1996) and later modified to measure leaf hydraulic conductance

(Martre *et al.*, 2001; Nardini *et al.*, 2001; Sack *et al.*, 2002; Brodribb & Holbrook, 2003; Lo Gullo *et al.*, 2003). In this method, the hydraulic conductance is determined as the slope of the change in flow rate over the change in vacuum level. Here, we modified this technique to measure K_x.

Shoots of at least three leaves were cut under water from the larger rehydrated shoots and were allowed to dehydrate on the bench (or on a fan) to achieve a wide range of water potentials. Then, the leaves on the shoots were individually sealed in bags (Whirl-Pak; Nasco, Fort Atkinson, WI, USA), which had been previously exhaled in, and then the entire shoot with bagged leaves was placed inside a larger sealable bag with wet paper towel, to equilibrate for at least 30 minutes. For the maximum K_x values, rehydrated shoots were immediately bagged in this way. After equilibration was reached, the top and bottom leaf from each shoot were excised and measured for leaf water potential (Ψ_{leaf} = leaf xylem potential since leaves were equilibrated) using the pressure chamber (Plant Moisture Stress, Model 1000, Albany, OR, USA). If the values differed by more than 0.2 MPa (or 0.3 MPa in very dehydrated leaves), the shoot was discarded.

The lamina of a third leaf (still connected to the shoot) was then placed under ultra-pure water over a white-light transilluminator table (Model TW, UVP, Upland, CA, USA), allowing visualization of minor veins (4^{th} order and higher). Cuts were made to open up the bulk of the minor vein network using a scalpel with cuts between approximately 95% of tertiary veins throughout the leaf, so that the number of cuts per leaf area ranged 7.3-34 cuts/ cm^2 depending on species, enough such that water would move directly out of the cut minor veins, "shorting" out the resistance outside the xylem (Sack *et al.*, 2004). Because species with larger leaves have their tertiary veins spaced apart further (Sack *et al.*, 2012) than smaller leaves, fewer, longer cuts

were made in larger leaves (length of cuts ranged 0.8 to 4 mm depending on leaf size). Special care was taken that no major veins (first, second and third orders) were severed in the process. Cuts were rapidly made within 5-15 min. Once all the cuts were made, the leaf was excised from the shoot at the base of the petiole under ultra-pure water, and stretched parafilm was quickly wrapped around it before it was re-cut at the end (≤1 mm) under water using a fresh razor blade, and connected under ultrapure water to silicone tubing (Cole-Parmer, Vernon Hills, IL, USA) or compression fitting (Omnifit A2227 bore adaptor; Omnifit, Cambridge, UK) connected to hard tubing running to a water source on a balance (models XS205 and AB265, ± 10 μg sensitivity; Mettler Toledo, Colombus, OH, USA). The water was degassed overnight using a vacuum pump (Gast, Benton Harbor, MI, USA) and refiltered (0.2 μm; Syringe filter; Cole-Parmer). For species with smaller petioles for which silicone tubing was preferred (*C. diversifolia* and *Q. agrifolia*), vacuum tight seals between the petiole and tubing were obtained by tightening the tubing around the petiole with zipties and sealing off the exposed end of the tubing to the petiole using super glue (Loctite 409 Glue; McMaster-Carr, Los Angeles, CA, USA) with accelerator (Loctite 712 accelerator). Leaves were then placed along with a thermocouple (Cole-Parmer) in vacuum flasks connected by a four-way valve to a vacuum pump (Gast) and a pressure gauge (± 0.002 MPa; J4605 Marsh/Bellofram; Marshall Instruments Inc., Anaheim, CA, USA).

Five vacuum levels were applied, starting at approximately 0.06 MPa and then reducing by 0.01 MPa intervals until 0.02 MPa was reached. The mass of water on the balance was logged to a computer every 30s for the calculation of flow rate through the leaf xylem. Leaves were left under a given vacuum until stable flow rate was achieved, with a coefficient of variation <5% for at least 5 min. It took about 30 min to 2 h for the flow rate under the first vacuum level to achieve stability depending on the species and leaf size (the larger the leaf, the longer the

equilibration times). For the subsequent vacuum levels, stabilization time ranged from about 10 min to 1 h. Once the flow was stable, the vacuum level inside the flask was recorded from the pressure gauge, as well as the leaf temperature from the thermocouple (20-25°C for all experiments). Once all five points of flow rates vs. vacuum pressure were measured, we tested for possible leaks from the system by cutting the leaf lamina off under water, and sealing the petiole end with superglue. Leak flow rate for given vacuum levels were measured in the same way as described above. Leaf xylem hydraulic conductance (K_x) was calculated as the slope of the flow rate against vacuum pressures, normalized for leaf area, and for the effect of temperature on the viscosity of water (Weast, 1974 ; Yang & Tyree, 1993; Sack *et al.*, 2002). The leak hydraulic conductance was calculated in the same way as described above. Only 11% (18/161) of measurements across all leaves and species were found to have small leaks during the measurement. Because flow through the leak would be in parallel with that of the leaf, the leak hydraulic conductance values were subtracted from K_x. To construct leaf xylem vulnerability curves, we plotted K_x values against the average of the two Ψ_{leaf} values determined at the start of the experiment for a given shoot. We note that, with this method, leaf xylem hydraulic vulnerability curves can take two weeks to a month to construct, depending on the species.

Testing for a "cutting artifact" on leaf xylem hydraulic conductance

We designed a "standard protocol" for measuring K_x for vulnerability curves, reducing the time the petiole is in contact with water. We cut the leaf from the shoot under water after having previously made the cuts to the minor veins with the lamina under water (Fig. 5.1A). According to Wheeler *et al*. (2013), this standard protocol could potentially create artifactual embolims in

the leaf minor veins since minor veins are cut under water while the leaf is under tension. Alternatively, because conduit sizes in the minor veins are very small, and thus potentially less prone to be affected by artifactual bubble formation at the cut ends, this standard protocol might instead be simply relaxing the tension in the leaf xylem before the leaf is cut from the shoot, thus acting to prevent the "cutting artifact" from occurring. Thus, we applied two additional treatments to determine whether a "cutting artifact" might influence leaf xylem conductance (K_x) (Fig. 5.2).

We first tested a "petiole cut under tension" treatment: i.e., whether excising the leaf under water while the shoot xylem is still under tension could induce an embolism artifact in the petiole that would impact K_x (Fig. 5.1B). This treatment parallels most closely the scenario experienced by the leaf xylem for leaves measured for K_{leaf} during the construction of typical whole leaf hydraulic vulnerability curves. Here, we prepared 5-6 shoots per species of at least three leaves dehydrated to approximately the xylem water potential values corresponding to 50% loss of K_x (see Result section *"Leaf xylem hydraulic vulnerability curves: results from maximum likelihood analysis"*; Table 5.1); as assessed from the Ψ_{leaf} of the top and bottom leaf on the shoot. For this treatment, the measurement leaf was excised under water while shoot xylem was under tension, prior to making the minor vein cuts with the leaf under water. Here, we might have expected the "cutting artifact" to occur at the petiole, which was cut under strong negative pressures (Fig. 5.2). Once all the minor vein cuts were made, the leaf was connected to the system, and K_x determined in the same way as described for the standard protocol.

We then tested a "relaxed tension" treatment (Fig. 5.1C). To do so, we prepared 5-6 shoots per species of at least four leaves dehydrated to approximately the xylem water potential values corresponding 50% loss of K_x based on the K_x vulnerability curves (see Result section

"Leaf xylem hydraulic vulnerability curves: results from maximum likelihood analysis"; Table 5.1); as assessed from the Ψ_{leaf} of the top and bottom leaf on the shoot. Then, before making cuts to the leaf veins under water, we first cut a different leaf from the shoot under water, relaxing xylem tension throughout the whole shoot, and then 1-2 min later we performed the cuts to the veins of the leaf to be measured for K_x. Once the cuts were made, the leaf was excised and cut under water and K_x was measured as described by the standard protocol. This treatment was designed to prevent any "cutting artifacts" from occurring either when making the cuts to the veins or when excising the leaf petiole under water before it is connected to the system (Fig. 5.2).

Construction of whole-leaf hydraulic vulnerability curves and calculation of the percent resistance in the xylem

For three of the four species, we used values of maximum leaf hydraulic conductance ($K_{leaf,\ max}$) and the water potential at 80% loss of hydraulic conductance reported in a previous paper for the same species and individuals (Scoffoni *et al.*, 2012). A leaf hydraulic vulnerability curve was constructed for *Salvia canariensis* using the Evaporative Flux Method following the previously described and filmed protocol (Sack & Scoffoni, 2012). An exponential function ($K_{\mathrm{leaf}} = -0.82 + 53.7 \times e^{-2.63\Psi_{\mathrm{leaf}}}$) was found to best fit the data using maximum likelihood (Fig. S5.1).

Measurement of maximum xylem conduit length

To test whether maximum xylem conduit length would explain our findings for the "cutting artifact", we selected three to 10 leaves from shoots of three individuals per species that had been rehydrated overnight as described above. Leaves were connected by silicone tubing to a four way

valve connected to a syringe. Zipties were applied around the tubing and petiole to ensure a tight seal. Air pressure was applied using a caulking gun while the leaf was placed under water, over the transilluminator table. Using a scalpel, cuts were made throughout the leaf beginning with the highest order veins, and progressively to lower order veins, and finally along the midrib toward the leaf base, until air bubbles first emerged from the xylem, indicating maximum conduit length.

Statistics

Maximum likelihood was used to select the best fit function for each species' leaf xylem hydraulic conductance using the *optim* function in R 3.0.0 as previously described in the literature (http://www.r-project.org; Burnham & Anderson, 2002; Burnham & Anderson, 2004; Scoffoni *et al.*, 2012). Five functions were tested (Scoffoni *et al.*, 2012; Scoffoni *et al.*, 2014): linear ($K_x = a\Psi_x + y_o$), two-parameter sigmoidal ($K_x = \frac{100}{1+e^{(a(\Psi_x - b)}}$), three-parameter sigmoidal ($K_x = \frac{a}{1+e^{-(\frac{\Psi_x - x_o}{b})}}$), logistic ($K_x = \frac{a}{1+(\frac{\Psi_x}{x_o})^b}$), and exponential ($K_x = y_o + ae^{-b\Psi_x}$). For each data set, functions were compared with the Akaike Information Criterion (AIC) corrected for low *n*, and the function with the lowest AIC score and highest r^2 value was chosen. From the best fit function, we calculated the maximum K_x ($K_{x,max}$) for each species. The % resistance in the xylem was then obtained as the inverse of $K_{x,max}$ / $K_{leaf,max}$, (since hydraulic resistance = 1/hydraulic conductance).

To test whether K_x values differed across treatments, we calculated the average and standard deviation of K_x and leaf xylem water potential for the leaves in each treatment and compared them using a one-sample two-tailed *t*-test to the K_x obtained from the species' K_x vulnerability curve at that same water potential (Minitab Release 16).

RESULTS

Leaf xylem hydraulic vulnerability curves: results from maximum likelihood analysis

The vacuum pump method was effective for construction of leaf K_x vulnerability curves (Fig. 5.3). Species differed in the shape of their K_x vulnerability curves (Fig. 5.3, Table S5.1): *S. canariensis* showed a linear decline whereas the other three species showed a non-linear decline (sigmoidal functions were selected by maximum likelihood for *C. diversifolia* and *H. canariensis* and logistic function for *Q. agrifolia*). Species also differed in their % leaf hydraulic resistance in the xylem at full hydration, ranging from 8.4% in the California chapparal species *C. diversifolia* to 77% in the herb *S. canariensis* (Table 5.1). Xylem water potential at 50% loss of K_x ranged from -0.89 MPa in *S. canariensis* to -5.59 MPa in *C. diversifolia* (Table 5.1).

Testing for a "cutting artifact" in leaf xylem hydraulic conductance

No significant differences in the K_x of dehydrated leaves were observed when applying the three cutting treatments for any of the four species (Table 5.2, Fig. 5.3). Indeed, neither mean K_x values from leaves of shoots with relaxed tension (white triangles in Fig. 5.3) or from leaves with petioles cut under tension (grey squares in Fig. 5.3) differed statistically from the predicted K_x value from the best fit function through data points obtained from the "standard protocol" in which minor veins were cut under tension before cutting the petiole from the stem under water ($p = 0.097$-0.56 across treatments and species; Table 5.2, Fig. 5.3).

Species variation in maximum xylem conduit length

Vein orders in which the longest xylem conduits from the petiole ended differed across individuals even for given species (Table 5.1). For all leaves of all species, the longest xylem

conduits from the petiole had ended by the secondaries or tertiaries, i.e., before the minor vein network.

DISCUSSION

"Don't think twice, it's alright" —, Bob Dylan,"The Freewheelin' Bob Dylan" (1963)

This study demonstrated that the "cutting artifact" had no impact on leaf xylem hydraulic conductance measured for dehydrated leaves. These findings provide the first validation of previous measurements of leaf hydraulic vulnerability against this potential artifact. Indeed, our results showed no significant differences in leaf xylem hydraulic conductance (K_x) of leaves cut off shoots after relaxing the xylem tension relative to shoots with high xylem tensions, for four diverse species differing in their initial % allocation to xylem vs. outside-xylem conductance.

This finding for leaves contrasted strongly with the effect shown to occur for the stem xylem for some species (Wheeler *et al.*, 2013). Indeed, for two maple species, Wheeler *et al.* found that stem percent loss of hydraulic conductance (PLC) was 43 to 71% lower when shoot xylem tension was relaxed prior to cutting after shoots were dehydrated to around water potentials at 50% loss of hydraulic conductance, thus indicating that these species were slightly less vulnerable to cavitation than previously thought. However, no significant difference was found in *Betula papyrifera* stem vulnerability curves for relaxed vs. non-relaxed shoots, suggesting that for stem tissue this "cutting artifact" is dependent on species and potentially depends on xylem anatomical traits, such as conduit diameter, length and/or presence of perforation plates (Wheeler *et al.*, 2013; Rockwell *et al.*, 2014).

Why should leaf xylem show no sensitivity to a Wheeler-type effect? Although no mechanistic explanation has been tested to explain this effect in stems, several hypotheses have

been raised. The main goal of our paper was to test, as it has been done in stems, whether this artifact has an effect in leaf hydraulics measurement. Since no effect was found, we discuss the possible explanation as to why leaves were found to differ from stems. A first possibility is that the difference arises because xylem conduits in petioles are narrower than those in stems, given that air bubbles may form more rapidly or enter more easily in wider conduits (Wheeler *et al.*, 2013; Rockwell *et al.*, 2014). We do not have data on petiole xylem conduit diameters, but values are available for mean midrib xylem conduit diameters for the same plants of these species, and these midrib conduit diameters would be yet narrower than those in the petiole: 27.8, 59.5, 27.2 and 198 μm for *C. diversifolia*, *H. canariensis*, *Q.agrifolia* and *S. canariensis* respectively (John *et al.*, 2013). This range of diameters encompassed that for stem mean vessel diameters previously reported for *Acer rubrum*, and *Betula papyrifera* used in the study by Wheeler *et al.* (45.3 and 34.0 μm respectively; Jacobsen *et al.*, 2012). If xylem conduit diameter was an important factor in determining the "cutting artifact", then we would have expected *S. canariensis* to show a strong effect, given its midrib conduit diameter over 4-fold greater than that of *A. rubrum*, which had showed the strongest "cutting artifact" (Wheeler *et al.*, 2013).

A second possibility for the lack of a "cutting artifact" in leaves is that it could be due to shorter xylem conduit lengths in leaves. Indeed, in shorter conduits, any embolism created artifactually by cutting under tensions would be expected to be stopped at end walls close to the cut, and thus these might have been trimmed off when trimming the petiole with a clean cut before it is placed on the system (Wheeler *et al.*, 2013; Rockwell *et al.*, 2014). Maximum conduit lengths have been reported to be of 0.14 m in *A. rubrum*, and mean vessel lengths of 0.03, 0.03 and 0.02 m in *A. rubrum*, *A. saccharum* and *B. papyrifera* (Jacobsen *et al.*, 2012). Although not as long as vessel lengths in stems, xylem conduits in leaves of our study species showed

continuity up to third order veins (Table 5.1). Of course, mean conduit length might play a more important role than maximum conduit length; however, it is unlikely that xylem conduits in the petiole are on average ≤ 1 mm long (the length of the final cut we make before connecting the leaf on the system), enabling the removal of any artifactual embolism that might have formed in these small enclosed conduits. Further studies of xylem conduit distributions in petioles and leaf veins are needed to fully verify our rejection of the idea that conduits are so short that trimming the petiole would remove embolisms that entered during cutting.

If neither conduit diameters nor lengths play a role in explaining the lack of a "cutting artifact" in leaves, we posit three other possible explanations for consideration. First, it is possible that if this effect arises from bubbles introduced from the blade itself (Dixon, 1914), our use of a fresh razor blade and partially degassed water might both reduce the bubbles and draw any small bubbles out of the cut petiole on attaching it to the tubing. Second, it is possible that the Wheeler effect is in part or entirely caused by air entering from airspaces within the stem aggravated by the mechanical disturbance generated by the act of cutting stems, especially as this would generate high and low pulses of pressure by deforming conduits (Lopez *et al.*, 2014; Mayr *et al.*, 2014). Such pressure pulses within the xylem would be expected to cause transient expansion of vapor spaces within xylem conduits as the conduits shrink and stretch and/or might cause air seeding across pit membranes. Any such effects due to physical disturbances during cutting would be much reduced in a petiole relative to the stem given their reduced diameters, densities and mechanical strength. Indeed, the xylem conduits and their pit membranes within leaves might be adapted to cope with the effects of transient pressures in the xylem caused by mechanical disturbances of the magnitude as that imposed by cutting the petiole with a sharp blade, whereas stems might not be adapted to the effects of disturbances as severe as those

imposed when cutting them for hydraulics measurements. Indeed, leaves suffer major mechanical stresses such as when they are blowing in the wind, or if a hard rain is to fall on them.

A third possible explanation for the lack of a "cutting artifact" in leaves is that this artifact arises itself from an artifact of hastening xylem refilling in a stem with its xylem tension relaxed (Trifilo *et al.*, 2014). Indeed, the "cutting artifact" disappeared in two Mediterranean tree species, *Laurus nobilis* and *Olea europaea*, when stems were girdled or exposed to Sodium orthovanadate (Na_3VO_4) prior to measurements, both of which treatments would impede xylem refilling. The authors concluded that relaxing the stem xylem tension before cutting, as proposed by Wheeler et al., could in fact be inducing xylem refilling before the sample is placed on the system, and thus under estimating PLC values. If such a scenario were true, we would expect to find a Wheeler effect only in those species in which xylem refilling occurs. In leaves, recovery of K_{leaf} with rehydration was found for four species with petioles under water for up to 1 h including *C. diversifolia* which recovered completely in K_{leaf} after 1h (Trifilo *et al.*, 2003; Scoffoni *et al.*, 2012). However, this could be due to recovery in K_{ox} rather than K_x (Scoffoni *et al.*, 2014). Only one study to our knowledge, for *Helianthus annuus*, using dye experiments has showed that after rehydration vein staining after infiltration with Phloxine B, an apoplastic dye, was greater than for dehydrated ones, suggesting embolism refilling had occured in the leaf veins, though the time scale of the process was not clear (Trifilo *et al.*, 2003). More studies are needed to confirm embolism recovery in leaves after rapid rehydration.

More study will be needed of stem xylem tissue to fully understand the mechanism(s) underlying the "cutting artifact". For leaves, based on this first detailed study, until an artifact is

shown, one may consider the previous literature on leaf hydraulic vulnerability to be validated against this effect.

ACKNOWLEDGMENTS

We thank Megan Bartlett, Marissa Caringella and Grace John for valuable comments on the manuscript, and Brendan Choat for discussion. This study was funded by the National Science Foundation (grants IOS-0753233 and IOS-1147292) and the UCLA Dissertation Year Fellowship.

Table 5.1. Study species, family and mean ± standard error for drought tolerance leaf traits and hydraulics. *LA*, leaf area; *TLP*, turgor loss point; *LMA*, leaf mass per unit leaf area; K_{max}, leaf hydraulic conductance at full turgor; $\%R_x$, percent hydraulic resistance in the xylem; Leaf P_{80}, water potential at which 80% of leaf hydraulic conductance is lost; Xylem P_{50}, xylem water potential at which 50% of the xylem hydraulic conductance is lost. Data for *TLP*, *LMA*, K_{max} and leaf P_{80} are from previous papers (Scoffoni *et al.*, 2012; Scoffoni *et al.*, 2014), except for K_{max} and leaf P_{80} of *S. canariensis* which were obtained in this study.

Species	Family	Growth form	LA (cm^2)	TLP (MPa)	LMA ($g\ m^{-2}$)	K_{max} (mmol $m^{-2}\ s^{-1}\ MPa^{-1}$)	$\%R_x$	Maximum vessel length	Leaf P_{80} (MPa)	Xylem Px_{50} (MPa)
Comarostaphyllos diversifolia	Ericaceae	Tree	9.64 ± 0.42	3.45 ± 0.34	253 ± 16.9	2.96	8.4	2o (2/5 leaves)	-4.56	-5.59
Hedera canariensis	Araliaceae	Shrub	81.0 ± 4.52	1.98 ± 0.09	84.1 ± 11.0	5.73	23	3o (3/10)	-1.18	-1.89
Quercus agrifolia	Fagaceae	Tree	9.41 ± 0.42	3.00 ± 0.12	188 ± 7.53	3.96	14	2o (3/3)	-3.83	-5.43
Salvia canariensis	Lamiacaeae	Herb	20.7 ± 2.28	1.18 ± 0.07	41.4 ± 6.01	52.9	77	2o (2/5)	-0.59	-0.89

Table 5.2. Testing the "cutting artifact": number of samples (*n*), xylem water potential ± standard deviation, predicted xylem hydraulic conductance (K_x) for leaves of the three treatments depicted in Fig. 5.1, based on the mean xylem water potential obtained from the leaf xylem vulnerability curve using the "standard protocol treatment", along with the expected and resulting trends and *p*-value from one-sample *t*-test. A $p > 0.05$ is considered non-significant. According to the framework depicted in Fig. 5.2, one would expect the "standard protocol" treatment to either have relaxed the xylem tension by cutting the leaf veins under water or to introduce embolism into minor veins during that cutting; thus, K_x should either be the same or lower than that for the "relaxed tension treatment". By contrast, leaves of "petioles cut under tension treatment" should show significantly lower K_x due to embolism in their petioles.

Treatment	"Relaxed tension treatment"				"Petiole cut under tension treatment"			
Species	*n*	Ψ_x ± SD	Predicted K_x from the "standard protocol"	Mean K_x ± SD (*p*-value for comparison with "standard protocol"	*n*	Ψ_x ± SD	Predicted K_x from the "standard protocol"	Mean K_x ± SD (*p*-value for comparison with "standard protocol"
C. diversifolia	6	-5.41 ± 0.35	18.8	20.5 ± 1.13 (0.25)	6	-4.38 ± 0.23	25.7	27.7 ± 1.73 (0.30)
H. canariensis	5	-2.72 ± 0.16	3.21	4.13 ± 1.46 (0.56)	6	-1.82 ± 0.09	13.6	15.7 ± 1.26 (0.16)
Q. agrifolia	6	-5.63 ± 0.07	12.0	8.70 ± 2.15 (0.19)	5	-5.24 ± 0.09	16.9	15.4 ± 1.18 (0.27)
S. canariensis	6	-1.17 ± 0.05	23.4	18.4 ± 3.89 (0.26)	5	-1.10 ± 0.16	26.1	35.5 ± 4.35 (0.097)

FIGURE CAPTIONS

Figure 5.1. Experimental design: (A) "Standard treatment": minor vein cuts were applied on leaves with xylem under tension before the petiole was cut under water, for measurement of xylem hydraulic conductance (K_x). (B) "Petiole cut under tension treatment": the petiole was cut under water for a leaf with xylem under tension before minor vein cuts were applied and the leaf measured for K_x. (C) "Relaxed tension treatment": Another leaf on the shoot was cut under water releasing the xylem tension, before minor vein cuts were made for the measurement leaf, and the petiole was cut under water for measurement of K_x. Red asterisk indicates when the xylem is cut under tension: in treatments A and B, cuts could potentially cause an artifact in petioles and minor veins; in treatment C, no "cutting artifact" would be observed.

Figure 5.2. Flowchart presenting the interpretation of differences between the "Standard protocol treatment" and the two other treatments depicted in Fig. 5.1 ("Relaxed tension" and "Petiole cut under tension").

Figure 5.3. Leaf xylem hydraulic vulnerability curves for four diverse species in phylogeny, growth form, drought tolerance and xylem anatomy, ordered from most vulnerable on top to least on bottom. The line fitted through the black dots (obtained using the standard protocol) was selected as best fit function using maximum likelihood (see Methods and Table S5.1). A linear function was selected *for S. canariensis*: $K_x = -38.6 \times \Psi_x + 68.6$), a three-parameter sigmoidal function was selected for *H. canariensis* and *C. diversifolia*: ($K_x = \frac{25.5}{1+e^{-(\frac{\Psi_x - 1.87}{-0.44})}}$) and ($K_x = \frac{36.0}{1+e^{-(\frac{\Psi_x - 5.54}{-1.42})}}$) respectively. Finally, a logistic function was selected for *Q. agrifolia*: ($K_x = \frac{28.8}{1+(\frac{\Psi_x}{5.43})^{9.67}}$).

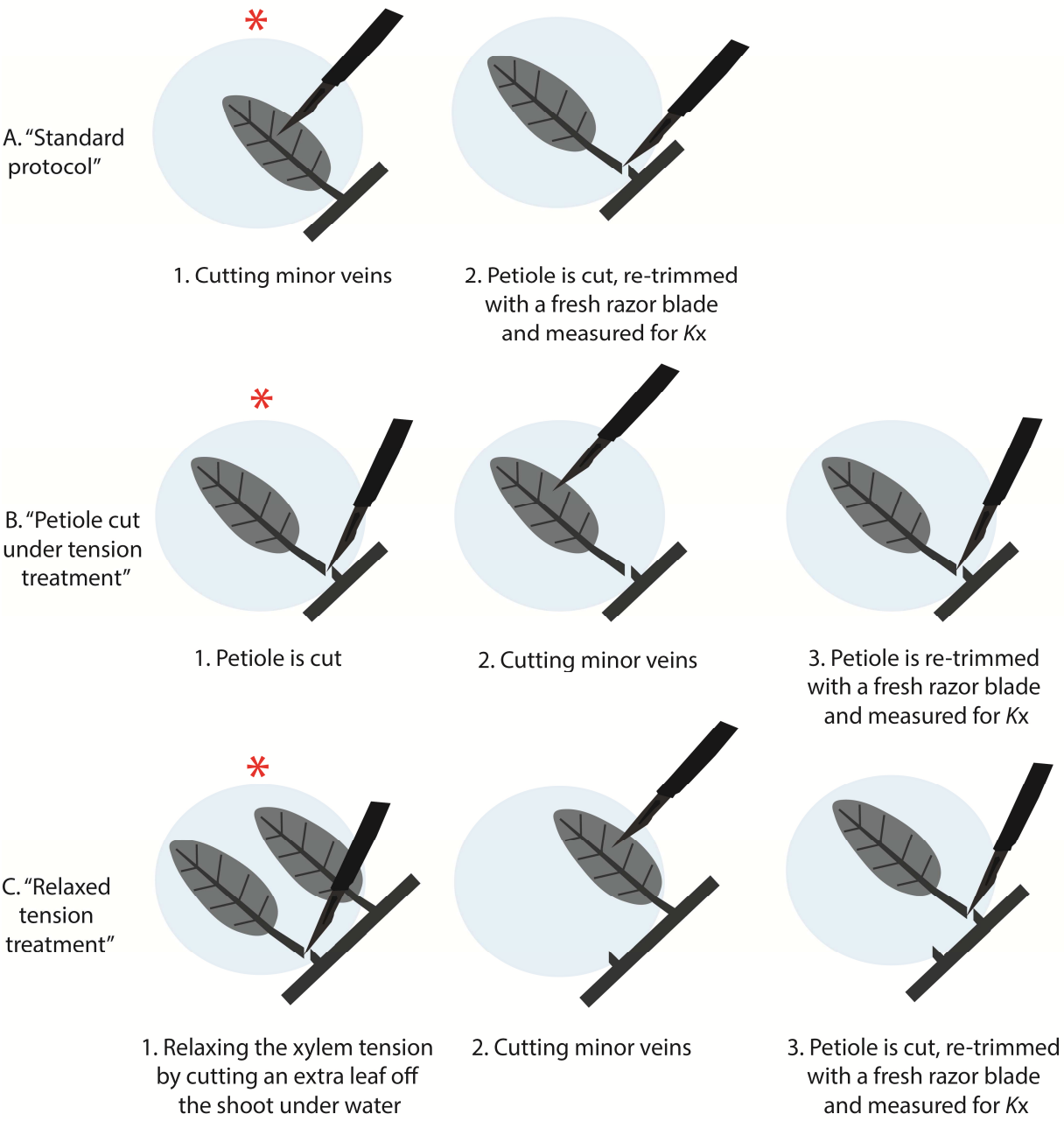
A. "Standard protocol"
1. Cutting minor veins
2. Petiole is cut, re-trimmed with a fresh razor blade and measured for Kx
B. "Petiole cut under tension treatment"
1. Petiole is cut
2. Cutting minor veins
3. Petiole is re-trimmed with a fresh razor blade and measured for Kx
C. "Relaxed tension treatment"
1. Relaxing the xylem tension by cutting an extra leaf off the shoot under water
2. Cutting minor veins
3. Petiole is cut, re-trimmed with a fresh razor blade and measured for Kx

Figure 5.1

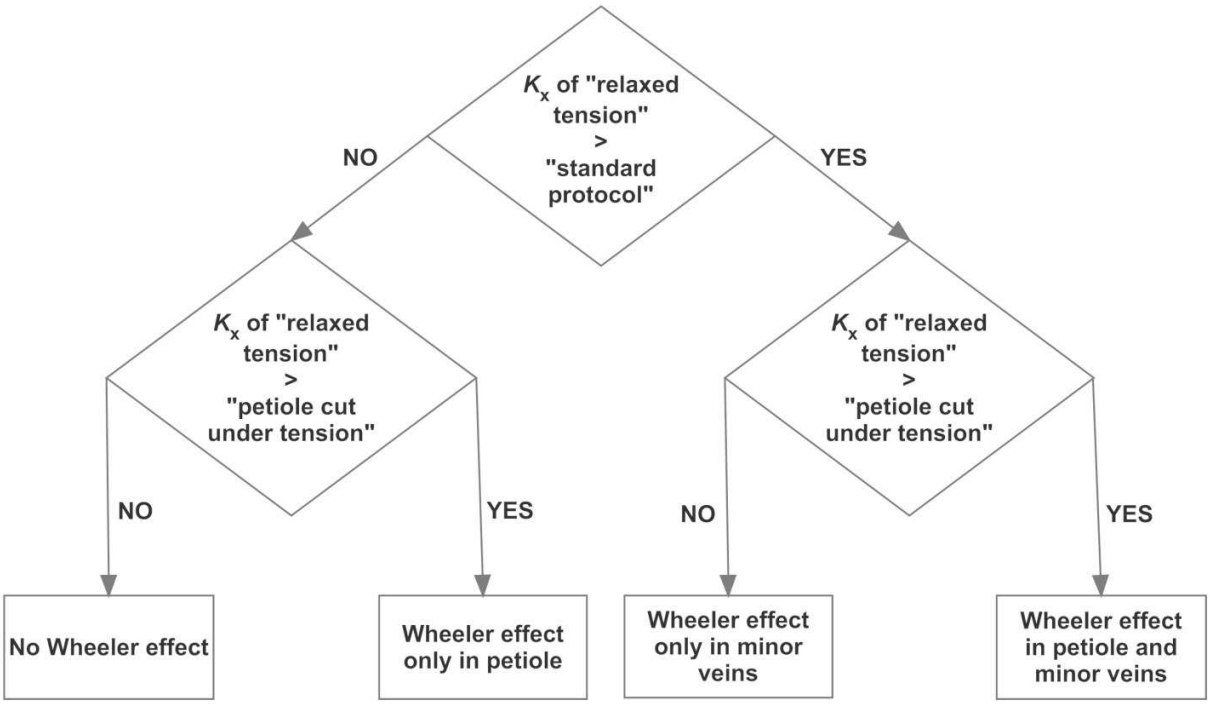
K_x of "relaxed tension" > "standard protocol"
NO
YES
K_x of "relaxed tension" > "petiole cut under tension"
K_x of "relaxed tension" > "petiole cut under tension"
NO
YES
NO
YES
No Wheeler effect
Wheeler effect only in petiole
Wheeler effect only in minor veins
Wheeler effect in petiole and minor veins

Figure 5.2

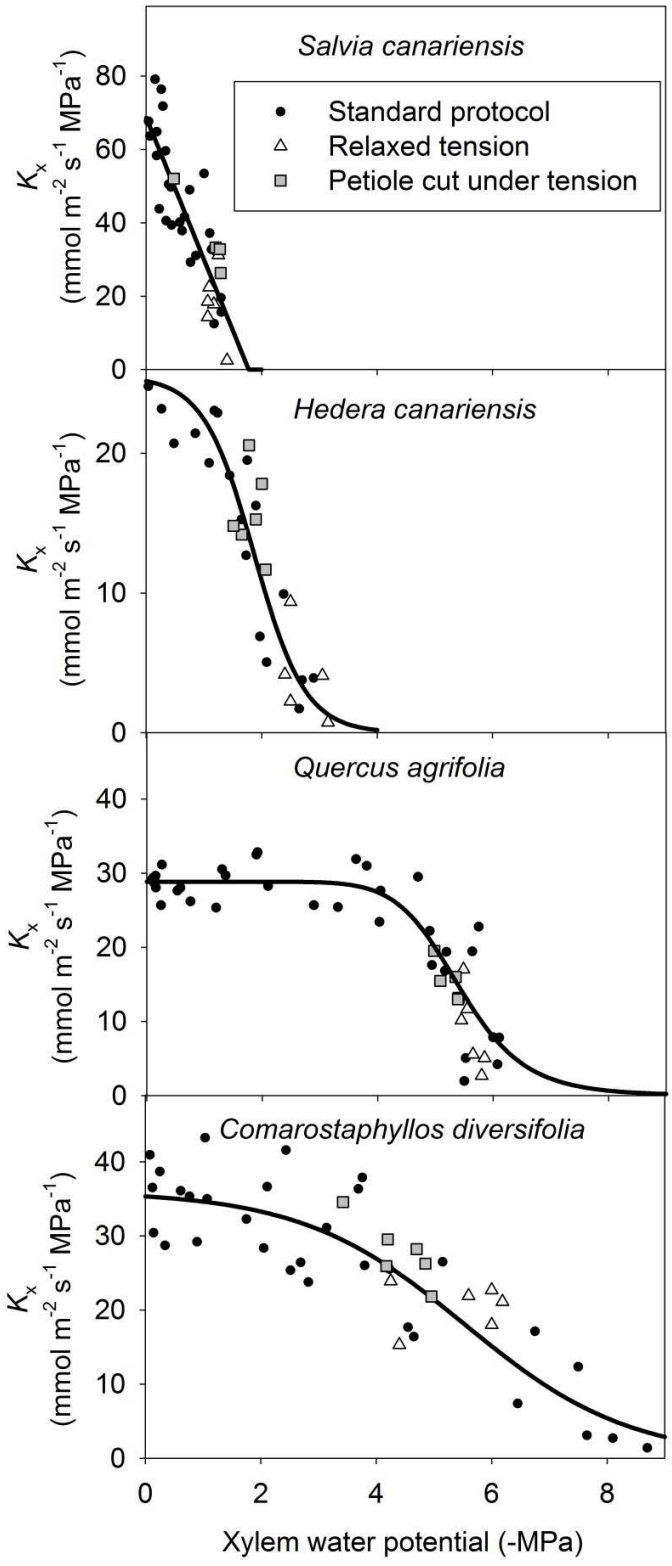
Salvia canariensis
Standard protocol
Relaxed tension
Petiole cut under tension
Hedera canariensis
Quercus agrifolia
Comarostaphyllos diversifolia
K_x (mmol m^{-2} s^{-1} MPa^{-1})
Xylem water potential (-MPa)

Figure 5.3

SUPPLEMENTAL MATERIAL

Table S5.1. Parameters (and standard errors) for the decline of xylem hydraulic conductance with dehydration for four species fitted with five different functions. Values in bold indicate the best-fit model for each species, r^2 for observed values plotted against predicted values, and values for the Akaike Information Criterion (AIC) corrected for low *n*.

Figure S1. Leaf hydraulic vulnerability of *Salvia canariensis* obtained using the Evaporative Flux Method. Best-fit function selected by maximum likelihood is fitted through the points: ($K_{\mathrm{leaf}} = -0.82 + 53.7 \times e^{-2.63\Psi_{\mathrm{leaf}}}$).

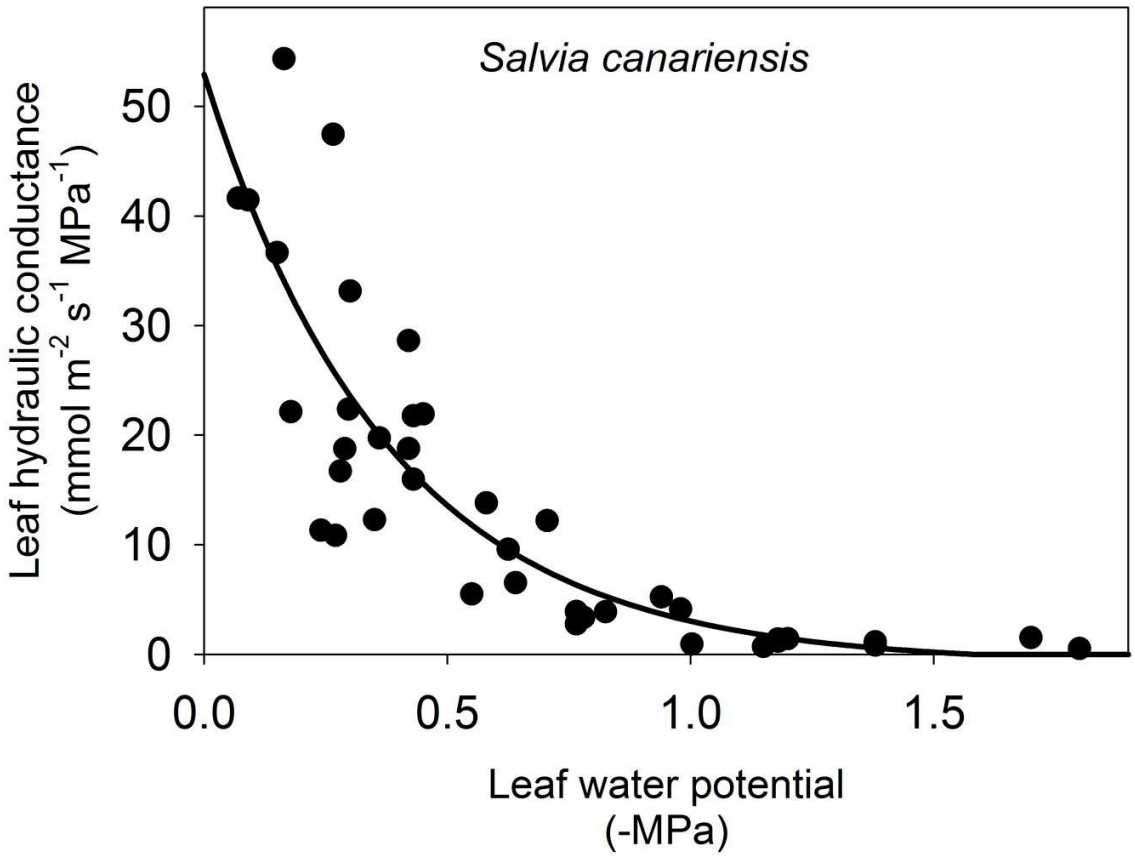
Salvia canariensis
Leaf hydraulic conductance
(mmol m-2 s-1 MPa-1)
50
40
30
20
10
0
0.0
0.5
1.0
1.5
Leaf water potential
(-MPa)

Figure S1

REFERENCES

Brodribb TJ, Holbrook NM. 2003. Changes in leaf hydraulic conductance during leaf shedding in seasonally dry tropical forest. *New Phytologist* **158**(2): 295-303.

Burnham KP, Anderson DR. 2002. *Model selection and multimodel inference, 2nd ed*. New York, New York, USA. : Springer.

Burnham KP, Anderson DR. 2004. Multimodel inference - understanding AIC and BIC in model selection. *Sociological Methods & Research* **33**(2): 261-304.

Cochard H, Nardini A, Coll L. 2004. Hydraulic architecture of leaf blades: where is the main resistance? *Plant Cell and Environment* **27**(10): 1257-1267.

Dixon HH. 1914. *Transpiration and the ascent of sap in plants*. MacMillan and Co., London, UK.

Jacobsen AL, Pratt RB, Tobin MF, Hacke UG, Ewers FW. 2012. A global analysis of xylem vessel length in woody plants. *American Journal of Botany* **99**(10): 1583-1591.

John GP, Scoffoni C, Sack L. 2013. Allometry of cells and tissues within leaves. *American Journal of Botany*: 100: 1936-1948.

Kolb KJ, Sperry JS, Lamont BB. 1996. A method for measuring xylem hydraulic conductance and embolism in entire root and shoot systems. *Journal of Experimental Botany* **47**(304): 1805-1810.

Lo Gullo MA, Nardini A, Trifilo P, Salleo S. 2003. Changes in leaf hydraulics and stomatal conductance following drought stress and irrigation in *Ceratonia siliqua* (Carob tree). *Physiologia Plantarum* **117**(2): 186-194.

Lopez R, Badel E, Peraudeau S, Leblanc-Fournier N, Beaujard F, Julien J-L, Cochard H, Moulia B. 2014. Tree shoot bending generates hydraulic pressure pulses: a new long-distance signal? *Journal of Experimental Botany* **65**(8): 1997-2008.

Martre P, Cochard H, Durand JL. 2001. Hydraulic architecture and water flow in growing grass tillers (*Festuca arundinacea* Schreb.). *Plant Cell and Environment* **24**(1): 65-76.

Mayr S, Bertel C, Damon B, Beikircher B. 2014. Static and dynamic bending has minor effects on xylem hydraulics of conifer branches (*Picea abies, Pinus sylvestris*). *Plant, Cell & Environment* **In press.**

Nardini A, Ramani M, Gortan E, Salleo S. 2008. Vein recovery from embolism occurs under negative pressure in leaves of sunflower (*Helianthus annuus*). *Physiologia Plantarum* **133**(4): 755-764.

Nardini A, Tyree MT, Salleo S. 2001. Xylem cavitation in the leaf of *Prunus laurocerasus* and its impact on leaf hydraulics. *Plant Physiology* **125**(4): 1700-1709.

Rockwell FE, Wheeler JK, Holbrook NM. 2014. Cavitation and its discontents: opportunities for resolving current controversies. *Plant Physiology* **164**(4): 1649-1660.

Sack L, Melcher PJ, Zwieniecki MA, Holbrook NM. 2002. The hydraulic conductance of the angiosperm leaf lamina: a comparison of three measurement methods. *Journal of Experimental Botany* **53**(378): 2177-2184.

Sack L, Scoffoni C. 2012. Measurement of leaf hydraulic conductance and stomatal conductance and their responses to irradiance and dehydration using the evaporative flux methods (EFM). *Journal of Visualized Experiments*.

Sack L, Scoffoni C, McKown AD, Frole K, Rawls M, Havran C, Tran H, Tran T. 2012. Developmentally-based scaling of leaf venation architecture explains global ecological patterns. *Nature Communications* **3** 837.

Sack L, Streeter CM, Holbrook NM. 2004. Hydraulic analysis of water flow through leaves of sugar maple and red oak. *Plant Physiology* **134**(4): 1824-1833.

Sack L, Tyree MT, Holbrook NM. 2005. Leaf hydraulic architecture correlates with regeneration irradiance in tropical rainforest trees. *New Phytologist* **167**(2): 403-413.

Scoffoni C, McKown AD, Rawls M, Sack L. 2012. Dynamics of leaf hydraulic conductance with water status: quantification and analysis of species differences under steady-state. *Journal of Experimental Botany* **63**: 643-658.

Scoffoni C, Vuong C, Diep S, Cochard H, Sack L. 2014. Leaf shrinkage with dehydration: coordination with hydraulic vulnerability and drought tolerance. *Plant Physiology* **164**: 1772-1788.

Trifilo P, Gasco A, Raimondo F, Nardini A, Salleo S. 2003. Kinetics of recovery of leaf hydraulic conductance and vein functionality from cavitation-induced embolism in sunflower. *Journal of Experimental Botany* **54**(391): 2323-2330.

Trifilo P, Raimondo F, Lo Gullo MA, Barbera PA, Salleo S, Nardini A. 2014. Relax and refill: xylem rehydration prior to hydraulic measurements favours embolism repair in stems and generates artificially low PLC values. *Plant, Cell & Environment* **In press.**

Tyree MT, Zimmermann MH. 2002. *Xylem Structure and the Ascent of Sap*. Berlin, Germany.: Springer.

Weast RC. 1974 *Handbook of chemistry and physics*: , 54th edn, Cleveland, OH: CRC Press.

Wheeler JK, Huggett BA, Tofte AN, Rockwell FE, Holbrook NM. 2013. Cutting xylem under tension or supersaturated with gas can generate PLC and the appearance of rapid recovery from embolism. *Plant Cell and Environment* **36**(11): 1938-1949.

Yang SD, Tyree MT. 1993. Hydraulic resistance in *Acer saccharum* shoots and its influence on leaf water potential and transpiration. *Tree Physiology* **12**(3): 231-242.

CHAPTER 6

THE INTEGRATED LIGHT-INDUCED PLASTICITY OF LEAF HYDRAULICS, GAS EXCHANGE AND ANATOMY: TESTING HYPOTHESES IN HAWAIIAN LOBELIADS DIVERSE IN LIGHT ADAPTATION

ABSTRACT

The leaf hydraulic conductance (K_{leaf}) quantifies the capacity of a leaf to transport liquid water and is a major constraint on light-saturated stomatal conductance (g_s) and photosynthetic rate (A_{max}). Few studies have considered the plasticity of K_{leaf} and anatomy across growth environments. The Hawaiian lobeliads are an excellent system to examine plasticity, given their striking diversity in light regime occupied, and their correspondingly wide range of A_{max} allowing maximal carbon gain for success in given environments. We measured K_{leaf}, A_{max}, g_s and leaf anatomy, structure and composition for six species of lobeliads grown in a common garden under two irradiances (300 and 800 μmol·photons·m^{-2}·s^{-1}). We tested hypotheses for light-induced plasticity based on expectations from optimality. K_{leaf}, A_{max} and g_s differed strongly among these closely related species. Sun-shade plasticity was observed in K_{leaf} and A_{max} and in numerous traits relating to leaf lamina and xylem anatomy, venation and composition but g_s was conservative across growth irradiances. Species adapted to higher irradiance showed greater hydraulic supply relative to demand, i.e., a higher K_{leaf} /g_s. Similarly, within species, plants grown under higher irradiance had higher K_{leaf} /g_s. This work suggests a high K_{leaf} /g_s as a key mechanism for additional tolerance of environmental stresses such as heat load and drought during adaptation and plasticity.

Key words: Adaptive radiation, evolution, gas exchange, leaf anatomy, LMA, sun/shade plasticity

INTRODUCTION

Leaf hydraulic conductance (K_{leaf}), the efficiency of liquid water transport through the leaf, is an important constraint on rates of transpiration, photosynthesis and growth (Sack & Holbrook, 2006). Water first moves through the petiole then vein xylem, then traverses the bundle sheath and mesophyll before evaporating and diffusing through stomata. Because water moves through both xylem and living cells, K_{leaf} responds to many environmental factors including leaf water status, temperature and irradiance (Sack *et al.*, 2004; Sack & Holbrook, 2006; Scoffoni *et al.*, 2008; Scoffoni *et al.*, 2012). Several studies have examined the basis of K_{leaf} and its dynamics in the structure and anatomy of the leaf, such as venation and mesophyll internal anatomy, and their correlation with stomatal anatomy and rates of gas exchange across species (e.g., Sack & Frole, 2006; Sack & Holbrook, 2006; Brodribb *et al.*, 2007; Sack & Scoffoni, 2013); indeed, the coordination of hydraulics and gas exchange is often so strong that it can be shown even among 4-6 species (Aasamaa & Sober, 2001; Nardini *et al.*, 2012a). However, very few studies have examined this coordination among closely-related species within a genus, or for given species after acclimation to sun vs. shade, though these would give strong insight into the correspondence of these traits to ecological specialization. Only one study to our knowledge quantified the plastic responses of K_{leaf} and anatomy in relation to growth irradiance, for a single species (Murphy *et al.*, 2012). The aim of this study was to determine the degree to which sun-shade plasticity in hydraulics, structure and function are integrated for leaves within a model adaptive radiation, the Hawaiian lobeliads.

The endemic Hawaiian lobeliads (Campanulaceae) include six genera and 141 species, and arose from a single ancestor about 13 Myr ago (Givnish 2009). They are a spectacular example of adaptive radiation, given their exceptional rapid diversification into a variety of

ecological niches (Losos & Miles, 2002). In particular, lobeliads have radiated into a wide range of light regimes, particularly diversifying in their maximum photosynthetic rate (A_{max}) to optimize the carbon gain of each species in its own environment (Givnish *et al.*, 2004; Givnish & Montgomery, 2014). High sun-shade plasticity in physiological and anatomical traits might have contributed to the establishment of Hawaiian lobeliads in such strikingly different light environments. To test the adaptation of leaf hydraulics and gas exchange and their sun-shade plasticity in closely related lobeliads, we addressed four main questions:

1) Is K_{leaf} higher in plants grown in sun vs. shade, and how does it relate to anatomy? Although many studies have found K_{leaf} to be higher in sun rather than shade exposed leaves for diverse species (Table 6.1), to our knowledge only one study focusing on one species tested K_{leaf} plasticity to growth irradiance and found higher values in high irradiance, which corresponded to higher vein length per area (VLA) (Murphy *et al.*, 2012). Here we tested and extended these findings to hydraulic and anatomical variables in an integrated way within a rapidly diversified lineage. We hypothesized that K_{leaf} would be higher for plants grown under high irradiance. Moreover, several studies have proposed different anatomical traits as "drivers" of K_{leaf}, such as major and minor VLA (Brodribb *et al.*, 2007; McKown *et al.*, 2010), higher mesophyll surface area per leaf area (Sack & Scoffoni, 2013), and higher theoretical midrib conductance corresponding to wider and/or more numerous conduits (Sack & Frole, 2006; McKown *et al.*, 2010; Sommerville *et al.*, 2012). Here we tested these different potential drivers for the first time within a rapidly evolved lineage.

2) How does sun/shade plasticity affect the coordination of K_{leaf} and gas exchange? Previous work has shown K_{leaf} was higher for sun leaves than shade leaves within a canopy, consistent with a matching of hydraulic supply with hydraulic demand (g_s) (Sack *et al.*, 2003a;

Sellin & Kupper, 2007; Brodribb & Jordan, 2011). While this direct coordination of K_{leaf} and g_s has not been shown across plants of a given species grown in sun versus shade, it is consistent with the correlation of stomata and xylem traits reported in studies across diverse species and across species within lineages (Edwards, 2006; Dunbar-Co *et al.*, 2009; Zhang *et al.*, 2012; Brodribb *et al.*, 2013). Here, we aimed to directly test these hypotheses within the Hawaiian lobeliads across light treatments. We hypothesized that individuals grown in higher irradiance would achieve higher CO_2 assimilation rates (A_{max}) and stomatal conductance (g_s), with K_{leaf} either matching g_s, or, a higher K_{leaf} / g_s ratio in high irradiance, representing a greater supply over demand. Indeed, a higher K_{leaf} / g_s has been observed in leaves of *Toona ciliata* grown in higher vapor pressure deficit treatments (Murphy *et al.*, 2014), and for sun leaves of given species acclimating rapidly to high versus low irradiance during simulated transpiration (Guyot *et al.*, 2012) and would indicate a possible mechanism of additional environmental tolerances such as drought or heat load.

3) To what extent do species differ in the sun-shade plasticity of leaf hydraulics and associated physiological and anatomical traits? In the 11 previous studies comparing K_{leaf} for leaves within canopies or across growth irradiances, K_{leaf} was higher in sun than shade leaves for 12/14 species, from 18% in *Betula papyrifera* to 238% in *Prunus dulcis*, but no significant differences were found in *Olea europea* (Table 6.1). Previous studies have argued that species tend to show a narrow range in leaf traits due to sun-shade plasticity within canopies (Sack *et al.*, 2003b; Sack *et al.*, 2006). However, species may differ strongly in the sun-shade plasticity of leaf traits when plants are grown in different conditions (Walters & Reich, 1999), with species of higher irradiance, or faster-growing species in generally, often showing greater plasticity. We tested for the first time the differences in the magnitude of shifts in leaf hydraulic, gas exchange,

structural and anatomical traits from low to high irradiance across related species diversified across sun and shade. We hypothesized that species adapted to lower irradiances (i.e., with lower CO_2 assimilation rates) will experience more limited plasticity. Further, we hypothesized that plants grown in high light would have higher A_{max} and K_{leaf}, and leaves would be structurally and anatomically built to capture more direct light, and transport more water and sugars via higher vein length per area (VLA), greater leaf thickness (and thickness of the different tissues within the leaf), higher leaf mass per area (LMA) and leaf density, higher nitrogen and carbon concentrations, and with larger midribs, smaller cell sizes and greater % intercellular airspaces, and more numerous and wider conduits in the midrib. The opposite traits for leaves of plants grown in shade would be expected to confer a reduced construction cost (Givnish, 1988; Dunbar-Co *et al.*, 2009; Pasquet-Kok *et al.*, 2010; Pivovaroff *et al.*, 2014).

4) How quickly can physiology and anatomy evolve to diversify across species, and how does it correspond to anatomical and structural diversification? The Hawaiian lobeliads diversified rapidly in life form, height and leaf size (Ackerly, 2009; Givnish *et al.*, 2009), but very few studies have considered the evolution of fine scale physiological and anatomical traits within plant adaptive radiations. In the Hawaiian lobeliads, photosynthetic traits correlated with the light regime experienced by each species in their natural habitat (Givnish *et al.*, 2004) and similar patterns were found in *Schiedea* and *Sonchus* (Kapralov & Filatov, 2006; Santiago & Kim, 2009; Kapralov *et al.*, 2013), and for lineages that evolved CAM photosynthesis as key innovations in Bromeliaceae and Orchidaceae (Crayn *et al.*, 2004; Silvera *et al.*, 2009). Further, only a few studies investigated anatomical differences within plant adaptive radiations (Edwards, 2006; Dunbar-Co *et al.*, 2009; Jordan *et al.*, 2013). No studies to our knowledge have examined the variation of K_{leaf} within a rapidly diversified lineage. We investigated the diversification

across six species of lobeliads of K_{leaf} alongside gas exchange and anatomy, and their sun/shade plasticity. We hypothesized these traits would correlate with the light regime experienced in their natural habitat. We hypothesized based on expectations from optimality theory that all traits that benefit differential performance in sun vs. shade would tend to shift together in a coordinated way, because the benefit of shifting one trait would diminish if other traits that benefit performance did not (see shifts predicted for individual traits in Table 6.2; McKown *et al.*, 2010; Sack & Scoffoni, 2013; Sack *et al.*, 2013b). Thus, we expect traits that showed significant plasticity in plants grown from low to high irradiance (summarized above), to also show significant difference across species growing in contrasting habitat.

By using this integrated approach of plasticity in physiological, anatomical and structural traits with relation to light, we aim to understand the mechanisms underlying rapid species diversification across light environments.

MATERIAL AND METHODS

Species and plant cultivation

Six species of Hawaiian lobeliads were selected to span the range of light and moisture regimes occupied by the lobeliad lineage: *Clermontia clermontioides*, *Clermontia parviflora*, *Cyanea leptostegia, Delissea rhytidosperma, Lobelia niihauensis* and *Lobelia yuccoides* (Fig. 6.1, Table 6.2). These species were grown in a common garden greenhouse at the Hawai'i Agricultural Experiment Station of the University of Hawai'i in Volcano, HI (Big Island), in the heart of the elevational range of the lobeliad lineage (~1190 m). These six species were grown under low and high irradiance (300 vs. 800 μmol photons m^{-2} s^{-1}). The greenhouse consisted of a hoop house with plastic cover, open to ambient air along the lower walls (0–1 m off the ground) and at both

ends of the structure. The greenhouse was divided into two irradiance treatments that provided approximately 6-7% transmission of full sunlight (low irradiance treatment) and 33-35% of full sunlight (high irradiance treatment). Irradiance levels were achieved using a combination of neutral density shade cloth and the plastic cover. Air temperature and relative humidity were recorded with EL-USB-2+ Hobo data loggers (Lascar Electronics, Erie, PA). In the low irradiance treatment the mean daily minimum, maximum and average values for temperature (± SE) were 11.4 ± 0.08 ^{o}C, 26.8 ± 0.11 ^{o}C and 17.3 ± 0.04^{o}C, respectively, and the values for relative humidity were 62.5 ± 1.1%, 87.9 ± 0.3% and 78.3 ± 0.16 %, respectively; in the high irradiance treatment, values were 11.3 ± 0.15 ^{o}C, 27.7 ± 1.43 ^{o}C and 17.3 ± 0.40^{o}C, and 56.7 ± 4.2%, 90.1 ± 1.9% and 78.9 ± 3.0 %, respectively.

Seeds were germinated in 8" diameter bulb pans filled with an equal mixture of sifted cinder (~0.25") and perlite (~0.25"), and germinant seedlings were transplanted to individual pots when they were ~2-5 cm tall, and transplanted again regularly as they grew to minimize pot effects. Seedlings were transplanted into 0.04 liter deep, 3.8 liter or 11.4 liter pots with a 3:1 mixture of cinder to potting soil (Sunshine Mix #3; Sun Gro Horticulture Canada Ltd., Canada). Cinder was used in the experimental soil because it improves the growth of native Hawaiian species, including Hawaiian lobeliads, adapted to volcanic soils (Lilleeng-Rosenberger, 2005).

We applied fertilizer (Gaviota 60, 19-19-19; J. R. Simplot, Boise, ID, USA) to germination bulb pans bi-weekly until the germinant seedlings were transplanted to individual pots after which we applied slow release fertilizer on the surface of soil media (Osmocote, 19-6-12 N-P-K; The Scotts Miracle-Gro Company, Marysville, OH, USA) at initial transplant date and every 3-4 months afterward. To control white flies (Hemiptera, Alevrodidae) we applied GC-MITE (JH Biotech, Inc., Ventura, CA, USA) bi-weekly.

Measurements were made when species were 10-85 cm tall (~1.5-2 years old).

Measurements of leaf hydraulic conductance

Leaf hydraulic conductance (K_{leaf}) was measured in May 2010, using the evaporative flux method (Sack *et al.*, 2002; Sack & Scoffoni, 2012). The night prior to measurements, individuals in their pots were transported to the lab, the soil was watered to saturation and pots were enclosed in dark plastic bags filled with wet paper towels to ensure complete plant hydration. Measurements were made for 2-3 leaves per individual for 5-6 individuals per species (10-16 leaves per species). Leaves were cut from the plants in the lab under ultrapure water (Barnstead E-pure, Thermo Scientific) using a fresh razor blade. The petiole was wrapped in parafilm and re-cut under pure water with a fresh razor blade. Petioles were kept under ultrapure water for approximately 10 min until mucilage no longer bled out. The leaf was then re-cut with a fresh razor blade under pure water and if no mucilage appeared the leaf was connected to silicone tubing (Cole-Parmer) under flow solution (ultrapure water, degassed overnight, and re-filtered (0.2 μm; Syringe filter, Cole-Parmer, Vernon Hills, IL.USA). The tubing connected the leaf to a flowmeter (Brodribb & Cochard, 2009; Sack *et al.*, 2011) that logged data every second to a computer for the calculation of flow rate through the leaf (*E*). The leaf was held adaxial face up over a large box fan (Lakewood Engineering & Manufacturing Company, Chicago, IL, USA) and under floodlights (model 73828 1000W, 'UV filter'; Sears, Roebuck, Hoffman Estates, IL, USA) illuminating the leaf surface with >1000 mmol m^{-2} s^{-1} photosynthetically active radiation. A Pyrex container filled with water between the leaf and the floodlights enabled the maintenance of leaf temperature between 23-28°C, determined using a thermocouple (Cole-Parmer). Leaves were allowed to transpire over the fan for at least 30 min, and until the *E* stabilized with a

coefficient of variation <5% for at least 5 min, with no upward or downward trend. Measurements were discontinued if the flow suddenly changed, likely due to air bubbles, particles/mucilage blocking the flow of water, or stomatal closure. Following flow stabilization, leaf temperature was recorded, and the leaf was removed from the system, its petiole dabbed dry and immediately placed into a sealable bag (Whirl-Pack; Nasco, Fort Atkinson, WI, USA) previously humidified with human breath to halt transpiration. The leaf water potential driving force (Ψ_{leaf}) was measured after 30 min equilibration time in the bag using a Pressure Chamber (Plant Moisture Stress, Model 1000, Albany, OR, USA). K_{leaf} was calculated as $E/-\Psi_{leaf}$ and further normalized by leaf area, obtained by measuring scanned images using ImageJ software version 1.42q (National Institutes of Health). To correct for the effect of water viscosity, K_{leaf} values were further standardized to 25 °C (Weast, 1974 ; Yang & Tyree, 1993; Sack *et al.*, 2002).

To obtain maximum K_{leaf} values, we plotted the K_{leaf} values obtained against the Ψ_{leaf} obtained at the end of the measurement, which in some cases reached relatively low values (down to -1.4MPa), and fitted linear functions to the data. The regression was significant in 8/12 cases ($p < 0.05$); we calculated K_{leaf} as the intercept of the function fitted through the points (Brodribb *et al.*, 2007) for plots that showed significant regressions, while we averaged K_{leaf} values in the other 4 cases.

Measurements of photosynthetic rate and stomatal conductance

We measured light-saturated photosynthetic rate (A_{max}) and stomatal conductance (g_s) in the greenhouse using a portable gas exchange system (LI-6400; LI-Cor, Lincoln, NE, USA). All measurements were made between 0800 and 1300. The LI-6400 was equipped with a red/blue

LED light source and a CO_2 mixing system. A_{max} was sampled on the newest fully expanded leaf on 4-5 individuals of each species within both irradiance treatments. Leaves were clamped into the cuvette and they were exposed to saturating light (1000 μmol m^{-2} s^{-1}). We maintained relative humidity, leaf temperature and cuvette CO_2 concentration at near ambient conditions (ca. 75% relative humidity, 20^o – 25^o C, and 400 ppm, respectively). Gas exchange was logged when the photosynthetic rate had been stable for at least 60 s.

Measurements of leaf structure and composition

Leaf area (*LA*; cm^2) was measured for 8-12 leaves from 4-6 individuals per species on scanned images using ImageJ (http://imagej.nih.gov/ij/; Abramoff *et al.*, 2004). Fresh leaf thickness was measured on those same leaves prior to sampling from the plant using digital calipers (± 0.01 mm; Fowler, Chicago, IL). After leaves were scanned for leaf areas, they were placed in an oven at 70°C for 3 days and their dry mass was measured using an analytical balance (± 0.01 mg; XS205; Mettler Toledo, OH). Leaf mass per area (LMA; g m^{-2}; dry mass / turgid leaf area) and leaf density (LD; g cm^{-3}; LMA/ leaf thickness) were obtained.

To determine leaf chemical and isotopic composition, five leaves from five individuals per species were oven dried at 70 °C for 72h, and ground, weighed and sealed in tin capsules, according to standard protocols of the UC Davis Stable Isotope Facility (http://stableisotopefacility.ucdavis.edu/). Leaves were analyzed for carbon isotope ratio ($\delta^{13}C$), carbon per mass (C_{mass}), and nitrogen per mass (N_{mass}) using an elemental analyzer interfaced to a continuous flow isotope ratio mass spectrometer (IRMS). Carbon to nitrogen ratios (*C:N*) were calculated for individual leaves as C_{mass} /N_{mass} and averaged to the species and nitrogen per area

(N_{area}) was calculated for each species as N_{mass} × *LMA*. Maximum CO_2 assimilation rate per nitrogen mass per unit area was calculated as A_{max} / N_{area}.

Measurements of leaf venation architecture

For vein trait determination, one leaf from each of three individuals per species was chemically cleared in 5% NaOH solution and bleach following standard procedures (Scoffoni *et al.*, 2013). Leaves were then scanned (using a flatbed scanner; Epson Perfection 4490 Photo Scanner, CA, USA; 1,200 pixels per inch) and further imaged under a light microscope (Leica Lietz DMRB; Leica Microsystems) at the top, middle and bottom thirds of the leaves using a 5× objective with a camera (SPOT Imaging Solutions; Diagnostic Instruments Inc.; Sterling Heights, MI), resulting in 287× total image magnification (Sack *et al.*, In revision). Leaf area (cm^2), perimeter (cm), length (cm) and width (cm), major vein length per area (major VLA; mm mm^{-2}), minor vein length per area (minor VLA; mm mm^{-2}), total vein length per area (VLA; mm mm^{-2}), number of secondary veins and numbers of free vein endings per area (FEV; number per mm^{-2}) and midrib diameters were measured using ImageJ (http://imagej.nih.gov/ij/; Abramoff *et al.*, 2004) following procedures previously described (Scoffoni *et al.*, 2013).

Measurements of leaf cross sectional anatomy

For measurements of leaf cross sectional anatomy, one leaf from each of three individuals per species was sampled. From each leaf center, a 1 × 0.5 cm rectangle was cut and gradually infiltrated with mixtures of increasing strength low viscosity acrylic resin (L.R. White; London Resin Company, England) in ethanol, under vacuum over the course of a week. Once fully infiltrated, the samples were embedded in resin in gelatin capsules in an oven at 55 °C overnight.

Using glass knives (cut using a LKB 7800 KnifeMaker; LKB Produkter; Bromma, Sweden), samples were sectioned in the transverse plane at 1 μm thickness in a rotary microtome (Leica Ultracut E, Reichter-Jung, Ca, USA). Sections were then placed on slides and stained with 0.01% toluidine blue in 1% sodium borate and imaged using a 5, 10, 20 and 40× objective using a light microscope (Leica Lietz DMRB; Leica Microsystems) with camera utilizing SPOT advanced imaging software (SPOT Imaging Solutions; Diagnostic Instruments Inc.; Sterling Heights, MI) for a total image magnification of 287× to 2303×.

We measured cell and tissue dimensions using ImageJ. In the middle of the left, center and right thirds of the cross-sections, we measured tissue thicknesses. For the upper and lower cuticles and epidermises, and for the palisade and spongy mesophyll, cell cross-sectional areas were averaged for three cells per tissue per leaf cross-section.

Palisade and spongy mesophyll surface area per leaf area ($A_{mes,p}/A$; $A_{mes,spo}/A$) were estimated from cross-sectional anatomy (Chatelet *et al.*, 2013; Sack *et al.*, 2013a), with a novel correction for the mesophyll volume taken up by minor veins and bundle sheath cells:

$$A_{\mathrm{mes,x}}/A = \frac{SA_{\mathrm{x}}\times(T_{\mathrm{pt}}-(ASF_{\mathrm{xt}}\times T_{\mathrm{xt}})-(0.5\times(CSA_{\mathrm{bs}}\times minor\ VLA)))}{VC_{\mathrm{x}}} \qquad \text{eqn 1,}$$

Where SA_x is the palisade or spongy cell surface area, T_{xt} is the thickness of the palisade or spongy mesophyll tissue, ASF_{xt} is the airspace fraction of the palisade or spongy mesophyll tissue, CSA_{bs} is the bundle sheath cross-sectional area, and VC_x is the palisade or spongy mesophyll cell volume. This equation treats the minor veins as if distributed half in the palisade tissue and half in the spongy tissue, and thus half their volume is subtracted from each tissue. All component traits were calculated according to published detailed protocols (Sack *et al.*, 2013a). We calculated the bundle sheath surface area per area ($A_{mes,bs}/A$) as the mean perimeter of bundle

sheath cell × minor VLA. The total mesophyll surface area per area ($A_{mes,bs}/A$) was then calculated as the sum of $A_{mes,p}/A$, $A_{mes,spo}/A$ and $A_{mes,bs}/A$.

We note we didn't calculate the mean maximum mesophyll pathway (D_m) that has been used in the past (Brodribb *et al.*, 2007) for several reasons. First, D_m is calculated based on measurements of internal vein distance (IVD) and the distance from vein to epidermis (LE), both of which cannot be measured properly from cross-sections in our opinion. Indeed, the distance between veins can be greatly variable in reticulate venation (except when looking at grass leaves, which have more of a regular pattern), thus the distance measured in a cross-sections between two veins would depend on the angle and location at which the section was made in the leaf. Second, LE could only be compared across species if measured for a given vein order. However, in cross sections, it is hard to tell what minor vein order a vein is. Finally, D_m is essentially driven by VLA (Brodribb *et al.*, 2007), and LE has been shown to be positively correlated to K_{leaf} across species, rather than negatively as would imply a correlation of D_m with K_{leaf} (Aasamaa & Sober, 2001; Sack *et al.*, 2003a; Brodribb & Jordan, 2011). Thus, recent papers have focused on VLA rather than D_m to investigate correlations with physiology (Brodribb & Feild, 2010; Brodribb *et al.*, 2010; Brodribb & Jordan, 2011).

To characterize the xylem anatomy, we measured major and minor axis diameters of all xylem conduits in the midrib of each leaf sampled for anatomy. The total number of conduits and maximum conduit diameter were averaged across the midribs of the three sections. Additionally, we determined the theoretical conductivity of xylem conduits in the midrib of each leaf using Poiseuille's equation modified for ellipses (Lewis & Boose, 1995; Cochard *et al.*, 2004):

$$K_t = \sum \frac{\pi a^3 b^3}{64\eta(a^2+b^2)} \qquad \text{eqn 2}$$

where *a* and *b* are the major and minor axes of xylem conduit and η is water viscosity at 25°C. We then calculate the theoretical hydraulic conductance normalized by leaf area by dividing K_t / *LA.*

Statistics

We tested differences in traits among species, irradiance growth treatments, and their interaction, using two-way analyses of variance (ANOVAs; Minitab Release 16). All data were log-transformed prior to analyses to improve normality and heteroscedasticity (Sokal & Rohlf, 1995). To test species-differences in K_{leaf} we performed an additional analysis, accounting for differences in the leaf water potential during measurement, because K_{leaf} is dynamic with leaf water status even at high water potentials (Scoffoni *et al.*, 2012; Scoffoni *et al.*, 2014). Thus, for K_{leaf} we repeated the ANOVA described above, adding leaf water potential as a co-variate, effectively comparing species in their K_{leaf} at a given leaf water potential. Given the large number of traits in our analyses, to account for multiple significance testing we applied the sequential Bonferroni correction and the False detection rate method to all ANOVA results (Rice, 1989; Benjamini & Hochberg, 1995); results were considered non-significant when so indicated by both methods.

Multiple regressions were used to predict K_{leaf} from major VLA, minor VLA, A_{mes}/A and theoretical midrib conductivity across species and growth irradiances combined (Minitab Release 16). We selected the multiple regression that exhibited the highest r^2 and in which the influence of given traits was in the realistic direction based on previous studies (see Introduction).

RESULTS

Variation across species in leaf physiological, structural and anatomical traits

We found substantial variation across the six lobeliad species in hydraulic, stomatal and photosynthetic physiology, as well as leaf venation, tissue anatomy and composition. Averaging for each species across the two growth irradiances, leaf hydraulic conductance (K_{leaf}) varied by 4.5-fold, CO_2 assimilation rate per leaf area (A_{max}) by 1.4-fold and stomatal conductance (g_s) by 2.1-fold (ANOVA, $p < 0.01$; Fig. 6.2, Table 6.3). Species varied by 3.2 to 11-fold in leaf area, LMA, and in leaf thickness and density. The species also varied significantly in all nutrient composition and isotope traits (Table 6.4). Species varied by 1.6 to 6-fold in vein diameters and venation lengths per area for each vein order (Table 6.5). Species varied by 1.4 to 5.1-fold in leaf tissue anatomical traits across species, except for the upper epidermis thickness, the number of spongy cell layer, the % intercellular airspace in the palisade mesophyll and the bundle sheath cell area, which were statistically similar across species (Table 6.5). Species varied by 2.0 to 13-fold in all their midrib cross-sectional anatomical traits, except in their conduit numbers (Table 6.5).

Plasticity across growth irradiances in leaf hydraulic and gas exchange traits

On average, both K_{leaf} and A_{max} values for leaves developed under high irradiance were higher for plants grown under low irradiance (ANOVA, $p < 0.01$; Fig. 6.2, Table 6.3 and Table S6.1). By contrast, no differences were found in g_s measured under saturating irradiance for plants grown in the two irradiance treatments. Notably, one of the six species showed a contrary response: *Cyanea leptostegia* showed a 2.5-fold higher K_{leaf} in plants grown in low vs high light.

The hydraulic plasticity of a given species was strongly correlated with the irradiance of its native habitat, as approximated by A_{max}, which correlates with native habitat across species (Givnish *et al.*, 2004; Montgomery & Givnish, 2008). Across species, the relative increase of K_{leaf} values from low to high growth irradiance was strongly positively related to A_{max} (r^2 = 0.92; Fig. 6.4), as was the relative increase of A_{max} from low to high growth irradiance (r^2 = 0.92, p = 0.005). Because there were no significant differences in g_{max} in species grown in high vs. low light, species with greater hydraulic plasticity had greater increases in hydraulic supply (K_{leaf}) relative to demand (g_{max}) in high vs. low light (Fig. 6.5, Table S6.1). Similarly, because of the greater variation in hydraulic plasticity than in A_{max}, we found a strong positive correlation between hydraulic plasticity and the ratio of K_{leaf}/A_{max} (Fig. 6.5, Table S6.1). Thus, species with greater K_{leaf} in high vs low irradiance had higher investment in hydraulic capacity relative to their improved gain in photosynthetic rate.

Plasticity across growth irradiances in leaf venation architecture, and leaf structure and composition

Plastic responses to light in the expected directions, based on previous studies of other species, were found in 19/36 of the leaf structure, venation and anatomical traits ($p < 0.05$ in ANOVAs after correction for multiple tests); only mean conduit diameter and N:C ratio shifted in a direction contrary to expectation (Tables 6.3, 6.4 and 6.5). Of the four potential anatomical drivers of K_{leaf}, only K_t didn't show significant plasticity across growth treatments. Major and minor VLA, as well as A_{mes}/A all showed expected sun-shade plasticity (Table 6.5). Plants grown under high irradiance had leaves on average 1.2-fold higher in major vein length per area (major VLA), 1.1-fold higher in minor vein length per area (minor VLA) and 1.1-fold higher in total

vein length per area (VLA) ($p < 0.05$; Fig. 6.1, Fig. 6.3, Table 6.5 and Table S6.1).For plants grown under high irradiance, leaf area was on average 1.7-fold smaller, leaves tended to be 1.2-fold thicker and 1.6-fold more dense, yielding 2.2-fold higher LMA values. No significant plastic differences were found in species' free ending veins per area (FEVs) across growth irradiances ($p > 0.05$; Table 6.5). Across species, there was a significant increase of the upper and lower cuticle thickness, the palisade thickness, and the number of palisade and spongy cell layer (Fig. 6.3, Table 6.5 and Table S6.1). Similarly, high-irradiance grown plants had greater values of total mesophyll, spongy, palisade and bundle sheath surface area per leaf area (Table 6.5 and Table S6.1). However, no differences between light treatments were found in xylem anatomical traits, except the mean midrib xylem conduit diameter was smaller in species grown under high irradiance (Table 6.5 and sup Table S6.1).

Plants grown under high irradiance had less negative values for $\delta^{13}C$, higher A_{max}/ N_{area} and lower *N:C* (Fig. 6.3, Table 6.4 and Table S6.1). We found no significant differences in N_{area} and N_{mass} across growth irradiances (Table 6.4 and Table S6.1).

Species differed in their plastic responses of leaf area, thickness, LMA, major VLA and midrib diameter in the upper cuticle thickness, the lower epidermis thickness, the % airspace in the spongy mesophyll as well as in theoretical midrib conductivity and conduit sizes ($p < 0.05$ for species × growth irradiance interaction; Tables 6.4 and 6.5). No significant interaction was found in leaf density, minor VLA, VLA and FEVs, or for tissue thicknesses, cell areas, number of cells and mesophyll surface area per leaf area or the average conduit numbers in the midrib ($p > 0.05$ for species × growth irradiance interaction; Table 6.5).

Species adapted to higher irradiance had greater plasticity in given traits in addition to K_{leaf} and gas exchange (described in the previous section). Thus, species with higher A_{max} in high

light also had a greater plastic response of the N/C ratio, % airspace in the palisade, palisade cell area and bundle sheath surface area per leaf area (r_p= 0.86-0.94, r_s= 0.83-1, $p < 0.05$).

Structural and anatomical basis for variation among species and irradiance treatments in hydraulic capacity

Across species, whether considering the high or low irradiance treatments individually, or both treatments together, K_{leaf} was not associated with individual putative anatomical driver variables: major and minor vein length per area (VLA), the theoretical hydraulic conductivity through the midrib (K_t) or the mesophyll surface area per leaf area (A_{mes}/A) ($p > 0.05$; Table S6.1). However, K_{leaf} was significantly correlated with multiple factors; combining the effect of each of these anatomical traits on K_{leaf} using equation 3 explained 40% of the variation observed in K_{leaf} ($p < 0.01$; Fig. 6.6):

$$K_{\mathrm{leaf},pred.} = -0.41 + 0.19 \times major\ VLA + 0.09\ A_{\mathrm{mes}}/A \qquad \text{eqn3.}$$

DISCUSSION

Our results provide a first demonstration of sun/shade plasticity in leaf hydraulic conductance for species within a highly diversified lineage. Indeed, this study provides a new level of detail for sun-shade leaf plasticity in general, integrated view of hydraulics, gas exchange, mesophyll and xylem anatomy, leaf venation architecture and leaf composition. Additionally, our results highlight the enormous extent of physiological diversification that has evolved rapidly among closely related species with implications for the hydraulic control of gas exchange.

Plastic response of the leaf hydraulic conductance to growth irradiance and anatomical drivers

We found strong plasticity in leaf hydraulic conductance (K_{leaf}) with growth irradiance, extending the findings of two recent studies of single species (Raimondo *et al.*, 2009; Murphy *et al.*, 2012) by examining closely related species within a lineage that has been shown to have diverse physiological responses to irradiance (Givnish *et al.*, 2004; Givnish & Montgomery, 2014). Previous studies reported that K_{leaf} tends to be higher in sun vs. shade leaves within canopies of given species (Table 6.1), and higher for sun vs shade adapted species (Nardini *et al.*, 2005; Sack & Frole, 2006; Lo Gullo *et al.*, 2010).

What causes K_{leaf} to differ with growth irradiances? A species can increase its K_{leaf} by modifying its xylem anatomy, its mesophyll anatomy, and/or its biochemistry. Across species, anatomical changes statistically explained 40% of observed variation in K_{leaf}. Plants of given species grown under higher irradiance tended to develop smaller and thicker leaves with higher major vein length per leaf area (Major *VLA*) and mesophyll surface area per leaf area (A_{mes}/A), traits that would increase both vein xylem conductivities (McKown *et al.*, 2010) and outside-xylem conductivity (an increase in A_{mes}/A could increase the evaporative surface inside the leaf; Sack & Scoffoni, 2013). Future studies are required to focus on sun/shade plasticity in leaf biochemistry such as changes in the amount of aquaporin expression and/or distribution throughout the outside-xylem pathways (Kim & Steudle, 2007; Shatil-Cohen *et al.*, 2011), which our results suggest might play an important role in the plasticity of K_{leaf}.

Physiological benefits of the plastic response of the leaf hydraulic conductance

In the Hawaiian lobeliads, while K_{leaf} tended to increase in higher irradiance, g_s did not shift upward correspondingly. This finding contrasted with two previous studies of intra-canopy

plasticity for two species, in which a higher K_{leaf} matched the higher hydraulic demand of sun exposed leaves within canopies (Sellin & Kupper, 2007; Brodribb & Jordan, 2011). Thus, in our study, for closely related species grown in contrasting light environments, K_{leaf} showed stronger plasticity than hydraulic demand (Fig. 6.5). Although we found higher A_{max} for plants of given species grown in high vs low irradiance due to their more efficient CO_2 assimilation rate per nitrogen, we found that apart from C. *leptostegia*, species still tended to invest more in their hydraulic supply relative to the carbon gain (Fig. 6.5). Previous studies indicate that increases in hydraulic supply relative to demand and carbon gain would provide physiological benefits, as the resulting excess hydraulic capacity in high irradiance would confer additional tolerance of environmental stresses such as heat load and drought (Brodribb & Jordan, 2008; Scoffoni *et al.*, 2011).

Adaptive significance of species differences in their sun-shade plasticity in leaf hydraulics

The six Hawaiian lobeliad species differed in their sun-shade plasticity of K_{leaf}. Indeed, K_{leaf} increased from low to high irradiance by 16% in *D. rhytidosperma* to 144% in *C. clermontioides*, but decreased by 164% from low to high irradiance in *C. leptostegia*. Indeed, the degree to which species responded to light treatment in their K_{leaf} strongly correlated with A_{max}, a trait that itself correlates with the light environment in which species are distributed ecologically (Fig. 6.4). These results point for the first time to potential adaptive significance of species differences in their sun-shade plasticity of $K_{leaf,}$ which would contribute to the ability to establish under contrasting light habitats.

Integrated adaptation and plasticity in response to sun vs shade of leaf physiological and anatomical traits

In addition to the sun-shade plasticity observed in leaf hydraulic conductance and assimilation rates, our results point to the integrated plasticity of a wide complex of leaf anatomical and compositional traits. Across these six Hawaiian lobeliad species, we found that traits benefiting differential performance in sun vs. shade shifted together in a coordinated way, as expected from optimality theory (McKown *et al.*, 2010; Sack & Scoffoni, 2013; Sack *et al.*, 2013b). Consistent with the many studies looking at sun vs. shade leaves, or sun vs. shade establishing species, leaves adapted or acclimated to high irradiance tended to be smaller, thicker and denser, yielding higher leaf mass per area, and thus allowing leaves, when grown under high irradiance, to capture more efficiently direct light and to have thinner boundary layers, reducing the heat load (e.g., Givnish, 1988; Popma *et al.*, 1992; Bragg & Westoby, 2002; Sack & Frole, 2006). The shifts in leaf thickness corresponded to increases in the thickness of the palisade tissue and the numbers of palisade and spongy cell layers, providing more photosynthetic tissue and cell/intercellular airspace contact for CO_2 and water exchange, consistent with the higher A_{mes}/A values (Kenzo *et al.*, 2004). Consistent with developmental constraints, smaller sun leaves had higher major VLA and smaller midrib diameter (Sack *et al.*, 2012). These coordinated shifts of leaf physiological and anatomical traits shown across closely related species points toward an optimal integration of leaf traits, with the entire complex showing a coordinated shift from low to high irradiance, both during plasticity and adaptation to ecologically diverse light regimes, to improve carbon gain under high irradiance and reduce construction and maintenance costs under low irradiance, and potentially improving tolerance of additional stresses experienced in given light regimes, such as high VPD and water stress under high irradiance.

ACKNOWLEDGMENTS

We thank Laura Arnold, Heraldo Farrington, David Foote, Tara Holitzki, Lucas Mead and Kim Tavares for logistical assistance and Phil Rundel and Louis Santiago for valuable comments on the manuscript; Hawai‘i Volcanoes National Park, the National Tropical Botanical Garden, the Koke‘e Natural History Museum, Limahuli Garden and the University of Hawai‘i Agricultural Experiment Station in Volcano for important research support; Kaua‘i State Parks, the Kaua‘i Division of Forestry and Wildlife, and the Hawai‘i Natural Areas Reserves Program for helping us obtain research permits; and the National Science Foundation (Grants # 0546784 and # 0614813) and the UCLA Department of Ecology and Evolutionary Biology for support.

Table 6.1. Results of previous studies of the plasticity of leaf hydraulic conductance (K_{leaf}) in response to irradiance, indicating species name, light treatment applied in the study and values of K_{leaf} in low and high irradiances.

Species	Study	% Increase from low to high irradiance	K_{leaf} low light (mmol m^{-2} s^{-1} MPa^{-1})	K_{leaf} high light (mmol m^{-2} s^{-1} MPa^{-1})
Comparing plants grown in low and high irradiance				
Olea europaea cv Leccino	Raimondo *et al.*, 2009	0	4.7	4.7
Toona ciliata	Murphy *et al.*, 2012	122	5.5	12.2
Comparing sun and shade leaves within canopies				
Acer rubrum	Sack *et al.*, 2003a	18	8.5	10.1
Betula papyrifera	Sack *et al.*, 2003a	18	14.3	12.1
Retanilla patagonica	Iogna *et al.*, 2011	30	11.5	15
Quercus rubra	Sack *et al.*, 2003a	53	9.96	15.2
Betula pendula	Ounapuu & Sellin, 2013	56	2.4	3.75
Acer saccharum	Sack *et al.*, 2003a	73	4.06	7.04
Quercus ilex	Nardini *et al.*, 2012b	93	4.1	7.9
Tilia cordata	Sellin & Kupper, 2007	158	1.2	3.1
Nothofagus cunninghamii	Brodribb & Jordan, 2011	164	3.24	8.55
Colliguaja integerrima	Iogna *et al.*, 2011	218	5.5	17.5
Prunus dulcis	Egea *et al.*, 2012	238	4	13.5

Table 6.2. Study species, habitat, elvation, rainfall, light regimes and geographic locations.

Species	Habitat	Elevation (m)	Annual rainfall (mm)	Light regimes	Localities (islands)
Clermontia clermontioides	Mesic and wet forest	670-1825	1000-2500	Forest, gaps, forest edges	TNC Kaʻū Preserve, TNC Kona Heme Preserve (Hawaiʻi)
Clermontia parviflora	Wet forest	120-1460	2500-5000	Gaps, forest edges	Olaʻa forest, Hawaii Volcanoes National Partk (Hawaiʻi)
Cyanea leptostegia	Diverse mesic forest	970-1300	1500-2500	Open forest, subcanopy	Forest off Mohihi Road above YMCA camp, Canyon Trail, Kōkeʻe (Kauaʻi)
Delissea rhytidosperma	Diverse mesic forest	300-1000	1000-2500	Open forest, understory	Limahuli Preserve (Kauaʻi)
Lobelia niihauensis	Forest, seeps in dry regions	125-725	500-2000	Open cliffs, ridges, broken crests	Limahuli Living Collection (Kauaʻi)
Lobelia yuccoides	Diverse mesic and wet forest	750-1200	1500-3000	Open cliffs, ridges, broken crests	Kalalau Valley rim and forest near Hongwanji camp, Kōkeʻe (Kauaʻi)

Table 6.3. Expected plastic and adaptive responses to irradiance for leaf hydraulic and gas exchange traits and results of the analysis of variance for six ecologically diverse species of Hawaiian lobeliads testing the effects of species differences, growth irradiance, and for an interaction We performed the analysis of variance on leaf hydraulic conductance (K_{leaf}) with and without mean measurement Ψ_{leaf} as a covariate, to account for hydraulic vulnerability during the measurement (see Methods). Mean square values, % variance, are shown with degrees of freedom in parentheses. For variables calculated from mean species values, paired *t*-test were conducted between species-means for low vs high irradiance, and only *p*-values are shown. Values in bold indicate a significant impact of growth irradiance (i.e., significant plasticity). $p < 0.001$***, $p < 0.01$**, $p < 0.05$*, $p > 0.05^{NS}$. †indicates the loss of significance when accounting for multiple tests using the sequential Bonferroni analysis and the False detection rate method (Table S6.2).

Trait	Symbol	Unit	Expected plastic and adaptive response to irradiance	Leaf water potential (covariate)	Species	Growth irradiance (%increase or decrease averaged across species mean)	Species × Growth Irradiance	Error
Leaf hydraulics								
Leaf hydraulic conductance	K_{leaf}	mmol m^{-2} s^{-1} MPa^{-1}	+		**0.532, 12.0, (5)****	**1.61, 7.05, (1)**** **(26% increase)**	0.186, 4.12, $(5)^{NS}$	0.128, 76.9, (135)
Leaf hydraulic conductance	K_{leaf}	mmol m^{-2} s^{-1} MPa^{-1}	+	**6.60, 33.1, (1)*****	**0.587, 12.6, (5)*****	**0.567, 2.53, (1)****	**0.184, 4.08, (5)*** †**	0.080, 47.6, (134)
Leaf gas exchange								
CO_2 assimilation rate	A_{max}	μmol m^{-2} s^{-1}	+		**0.013, 34.4, (5)*****	**0.016, 8.68, (1)**** **(8% increase)**	0.002, 5.16, $(5)^{NS}$	0.002, 51.8, (47)
Stomatal conductance	g_s	mol m^{-2} s^{-1}	+		**0.080, 29.2, (5)****	0005, 0.382, $(1)^{NS}$	0.014, 4.93, $(5)^{NS}$	0.019, 65.5, (47)
Hydraulic supply to demand ratio	K_{leaf}/g_s	MPa^{-1}	+	$p = 0.59$				

Table 6.4. Expected plastic and adaptive responses to irradiance for gross leaf structure and nutrient and isotope composition traits and results of the analysis of variance for six ecologically diverse species of Hawaiian lobeliads testing the effects of species differences, growth irradiance, and for an interaction. Mean square values, % variance, are shown with degrees of freedom in parentheses. For variables calculated from mean species values, paired *t*-test were conducted between species-means for low vs high irradiance, and only *p*-values are shown. Values in bold indicate a significant impact of growth irradiance (i.e., significant plasticity). $p < 0.001$***, $p < 0.01$**, $p < 0.05$*, $p > 0.05^{NS}$. †indicates the loss of significance when accounting for multiple tests using the sequential Bonferroni analysis and the False detection rate method (Table S6.2).

Trait	Symbol	Unit	Expected plastic and adaptive response to irradiance	Species	Growth irradiance (%increase)	Species × Growth Irradiance	Error
Gross leaf structure							
Leaf area	*LA*	cm^2	-	**0.673, 66.3, (5)*** **	**0.832, 17.0, (1)*** (67% decrease)**	**0.054, 5.50, (5)****	0.011, 11.2, (50)
Leaf thickness	T_{leaf}	mm	+	**0.113, 48.6, (5)*** **	**0.150, 11.8, (1)*** (23% increase)**	**0.043, 17.8, (5)*** **	0.005, 21.8, (50)
Leaf mass per area	LMA	$g\ m^{-2}$	+	**0.246, 33.0, (5)*** **	**1.50, 39.2, (1)*** (124% increase)**	**0.102, 13.6, (5)*** **	0.011, 14.2, (50)
Leaf density	LD	$g\ cm^{-3}$	+	**0484, 61.3, (5)*** **	**0.698, 18.1, (1)*** (63% increase)**	0.022, 2.80, $(5)^{NS}$	0.014, 17.8, (50)
Midrib diameter	-	mm	-	**0.230, 65.9, (5)*** **	0.006, 0.346, $(1)^{NS}$	**0.082, 23.5, (5)*** **	0.007, 10.3, (24)
Nutrient and isotope composition							
Carbon isotope ratio	$\delta^{13}C$	‰	+	**0.004, 37.3, (5)*** **	**0.013, 23.1, (1)*** (7% increase)**	0.001, 4.65, $(5)^{NS}$	0.0004, 34.9, (48)
Carbon concentration per mass	C_{mass}	%	+	**0.016, 14.6, (5)* †**	0.0004, 0.079, $(1)^{NS}$	**0.038, 35.1, (5)*** **	0.006, 50.2, (48)
Nitrogen concentration per mass	N_{mass}	%	+	**0.119, 35.9, (5)*** **	0.075, 4.51, $(1)^{NS}$	0.017, 4.98, $(5)^{NS}$	0.019, 54.6, (48)
Nitrogen concentration per area	N_{area}	$g\ m^{-2}$	+	$p = 0.09$			
Photosynthesis per nitrogen concentration per area	A_{max} / N_{area}	$\mu mol\ g^{-1}\ s^{-1}$	+	***p* = 0.03**	**(89% increase)**		
Nitrogen: carbon ratio	*N:C*	-	+	**0.091, 39.4, (5)*** **	**0.064, 5.54, (1)* (13% decrease)**	0.024, 10.5, $(5)^{NS}$	0.011, 44.6, (48)

Table 6.5. Expected plastic and adaptive responses to irradiance for leaf venation architecture and anatomical traits and results of the analysis of variance for six ecologically diverse species of Hawaiian lobeliads testing the effects of species differences, growth irradiance, and for an interaction. Mean square values, % variance, are shown with degrees of freedom in parentheses. Values in bold indicate a significant impact of growth irradiance (i.e., significant plasticity). $p < 0.001$***, $p < 0.01$**, $p < 0.05$*, $p > 0.05^{NS}$. †indicates the loss of significance when accounting for multiple tests using the sequential Bonferroni analysis and the False detection rate method (Table S6.2).

Trait	Symbol	Unit	Expected plastic and adaptive response to irradiance	Species	Growth irradiance	Species × Growth Irradiance	Error
Leaf venation architecture							
Major vein length per area	Major VLA	mm mm^{-2}	+	**0.117, 68.1, (5)*** **	**0.070, 8.12, (1)*** (19% increase)**	**0.004, 12.0, (5)****	0.004, 11.7, (24)
Minor vein length per area	Minor VLA	mm mm^{-2}	+	**0.020, 49.3, (5)*** **	**0.013, 6.53, (1)*** † (9% increase)**	0.004, 9.12, (5)^{NS}	0.003, 35.0, (24)
Total vein length per area	VLA	mm mm^{-2}	+	**0.029, 60.0, (5)*** **	**0.020, 8.25, (1)**** (10% increase)**	0.005, 10.4, (5)^{NS}	0.002, 21.4, (24)
Number of free ending veins per area	FEVs	number mm^{-2}	=	**0.43, 88.2, (5)*** **	0.024, 0.99, (1)^{NS}	0.014, 2.96, (5)^{NS}	0.008, 7.84, (24)
Epidermal and mesophyll cross-sectional anatomy							
Upper cuticle thickness	$T_{cut,ad}$	µm	+	**0.071, 20.5, (5)****	**0.578, 33.3, (1)*** (79% increase)**	**0.078, 22.5, (5)****	0.017, 23.7, (24)
Lower cuticle thickness	$T_{cut,ab}$	µm	+	**0.112, 30.1, (5)****	**0.420, 22.0, (1)**** (64% increase)**	0.048, 12.5, (5)^{NS}	0.028, 35.3, (24)
Upper epidermal thickness	$T_{ep,ad}$	µm	+	0.008, 23.2, (5)^{NS}	0.002, 0.971, (1)^{NS}	0.007, 20.7, (5)^{NS}	0.004, 55.2, (24)
Lower epidermal thickness	$T_{ep,ab}$	µm	+	**0.036, 56.0, (5)*** **	0.003, 0.997, (1)^{NS}	**0.011, 16.5, (5)*** †	0.004, 26.5, (24)
Thickness spongy mesophyll	T_{spo}	µm	+	**0.137, 60.5, (5)*** **	0.018, 1.56, (1)^{NS}	0.016, 6.93, (5)^{NS}	0.016, 6.93, (24)
Thickness palisade mesophyll	T_{pal}	µm	+	**0.048, 33.4, (5)****	**0.187, 26.2, (1)*** (40% increase)**	0.015, 10.3, (5)^{NS}	0.015, 10.3, (24)
Number of spongy cell layers		-	+	0.025, 20.4, (50)^{NS}	**0.112, 18.4, (1)**** (30% increase)**	0.006, 5.29, (5)^{NS}	0.014, 5.29, (24)
Number of palisade cell layers		-	+	**0.106, 42.5, (5)*** **	**0.339, 27.3, (1)*** (50% increase)**	0.027, 10.7, (5)^{NS}	0.010, 19.6, (24)
Air space spongy mesophyll	$\%Air_{spo}$	%	-	**0.112, 60.4, (5)*** **	0.010, 1.11, (1)^{NS}	**0.027, 14.4, (5)*** †	0.009, 24.2, (24)
Air space palisade mesophyll	$\%Air_{pal}$	%	-	0.132, 19.2, (5)^{NS}	0.156, 4.51, (1)^{NS}	0.089, 14.7, (5)^{NS}	0.089, 61.6, (24)
Upper epidermis cell area	$A_{ep,ad}$	µm^2	-	**0.076, 40.5, (5)****	0.018, 1.87, (1)^{NS}	0.036, 18.9, (5)^{NS}	0.015, 38.8, (24)
Lower epidermis cell area	$A_{ep,ab}$	µm^2	-	**0.120, 55.7, (5)*** **	0.015, 1.34, (1)^{NS}	0.016, 7.53, (5)^{NS}	0.016, 35.4, (24)
Palisade cell area	A_{pal}	µm^2	-	**0.133, 57.2, (5)*** **	0.004, 0.367, (1)^{NS}	0.030, 12.7, (5)^{NS}	0.014, 29.7, (24)
Spongy cell area	A_{spo}	µm^2	-	**0.016, 44.8, (5)****	0.008, 4.38, (1)^{NS}	0.004, 12.0, (5)^{NS}	0.003, 38.8, (24)
Bundle sheath cell area	A_{bs}	µm^2	-	0.051, 22.0, (5)^{NS}	0.062, 5.29, (1)^{NS}	0.019, 9.67, (5)^{NS}	0.027, 63.0, (22)

Bundle sheath surface area per leaf area	$A_{mes,bs}/A$	-	+	**0.042, 38.4, (5)***	**0.068, 12.3, (1)* (21% increase)**	0.002, 1.40, (5)^{NS}	0.011, 47.9, (24)
Spongy surface area per leaf area	$A_{mes,spo}/A$	-	+	**0.031, 28.2, (5)***	**0.077, 14.0, (1)** (26% increase)**	0.022, 20.1, (5)^{NS}	0.009, 37.6, (24)
Palisade surface area per leaf area	$A_{mes,pal}/A$	-	+	**0.182, 70.7, (5)*****	**0.242, 18.8, (1)*** (48% increase)**	0.005, 1.94, (5)^{NS}	0.005, 8.55, (24)
Mesophyll surface area per leaf area	$A_{mes,corr}/A$	-	+	**0.072, 55.3, (5)*****	**0.192, 24.8, (1)*** (37% increase)**	0.007, 5.34, (5)^{NS}	0.004, 14.5, (24)
Midrib xylem cross-sectional anatomy							
Theoretical conductance per leaf area	$K_{t,\ area}$	mmol m^{-2} s^{-1} MPa^{-1}	+	**0.440, 46.7, (5)*****	0.001, 0.013, (1)^{NS}	**0.267, 28.3, (5)****	0.049, 24.9, (24)
Theoretical conductance per leaf length and area	$K_{t,\ length/area}$	mmol m^{-1} s^{-1} MPa^{-1}	+	**0.632, 50.2, (5)*****	0.032, 0.505, (1)^{NS}	**0.304, 24.1, (5)****	0.066, 25.2, (24)
Number of conduits in the midrib		-	+	0.040, 25.2, (5)^{NS}	0.062, 7.91, (1)^{NS}	0.029, 18.2, (5)^{NS}	0.016, 48.7, (24)
Maximum conduit diameter		μm	+	**0.029, 43.2, (5)*****	0.017, 4.97, (1)^{NS}	**0.014, 21.2, (5)**** †	0.004, 30.6, (24)
Mean conduit diameter		μm	+	**0.027, 36.5, (5)****	**0.053, 14.4, (1)** (15% decrease)**	**0.016, 22.1, (5)***	0.004, 27.0, (24)

FIGURE CAPTIONS

Figure 6.1: Plasticity of leaf anatomy and structure in response to growth irradiance for six ecologically diverse species of Hawaiian lobeliads. Photograph of a representative plant, chemically cleared leaf, micrograph of the minor vein system and lamina cross-section for each species grown under low irradiance (300 μmol photons m^{-2} s^{-1}; left images) and high irradiance (800 μmol photons m^{-2} s^{-1}; right images).

Figure 6.2: Plastic response of physiological traits in response to growth irradiance for six ecologically diverse species of Hawaiian lobeliads. Mean ± standard error for (A) leaf hydraulic conductance (K_{leaf}), (B) light-saturated CO_2 assimilation rate (A_{max}), and (C) stomatal conductance (g_s) in low irradiance (filled bars) and high irradiance (open bars). All traits showed significant variation across species ($p < 0.01$; ANOVA, Table 6.2): ** $p < 0.01$; ^{NS} $p > 0.05$).

Figure 6.3: Plastic response of anatomical and structural traits to growth for six ecologically diverse species of Hawaiian lobeliads. Mean ± standard error for (A) leaf area, (B) leaf mass per area (LMA), (C) leaf thickness, (D) leaf density, (E) major vein length per area (Major *VLA*), (F) total vein length per area (*VLA*), palisade tissue thickness, and (G) mesophyll surface area per leaf area (A_{mes}/A) for individuals grown in low irradiance (filled bars) and high irradiance (open bars). All the above traits varied significantly across species ($p < 0.01$; ANOVA, Table 6.2): *** $p < 0.001$; ** $p < 0.01$.

Figure 6.4: Strong correlation of the leaf hydraulic response to growth irradiance (K_{leaf} at high irradiance/ K_{leaf} at low irradiance) and native light habitat (using A_{max} in high growth irradiance as a proxy; Givnish et al. 2004) across six ecologically diverse species of Hawaiian

lobeliads. Fitted standard major axis: $K_{\mathrm{leaf}}\ light\ response = 0.58\ \times\ A_{\mathrm{area}}\ - 5.60$. Clecle, *Clermontia clermontioides;* Clepar, *Clermontia parviflora;* Cyalep, *Cyanea leptostegia;* Delrhy, *Delissea rhytidosperma;* Lobnii, *Lobelia niihauensis;* and Lobyuc, *Lobelia yuccoides.* ** $p < 0.01$.

Figure 6.5: Strong correlation of plastic responses to growth irradiance for six ecologically diverse species of Hawaiian lobeliads: (A) the plastic response of index of hydraulic supply to photosynthetic capacity ($K_{\mathrm{leaf}}/A_{\mathrm{max}}$) vs that of leaf hydraulic conductance (K_{leaf}), (B) that of the index of hydraulic supply to demand ($K_{\mathrm{leaf}}/g_{\mathrm{s}}$) vs that of leaf hydraulic conductance (K_{leaf}). Fitted standard major axis: (A) $K_{\mathrm{leaf}}/A_{\mathrm{area}} in\ high\ vs. low\ light = 0.87\ \times K_{\mathrm{leaf}}\ in\ high\ vs\ lowlight + 0.07$; and (B) $K_{\mathrm{leaf}}/g_{\mathrm{s}} in\ high\ vs. low\ light = 1.14\ \times K_{\mathrm{leaf}}\ in\ high\ vs\ lowlight - 0.25$. *** $p < 0.001$, ** $p < 0.01$.

Figure 6.6: Partially explaining leaf hydraulic conductance (K_{leaf}) from leaf anatomy for six ecologically diverse species of Hawaiian lobeliads grown at two different irradiances. On the y-axis, K_{leaf} is predicted from major vein length per area (major VLA) and the mesophyll surface area per leaf area (A_{mes}/A) for mean values of species grown in low and high irradiance, using equation 3: $K_{\mathrm{leaf,pred}} = -0.41 + 0.19 \times major\ VLA + 0.09\ A_{\mathrm{mes}}/A$. Plotted line was forced through the origin to allow comparison with the 1:1 line. The presented r^2 value is for the line fitted through the points. * $p = 0.027$. *Clermontia clermontioides* (Clecle; triangles); *Clermontia parviflora* (Clepar, squares); *Cyanea leptostegia* (Cyalep, circles); *Delissea rhytidosperma* (Delrhy, diamonds); *Lobelia niihauensis;* (Lobnii, stars); *Lobelia yuccoides* (Lobyuc, reverse triangles). Open and closed symbols are for plants grown in high and low irradiance respectively.

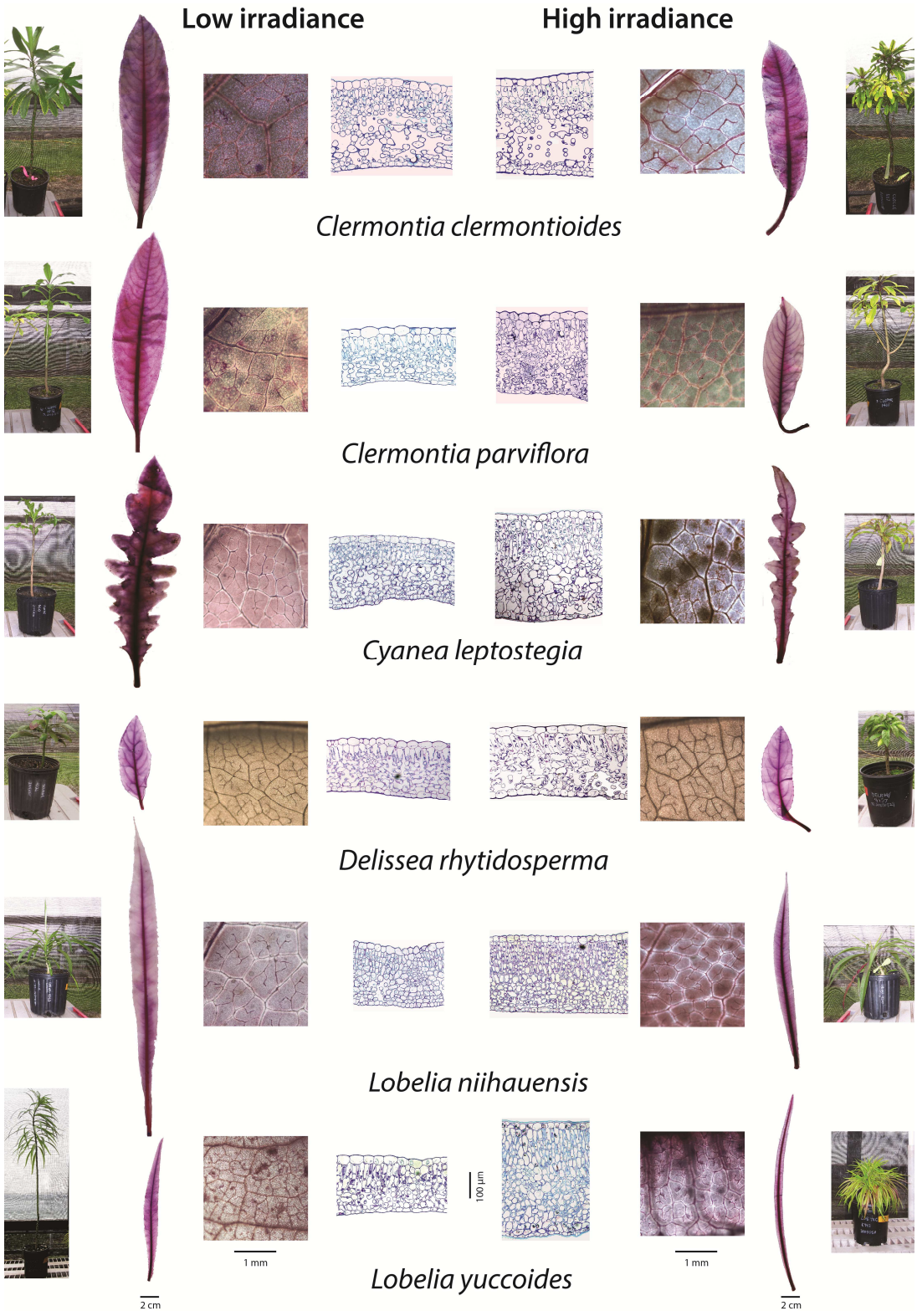
Low irradiance
High irradiance
Clermontia clermontioides
Clermontia parviflora
Cyanea leptostegia
Delissea rhytidosperma
Lobelia niihauensis
Lobelia yuccoides
100 µm
1 mm
1 mm
2 cm
2 cm

Figure 6.1

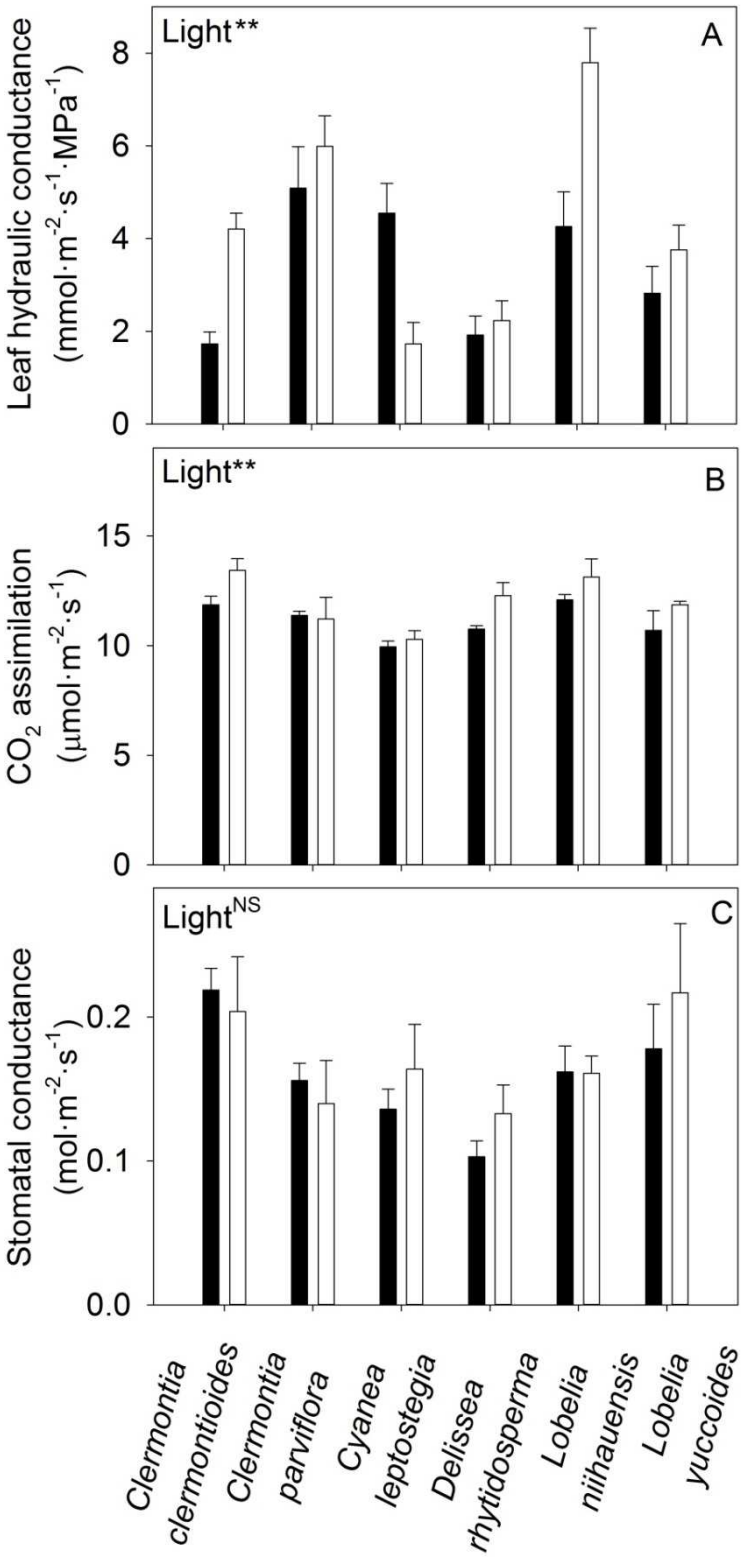
Light**
A
Leaf hydraulic conductance (mmol·m-2·s-1·MPa-1)
0
2
4
6
8
Light**
B
CO2 assimilation (μmol·m-2·s-1)
0
5
10
15
LightNS
C
Stomatal conductance (mol·m-2·s-1)
0.0
0.1
0.2
Clermontia clermontioides
Clermontia parviflora
Cyanea leptostegia
Delissea rhytidosperma
Lobelia niihauensis
Lobelia yuccoides

Figure 6.2

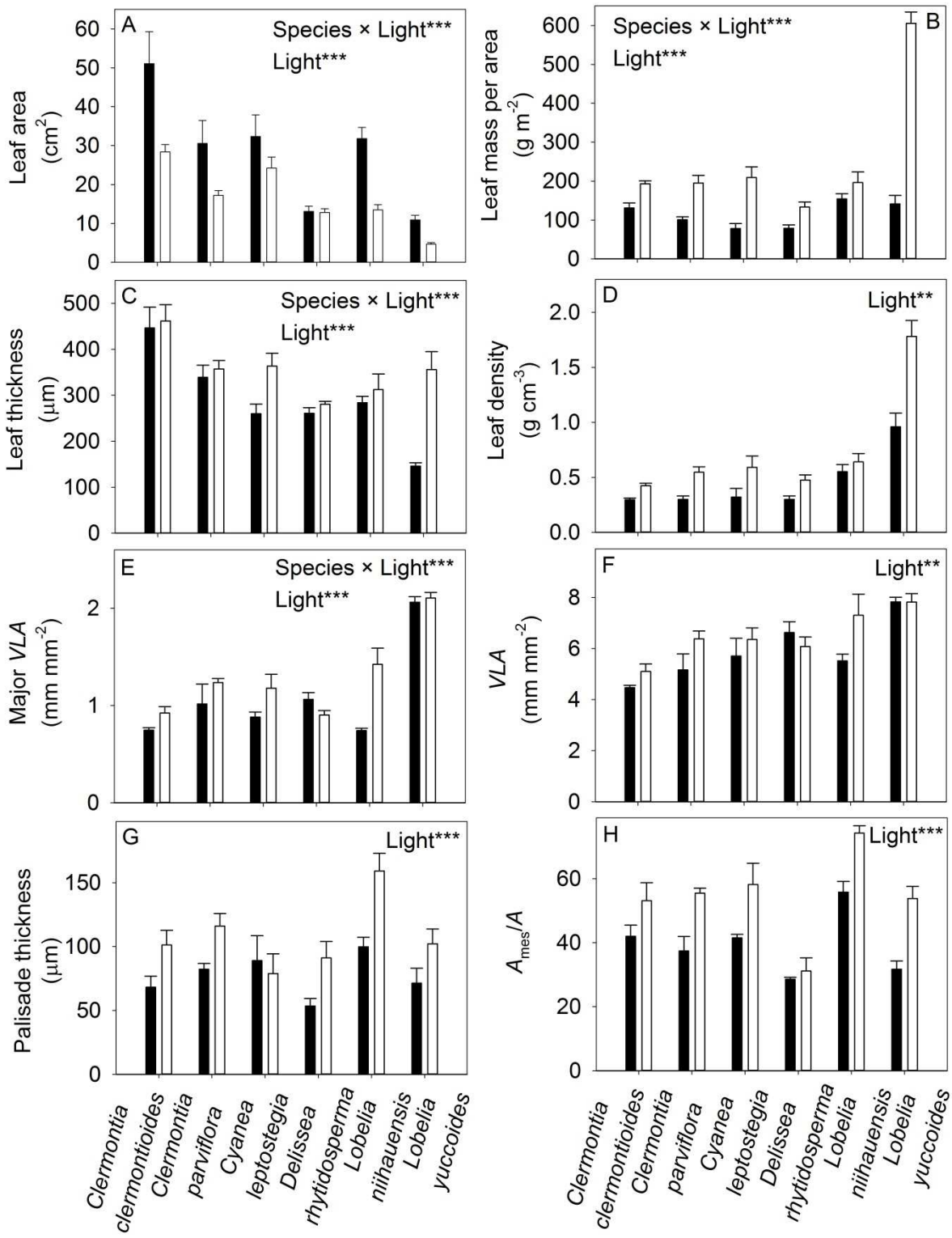
A
Species × Light***
Light***
Leaf area (cm²)
B
Species × Light***
Light***
Leaf mass per area (g m⁻²)
C
Species × Light***
Light***
Leaf thickness (µm)
D
Light**
Leaf density (g cm⁻³)
E
Species × Light***
Light***
Major VLA (mm mm⁻²)
F
Light**
VLA (mm mm⁻²)
G
Light***
Palisade thickness (µm)
H
Light***
Ames/A
Clermontia
clermontioides
Clermontia
parviflora
Cyanea
leptostegia
Delissea
rhytidosperma
Lobelia
niihauensis
Lobelia
yuccoides

Figure 6.3

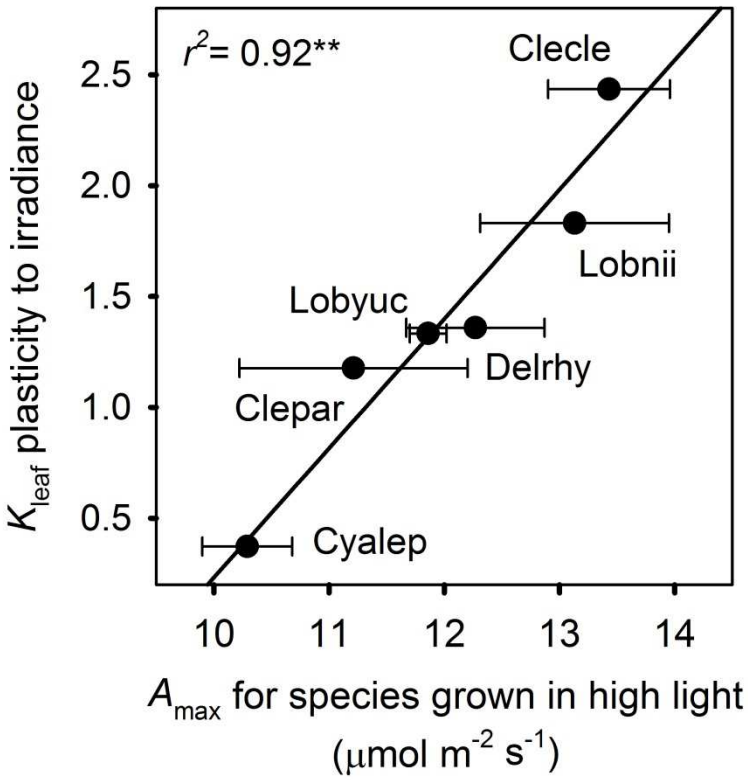
r^2= 0.92**
Clecle
Lobnii
Lobyuc
Delrhy
Clepar
Cyalep
K_{leaf} plasticity to irradiance
2.5
2.0
1.5
1.0
0.5
10
11
12
13
14
A_{max} for species grown in high light
(μmol m^{-2} s^{-1})

Figure 6.4

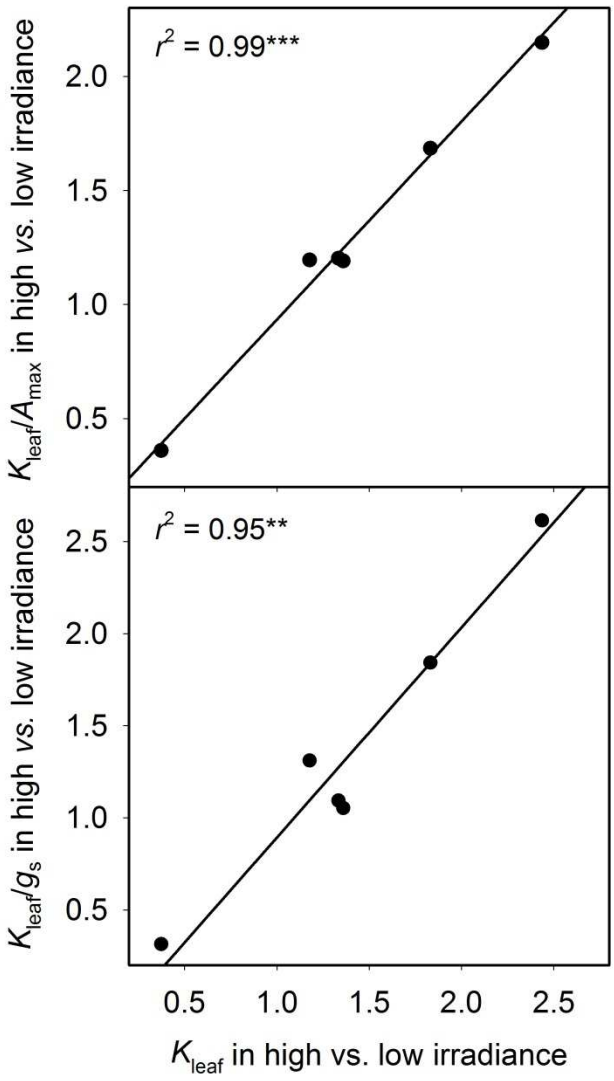
r^2 = 0.99***
K_{leaf}/A_{max} in high *vs.* low irradiance
2.0
1.5
1.0
0.5
r^2 = 0.95**
K_{leaf}/g_s in high *vs.* low irradiance
2.5
2.0
1.5
1.0
0.5
0.5
1.0
1.5
2.0
2.5
K_{leaf} in high vs. low irradiance

Figure 6.5

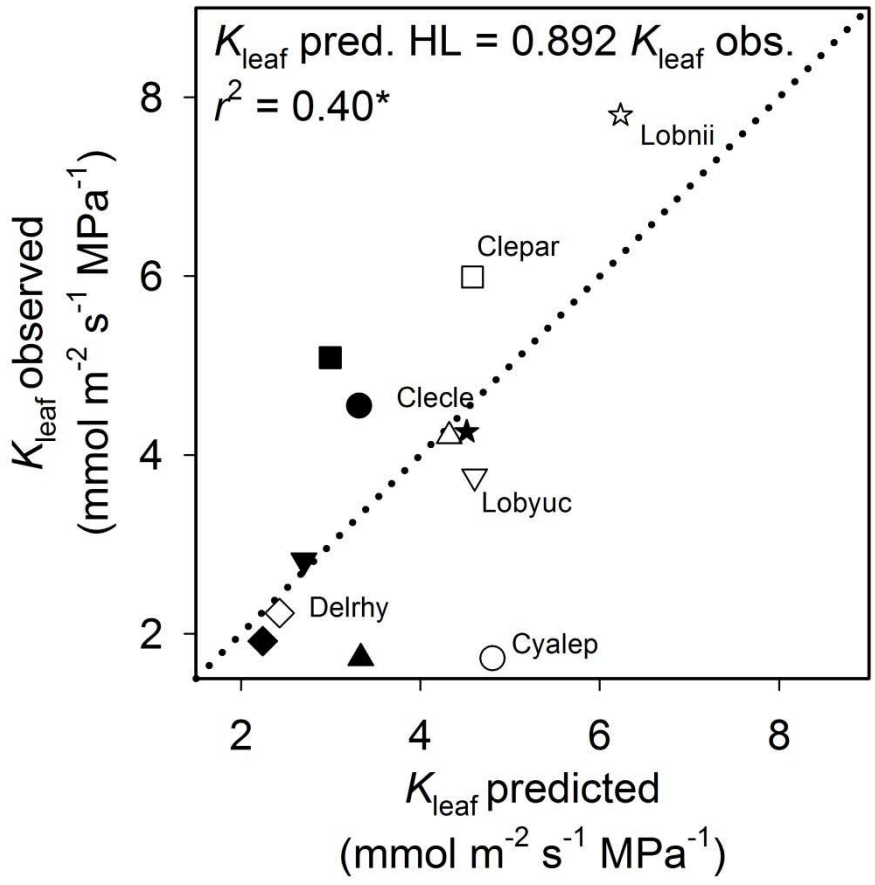
K_{leaf} pred. HL = 0.892 K_{leaf} obs.
r^2 = 0.40*
Lobnii
Clepar
Clecle
Lobyuc
Delrhy
Cyalep
K_{leaf} observed
(mmol m^{-2} s^{-1} MPa^{-1})
K_{leaf} predicted
(mmol m^{-2} s^{-1} MPa^{-1})
2
4
6
8

Figure 6.6

SUPPLEMENTAL MATERIAL

Table S6.1. Mean and standard errors for 45 traits relating to leaf hydraulics, gas exchange, structure, venation, nutrient and isotope composition, mesophyll anatomy and midrib cross-sectional anatomy for six ecologically diverse species of Hawaiian lobeliads. Trait units and symbol definition are given in Tables 6.3-6.5.

Table S6.2. Results for sequential Bonferroni and false detection rate analyses, testing the tablewide significance of physiological, structural and anatomical trait variance. The table displays r^2 values and *p*-values for the relationships presented in Tables 6.3-6.5, and *p*-values required by the sequential Bonferroni analysis (BF), i.e., by beginning with the most significant relationship and for each relationship dividing the critical *p* value of 0.05 by the number of remaining relationships to be tested, a yes or no indicating the tablewide significance (TWS) of the relationship according to the BF *p* value, and a yes or no indicating the significance of the relationship according to the false rate detection (FDR) test.

REFERENCES

Aasamaa K, Sober A. 2001. Hydraulic conductance and stomatal sensitivity to changes of leaf water status in six deciduous tree species. *Biologia Plantarum* **44**(1): 65-73.

Abramoff MD, Magalhaes PJ, Ram SJ. 2004. Image Processing with ImageJ. . *Biophotonics International* **11** (7): 36-42.

Ackerly D. 2009. Conservatism and diversification of plant functional traits: Evolutionary rates versus phylogenetic signal. *Proceedings of the National Academy of Sciences of the United States of America* **106**: 19699-19706.

Benjamini Y, Hochberg Y. 1995. Controlling the false discovery rate: a practical and powerful approach to multiple testing. *Journal of the Royal Statistical Society Series B-Methodological* **57**(1): 289-300.

Bragg JG, Westoby M. 2002. Leaf size and foraging for light in a sclerophyll woodland. *Functional Ecology* **16**(5): 633-639.

Brodribb TJ, Cochard H. 2009. Hydraulic Failure Defines the Recovery and Point of Death in Water-Stressed Conifers. *Plant Physiology* **149**(1): 575-584.

Brodribb TJ, Feild TS. 2010. Leaf hydraulic evolution led a surge in leaf photosynthetic capacity during early angiosperm diversification. *Ecology Letters* **13**(2): 175-183.

Brodribb TJ, Feild TS, Jordan GJ. 2007. Leaf maximum photosynthetic rate and venation are linked by hydraulics. *Plant Physiology* **144**(4): 1890-1898.

Brodribb TJ, Feild TS, Sack L. 2010. Viewing leaf structure and evolution from a hydraulic perspective. *Functional Plant Biology* **37**(6): 488-498.

Brodribb TJ, Jordan GJ. 2008. Internal coordination between hydraulics and stomatal control in leaves. *Plant Cell and Environment* **31**(11): 1557-1564.

Brodribb TJ, Jordan GJ. 2011. Water supply and demand remain balanced during leaf acclimation of Nothofagus cunninghamii trees. *New Phytologist* **192**(2): 437-448.

Brodribb TJ, Jordan GJ, Carpenter RJ. 2013. Unified changes in cell size permit coordinated leaf evolution. *New Phytologist* **199**(2): 559-570.

Chatelet DS, Clement WL, Sack L, Donoghue MJ, Edwards EJ. 2013. The evolution of photosynthetic anatomy in *Viburnum* (Adoxaceae). *International Journal of Plant Sciences* **174**(9): 1277-1291.

Cochard H, Nardini A, Coll L. 2004. Hydraulic architecture of leaf blades: where is the main resistance? *Plant Cell and Environment* **27**(10): 1257-1267.

Crayn DM, Winter K, Smith JAC. 2004. Multiple origins of crassulacean acid metabolism and the epiphytic habit in the Neotropical family Bromeliaceae. *Proceedings of the National Academy of Sciences of the United States of America* **101**(10): 3703-3708.

Dunbar-Co S, Sporck MJ, Sack L. 2009. Leaf trait diversification and design in seven rare taxa of the Hawaiian *Plantago* radiation. *International Journal of Plant Sciences* **170**(1): 61-75.

Edwards EJ. 2006. Correlated evolution of stem and leaf hydraulic traits in Pereskia (Cactaceae). *New Phytologist* **172**(3): 479-489.

Egea G, Gonzalez-Real MM, Baille A, Nortes PA, Conesa MR, Ruiz-Salleres I. 2012. Effects of water stress on irradiance acclimation of leaf traits in almond trees. *Tree Physiology* **32**(4): 450-463.

Givnish TJ. 1988. Adaptation to sun and shade: a whole plant perspective. *Australian Journal of Plant Physiology* **15**(1-2): 63-92.

Givnish TJ, Millam KC, Mast AR, Paterson TB, Theim TJ, Hipp AL, Henss JM, Smith JF, Wood KR, Sytsma KJ. 2009. Origin, adaptive radiation and diversification of the Hawaiian lobeliads (Asterales: Campanulaceae). *Proceedings of the Royal Society B-Biological Sciences* **276**(1656): 407-416.

Givnish TJ, Montgomery RA. 2014. Common-garden studies on adaptive radiation of photosynthetic physiology among Hawaiian lobeliads. *Proceedings of the Royal Society B-Biological Sciences* **281**(1779).

Givnish TJ, Montgomery RA, Goldstein G. 2004. Adaptive radiation of photosynthetic physiology in the Hawaiian lobeliads: Light regimes, static light responses, and whole-plant compensation points. *American Journal of Botany* **91**(2): 228-246.

Guyot G, Scoffoni C, Sack L. 2012. Combined impacts of irradiance and dehydration on leaf hydraulic conductance: insights into vulnerability and stomatal control. . *Plant, Cell & Environment*.

Iogna PA, Bucci SJ, Scholz FG, Goldstein G. 2011. Water relations and hydraulic architecture of two Patagonian steppe shrubs: Effect of slope orientation and microclimate. *Journal of Arid Environments* **75**(9): 763-772.

Jordan GJ, Brodribb TJ, Blackman CJ, Weston PH. 2013. Climate drives vein anatomy in Proteaceae. *American Journal of Botany* **100**(8): 1483-1493.

Kapralov MV, Filatov DA. 2006. Molecular Adaptation during Adaptive Radiation in the Hawaiian Endemic Genus Schiedea. *Plos One* **1**(1).

Kapralov MV, Votintseva AA, Filatov DA. 2013. Molecular Adaptation during a Rapid Adaptive Radiation. *Molecular Biology and Evolution* **30**(5): 1051-1059.

Kenzo T, Ichie T, Yoneda R, Kitahashi Y, Watanabe Y, Ninomiya I, Koike T. 2004. Interspecific variation of photosynthesis and leaf characteristics in canopy trees of five species of Dipterocarpaceae in a tropical rain forest. *Tree Physiology* **24**(10): 1187-1192.

Kim YX, Steudle E. 2007. Light and turgor affect the water permeability (aquaporins) of parenchyma cells in the midrib of leaves of *Zea mays*. *Journal of Experimental Botany* **58**(15-16): 4119-4129.

Lewis AM, Boose ER. 1995. Estimating volume flow-rates through xylem conduits. *American Journal of Botany* **82**(9): 1112-1116.

Lilleeng-Rosenberger KL. 2005. *Growing Hawaii's native plants: a simple step-by-step approach for every species*: Mutual Publishing.

Lo Gullo MA, Raimondo F, Crisafulli A, Salleo S, Nardini A. 2010. Leaf hydraulic architecture and water relations of three ferns from contrasting light habitats. *Functional Plant Biology* **37**(6): 566-574.

Losos JB, Miles DB. 2002. Testing the hypothesis that a clade has adaptively radiated: Iguanid lizard clades as a case study. *American Naturalist* **160**(2): 147-157.

McKown Athena D, Cochard H, Sack L. 2010. Decoding leaf hydraulics with a spatially explicit model: principles of venation architecture and implications for its evolution. *The American Naturalist* **175**(4): 447-460.

Montgomery RA, Givnish TJ. 2008. Adaptive radiation of photosynthetic physiology in the Hawaiian lobeliads: dynamic photosynthetic responses. *Oecologia* **155**(3): 455-467.

Murphy MRC, Jordan GJ, Brodribb TJ. 2012. Differential leaf expansion can enable hydraulic acclimation to sun and shade. *Plant Cell and Environment* **35**(8): 1407-1418.

Murphy MRC, Jordan GJ, Brodribb TJ. 2014. Acclimation to humidity modifies the link between leaf size and the density of veins and stomata. *Plant Cell and Environment* **37**(1): 124-131.

Nardini A, Gortan E, Salleo S. 2005. Hydraulic efficiency of the leaf venation system in sun- and shade-adapted species. *Functional Plant Biology* **32**(10): 953-961.

Nardini A, Pedà G, La Rocca N. 2012a. Trade-offs between leaf hydraulic capacity and drought vulnerability: morpho-anatomical bases, carbon costs and ecological consequences. *New Phytologist*.

Nardini A, Peda G, Salleo S. 2012b. Alternative methods for scaling leaf hydraulic conductance offer new insights into the structure-function relationships of sun and shade leaves. *Functional Plant Biology* **39**(5): 394-401.

Ounapuu E, Sellin A. 2013. Daily dynamics of leaf and soil-to-branch hydraulic conductance in silver birch (Betula pendula) measured in situ. *Plant Physiology and Biochemistry* **68**: 104-110.

Pasquet-Kok J, Creese C, Sack L. 2010. Turning over a new 'leaf': multiple functional significances of leaves versus phyllodes in Hawaiian *Acacia koa*. *Plant Cell and Environment* **33**(12): 2084-2100.

Pivovaroff A, Sharifi R, Scoffoni C, Sack L, Rundel P. 2014. Making the best of the worst of times: traits underlying combined shade and drought tolerance of Ruscus aculeatus and Ruscus microglossum (Asparagaceae). *Functional Plant Biology* **41**(1): 11-24.

Popma J, Bongers F, Werger MJA. 1992. Gap-dependence and leaf characteristics of trees in a tropical lowland rainforest in Mexico. *Oikos* **63**(2): 207-214.

Raimondo F, Trifilo P, Lo Gullo MA, Buffa R, Nardini A, Salleo S. 2009. Effects of reduced irradiance on hydraulic architecture and water relations of two olive clones with different growth potentials. *Environmental and Experimental Botany* **66**(2): 249-256.

Rice WR. 1989. Analyzing tables of statistical tests. *Evolution* **43**(1): 223-225.

Sack L, Bartlett M, Creese C, Guyot G, Scoffoni C 2011. Constructing and operating a hydraulics flow meter. http://prometheuswiki.publish.csiro.au/tiki-index.php?page=Constructing+and+operating+a+hydraulics+flow+meter: Prometheus Wiki.

Sack L, Caringella M, Scoffoni C, Mason C, Rawls M, Markesteijn L, Poorter L. In revision. Leaf vein length per area is not intrinsically scale dependent: avoiding measurement artifacts for accuracy and precision.

Sack L, Chatelet DS, Scoffoni C 2013a. Estimating the mesophyll surface area per leaf area from leaf cell and tissue dimensions measured from transverse cross-sections. http://prometheuswiki.publish.csiro.au/tiki-index.php?page=Estimating+the+mesophyll+surface+area+per+leaf+area+from+leaf+cell+and+tissue+dimensions+measured+from+transverse+cross-sections: Prometheus Wiki.

Sack L, Cowan PD, Jaikumar N, Holbrook NM. 2003a. The 'hydrology' of leaves: co-ordination of structure and function in temperate woody species. *Plant Cell and Environment* **26**(8): 1343-1356.

Sack L, Frole K. 2006. Leaf structural diversity is related to hydraulic capacity in tropical rain forest trees. *Ecology* **87**(2): 483-491.

Sack L, Grubb PJ, Maranon T. 2003b. The functional morphology of juvenile plants tolerant of strong summer drought in shaded forest understories in southern Spain. *Plant Ecology* **168**(1): 139-163.

Sack L, Holbrook NM. 2006. Leaf hydraulics. *Annual Review of Plant Biology* **57**: 361-381.

Sack L, Melcher PJ, Liu WH, Middleton E, Pardee T. 2006. How strong is intracanopy leaf plasticity in temperate deciduous trees? *American Journal of Botany* **93**(6): 829-839.

Sack L, Melcher PJ, Zwieniecki MA, Holbrook NM. 2002. The hydraulic conductance of the angiosperm leaf lamina: a comparison of three measurement methods. *Journal of Experimental Botany* **53**(378): 2177-2184.

Sack L, Scoffoni C. 2012. Measurement of leaf hydraulic conductance and stomatal conductance and their responses to irradiance and dehydration using the evaporative flux methods (EFM). *Journal of Visualized Experiments*.

Sack L, Scoffoni C. 2013. Leaf venation: structure, function, development, evolution, ecology and applications in past, present and future. *New Phytologist*.

Sack L, Scoffoni C, John GP, Poorter H, Mason CM, Mendez-Alonzo R, Donovan LA. 2013b. How do leaf veins influence the worldwide leaf economic spectrum? Review and synthesis. *Journal of Experimental Botany* **64**(13): 4053-4080.

Sack L, Scoffoni C, McKown AD, Frole K, Rawls M, Havran C, Tran H, Tran T. 2012. Developmentally-based scaling of leaf venation architecture explains global ecological patterns. *Nature Communications* **3** 837.

Sack L, Streeter CM, Holbrook NM. 2004. Hydraulic analysis of water flow through leaves of sugar maple and red oak. *Plant Physiology* **134**(4): 1824-1833.

Santiago LS, Kim SC. 2009. Correlated evolution of leaf shape and physiology in the woody *Sonchus* alliance (Asteraceae: Sonchinae) in Macaronesia. *International Journal of Plant Sciences* **170**(1): 83-92.

Scoffoni C, McKown AD, Rawls M, Sack L. 2012. Dynamics of leaf hydraulic conductance with water status: quantification and analysis of species differences under steady-state. *Journal of Experimental Botany* **63**: 643-658.

Scoffoni C, Pou A, Aasamaa K, Sack L. 2008. The rapid light response of leaf hydraulic conductance: new evidence from two experimental methods. *Plant Cell and Environment* **31**(12): 1803-1812.

Scoffoni C, Rawls M, McKown A, Cochard H, Sack L. 2011. Decline of leaf hydraulic conductance with dehydration: relationship to leaf size and venation architecture. *Plant Physiology* **156**(2): 832-843.

Scoffoni C, Sack L, contributors P 2013. Quantifying leaf vein traits. http://prometheuswiki.publish.csiro.au/tiki-index.php?page=Quantifying+leaf+vein+traits: Prometheus Wiki.

Scoffoni C, Vuong C, Diep S, Cochard H, Sack L. 2014. Leaf shrinkage with dehydration: coordination with hydraulic vulnerability and drought tolerance. *Plant Physiology* **164**: 1772-1788.

Sellin A, Kupper P. 2007. Temperature, light and leaf hydraulic conductance of little-leaf linden (*Tilia cordata*) in a mixed forest canopy. *Tree Physiology* **27**(5): 679-688.

Shatil-Cohen A, Attia Z, Moshelion M. 2011. Bundle-sheath cell regulation of xylem-mesophyll water transport via aquaporins under drought stress: a target of xylem-borne ABA? *Plant Journal* **67**(1): 72-80.

Silvera K, Santiago LS, Cushman JC, Winter K. 2009. Crassulacean Acid Metabolism and Epiphytism Linked to Adaptive Radiations in the Orchidaceae. *Plant Physiology* **149**(4): 1838-1847.

Sokal RR, Rohlf FJ. 1995. *Biometry: the principles and practice of statistics in biological research. Third edition*: W.H. Freeman and Company, New York, New Yord, USA.

Sommerville KE, Sack L, Ball MC. 2012. Hydraulic conductance of Acacia phyllodes (foliage) is driven by primary nerve (vein) conductance and density. *Plant Cell and Environment* **35**(1): 158-168.

Walters MB, Reich PB. 1999. Low-light carbon balance and shade tolerance in the seedlings of woody plants: do winter deciduous and broad-leaved evergreen species differ? *New Phytologist* **143**(1): 143-154.

Weast RC. 1974 *Handbook of chemistry and physics*: , 54th edn, Cleveland, OH: CRC Press.

Yang SD, Tyree MT. 1993. Hydraulic resistance in *Acer saccharum* shoots and its influence on leaf water potential and transpiration. *Tree Physiology* **12**(3): 231-242.

Zhang S-B, Guan Z-J, Sun M, Zhang J-J, Cao K-F, Hu H. 2012. Evolutionary Association of Stomatal Traits with Leaf Vein Density in Paphiopedilum, Orchidaceae. *Plos One* **7**(6).

CHAPTER 7

THE INFLUENCE OF LEAF HYDRAULIC ARCHITECTURE ON THE EVOLUTION OF PHOTOSYNTHETIC CAPACITY

ABSTRACT

Theory and experimental work have indicated that leaf hydraulic conductance (K_{leaf}) is a critical determinant of whole plant performance. As leaves open their stomata to capture CO_2 for photosynthesis, water is lost to the atmosphere by transpiration, and K_{leaf} determines the efficiency with which the water loss is replaced, allowing stomata to remain open. Thus, K_{leaf} has been shown to correlate with maximum CO_2 assimilation rate (A_{max}) and stomatal conductance (g_s) across phylogenetically diverse species sets. However, no studies have investigated whether these traits evolved in a coordinated way within a phylogenetically well-resolved lineage with exceptional leaf diversity. Here, we test for the first time for a coordinated evolution of the hydraulic efficiency of K_{leaf}, and its determinants, the xylem and outside xylem pathways; of photosynthetic gas exchange; and of the anatomy of leaf venation and mesophyll, testing explicitly hypotheses for the evolution of leaf water relations for 30 *Viburnum* species in a common garden. We found a strong diversification in K_{leaf}, mainly explained by variation in the outside-xylem pathways, and coordinated in evolution with photosynthetic gas exchange, and with stomatal conductance and leaf venation architecture. Our data also supported an evolutionary trade-off between hydraulic efficiency and safety at the leaf level. These results support and extend key theory for the mechanistic basis of evolutionary physiological diversification during adaptation across environments.

Key words: Leaf size, phylogeny, major vein length per area, minor vein length per area

INTRODUCTION

In the past few decades, leaf hydraulic conductance (K_{leaf}; the capacity of water to move through the leaf) has emerged as a critical trait to understand plant growth and function (e.g., Nardini et al., 2001; Brodribb and Holbrook, 2003; Sack and Holbrook, 2006; Flexas et al., 2013). Indeed, as leaves open their stomata to capture the CO_2 for photosynthesis, water is lost to the dry atmosphere by transpiration, and the capacity with which the leaf can replace that water loss, especially when experiencing environmental stresses such as soil drought, will have a great impact on leaf and whole plant function. As such, studies have found hydraulic supply (K_{leaf}) to be coordinated with carbon gain (maximum CO_2 assimilation rates, A_{max}; Brodribb et al., 2005; Brodribb et al., 2007), and hydraulic demand (stomatal conductance, g_s; Aasamaa and Sober, 2001; Sack et al., 2003; Brodribb and Holbrook, 2004) across species. Studies of animal systems have indicated that such mechanistic correlations should also appear as patterns of coordinated trait evolution (e.g., Price et al., 2013; Santana et al., 2013). However, the theory for leaf hydraulic trait coordination has not been tested in an evolutionary context—i.e., for a lineage with highly diverse leaves with a well resolved phylogeny. The aim of our study was to test, for the first time across closely related species, for a coordinated evolution of hydraulics and gas exchange traits, and whether these traits repeatedly co-evolved through time as well as to understand the mechanisms by which K_{leaf} diversified through time.

The leaf hydraulic conductance is composed of two pathways: the xylem pathways in which water moves through the xylem, from the petiole to different vein orders (K_x), and the outside-xylem pathways, in which water moves across the bundle sheath and mesophyll cells until it reaches the sites of evaporation in the leaf (K_{ox}). Past studies have found that species vary greatly in the proportion of hydraulic resistance distributed in the xylem vs. outside xylem pathways. Across 14 tropical and temperate tree species in which the partitioning of leaf

hydraulic resistance was examined, the % resistance outside the xylem (R_{ox}) varied from 11% for *Lindackeria laurina*, to 88% in *Juglans regia* (Cochard et al., 2004; Sack et al., 2004; Sack et al., 2005), and for tropical tree species, sun-establishing species allocated less resistance to outside-xylem pathways compared to shade-establishing species (Sack et al., 2005). Outside-xylem pathways also influence drought responses: a spatially explicit model suggested that higher resistance outside the xylem could provide the leaf with higher tolerance to K_{leaf} decline by acting as a stronger bottleneck in the leaf hydraulic pathway, reducing tensions in the xylem, and preventing cavitation from occurring, which would otherwise induce dramatic declines in K_{leaf} (Scoffoni et al., 2014).

What drives differences in conductance through these different water pathways in the leaf? Theory, model and empirical work have identified several anatomical drivers influencing K_x and K_{ox}. A high minor vein length per area (*VLA*) can increase both K_x and K_{ox} by increasing the number of flow pathways in the xylem and reducing the length water has to move outside the xylem (Sack and Scoffoni, 2013). Higher major *VLA* reduced vulnerability to hydraulic decline by providing redundancy in high capacity flow pathways across ten diverse species, consistent with expectations based on modelling work (Scoffoni et al., 2011). The hydraulic conductivity of the midrib, estimated from midrib xylem anatomy, strongly correlated with K_{leaf} across 10 tropical trees and 44 species of *Acacia*s (Sack and Frole, 2006; Sommerville et al., 2012). However, no studies have tested these key relationships in an evolutionary context.

Viburnum (Adoxaceae) is an ideal model system for testing theory of the evolution of leaf physiology (Schmerler et al., 2012; Chatelet et al., 2013) including water transport in leaves. *Viburnum* consists of ca. 170 species from temperate and tropical forests, extremely diverse in leaf shape and photosynthetic anatomy (Schmerler et al., 2012; Chatelet et al., 2013). We

quantified K_{leaf} and gas exchange, and their anatomical correlates, in 30 *Viburnum* species grown in a common garden, and tested for a correlated trait evolution. For 17 species, we analyzed the partitioning of resistances inside and outside the xylem and how these co-evolved with and influenced K_{leaf}. According to the theory of the integration of water transport and gas exchange, we hypothesized that across species, during the evolution of shifts in leaf traits, 1) hydraulic supply matches demand and carbon gain, 2) vein length per area and mesophyll structure drive K_{leaf}. Because mesophyll anatomy has been shown to be so diverse across *Viburnum* (Chatelet et al., 2013), we hypothesized 3) that outside xylem pathways would be especially important in determining K_{leaf} variation across species. Finally, as it has been observed in stems, especially in closely related species (Pittermann et al., 2010), we hypothesized 4) a trade-off between hydraulic efficiency (maximum leaf hydraulic conductance; K_{max}) and safety *Viburnum* species.

MATERIAL AND METHODS

Viburnum *phylogeny*

We used the well supported Viburnum phylogeny from Chatelet et al (2013) that describes the phylogenetic relationships for 80 species. Here we focused on a subset of 30 species (Table 7.1; Figure 7.1) spanning the 10 clades within the tree (Clement and Donoghue, 2011) and growing in a common garden at the Arnold Arboretum of Harvard University (Jamaica Plain, MA).

Leaf hydraulic conductance

In July 2010, mature, sun-exposed shoots from 2-3 individuals per species were collected the day prior to measurements and placed in dark plastic bags filled with wet paper towels, and transported directly to the lab at Brown University (Providence, RI), where they were recut under

ultra-pure water (Millipore Milli-Q Academic), by at least two nodes, and placed in buckets filled with ultra-pure water and covered in double dark plastic bags filled with wet paper towels to halt transpiration and enable the shoots to rehydrate overnight.

The next day, leaf hydraulic conductance measurements were made on 3-8 leaves per individuals per species (9-16 leaves per species) using the evaporative flux method (Sack and Scoffoni, 2012). Leaves were excised from shoots under ultra-pure water, parafilm was wrapped around their petiole, and petioles were re-cut under water using a fresh razor blade. Petioles were sealed into compression fittings (Omnifit A2227 bore adaptor; Omnifit, Cambridge, UK) connected to a pressure-drop hydraulic flowmeter (Brodribb and Cochard, 2009; Sack et al., 2011) that logged data every second to the computer to calculate flow rate (*E*). The flow solution was ultra-pure water degassed overnight with a vacuum pump, and re-filtered (0.2 μm; Syringe filter, Cole-Parmer, Vernon Hills, IL.USA). To ensure the leaf was transpiring, it was held adaxial face up over a large box fan (Lakewood Engineering & Manufacturing Company, Chicago, IL, USA) and under floodlights (model 73828 1000W, 'UV filter'; Sears, Roebuck, Hoffman Estates, IL, USA) illuminating the leaf surface with >1000 μmol m^{-2} s^{-1} photosynthetically active radiation. Leaf temperature was maintained between 23-28°C by using a Pyrex container filled with water between the leaf and the floodlights. Leaves were allowed to transpire over the fan for at least 30 min and up to 4 hours, until the *E* stabilized with a coefficient of variation <5% for at least 5 min, with no upward or downward trend. Measurements were discontinued if the flow suddenly changed, likely due to air bubbles, particles/mucilage blocking the flow of water, or stomatal closure. Leaf temperature was recorded once flow stabilized, before it was removed from the system, its petiole dabbed dry and immediately placed into a sealable bag (Whirl-Pack; Nasco, Fort Atkinson, WI, USA) previously

inhaled in to halt transpiration. The leaf water potential driving force (Ψ_{leaf}) was measured after 30 min equilibration time in the bag using a pressure chamber (Plant Moisture Stress, Model 1000, Albany, OR, USA). K_{leaf} was calculated as $E/-\Psi_{leaf}$ and further normalized by leaf area, obtained by measuring scanned images using ImageJ software (http://imagej.nih.gov/ij/; Abramoff et al., 2004). To correct for the effect of water viscosity, K_{leaf} values were further standardized to 25 °C (Weast, 1974 ; Yang and Tyree, 1993; Sack et al., 2002).

Because K_{leaf} has been shown to respond to leaf water potential (Ψ_{leaf}) even at moderately negative water potentials (Scoffoni et al., 2012), we plotted the K_{leaf} values obtained against the Ψ_{leaf} obtained at the end of the measurement, which in some cases reached relatively low values (down to -1.5MPa), and fitted linear functions to the data. In 16/30 cases, the regression was significant ($p < 0.05$) and we calculated K_{max} as the intercept of the function fitted through the points (Brodribb et al., 2007). Because K_{max} values were very high, also from the linear function, we obtained a K_{leaf} value within the realistic range of leaf transpiration at Ψ_{leaf} = -0.3MPa ($K_{0.3MPa}$) to allow comparisons across species. We also estimated the water potential at which 50% of K_{leaf} was lost (P_{50}). In the 14 other species that did not show a significant decline in K_{leaf} over the range of measured Ψ_{leaf}, K_{max} and $K_{0.3MPa}$ were calculated as the average of all K_{leaf} measurements.

Partitioning of leaf hydraulic resistances inside and outside the xylem

We used the high pressure flowmeter method (HPFM) to measure hydraulic conductance through the different vein orders on a subset of 17 *Viburnum* species, spanning the different clades within the genus (Sack *et al.* 2004, 2005), One to two leaves per 2-3 individuals per species were excised under water from the rehydrated shoots, and petioles wrapped with parafilm before they were re-cut under water using a fresh razor blade. Leaves were connected to the

HPFM via a compression fitting. Pressurized degassed and re-filtered flow solution (0.5-0.6MPa) was forced through a system of silicone and high resistance tubing (PEEK; 0.125 mm internal diameter; Upchurch Scientific, Oak Harbor, WA, USA) before entering the leaf. The hydraulic conductance was calculated using pressure transducers (Omega PX-180; Omega Engineering, Stamford, CT, USA) before (P_1) and after (P_2) PEEK tubing of known resistance (R_{PT}), as (P_1-P_2)/ ($P_2 \times R_{PT}$). R_{PT} was obtained from the slope of the delivery pressure vs. flow rate measured using an analytical balance (model XS205, ±10 μg sensitivity; Mettler Toledo, Columbus, OH, USA) and standardized to 25°C to correct for the effect of viscosity of water through the tubing (Weast, 1974 ; Yang and Tyree, 1993; Sack et al., 2002).

To determine the hydraulic resistance of the leaf xylem (R_x), we first applied 1- 2 mm wide cuts to the minor vein system using a scalpel, by cutting between tertiary veins in the leaf, resulting in 4-22 cuts/ cm^2. Care was taken to avoid cutting any major veins (1^o, 2^o and 3^o). To ensure this was enough cuts, we increase the number of cuts and found no significant differences in flow rate between before and after the extra cuts. Measurements were logged onto the computer every second, and once the flow stabilized with a coefficient of variation < 5% for at least 5 min with no upward or downward trend, the hydraulic conductance was reported, and temperature of the water flowing through the system was recorded, to correct for the viscosity effect on the resistance of the tubing and of the leaf. To determine the hydraulic resistance of the minor veins, we applied central cuts to all tertiary veins in the lamina, and measured the resistance (R_{3o}) as $R_{min} = R_x - R_{3o}$. To determine the hydraulic resistance of the petiole (R_{pet}), the lamina was cut off and the resistance measured. At the end of the petiole hydraulic conductance measurement, a leak test was conducted by sealing the petiole end with super glue (Loctite 409 Glue; McMaster-Carr, Los Angeles, CA, USA) and accelerator (Loctite 712 accelerator), and

hydraulic conductance was measured. Small leaks were found in only 19/63 measurements, and were subtracted from the conductances values in obtained in each measurement. Leaf area was measured at the end of the measurements using a flatbed scanner and calculated in ImageJ (http://imagej.nih.gov/ij/; Abramoff et al., 2004). All resistances were then normalized by leaf size. The hydraulic resistance of the major veins (R_{maj}) was obtained as $R_{maj} = R_{3o} - R_{pet}$. We obtained the outside-xylem hydraulic resistance using the formula $R_{ox} = (1/K_{max}) - R_x$, using K_{max} values obtained for the same plants with the evaporative flux method (EFM, see section above), The percent hydraulic resistance in the xylem ($\%R_x$), outside-xylem ($\%R_{ox}$), minor veins ($\%R_{min}$), major veins ($\%R_{maj}$) and petiole ($\%R_{pet}$) were obtained by dividing their given resistances by total leaf hydraulic resistance ($1/ K_{max}$). The hydraulic conductance of the xylem (K_x) was obtained as $1/R_x$ and K_{ox} was obtained as $1/ ((1/K_{max})-(1/K_x))$.

Gas exchange measurements

Mean values for light-saturated CO_2 assimilation rate (A_{max}) were the values previously published values for the same plants of the 30 *Viburnum* species grown at the Arnold Arboretum (Chatelet et al., 2013). Briefly, for each species, A_{max} was measured on several sun-exposed mature leaves of several individuals using a LiCOR 6400XT (Li-COR Biosciences, Lincoln, NB, USA). At the same time A_{max} measurements were taken, the stomatal conductances (g_s, mmol H_2O m^{-2} s^{-1}) were also recorded.

Leaf area and vein architecture

For each species, leaf area (*LA*) was obtained by collecting 13-20 sun-exposed mature leaves from several individuals between 2009 and 2010. Each leaf was photographed individually and leaf areas were measured using ImageJ.

Minor vein length per area (VLA) was measured for all 30 *Viburnum* species. For each species, three 2×3cm pieces were cut from 3 sun-exposed mature leaves from different individuals and cleared with sodium hydroxide followed by sodium hypochlorite on a hot plate (Scoffoni et al., 2013). Each leaf piece was cut at the center of the leaf and included all vein orders except for the primary vein. Veins were stained with Safranin O and digital images representing 7 mm^2 of leaf area were captured with Nikon DXM1200C digital camera coupled to a Nikon Eclipse E600 (Nikon, Melville, NY, USA) compound light microscope. From the digital images, the total length of the minor veins (4^{th} vein order and above) was measured with ImageJ and VLA was calculated.

For the 17 species selected for hydraulic partitioning, we cleared whole leaves to additionally characterize the major venation. Three leaves from 2-3 individuals per species were chemically cleared in 5% NaOH solution and bleach following standard procedures (Scoffoni et al., 2013). Leaves were then scanned (using a flatbed scanner; Epson Perfection 4490 Photo Scanner, CA, USA; 1,200 pixels per inch). Major vein length per area (major VLA; mm mm^{-2}) was measured using ImageJ (Scoffoni et al., 2013).

Leaf xylem anatomy

To characterize the midrib xylem anatomy, we measured major and minor axis diameters of all xylem conduits in the midrib from three leaves of 2-3 individuals of each of the 17 selected species measured for leaf hydraulic partitioning. The total number of conduits and maximum conduit diameter were averaged across the midribs of the three sections. We determined the theoretical midrib conductivity of by treating each conduit as an ellipse and using Poiseuille's equation modified for ellipses (Lewis and Boose, 1995; Cochard et al., 2004):

$$K_t = \sum \frac{\pi a^3 b^3}{64\eta(a^2+b^2)}, \quad \text{eqn 1,}$$

where *a* and *b* are the major and minor axes of the ellipse and η is water viscosity at 25°C. Theoretical hydraulic conductance normalized by leaf area was calculated by dividing K_t / *LA*, and theoretical hydraulic conductance normalized by midrib length and leaf area was calculated as K_t / (*LA*/Midrib length).

We measured maximum vessel length for 21 species (Table S7.1) by selecting 3-6 leaves from shoots of the different individuals that had been rehydrated overnight. Leaves were connected by silicone tubing to a four-way valve connected to a syringe. Zipties were applied around the tubing and petiole to ensure a tight seal. Air pressure was applied using a caulking gun while the leaf was placed under water, under a light source. Using a scalpel, cuts were made throughout the leaf beginning with the highest order veins, and progressively to lower order veins, and finally along the midrib toward the leaf base, until air bubbles first emerged from the xylem, indicating maximum conduit length.

Statistical and phylogenetic comparative analyses

We tested differences in traits among species using one-way analyses of variance (ANOVAs; Minitab Release 16). All data were log-transformed to improve normality and heteroscedasticity (Sokal and Rohlf, 1995). To test for variation across K_{leaf} values measured with the EFM, we performed a one-way ANOVA on log-transformed data, with mean leaf water potential (Ψ_{leaf}) as a covariate, to control for the decline of K_{leaf} with Ψ_{leaf} during measurements.

Correlations between two traits of interest were considered significant when both Spearman and Pearson coefficients (r_s and r_p respectively) were significant. Because many

relationships were non-linear, we determined Pearson values for both raw and log-transformed data.

To control for the non-independence of our species in an evolutionary sense, and test whether two traits of interest repeatedly co-evolved in a coordinated way, we performed phylogenetic independent contrasts (PICs; Felsenstein, 1985) analyses which quantify trait variation that occurs at each node in a phylogeny based on the trait values of the descendent taxa or nodes and the branch lengths between the parent and daughter nodes. The PICs were calculated using the *pic* and *fitcontinuous* functions from the packages APE and GEIGER in R.3.1.0 following two evolutionary models: the Brownian Motion model (BM) and the Ornstein-Uhlenbeck model (OU; Butler and King, 2004). The BM model assumes that traits have evolved under random drift, whereas in the OU model, traits are assumed to evolve under stabilizing selection and are pulled toward an optimum value. For each trait comparison, these two models were compared using the Akaike Information Criterion corrected for low *n* (AIC). We present the r^2 of the PICs for the best fit evolutionary model. When evolutionary models were within 2 AIC scores of one another, we presented the PICs with highest r^2.

RESULTS

Species variation in leaf physiological, structural and anatomical traits

Strong diversification was observed across species in leaf hydraulic conductance: K_{max} varied 53-fold across all 30 species from 0.48 to 25.8 mmol m^{-2} s^{-1} MPa^{-1}, from *V. wrightii* and *V. ichangense* respectively ($p < 0.001$; ANOVA), with 4-fold variation observed in K_x ($p = 0.035$; ANOVA), and 87-fold variation in K_{ox} across the 17 species for which leaf hydraulic resistance was partitioned (Table 7.1). Across all 30 species, light-saturated CO_2 assimilation rate (A_{max})

varied 2.5-fold ($p < 0.001$; ANOVA; Table 7.1) and stomatal conductance (g_s) varied by 3.3-fold ($p < 0.001$; ANOVA; Table S7.1).

Species also varied strongly in the partitioning of their leaf hydraulic conductance (Fig. 7.2). The percent hydraulic resistance distributed outside the xylem (%R_{ox}) varied from 22% for *V. lentago* to 97% for *V. wrightii*; that in the minor veins (%R_{min}) from 0.3 for *V. wrightii* to 12% for *V. lentago* (Fig. 7.2, Table S7.1); that in the major veins (%R_{maj}) from 1.8 for *V. wrightii* to 36% for *V. lentago*; and that in the petiole (%R_{pet}) from 0.9 for *V. wrightii* to 50% for *V .plicatum* (Tables 7.1 and S1; Fig. 7.2). Across species, on average, %R_{ox} accounted for most of the leaf hydraulic resistance (60%), followed by % R_{pet} (22%) and % R_{maj} (14%) and the minor vein xylem the least (5%) (Fig. 7.2). Maximum vessel length also varied strongly across species, i.e., ending in the midrib in *V. betulifolium* and *V. bitchiuense* and in the minor veins in *V. cassinoides*, with most species having their longest vessels ending in the secondary veins (14/21) (Table S7.1).

Leaf area varied 8-fold across the 30 species from 18.6 for *V. burejaeticum* to 149 cm^2 for *V. furcatum* ($p < 0.001$; ANOVA; Table S7.1). Species also varied in leaf venation traits. Indeed, minor vein length per area (VLA) varied by 2-fold across 30 species ($p < 0.001$; ANOVA; Table 7.1), major VLA varied by 1.8-fold across 17 species ($p < 0.001$; ANOVA; Table 7.1).

The coordinated evolution of leaf hydraulics, gas exchange and anatomy

Leaf hydraulic conductance was strongly coordinated with both A_{max} and g_s, across species (Figures 7.1 and 7.3). These relationships arose from evolutionary correlation: phylogenetically independent contrasts were significantly correlated under both the Brownian Motion model (BM; r_{BM}^2 shown in Fig. 7.3) and Ornstein-Uhlenbeck model (OU; $r_{OU}^2 = 0.46$, $p < 0.001$ for both K_{leaf}

and A_{max}, and K_{leaf} and g_s), with the BM model of evolution selected by maximum likelihood as best fit to explain the correlated evolution of all three traits

The variation observed in K_{max} was mainly explained by K_{ox} rather than K_x (Fig. 7.4). Indeed, K_{max} was tightly correlated with K_{ox} across the 17 species tested for hydraulic partitioning, whereas K_{max} was statistically independent of K_x across species. Phylogenetically independent contrasts of K_{ox} vs. K_{max} were significantly correlated under both Brownian motion (BM; r_{BM}^2 shown in Fig. 7.4) and Ornstein-Uhlenbeck (OU; $r_{OU}^2 = 0.96$, $p < 0.001$) models of evolution, with the BM model selected by maximum likelihood as best fit to explain the correlated evolution of these traits (Table S7.2).

Across the 16 species for which data were available for leaf hydraulic vulnerability (P_{50}, see *Methods*), we found a trade-off between hydraulic capacity and vulnerability. Thus K_{max} was tightly correlated with P_{50} (Fig. 7.5). Phylogenetically independent contrasts of K_{max} vs. P_{50} were significantly correlated under both the Brownian motion model (BM; r_{BM}^2 shown in Fig. 7.5) and the Ornstein-Uhlenbeck model (OU; $r_{OU}^2 = 0.68$, $p < 0.001$), with the BM model of evolution selected by maximum likelihood as best fit to explain the correlated evolution of these traits (Table S7.2).

K_{max} and A_{max} correlated with leaf venation traits. Both K_{max} and A_{max} were tightly positively correlated with major *VLA* across species (Fig. 7.6). Phylogenetically independent contrast of K_{max} and major *VLA* were significantly correlated under both Brownian motion model (BM; r_{BM}^2 = 0.38-0.49 for major *VLA* and K_{max} and A_{max} respectively; $p < 0.005$) and the Ornstein-Uhlenbeck model (OU; r_{OU}^2= 0.26-0.69 for major *VLA* and K_{max} and with A_{max} respectively; $p < 0.02$). The BM model of evolution selected by maximum likelihood as best fit to explain the correlated evolution of K_{max} with major *VLA*, while the OU model of evolution

was selected to explain the correlated evolution of A_{max} and *VLA* (Table S7.2). No significant correlation of K_{max} with minor VLA was found (r_p = 0.046, p < 0.05; r_s = 0.31, p >0.005). Minor *VLA* was however slightly correlated with A_{max}, but no significant correlation between the phylogenetically independent contrast of these traits were found (r_{BM}^2= -0.01 and r_{OU}^2= 0.06 p > 0.05).

Correlation of physiological and anatomical traits

Across 17 species, the hydraulic resistance in the major veins (R_{maj}) correlated negatively with major *VLA* (r_p = -0.70, r_s= -0.72, p < 0.01). By contrast, no correlation was found between the hydraulic resistance in the minor veins (R_{min}) and minor *VLA* (r_p = 0.02, r_s= 0.08, p > 0.01). Leaf size scaled negatively with major *VLA* (r_p = -0.73, r_s= -0.66, p < 0.01). No significant correlation was found between either K_{max} or P_{50} and theoretical midrib hydraulic conductance (K_t) (whether normalized by area, or midrib length per area), number of conduits in the midrib, maximum xylem conduit size or maximum conduit length ($|r_p|$ = 0.03-0.44, $|r_s|$= 0.07-0.71, p > 0.05).

DISCUSSION

Our results provide the first support for the theory of leaf hydraulic-stomatal-photosynthetic coordination in an evolutionary model system, i.e., a well-resolved lineage with highly diverse leaves. Across the *Viburnum* species we found strong evolutionary diversification of leaf water transport, arising from diversification of vein traits, and coordinated with diversification of stomatal conductance and photosynthetic rate, consistent with the matching of hydraulic supply and demand.

Coordinated evolution of leaf hydraulics and gas exchange

Although leaf hydraulics and gas exchange have often been hypothesized to evolve in a coordinated way, given that a high K_{leaf} would allow stomata to remain open for CO_2

assimilation while water is lost by transpiration, no previous studies have investigated their coordinated evolution. A correlation between K_{leaf} and A_{max} had previously been shown across diverse lineages of bryophytes, lycopodes, ferns, gymnosperms and angiosperms (Brodribb et al., 2007), but the correlation of K_{leaf} and A_{max} across angiosperm species only was not clear (Brodribb et al., 2007). Past studies have shown that a leaf hydraulic-stomatal-photosynthetic coordination could arise from a K_{leaf} - g_s correlation, which would minimize the operating leaf water potential (Sack and Scoffoni, 2013; Sack et al., 2013), or a K_{leaf} - mesophyll conductance (g_m) correlation, which would indirectly link leaf hydraulics to gas exchange (Flexas et al., 2013). Additionally, in given environments, a higher supply (K_{leaf}) over demand (A_{max} and g_s) could be beneficial, especially if exposed to heat load and drought (Scoffoni et al., In review). The most rigorous approach to testing such mechanistic and evolutionary trait coordination is across closely related species. Our test demonstrated that higher K_{leaf} values co-evolved multiple times with shifts in light saturated CO_2 assimilation rates (A_{max}) and stomatal conductance (g_s) across closely related *Viburnum* species. These finding of a coordinated evolution of hydraulics and gas exchange point to a clear understanding of physiological adaptation across environments as the strong diversification observed in K_{leaf} across *Viburnum* species would thus have potentiated the diversification observed in A_{max} across different light environments (Chatelet et al., 2013).

Evolutionary diversification of leaf water transport

The *Viburnum* species diversified strongly in the partitioning of leaf hydraulic resistances, especially in the hydraulic resistance outside the xylem, i.e., for bulk water flow through the bundle sheath and mesophyll to the sites of evaporation in the leaf. The high variation observed in maximum leaf hydraulic conductance (K_{max}) across species was statistically independent of

the xylem hydraulic conductance (K_x), but tightly correlated with the outside-xylem conductance (K_{ox}). Indeed, K_x showed a more narrow range of variation than K_{ox} (4-fold vs. 87-fold variation respectively). The diversification of K_{ox} is consistent with previous findings of strong diversification in mesophyll anatomy for these same species (Chatelet et al., 2013). Indeed, a strong diversification especially in palisade cells was observed across 36 *Viburnum* species (including the ones in our study) which exhibited both branched H-cell palisade as well as the more typical elongated and packed type I-cell palisade mesophyll (Chatelet et al., 2013). These shifts in mesophyll anatomy were found to correlate with increasing photosynthetic capacity (Chatelet et al., 2013). Physical and computer models and meta-analyses have predicted that shifts in mesophyll anatomy would affect water movement outside the xylem to the site of evaporation in the leaf (Noblin et al., 2008; Flexas et al., 2013; Buckley, 2014). Differences in biochemistry could also play an important role in determining K_{ox}. Indeed, the abundance and activity of aquaporins in the outside xylem pathways—i.e., activation in bundle sheath and/or mesophyll cells—can strongly impact on K_{leaf} (e.g., Sack et al., 2002; Kim and Steudle, 2007; Scoffoni et al., 2008; Voicu et al., 2008). Diversification in biochemistry to evolve higher K_{leaf} values could be especially beneficial, as it would require no or few structural/anatomical changes.

Anatomical basis for the K_{leaf} - A_{max} *coordination*

We found evidence of an evolutionary coordination between K_{leaf}, A_{max} and major vein length per area (*VLA*). The stronger correlation between K_{leaf}, A_{max} and major *VLA* than with minor *VLA* (which make up the bulk of the leaf vein system) is at first sight surprising, especially because many studies reported a strong correlation between both K_{leaf} and minor *VLA*, and A_{max} and minor *VLA* across diverse species sets (Sack and Scoffoni, 2013). However, *Viburnum* species

showed a relatively narrow range of variation in minor *VLA* (only 2-fold variation, from 3 to 6 mm mm^{-2}), and the minor veins accounted for little of the total hydraulic resistance in the leaf (0.3 to 12% across species, see *Results*). Instead, the greater diversity of the major veins across *Viburnum* species produced a greater impact on total leaf hydraulic resistance via the hydraulic resistance in the major veins (R_{maj}) which accounted for 1.8 to 36% of R_{leaf} (see *Results*). The variation in major VLA was strongly linked with leaf size. Indeed, *Viburnum* leaves are especially known for their diversity in shape and size (Schmerler et al., 2012), and, consistent with a previous study on 485 globally distributed angiosperm species (Sack et al., 2012), leaf size across *Viburnum* species scaled negatively with major *VLA*, such that smaller leaves exhibited higher major *VLA*. Thus, it appears that *Viburnum* diversified more strongly in major than minor *VLA*, enabling higher K_{leaf}, g_s and A_{max}. We note however that there are many ways by which species can vary in their mesophyll/xylem anatomy, and biochemistry, influencing K_{leaf} (see above).

Leaf hydraulic safety-efficiency trade-off across closely related species

We found for the first time in leaves an evolutionary trade-off between hydraulic efficiency (K_{max}) and safety (P_{50}). Such a trade-off has been found to occur in stems especially for closely related species or species growing in similar environments, and has been shown to relate to conduit and pore diameters in the xylem (Hacke et al., 2001; Pittermann et al., 2006; Pittermann et al., 2006; Sperry et al., 2006; Pittermann et al., 2010). However, across diverse species or within certain families this trade-off does not always appear due to variation in the anatomy of the stem xylem (Maherali et al., 2004; Pittermann et al., 2006; Hacke et al., 2007). In leaves, one study has shown a correlation between K_{leaf} on a mass basis (K_{leaf} / LMA) and P_{50} across three maple and oak species (Nardini et al., 2012). However, a leaf hydraulic safety versus efficiency

trade-off was not found across diverse species sets (Blackman et al., 2010; Scoffoni et al., 2012). Here, we confirm this trade-off across closely related species and showed for the first time a correlated evolution of these traits. The lack of trade-off found in previous studies (Blackman et al., 2010; Scoffoni et al., 2012) had been attributed mainly to the fact that leaves, contrary to stems, have both xylem and outside-xylem pathways, and thus xylem anatomy might not have as strong an influence as for stems on hydraulic properties. Here, the leaf hydraulic safety-efficiency trade-off might not have related to xylem anatomy, but rather to differences in mesophyll anatomy. Indeed, no relationship was found between either P_{50} or K_{max} with xylem conduit size or maximum length. Thus, this hydraulic trade-off observed for the first time here for K_{leaf} on an area basis, most likely reflects differences in mesophyll anatomy that would confer a range of resistance to cell shrinkage, which has been recently shown to have a great impact on hydraulic decline, especially at mild stress (Scoffoni et al., 2014).

Conclusion

The hydraulic-stomatal-photosynthetic theory was tested here for the first time in an evolutionary context and strong evidence for repeated co-evolution of these traits in a coordinated way was found. This coordinated diversification observed of hydraulics and gas exchange traits would have most likely allowed species to adapt and occupy different environments throughout their evolutionary history.

ACKNOWLEDGMENTS

We would like to thank Mike Alfaro and Jonathan Chang for discussion and help with the phylogenetic analyses, and the staff at the Arnold Arboretum. This work was funded in part by the Department of Ecology and the Evolutionary Biology at UCLA, the UCLA Dissertation Year

Fellowship and NSF grants IOS-0842771 to L. Sack, IOS-0843231 to E. J. Edwards, IOS-0842800 to M. J. Donoghue.

Table 7.1. Species of *Viburnum* studied, clade and physiological and anatomical traits. K_{leaf}, leaf hydraulic conductance; $K_{leaf\ \_0.3\ MPa}$, leaf hydraulic conductance at -0.3MPa; K_x, xylem hydraulic conductance, K_{ox}, outside-xylem hydraulic conductance, $\%R_{ox}$, percent resistance outside the xylem; VLA, vein length per area. * p <0.005; *** p <0.001.

Species	Clade	K_{leaf}	$K_{leaf\_0.3MPa}$	K_x	K_{ox}	$\%R_{ox}$	A_{max}	*Major VLA*	*Minor VLA*
			mmol m^{-2} s^{-1} MPa^{-1}				µmol m^{-2} s^{-1}	mm mm^{-2}	
V. bitchiuense	Lantana	7.7	4.37	14.3 ± 3.6	16.7	35	11.1 ± 1.0	0.74 ± 0.04	4.81 ± 0.44
V. burejaeticum	Lantana	6.96	5.34	-	-	-	12.3 ± 1.4	-	4.75 ± 0.29
V. carlesii	Lantana	13.3	4.58	-	-	-	10.9 ± 0.64	-	6.21 ± 0.77
V. lantana	Lantana	5.39	4.65	13.1 ± 2.9	9.16	54	13.5 ± 1.8	0.69 ± 0.05	5.48 ± 0.51
V. lantana var. discolor	Lantana	11.6	8.89	-	-	-	16.9 ± 1.5	-	4.71 ± 0.26
V. rhytidophyllum	Lantana	3.99 ± 1.97	3.99 ± 1.97	16.7 ± 2.5	5.24	74	12.3 ± 0.81	0.66 ± 0.05	5.05 ± 0.26
V. veitchii	Lantana	14.9	7.92	-	-	-	12.4 ± 1.3	-	5.86 ± 0.24
V. cassinoides	Lentago	3.62 ± 0.66	3.62 ± 0.66	9.46 ± 1.7	5.87	58	12.7 ± 1.1	0.82 ± 0.01	5.48 ± 0.36
V. lentago	Lentago	7.62 ± 2.2	7.62 ± 2.2	11.3 ± 3.2	23.4	22	12.4 ± 1.7	0.76 ± 0.01	4.94 ± 0.55
V. prunifolium	Lentago	5.52 ± 0.49	5.52 ± 0.49	-	-	-	10.8 ± 0.66	-	4.80 ± 0.07
V. rufidulum	Lentago	5.92 ± 0.38	5.92 ± 0.38	20.6 ± 6.4	8.31	59	14.2 ± 0.93	0.85 ± 0.05	5.70 ± 0.14
V. acerifolium	Lobata	3.77 ± 0.59	3.77 ± 0.59	14.3 ± 4.0	5.12	68	6.78 ± 0.49	0.61 ± 0.04	3.65 ± 0.18
V. plicatum	Lutescentia	11.9	7.04	16.4 ± 1.9	43.4	25	11.1 ± 0.67	1.0 ± 0.03	4.78 ± 0.46
V. bracteatum	Mollodontotinus	10.7	8.41	-	-	-	9.04 ± 0.98	-	3.68 ± 0.27
V. molle	Mollodontotinus	5.85	3.8	14.6 ± 0.85	9.76	59	8.32 ± 0.50	0.58 ± 0.07	5.35 ± 0.12
V. opulus	Opulus	10.4	1.55	-	-	-	7.81 ± 1.2	-	4.82 ± 0.42
V. sargentii	Opulus	3.17 ± 0.88	3.17 ± 0.88	12.6 ± 3.5	4.24	68	13.1 ± 1.4	0.77 ± 0.08	4.26 ± 0.15
V. trilobum	Opulus	2.11 ± 0.36	2.11 ± 0.36	20.8 ± 5.3	2.35	86	10.2 ± 1.2	0.69 ± 0.02	4.99 ± 0.19
V. dentatum	Oreinodontotinus	5.76	2.73	14.0 ± 3.6	9.79	46	10.7 ± 1.8	0.82 ± 0.02	4.72 ± 0.34
V. furcatum	Pseudotinus	1.64 ± 0.24	1.64 ± 0.24	5.23 ± 0.91	2.38	66	7.00 ± 0.52	0.55 ± 0.02	3.05 ± 0.07
V. sieboldii	Solenotinus	5.71 ± 0.81	5.71 ± 0.81	15.9 ± 3.0	8.9	54	13.8 ± 1.1	0.94 ± 0.07	3.13 ± 0.09
V.betulifolium	Succodontotinus	4.16	3.13	-	-	-	9.71 ±1.6	-	4.18 ± 0.30
V. corylifolium	Succodontotinus	11.9	2.87	22.7 ± 1.9	25	41	9.94 ± 0.77	0.77 ± 0.02	4.46 ± 0.02
V. dilatatum	Succodontotinus	2.38 ± 0.48	2.38 ± 0.48	14.4 ± 2.1	2.85	82	8.04 ± 1.2	0.69 ± 0.03	3.84 ± 0.37
V. erosum	Succodontotinus	12.9	3.48	-	-	-	7.53 ±1.3	-	4.14 ± 0.07
V. hupehense	Succodontotinus	4.54 ± 0.65	4.54 ± 0.65	-	-	-	9.89 ± 1.5	-	3.41 ± 0.24
V. ichangense	Succodontotinus	25.8	-	-	-	-	7.29 ± 1.1	-	4.67 ± 0.19
V. lobophyllum	Succodontotinus	5.70 ± 0.30	5.70 ± 0.30	-	-	-	10.8 ± 1.8	-	3.48 ± 0.12
V. setigerum	Succodontotinus	12.3	5.72	-	-	-	9.36 ± 1.9	-	4.78 ± 0.16
V. bitchiuense	Lantana	7.7	4.37	14.3 ± 3.6	16.7	35	11.1 ± 1.0	0.74 ± 0.04	4.81 ± 0.44
ANOVA		***		*			***	***	***

Figure captions

Figure 7.1. Distribution of (A) leaf hydraulic conductance (K_{leaf} at -0.3 MPa; mmol m^{-2} s^{-1} MPa^{-1}), (B) light saturated CO_2 assimilation rate (A_{max}; μmol m^{-2} s^{-1}) and (C) stomatal conductance (g_s; mol m^{-2} s^{-1}) across the phylogenetic tree for 30 *Viburnum* species.

Figure 7.2. Partitioning of leaf hydraulic resistance in *Viburnum*. (A) Average allocation to hydraulic resistance in *Viburnum* species, (B) Allocation to hydraulic resistance for the species with least resistance outside the xylem, and (C) the greatest resistance outside the xylem. $\%R_{ox}$, Percent of hydraulic resistance outside the xylem; $\%R_{min}$, percent hydraulic resistance in the minor veins; $\%R_{maj}$, percent hydraulic resistance in the major veins; $\%R_{pet}$, percent hydraulic resistance in the petiole. Note that the percent resistance in the xylem $\%R_x = \%R_{pet} + \%R_{maj} + \%R_{min}$.

Figure 7.3. Coordinated evolution of leaf hydraulics and gas exchange across *Viburnum* species. (A) Light-saturated CO_2 assimilation rate (A_{max}) vs leaf hydraulic conductance at -0.3 MPa (K_{leaf} at 0.3MPa), (B) stomatal conductance (g_s) vs K_{leaf} at 0.3MPa (n = 29 species). Standard major axes (SMA) lines were fitted through the points. Both r^2 of the SMA line and the r^2 of the phylogenetic independent contrasts regression (not shown) calculated under the evolutionary model selected by maximum likelihood are given in the figures. Here, Brownian Motion model (BM) was chosen as best fit in both A and B. ** $p < 0.01$.

Figure 7.4. Drivers of leaf hydraulic conductance for *Viburnum* species. (A) Outside-xylem hydraulic conductance (K_{ox}) drives leaf hydraulic conductance (K_{leaf}) diversification, (B) Independence of K_{leaf} from xylem hydraulic conductance (K_x) (n = 17 species). Both r^2 of the SMA line and the r^2 of the phylogenetic independent contrasts regression (not shown) calculated

under the evolutionary model selected by maximum likelihood are given in the figures. Here, Brownian Motion model (BM) was chosen as best fit in A. *** $p < 0.001$; ^{NS} $p > 0.05$.

Figure 7.5. Trade-off between leaf hydraulic efficiency (maximum leaf hydraulic conductance, K_{max}) and hydraulic safety (Leaf water potential (Ψ_{leaf}) at which 50% of the initial conductance was lost calculated from the linear approximation of K_{leaf} vs. Ψ_{leaf}; P_{50}^{*}) across *Viburnum* species (n = 16 species). Both r^2 of the SMA line and the r^2 of the phylogenetic independent contrasts regression (not shown) calculated under the evolutionary model selected by maximum likelihood are given in the figures. Here, Brownian Motion model (BM) was chosen as best fit model. ** $p < 0.01$; *** $p < 0.001$.

Figure 7.6. Coordination of (A) maximum leaf hydraulic conductance (K_{max}) and (B) maximum CO_2 assimilation rate (A_{max}) with major vein length per area across *Viburnum* species (n = 17 species). Both r^2 of the SMA line and the r^2 of the phylogenetic independent contrasts regression (not shown) calculated under the evolutionary model selected by maximum likelihood are given in the figures. Here, Brownian Motion model (BM) was chosen as best fit model in A, while the Ornstein-Uhlenbeck model of evolution was chosen in B. * $p < 0.05$; ** $p < 0.01$; *** $p < 0.001$.

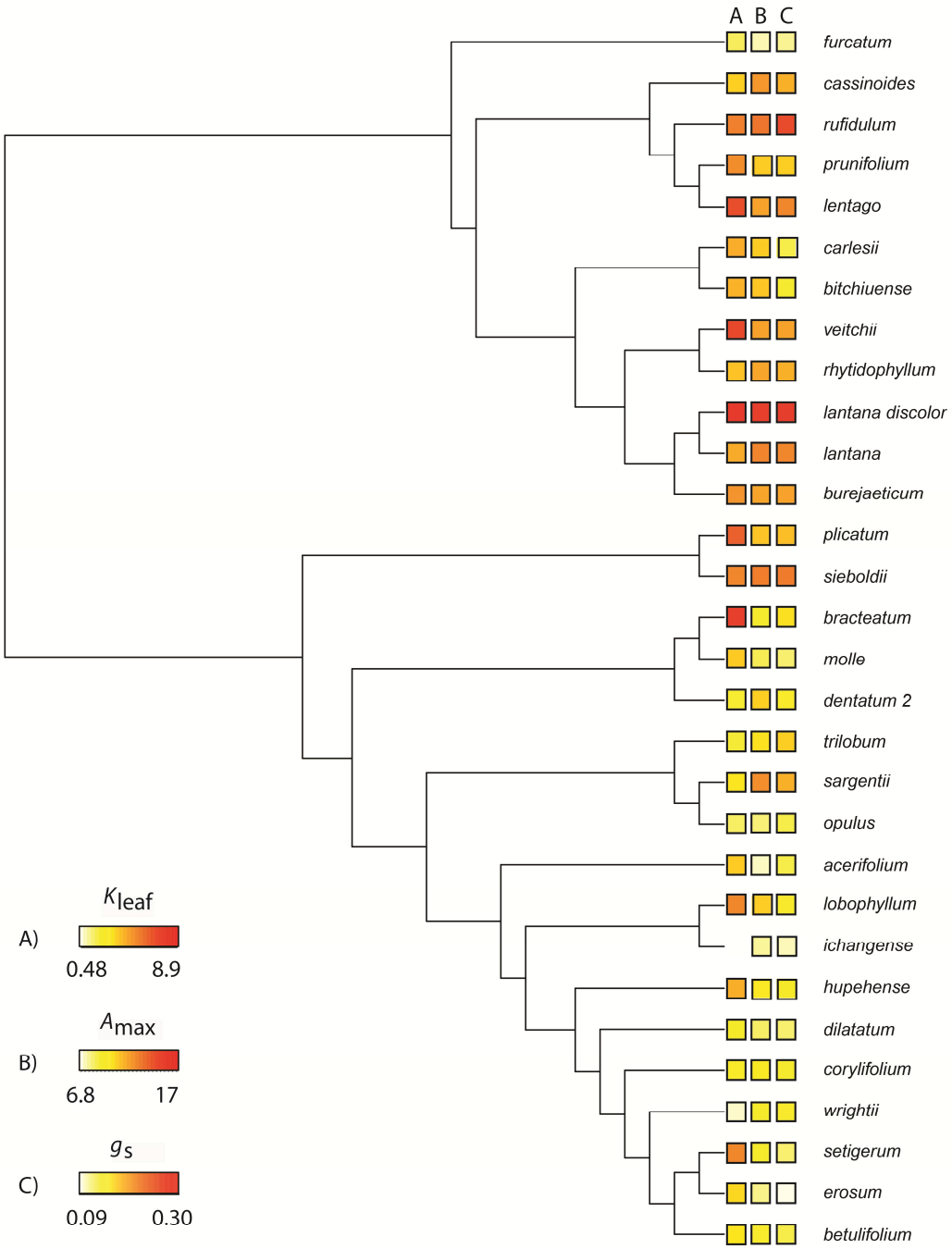
A B C
furcatum
cassinoides
rufidulum
prunifolium
lentago
carlesii
bitchiuense
veitchii
rhytidophyllum
lantana discolor
lantana
burejaeticum
plicatum
sieboldii
bracteatum
molle
dentatum 2
trilobum
sargentii
opulus
acerifolium
lobophyllum
ichangense
hupehense
dilatatum
corylifolium
wrightii
setigerum
erosum
betulifolium
A) Kleaf
0.48 8.9
B) Amax
6.8 17
C) gs
0.09 0.30

Figure 7.1

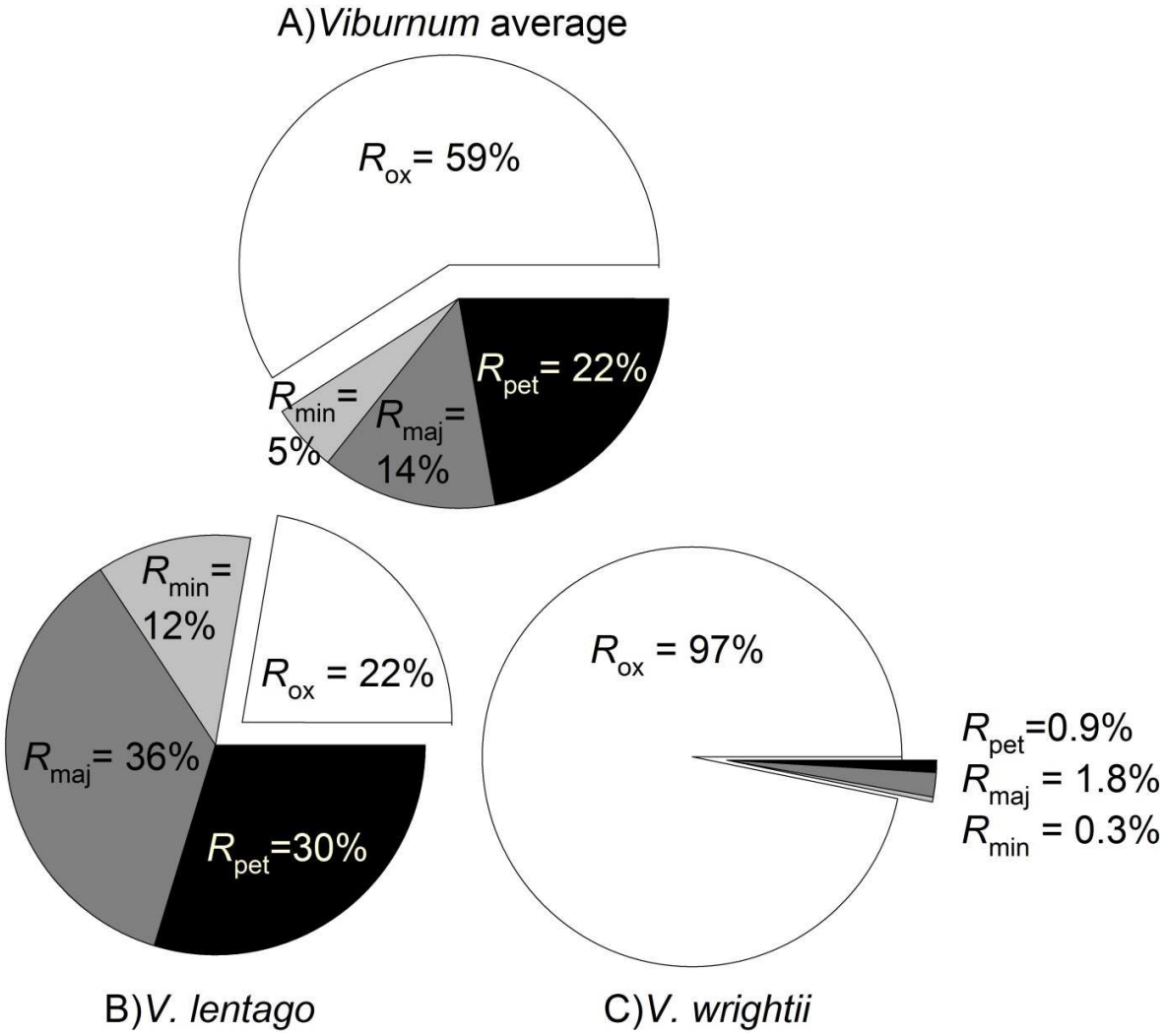
A) *Viburnum* average
R_{ox}= 59%
R_{pet}= 22%
R_{min}= 5%
R_{maj}= 14%
R_{min}= 12%
R_{ox} = 22%
R_{maj}= 36%
R_{pet}=30%
B) *V. lentago*
R_{ox} = 97%
R_{pet}=0.9%
R_{maj} = 1.8%
R_{min} = 0.3%
C) *V. wrightii*

Figure 7.2

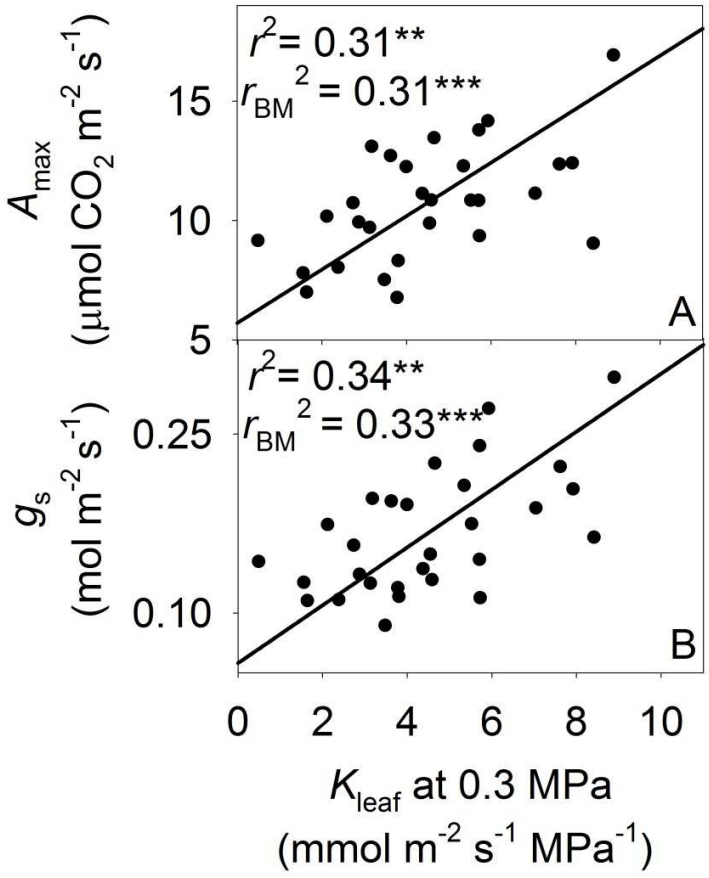
r^2= 0.31**
$r_{BM}{}^2$ = 0.31***
A_{max} (µmol CO_2 m^{-2} s^{-1})
15
10
5
A
r^2= 0.34**
$r_{BM}{}^2$ = 0.33***
g_s (mol m^{-2} s^{-1})
0.25
0.10
B
0
2
4
6
8
10
K_{leaf} at 0.3 MPa
(mmol m^{-2} s^{-1} MPa^{-1})

Figure 7.3

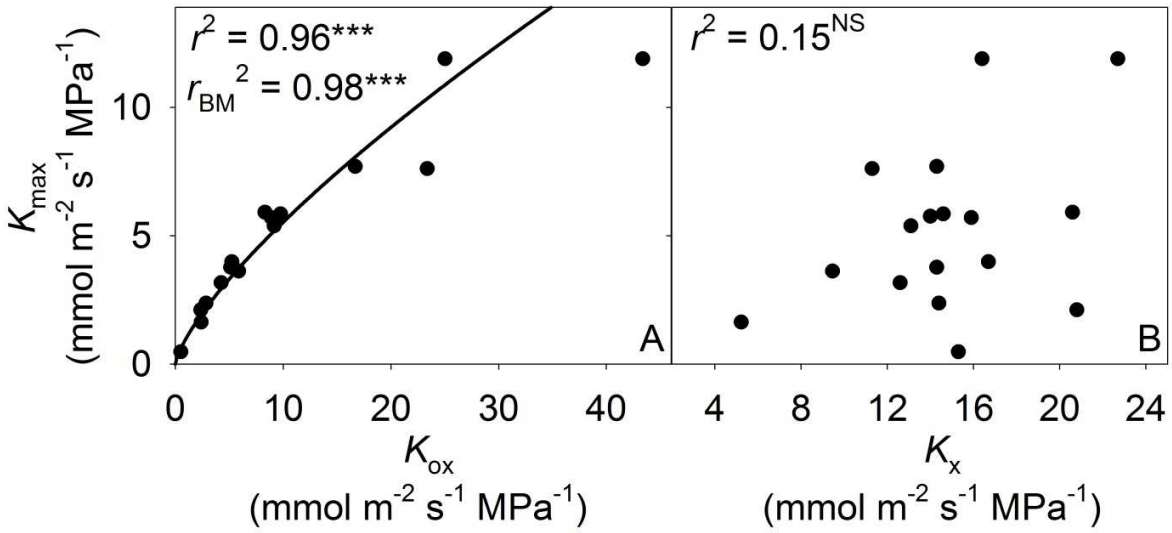
r^2 = 0.96***
r_{BM}^2 = 0.98***
r^2 = 0.15^{NS}
A
B
K_{max} (mmol m^{-2} s^{-1} MPa^{-1})
K_{ox} (mmol m^{-2} s^{-1} MPa^{-1})
K_x (mmol m^{-2} s^{-1} MPa^{-1})
0
5
10
0
10
20
30
40
4
8
12
16
20
24

Figure 7.4

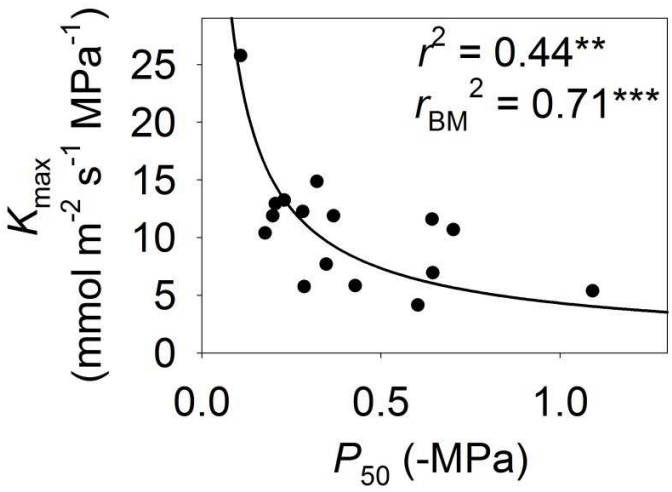
K_{max} (mmol m^{-2} s^{-1} MPa^{-1})
25
20
15
10
5
0
0.0
0.5
1.0
P_{50} (-MPa)
r^2 = 0.44**
r_{BM}^2 = 0.71***

Figure 7.5

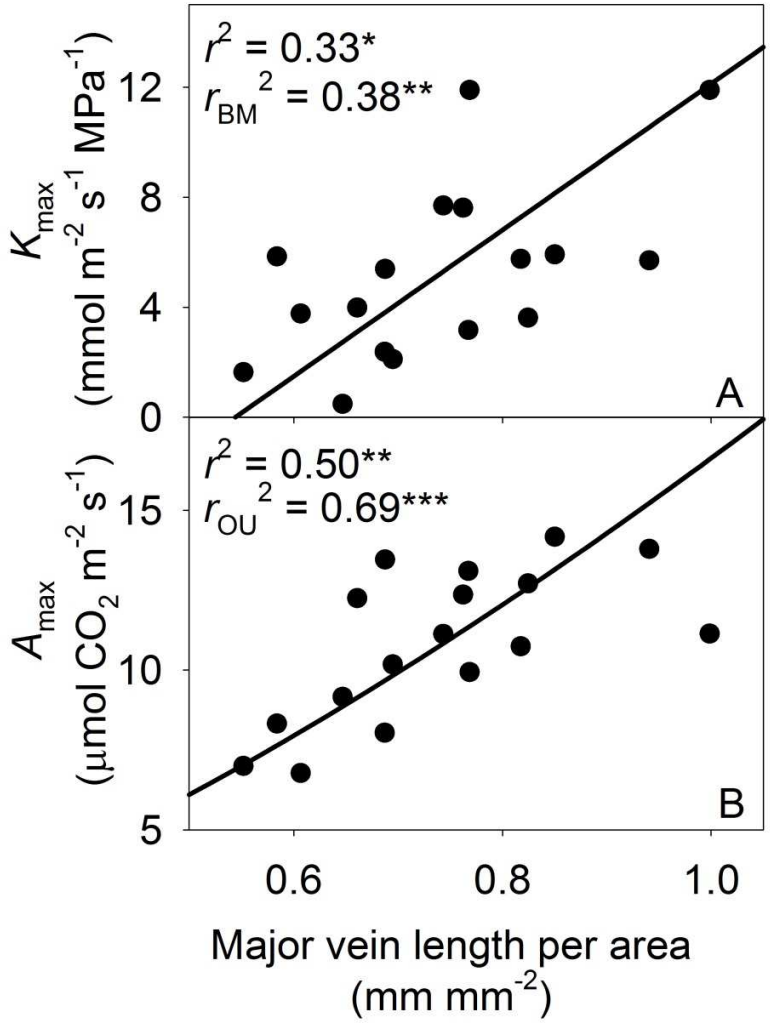
r^2 = 0.33*
$r_{BM}{}^2$ = 0.38**
K_{max} (mmol m^{-2} s^{-1} MPa^{-1})
A
r^2 = 0.50**
$r_{OU}{}^2$ = 0.69***
A_{max} (µmol CO_2 m^{-2} s^{-1})
B
0
4
8
12
5
10
15
0.6
0.8
1.0
Major vein length per area
(mm mm^{-2})

Figure 7.6

SUPPLEMENTAL MATERIAL

Table S7.1. Mean ± standard errors of all traits in the study.

Table S7.2. Akaike Information Criterion (AIC) scores for the two models of trait evolution in the different tested correlations. Model: Brownian motion (BM) and Ornstein-Uhlenbeck (OU). Best chosen model appears in bold.

REFERENCES

Aasamaa K, Sober A (2001) Hydraulic conductance and stomatal sensitivity to changes of leaf water status in six deciduous tree species. Biologia Plantarum **44**: 65-73

Abramoff MD, Magalhaes PJ, Ram SJ (2004) Image Processing with ImageJ. . Biophotonics International **11** 36-42

Blackman CJ, Brodribb TJ, Jordan GJ (2010) Leaf hydraulic vulnerability is related to conduit dimensions and drought resistance across a diverse range of woody angiosperms. New Phytologist **188**: 1113-1123

Brodribb TJ, Cochard H (2009) Hydraulic Failure Defines the Recovery and Point of Death in Water-Stressed Conifers. Plant Physiology **149**: 575-584

Brodribb TJ, Feild TS, Jordan GJ (2007) Leaf maximum photosynthetic rate and venation are linked by hydraulics. Plant Physiology **144**: 1890-1898

Brodribb TJ, Holbrook NM (2003) Stomatal closure during leaf dehydration, correlation with other leaf physiological traits. Plant Physiology **132**: 2166-2173

Brodribb TJ, Holbrook NM (2004) Stomatal protection against hydraulic failure: a comparison of coexisting ferns and angiosperms. New Phytologist **162**: 663-670

Brodribb TJ, Holbrook NM, Zwieniecki MA, Palma B (2005) Leaf hydraulic capacity in ferns, conifers and angiosperms: impacts on photosynthetic maxima. New Phytologist **165**: 839-846

Buckley TN (2014) The contributions of apoplastic, symplastic and gas phase pathways for water transport outside the bundle sheath in leaves Plant, Cell & Environment In Press

Butler MA, King AA (2004) Phylogenetic comparative analysis: A modeling approach for adaptive evolution. American Naturalist **164**: 683-695

Chatelet DS, Clement WL, Sack L, Donoghue MJ, Edwards EJ (2013) The evolution of photosynthetic anatomy in *Viburnum* (Adoxaceae). International Journal of Plant Sciences **174**: 1277-1291

Clement WL, Donoghue MJ (2011) Dissolution of *Viburnum* section *Megalotinus* (Adoxaceae) of southeast Asia and its implications for morphological evolution and biogeography. International Journal of Plant Sciences **172**: 559-573

Cochard H, Nardini A, Coll L (2004) Hydraulic architecture of leaf blades: where is the main resistance? Plant Cell and Environment **27**: 1257-1267

Felsenstein J (1985) Phylogenies and the comparative method. American Naturalist **125**: 1-15

Flexas J, Scoffoni C, Gago J, Sack L (2013) Leaf mesophyll conductance and leaf hydraulic conductance: an introduction to their measurement and coordination. Journal of Experimental Botany **64**: 3965-3981

Hacke UG, Sperry JS, Feild TS, Sano Y, Sikkema EH, Pittermann J (2007) Water transport in vesselless angiosperms: conducting efficiency and cavitation safety. International Journal of Plant Sciences **168**: 1113-1126

Hacke UG, Sperry JS, Pockman WT, Davis SD, McCulloch KA (2001) Trends in wood density and structure are linked to prevention of xylem implosion by negative pressure. Oecologia **126**: 457-461

Kim YX, Steudle E (2007) Light and turgor affect the water permeability (aquaporins) of parenchyma cells in the midrib of leaves of *Zea mays*. Journal of Experimental Botany **58**: 4119-4129

Lewis AM, Boose ER (1995) Estimating volume flow-rates through xylem conduits. American Journal of Botany **82**: 1112-1116

Maherali H, Pockman WT, Jackson RB (2004) Adaptive variation in the vulnerability of woody plants to xylem cavitation. Ecology **85**: 2184-2199

Nardini A, Pedà G, La Rocca N (2012) Trade-offs between leaf hydraulic capacity and drought vulnerability: morpho-anatomical bases, carbon costs and ecological consequences. New Phytologist

Nardini A, Tyree MT, Salleo S (2001) Xylem cavitation in the leaf of *Prunus laurocerasus* and its impact on leaf hydraulics. Plant Physiology **125**: 1700-1709

Noblin X, Mahadevan L, Coomaraswamy IA, Weitz DA, Holbrook NM, Zwieniecki MA (2008) Optimal vein density in artificial and real leaves. Proceedings of the National Academy of Sciences of the United States of America **105**: 9140-9144

Pittermann J, Choat B, Jansen S, Stuart SA, Lynn L, Dawson TE (2010) The Relationships between Xylem Safety and Hydraulic Efficiency in the Cupressaceae: The Evolution of Pit Membrane Form and Function. Plant Physiology **153**: 1919-1931

Pittermann J, Sperry JS, Hacke UG, Wheeler JK, Sikkema EH (2006) Inter-tracheid pitting and the hydraulic efficiency of conifer wood: The role of tracheid allometry and cavitation protection. American Journal of Botany **93**: 1265-1273

Pittermann J, Sperry JS, Wheeler JK, Hacke UG, Sikkema EH (2006) Mechanical reinforcement of tracheids compromises the hydraulic efficiency of conifer xylem. Plant Cell and Environment **29**: 1618-1628

Price SA, Tavera JJ, Near TJ, Wainwright PC (2013) Elevated rates of morphological and functional diversification in reff-dwelling haemulid fishes. Evolution **67**: 417-428

Sack L, Bartlett M, Creese C, Guyot G, Scoffoni C (2011) Constructing and operating a hydraulics flow meter. http://prometheuswiki.publish.csiro.au/tiki-

index.php?page=Constructing+and+operating+a+hydraulics+flow+meter. *In*. Prometheus Wiki

Sack L, Cowan PD, Jaikumar N, Holbrook NM (2003) The 'hydrology' of leaves: co-ordination of structure and function in temperate woody species. Plant Cell and Environment **26**: 1343-1356

Sack L, Frole K (2006) Leaf structural diversity is related to hydraulic capacity in tropical rain forest trees. Ecology **87**: 483-491

Sack L, Holbrook NM (2006) Leaf hydraulics. Annual Review of Plant Biology **57**: 361-381

Sack L, Melcher PJ, Zwieniecki MA, Holbrook NM (2002) The hydraulic conductance of the angiosperm leaf lamina: a comparison of three measurement methods. Journal of Experimental Botany **53**: 2177-2184

Sack L, Scoffoni C (2012) Measurement of leaf hydraulic conductance and stomatal conductance and their responses to irradiance and dehydration using the evaporative flux methods (EFM). Journal of Visualized Experiments

Sack L, Scoffoni C (2013) Leaf venation: structure, function, development, evolution, ecology and applications in past, present and future. New Phytologist

Sack L, Scoffoni C, John GP, Poorter H, Mason CM, Mendez-Alonzo R, Donovan LA (2013) How do leaf veins influence the worldwide leaf economic spectrum? Review and synthesis. Journal of Experimental Botany **64**: 4053-4080

Sack L, Scoffoni C, McKown AD, Frole K, Rawls M, Havran C, Tran H, Tran T (2012) Developmentally-based scaling of leaf venation architecture explains global ecological patterns. Nature Communications **3** 837

Sack L, Streeter CM, Holbrook NM (2004) Hydraulic analysis of water flow through leaves of sugar maple and red oak. Plant Physiology **134**: 1824-1833

Sack L, Tyree MT, Holbrook NM (2005) Leaf hydraulic architecture correlates with regeneration irradiance in tropical rainforest trees. New Phytologist **167**: 403-413

Santana SE, Alfaro JL, Noonan A, Alfaro ME (2013) Adaptive response to sociality and ecology drives the diversification of facial colour patterns in catarrhines. Nature Communications **4**

Schmerler SB, Clement WL, Beaulieu JM, Chatelet DS, Sack L, Donoghue MJ, Edwards EJ (2012) Evolution of leaf form correlates with tropical-temperate transitions in Viburnum (Adoxaceae). Proceedings of the Royal Society B-Biological Sciences **279**: 3905-3913

Scoffoni C, Kunkle J, Pasquet-Kok J, Vuong C, Patel AJ, Montgomery RA, Givnish TJ, L. S (In review) The integrated light-induced plasticity of leaf hydraulics, gas exchange and anatomy: testing hypotheses in Hawaiian lobeliads diverse in light adaptation.

Scoffoni C, McKown AD, Rawls M, Sack L (2012) Dynamics of leaf hydraulic conductance with water status: quantification and analysis of species differences under steady-state. Journal of Experimental Botany **63**: 643-658

Scoffoni C, Pou A, Aasamaa K, Sack L (2008) The rapid light response of leaf hydraulic conductance: new evidence from two experimental methods. Plant Cell and Environment **31**: 1803-1812

Scoffoni C, Rawls M, McKown A, Cochard H, Sack L (2011) Decline of leaf hydraulic conductance with dehydration: relationship to leaf size and venation architecture. Plant Physiology **156**: 832-843

Scoffoni C, Sack L, contributors P (2013) Quantifying leaf vein traits. http://prometheuswiki.publish.csiro.au/tiki-index.php?page=Quantifying+leaf+vein+traits. *In*. Prometheus Wiki

Scoffoni C, Vuong C, Diep S, Cochard H, Sack L (2014) Leaf shrinkage with dehydration: coordination with hydraulic vulnerability and drought tolerance. Plant Physiology **164**: 1772-1788

Sokal RR, Rohlf FJ (1995) Biometry: the principles and practice of statistics in biological research. Third edition. W.H. Freeman and Company, New York, New Yord, USA

Sommerville KE, Sack L, Ball MC (2012) Hydraulic conductance of Acacia phyllodes (foliage) is driven by primary nerve (vein) conductance and density. Plant Cell and Environment **35**: 158-168

Sperry JS, Hacke UG, Pittermann J (2006) Size and function in conifer tracheids and angiosperm vessels. American Journal of Botany **93**: 1490-1500

Voicu MC, Zwiazek JJ, Tyree MT (2008) Light response of hydraulic conductance in bur oak (Quercus macrocarpa) leaves. Tree Physiology **28**: 1007-1015

Weast RC (1974) Handbook of chemistry and physics, 54th edn, Cleveland, OH: CRC Press.

Yang SD, Tyree MT (1993) Hydraulic resistance in *Acer saccharum* shoots and its influence on leaf water potential and transpiration. Tree Physiology **12**: 231-242

CHAPTER 8

CONCLUSIONS AND FUTURE DIRECTIONS

The field of leaf hydraulics emerged only two decades ago, and has expanded rapidly since. As such, most of the fundamental discoveries regarding water movement have been made based on approaches focused at the stem or whole plant level. My dissertation work was aimed in large part to fill the gap of knowledge for leaves by combining anatomy, physiology, ecology and evolution.

The first study of water relations in plants dates from three centuries ago. Indeed, John Woodward in 1699 was the first to realize that water was at least as important to plant growth, if not more, than soil, as it had been thought at the time (Woodward, 1699). It was however Stephen Hales 30 years later, who invented the first potometer system consisting of tubing filled with water connected to detached shoots and measured the rate of water uptake, proving that roots are not needed for the uptake of water through plants, as had been previously assumed (Hales, 1727). In fact, that was such a well-established concept at the time that still over a century later scientists were testing this, though it is possible that Hales' book was not read by other scientists as these later studies on the topic did not cite Hales' work. Thus, in 1890, Strasburger at the University of Bonn investigated the question, cutting off an entire maple tree to remove the roots and placing it in water, establishing again that a tree without root was still able to take up water and apparently remain alive (Strasburger, 1891, 1893). This work sparked the interest of Dixon and Joly, of Trinity College in Dublin. While they were visiting Prof. E. Strasburger in Bonn, he showed them his experiments, which led them to investigate the cause of the ascent of sap in trees. Just a few years later, they published their famous study "On the ascent of sap" which changed the field of water relations forever (Dixon and Joly, 1895; Dixon, 1914).

They proposed that water ascended up the tree by tension and cohesion of water molecules. During the entire 20th century, very strong debate around this "cohesion-tension" theory occurred, and it was finally fully accepted by the scientific community a century later (Angeles et al., 2004). Although debating over this for a whole century might seem now to have been a waste of time, the excitement around this debate triggered widespread interest in the field of plant hydraulics, and a greater appreciation of its centrality in plant biology. By combining physical and biological sciences, tools and methods were developed to measure hydraulic conductance through the plant, with a special emphasis on what occurred to the water column in dehydrated plants. John Milburn in 1966 was the first to show cavitation—the process by which air is sucked into the water column, embolising the conduit—and that work was conducted in leaves (Milburn, 1966). This study was followed by many others focusing on this phenomenon in stems. It is interesting to note, that although cavitation was first shown in leaves, it took over 30 years for the field of leaf hydraulics to take off and thus for the understanding of the phenomenon in leaves to be studied in detail.

Leaves are complex organs for water movement, since water moves through both the xylem and outside the xylem toward the sites of evaporation. During the first decade of the 21st century, studies measuring leaf hydraulic decline in dehydrating leaves mostly focused on cavitation as the sole explanation. Consistent with those studies, I found in Chapter 3 using an experimental and modeling approach that species most tolerant to dehydration had higher major vein length per area, which would provide them with more routes for water to flow around embolised conduits during drought. However, I later found in Chapter 4 that cell shrinkage outside the xylem also has an impact on leaf hydraulic decline, especially during mild stress. Thus, I found that outside-xylem pathways had a strong impact on whole leaf hydraulic

conductance, and can act as an important bottleneck in the leaf water pathways, protecting the xylem from reaching its cavitation thresholds. Consistent with other recent studies showing the importance of aquaporins in water movement outside the xylem and its impact on whole leaf hydraulic conductance (e.g., Sack et al., 2002; Cochard et al., 2007; Kim and Steudle, 2007; Scoffoni et al., 2008), it has become evident that cavitation might only be playing a small role in leaf hydraulic decline, compared to stems which only contain a xylary pathway. Indeed, in Chapter 5, I found that decline of leaf xylem hydraulic conductance tends to only start occurring at severe levels of leaf dehydration, possibly indicating that most of the hydraulic conductance decline observed at the whole leaf level would mainly relate to changes in outside-xylem pathways.

I found in Chapter 6 that leaf hydraulic conductance was highly plastic with light across Hawaiian Lobeliads, and this plasticity seemed to be explained mostly by potential differences in biochemistry in leaves of plants grown in sun vs. shade, rather than their xylem anatomy.

Finally, I found in Chapter 7 that differences in leaf hydraulic conductance have evolved by diversification of outside-xylem pathways, rather than the xylem itself. Indeed, across 30 *Viburnum* species, leaf hydraulic conductance correlated strongly with the conductance outside the xylem, while it showed no correlation with leaf xylem hydraulic conductance. Leaf hydraulic conductance also drove the diversification of photosynthetic rates observed across these closely related species. To be able to match the hydraulic supply of an increase demand, it might have been more cost efficient for leaves to modify their biochemistry and/or cellular architectures to increase overall conductance, rather than changing xylem anatomy, which seems to have been more conserved.

The next step in plant hydraulics is probably the most challenging. Until we understand where the water evaporates in the leaf mesophyll, and the degree to which species differ in its location, and why, it will be challenging to fully understand water movement outside the xylem. Modelling studies have been initiated to focus on this question, and for now this might be the only approach to further understanding in this area. More detailed work on cell shrinkage of different tissues, especially at the epidermal level near stomata, will help bridge the gap between hydraulic transport and diffusion of water in the leaf.

While many questions remain, by building on key work just as my research has done, and by increasing the use of multiple approaches and collaborations across fields including modeling, biochemistry, hydraulics and gas exchange, and by conducting detailed experimental work alongside comparative work in an ecological and evolutionary context, the next few decades will provide exciting answers enabling a new level of understanding of the plant hydraulic system and its contribution to plant life.

REFERENCES

Angeles G, Bond B, Boyer JS, Brodribb T, Brooks JR, Burns MJ, Cavender-Bares J, Clearwater M, Cochard H, Comstock J, Davis SD, Domec JC, Donovan L, Ewers F, Gartner B, Hacke U, Hinckley T, Holbrook NM, Jones HG, Kavanagh K, Law B, Lopez-Portillo J, Lovisolo C, Martin T, Martinez-Vilalta J, Mayr S, Meinzer FC, Melcher P, Mencuccini M, Mulkey S, Nardini A, Neufeld HS, Passioura J, Pockman WT, Pratt RB, Rambal S, Richter H, Sack L, Salleo S, Schubert A, Schulte P, Sparks JP, Sperry J, Teskey R, Tyree M (2004) The Cohesion-Tension theory. New Phytologist **163:** 451-452

Cochard H, Venisse JS, Barigah TS, Brunel N, Herbette S, Guilliot A, Tyree MT, Sakr S (2007) Putative role of aquaporins in variable hydraulic conductance of leaves in response to light. Plant Physiology **143:** 122-133

Dixon HH (1914) Transpiration and the ascent of sap in plants, MacMillan and Co., London, UK

Dixon HH, Joly J (1895) On the ascent of sap. Philosophical Transactions of the Royal Society of London **186:** 563-576

Hales S (1727) Vegetable staticks. Oldbourne Book Co., London, UK

Kim YX, Steudle E (2007) Light and turgor affect the water permeability (aquaporins) of parenchyma cells in the midrib of leaves of *Zea mays*. Journal of Experimental Botany **58:** 4119-4129

Milburn JA (1966) Conduction of sap. I. Water conduction and cavitation in water stressed leaves. Planta **69:** 34-&

Sack L, Melcher PJ, Zwieniecki MA, Holbrook NM (2002) The hydraulic conductance of the angiosperm leaf lamina: a comparison of three measurement methods. Journal of Experimental Botany **53:** 2177-2184

Scoffoni C, Pou A, Aasamaa K, Sack L (2008) The rapid light response of leaf hydraulic conductance: new evidence from two experimental methods. Plant Cell and Environment **31:** 1803-1812

Strasburger E (1891) Über den Bau und Verrichtungen del Leitungsbahnen in den Pflanzen. Histologische Beitrage **3:** 607-625

Strasburger E (1893) Ueber das Saftsteigen. Histologische Beitrage **5:** 1-94

Woodward J (1699) Some thoughts and experiments concerning vegetation Philosophical Transactions **21:** 193-227